**Technische Universität München**

Fachgebiet Bioanorganische Chemie

# Unsymmetric Redoxactive Ligands for Mono- and Bimetallic Complexes; Synthesis and Characterisation

**Ruth Marlen Haas**

Vollständiger Abdruck der von der Fakultät Chemie der Technischen Universität München zur Erlangung des akademischen Grades eines

**Doktors der Naturwissenschaften (Dr. rer. nat.)**

genehmigten Dissertation.

Vorsitzende(r): Hon.-Prof. Dr. Richard W. Fischer

Prüfer der Dissertation:

1. Prof. Dr. Corinna Hess
2. Prof. Dr. Klaus Köhler

Die Dissertation wurde am 12.12.2017 bei der Technischen Universität München eingereicht und durch die Fakultät für Chemie am 16.01.2018 angenommen.

Die vorliegende Arbeit wurde im Fachgebiet Bioanorganische Chemie der Technischen Universität München in der Zeit von November 2014 bis Dezember 2017 angefertigt.

Teile dieser Arbeit wurden bereits veröffentlicht:

Haas, R. M., Arshad, M., Anthony, J. A., Altmann, P. J., Pöthig, A., Köhler, F. H., Hess, C. R. "Six- and seven-coordinate Fe(II) and Zn(II) compounds ligated by unsymmetrical xanthene-based ligands: characterization and magnetic properties." *Inorg. Chem. Front.*, **2016**, *3*, 616.

Haas, R. M., Hern, Z., Sproules, S., Hess, C. R. "An unsymmetric ligand framework for non-coupled homo- and heterobimetallic complexes." *Inorg. Chem.*, **2017**, doi:10.1021/acs.inorgchem.7b02294.

Besonders danken möchte ich meiner Doktormutter

**Frau Professor Corinna R. Hess**

Für die Aufnahme in den Lehrstuhl und das interessante Forschungsthema, welches mir vorgeschlagen wurde.

# Acknowledgment

Mein Dank gilt:

Meinem Mitstarter am Lehrstuhl Manuel Kaspar, der alles mit mir aufgebaut hat. Ich hätte es auch gerne mit dir beendet. Sophia Stark, die in der letzten Halbzeit eine großartige Rücken-an-Rücken Bürostuhlnachbarin war. Unsere Diskussionen waren immer sehr verwirrend, haben uns aber oft weitergebracht und auch die Kaffee-/Teepausen waren immer erholsam. Michael Grübel, der OCler, hat oft Chaos in unserem Labor verbreitet, uns aber auch mit organischen Reaktionen weitergeholfen, Ceren Tok, die neues Flair in unsere Gruppe gebracht hat ,sowie Andreas Hofmann, meinem Nachfolger und unserem Neuzugang Raphael Lauenstein.

Unseren zwei Postdocs, Dr. Anica Dose und Dr. Daniel Betz, die uns jeweils ein Jahr begleitet haben, waren immer für gute Ratschläge zu haben.

Pauline Fischer und Lukas Niederegger, unseren Masteranten, Auch wenn ich oft Recht hatte, ihr habt großartige Arbeit geleistet und unsere Gruppe bereichert.

Dr. Alexander Pöthig, der mich in die Geheimnisse der Röntgenstrukturanalyse eingeführt hat und mit guten Ratschlägen weiterhelfen konnte. Außerdem gilt mein Dank seinem Kristallographieteam, allen voran Philipp Altmann, aber auch Christan Jandl und David Mayer. Danke für eure Hilfe, ich habe nicht aufgegeben.

Dr. Gaby Raudaschl-Sieber und Dr. Markus Drees, die ich bei der Betreuung von Laborpraktika unterstützen konnte , von denen ich aber auch immer Hilfe und Ratschläge erhalten habe.

Meinen Studenten, Fabian Hörmann, Lorenz Pardatscher, Zach Hern und David Müller, die mein Thema mit vorangebracht und oft für entscheidende Fortschritte durch ihre unermüdliche Arbeit gesorgt haben.

Weiter möchte ich mich bei Dr. Lilian Graser bedanken. Sie hat mich zur metallorganischen Chemie gebracht und dafür begeistert. Sie war sowohl an der Universität als auch Privat eine großartige Persönlichkeit und ein Rückhalt. Das Gleiche gilt für Dr. Nadine Eckstein, die mir immer mit Rat und Tat zur Seite stand.

Danken möchte ich den Mitarbeitern der Lehrstühle von Professor Kühn und Professor Fischer. Sie haben oft ausgeholfen und uns Geräte und Materialen zur Verfügung gestellt.

Den Technikern, Jürgen Kudermann, Maria Weindl, Olaf Ackermann , Ulrike Ammari, Bircan Dilki, Petra Ankenbauer und Rodica Dumitrescu, die meine Proben immer zeitnah gemessen haben. Sie haben mir geduldig die Geräte erklärt und hatten Antworten auf meine Fragen.

Frau Kullick, die unserem Lehrstuhl als Sekretärin beistand  Sie hat uns entlastet und immer Antworten auf unsere Fragen gefunden.

Aus meiner Studienzeit sind mir Christina Schwarzenböck, Susanne Herden und Lena Böbel in guter Erinnerung geblieben, ebenso unser Freitag-Mittagstisch, Johannes Stecher, Christoph Brenninger, Maike Wahl und Christine Hutterer.

Zuletzt möchte ich meiner Familie danken, meiner Mama und meinem Papa, die mich immer unterstützt und mir das Studium ermöglichten. Sie haben frühzeitig dafür gesorgt, dass ich in verschiedene Bereiche der Chemie Einblicke erhielt. Meiner Schwester Sylvia und ihrem Mann Simon für die Fahrdienste nach München und unserem jüngsten Familienzuwachs Alexander, der für Unruhe sorgt.

Der erweiterten Familie, meinem inzwischen leider verstorbenen Opa, meiner Oma, meinen Tanten, Onkel, Cousins und Cousinen, welche immer gefragt haben, wie es grad läuft.

Michi möchte ich dafür danken, dass er immer zugehört hat, an meiner Seite war und mich auch mal abgelenkt hat

# Deutscher Abstract

In der vorliegenden Arbeit wurden zwei Projekte bearbeitet deren Gemeinsamkeit ein nicht-redox-inertes Ligandensystem ist. Nicht-redox-inerte Ligandensysteme erfahren in den letzten Jahren mehr Aufmerksamkeit, da sie Multielektronenreaktionen unterstützen. Bei der Umsetzung oder Bildung kleiner Moleküle (wie $CO_2$, $H_2$ oder $N_2$) sind Multielektronenreaktionen unumgänglich und werden daher intensiv erforscht. Die Aktivierung oder Umsetzung dieser Moleküle ist nötig aufgrund der wachsenden Bevölkerung und des damit verbundenen erhöhten Energiebedarfs und ermöglicht eine $CO_2$ neutrale Energiespeicherung.

In der Synthese der iXa und iXa-2 Liganden wurde eine nicht redox inerte Iminopyridine-Einheit eingebaut und die Eisen- und Zinkkomplexe dazu synthetisiert. Diese Komplexe wurden sowohl in Lösung, also auch im Feststoff, untersucht. Beide Komplexe konnten die Erwartungen an Redoxaktivität nur bedingt erfüllen, zeigten aber gerade in der Messung der magnetischen Suszeptibilität unerwartete Eigenschaften, welche einen möglichen Einsatz als magnetisches Material versprechen. Dafür wurden diese Komplexe noch genauer mit DFT-Rechnungen begutachtet und besonders für den ungewöhnlichen siebenfach koordinierten Fe(iXa)-Komplex, die Labilität der Liganden mit NMR-Spektroskopie untersucht. Der Versuch weiter Komplexe zu synthetisieren zeigt, dass das Ligandensystem nicht stabil gegenüber Nickelionen ist.

Ein größerer Teil dieser Arbeit umfasste die Entwicklung und Synthese des Ligandengerüsts der Korbliganden, der offenen Korbliganden und des sogenannten PDIpCy-Liganden. Mit diesen Systemen wurden nicht-redox-inerte Koordinationsstellen mit einer redox-inerten Koordinationsstelle in einem Liganden für bimetallische Komplexe kombiniert. Das am besten untersuchte System ist bisher der PDIpCy- Ligand mit seinen Komplexen, da hier strukturelle Nachweise existieren. In vielen anderen Fällen konnte die Koordination eines zweiten Metalls nicht sicher bestätigt werden. Der PDIpCy-Ligand bildet sowohl homo- als auch heterobimetallische Komplexe. Ein Vorteil dieses Systems sind die zwei unterschiedlichen aber dennoch sehr räumlich klaren Bindungsstellen, welche, soweit bisher erforscht, nicht direkt miteinander interagieren. Die bisher synthetisierten Nickel, Zink und Eisenkomplexe müssen nun noch auf ihre Reaktivität untersucht werden.

# English Abstract

In this work, two projects are presented based on redox-active ligand scaffolds. Over the last decades the non-innocent theory became more abundant as they support multi-electron reactions. Many reactions for the activation or formation of small molecules, like $CO_2$, $H_2$ or $N_2$, include a multi-electron step. The work on small molecules gained importance as the growing population has a rising energy demand.

In the first project, the iXa and iXa-2 ligands a non-innocent diimine moiety was incorporated into the ligand scaffolds and the iron and zinc complexes were isolated. The metal complexes were thoroughly examined in solution and in solid state. The redox-activity of the non-innocent complexes did not completely meet our expectation, but the measurement of the magnetic susceptibility gave surprising results, which need to be investigated for magnetic materials. Therefore, DFT calculations were set up and the ligand lability of the rare seven coordinate Fe(iXa)-complex was investigated by NMR spectroscopy. Further complex syntheses were set up with nickel ions, but showed that our ligand scaffold is not stable in reactions with nickel ions under applied conditions.

The second project was the development and synthesis of ligand scaffolds for the basket ligands, the open basket ligands and the PDIpCy ligand. The design of these scaffolds combined a redox-active coordination site alongside an innocent coordination site for the formation of bimetallic complexes. All obtained complexes and their scaffolds have advantages. The most thoroughly examined system is so far the PDIpCy ligand and its complexes as there are structural information for the complexes. A big problem is often the conformation of the coordination of a second metal in our scaffold. The PDIpCy ligand forms homo- and heterobimetallic complexes. A great advantage of this ligand is the two distinct binding sites, which are electronically uncoupled. The synthesised nickel-, zinc- and iron-complexes have to be screened for reactivity.

# List of Abbreviations

| | |
|---|---|
| B | magnetic flux density |
| B3LYP | Becke, three-parameter, Lee-Yang-Parr – Basis Set for DFT |
| BOC | di-*tert*-butylcarbonate |
| $CDCl_3$ | deuterated chloroform |
| cod | cyclooctadiene |
| cosy | correlation spectroscopy |
| CV | cyclic voltammetry |
| Cy | cyclam |
| d | day |
| DCM | dichloromethane |
| DFT | density functional theory |
| DPPE | bis(diphenylphosphino)ethane |
| emu | electromagnetic unit |
| EPR | electron paramagnetic resonance |
| eq | equivalent |
| ESI | electron spray ionisation |
| ESI | electronic spray ionisation |
| $Et_2O$ | diethylether |
| EtCN | propionitrile |
| EtOH | ethanol |
| FAB | fast atomic bombardment |
| Fc | ferrocene |
| h | hour |
| HMBC | heteronuclear multiple bond correlation |
| HOMO | highest occupied molecular orbital |
| HRMS | high resolution mass spectroscopy |
| HSQC | heteronuclear single quantum coherence |
| Hz | Hertz |
| IR | infrared |
| IR | infrared |
| K | Kelvin |
| LIESST | light induced excited spin state trapping |
| LIFDI | liquid injection field desorption ionisation |
| LUMO | lowest occupied molecular orbital |

| | |
|---|---|
| MAS NMR | magic angle spinning nuclear magnetic resonance |
| MeCN | acetonitrile |
| MeOH | methanol |
| MLCT | metal ligand charge transfer |
| MO | molecular orbital |
| $NEt_3$ | trimethylamine |
| NHE | normal hydrogen electrode |
| NIR | near-infrared |
| nm | nanometre |
| NMR | nuclear magnetic resonance |
| OAc | acetate |
| PDI | pyridine diimine |
| pip | piperidine |
| ppm | parts per million |
| pyr | pyridine |
| RT | room temperature |
| SCE | saturated calomel electrode |
| SHE | standard hydrogen electrode |
| SOMO | single occupied molecular orbital |
| SQUID | superconducting quantum interference device |
| T | tesla |
| TCE | tetrachloroethane |
| Tf | triflate |
| THF | tetrahydrofuran |
| UVVis | UV-visible light |
| V | Volt |
| VT | variable temperature |
| XRD | X-ray diffraction |
| $\varepsilon$ | absorption coefficient |
| $\lambda$ | wavelength |
| PSII | Photolyse II |

# Table of contents

# 1 Introduction

The rising global energy demand over the next decade will be one of the major challenges for human kind. The support of a growing population needs to be secured by providing at least basic material supplies for everyone as well as giving the possibility for advanced progress of the economy in developing and emerging countries. Fossil fuels, over centuries the only energy source, are limited and the predictions show that the reserves will meet the energy demand until 2050.[1] Furthermore, the use of these fossil fuels has negative consequences for our environment and climate and the calls for clean, renewable and carbon neutral energy sources become more frequent. The focus lays on $CO_2$ which, along with $CH_4$ are broadly known as “climate killers” but gets emitted in large quantities by the use of fossil fuels. Nevertheless, both compounds represent a non-toxic, highly abundant and cheap carbon feedstock for the industries.

One way to face the carbon induced climate change is to find alternative energy sources, like solar energy, wind and hydroelectric power. Nuclear energy sources have negative publicity and due to the production of the fuel elements are not completely resource-friendly. Another approach is the recovery of the climate active small molecules and hydrogen production. The reduction of $CO_2$ and protons will now be closer examined:

## 1.1 $CO_2$- and proton-reduction

### 1.1.1 $CO_2$-reduction

The conversion of $CO_2$ into fuels or basic chemicals is a big goal for catalytic chemistry. The recycling of $CO_2$, although it is a good electrophile, is difficult due to the inertness of the substrate. In most of the catalytic reactions, the stability of the products, the selectivity of the reaction and the efficiency of the reactions are the key parameters to be monitored. Several possible reaction products of $CO_2$ reductions are shown in Scheme 1. The one electron reduction of $CO_2$ to $CO_2^{\cdot-}$ has the highest activation barrier ($E^0$ = -1.90 V vs NHE)[2] and is unfavourable due to geometric rearrangements from linear to bent. The proton-coupled multi-electron reactions are preferred as thermodynamically more stable products, such as methanol, CO or methane, are formed (Scheme 1).[3]

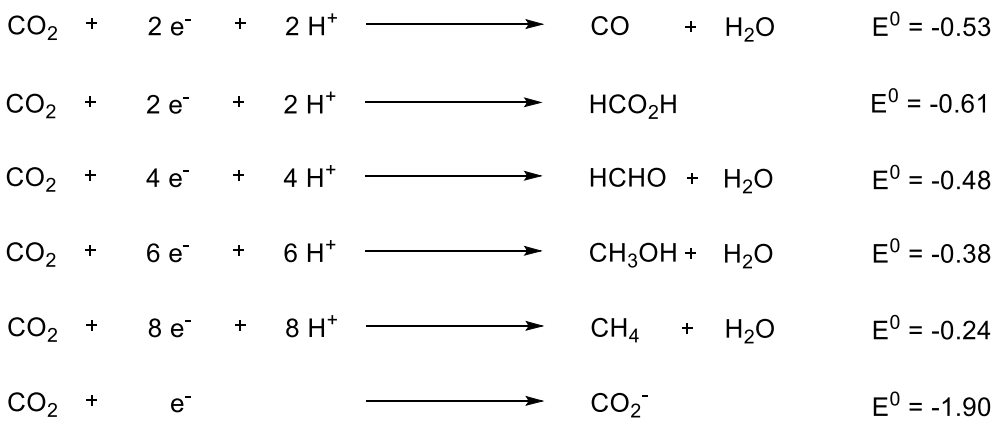


**Scheme 1.** Reduction of $CO_2$**.**

The activation barriers for the reactions, except the formation of the radical anion, are similar. The easiest way to perform the reaction to obtain liquid fuels is the reduction to CO, followed by the conversion to liquid fuels by the Fischer-Tropsch process.[4] The direct conversion of $CO_2$ to methanol or formiates is more difficult under electrochemical conditions as it can include the transfer of more than two electrons. The required catalyst needs to have functionalities which can support multi-electron catalysis and furthermore, guarantee the selectivity to one product.

In this short overview, select catalysts, which perform the reduction of $CO_2$ as electrocatalysts, will be discussed. Catalysts, which are used in photocatalytic reactions for $CO_2$ conversion, and the possibility to activate $CO_2$ with reducing chemicals, are not considered here. In the following section, select catalysts with earth abundant metals like iron or nickel will be presented. We are aware that there are more efficient catalysts with metals from the second and third transition metal row, but our interest is in cheap and earth abundant metals. Additionally, the attention lays on the active species in the catalysis, the mechanism and the ligand framework, developed for the reactions.

The reduction of $CO_2$ with earth abundant metals is restricted to two electron reductions and the formation of the radical anion $CO_2^-$. Oxalates are obtained by dimerization of the radical anion of $CO_2$ and have been observed in the direct reduction of $CO_2$ close to the standard potential in aprotic solvent as well as in catalysed reactions.[5-7]

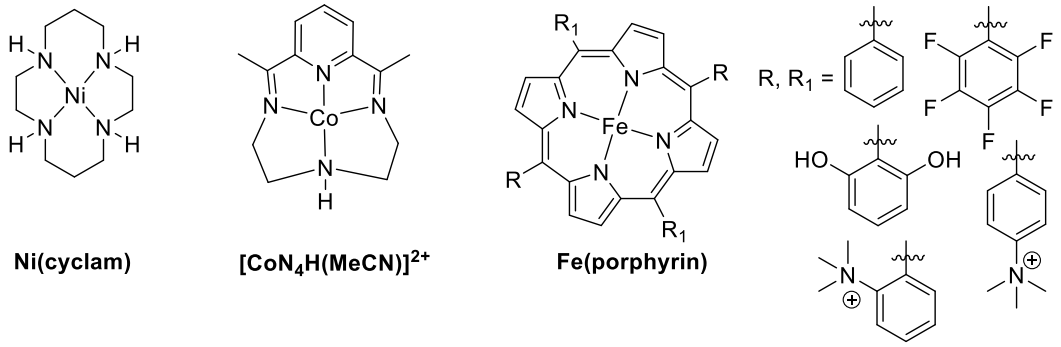


**Scheme 2.** Selected $CO_2$ reduction catalysts for the formation of CO.

The reduction of $CO_2$ to CO by nickel complexes has been performed *e.g.* with a Ni(cyclam) complex (Scheme 2). Eisenberg and Sauvage *et al.* discovered the high efficiency and selectivity of the cyclam complex. [8-9] The active species is supposed to be $Ni^{I}$, which binds $CO_2$ and forms a $Ni^{II}$-OCHO intermediate before releasing CO and $H_2O$. The catalysis is kinetically controlled as the $Ni^{I}$ species forms a stable $Ni^{I}$-CO adduct. The removal of CO and with it the formation of a $Ni^{II}$ species is the rate limiting step of the reaction. The addition of a tetramethylcyclam scavenger, to bind CO, increases the catalytic current in the electrochemical experiment by a factor of 10.[10]

Another tetraazamacrocycle was used for a cobalt containing catalyst. The catalyst $[Co^{II}N_4H(MeCN)]^{2+}$ (Scheme 2) was used already in the 1980s for $CO_2$ reduction experiments. Under the applied conditions the formation of CO was selective.[11] The active species was identified as $Co^{I}$ ligand radical. The two-electron reduced compound stores one electron in the ligand scaffold. Further investigations were carried out by Peters *et al.* who tested the faradaic efficiency upon adding water but herein lost the selectivity toward CO and produced hydrogen in the catalytic reaction.[12]

Fe(porphyrin) compounds (Scheme 2) belong to the more efficient earth abundant catalysts for $CO_2$ reduction. A $Fe^{0}$ species is obtained through a two electron reduction, which reacts with $CO_2$ to a $Fe^{I}$- $CO_2^{\cdot-}$ intermediate. CO is cleaved by the addition of two equivalents of acid. The first equivalent stabilises the intermediate, before the second equivalent cleaves the CO.[13] In these examples, only weak Brønsted acids ($H_2O$, phenol…) are necessary for the catalytic reaction. The substituents of the porphyrin have an influence on the rate constants, as acid functionalities increase the rate of the catalysis. Through these functionalities a slightly different mechanism is stated as the acid functionalities stabilise the intermediate.[14] The selectivity was enhanced by introducing trimethylanilinium groups. With the trimethylanilinium group in *ortho* position a selective formation of CO is obtained.

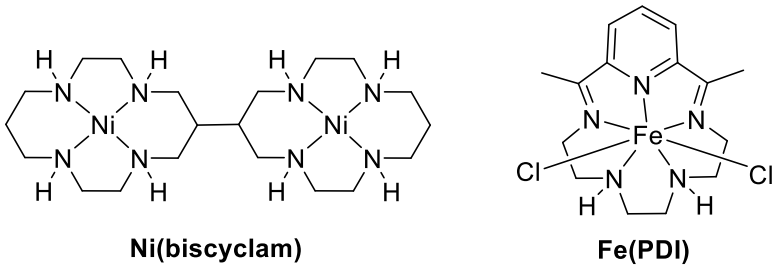


**Scheme 3.** Selected catalyst for the reduction of $CO_2$ to formic acid.

The formation of CO, in all three previous systems, is not completely selective. Beside hydrogen evolution as well the two electron reduction to formic acid or the formiate anion is possible. In DMF, the Ni(cyclam) (Scheme 2) and the Ni(biscyclam) (Scheme 3) have a higher selectivity toward formic acid compared to the catalytic reaction in MeCN/$H_2O$.[15] A similar example is the seven coordinate Fe(PDI) complex (Scheme 3), which has a high selectivity for formic acid.[16] For all mentioned catalysts, the mechanisms for the formation of the product were postulated without a hydride intermediate. The active species, which coordinates the $CO_2$, is $Fe^{I}$. Upon further reduction and the addition of a proton, an equilibrium between a $Fe^{II}$-OCHO and a $Fe^{II}$-$CO_2H$ species is formed. CO and $H_2O$ are not favoured under the reaction conditions, but with the addition of a second equivalent of proton formic acid is released (Scheme 4).

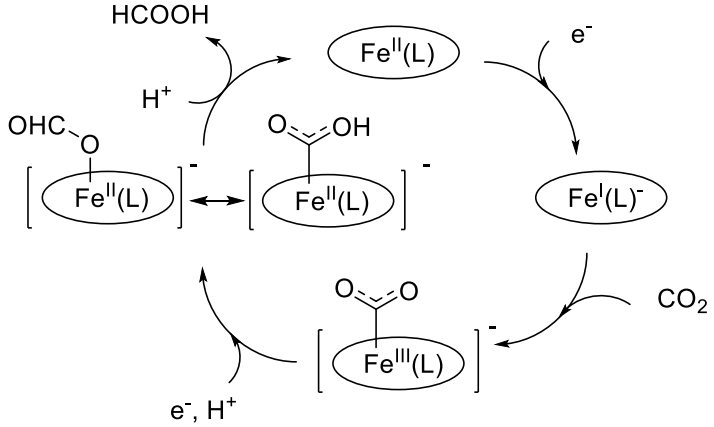


**Scheme 4.** Mechanism for HCOOH release with Fe(PDI) as catalyst.

In Table 1, the potential, at which the catalytic experiment was performed, and solvent of the electrolysis for the select catalyst are noted. The cyclam compounds show a dependence of the product distribution with the solvents.

**Table 1.** Select catalyst for $CO_2$ reduction, potential and product distribution.

| catalyst | | potential *vs.* SCE (V) | products | solvent |
|---|---|---|---|---|
| Ni(cyclam) | | -1.4 | $HCOO^-$ (75%) CO (24%) | DMF |
| | | -1.45 | CO (90%) | $H_2O$/MeCN |
| Ni(biscyclam) | | -1.4 | $HCOO^-$ (68%) CO (16%) | DMF |
| $[Co^{II}N_4H(MeCN)]^{2+}$ | | -1.54 | CO (20-30%) | MeCN |
| Fe(porphyrin) | R = phenyl | -1.7 | CO (94%) | DMF |
| | R = *o*-trimethylaniline | -1.2 | CO (100%) | DMF |
| Fe(PDI) | | -1.25 | $HCOO^-$ (75%) | DMF |

The catalysts show already relatively efficient $CO_2$ reduction with earth abundant metals. But so far, no catalyst is able to reduce carbon dioxide beyond the two electron reduction to CO or formic acid. One of the by-products in many catalytic experiments for $CO_2$ reduction is hydrogen. In the reduction of $CO_2$, the formation of hydrogen is undesirable but the reduction of protons itself is an important reaction for the production of non-carbon based energy resources. In the following chapter, the conditions for proton activation and hydrogen evolution will be discussed.

### 1.1.2 Proton reduction

Elemental hydrogen is a desirable product and can replace fossil fuels. Although hydrogen is a very abundant atom, almost all hydrogen is bound in hydrocarbons or water and cannot be easily accessed. Nowadays, hydrogen is obtained by the steam reforming process in the industry.[17] The evolution of hydrogen by water splitting or reduction of protons is aspired as it is carbon neutral.

Hydrogen can be obtained by water oxidation, which can be summarised in two reaction steps (Scheme 5). In the first part, oxygen evolution is induced by the oxidation of water and

protons are formed; in the second step the reduction of protons to molecular hydrogen completes the reaction.

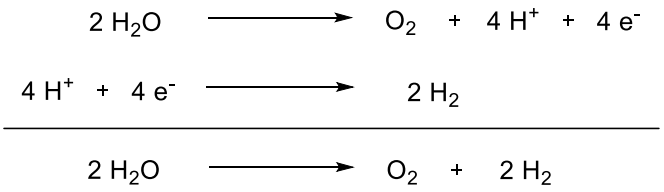

**Scheme 5.** Water oxidation.

The mechanisms of hydrogen evolution with metal catalysts are postulated with two competing pathways in the literature, homolytic and heterolytic, which can operate uniquely and simultaneously (Scheme 6). In the homolytic pathway a metal-hydride reacts with another metal-hydride to release hydrogen. With the addition of one electron, the obtained metal species is reduced after the hydrogen release, and can react with a proton to form a hydride again. In the heterolytic pathway, the metal hydride is reduced and hydrogen is released by reacting with a proton. The formation of the metal-hydride is achieved by addition of one proton and one electron to close the catalytic cycle. A bimetallic compound can favour one pathway and enhance the rate of the catalysis.[18]

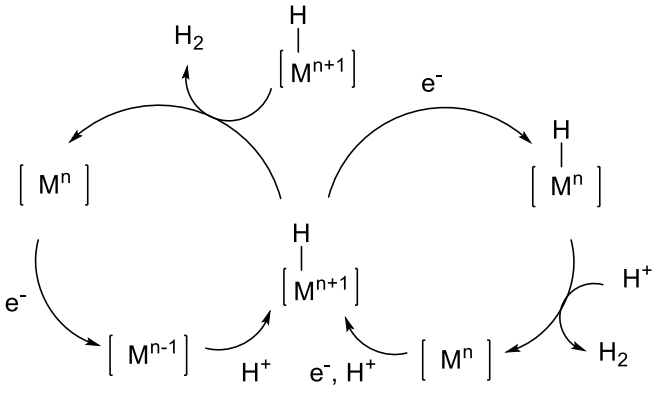

**Scheme 6.** Homolytic and heterolytic pathways for hydrogen evolution.

In this work, the focus will lay on, as above for $CO_2$ reduction, catalysts complexing earth abundant metals. The evolution of hydrogen is often observed as a side reaction to $CO_2$ reduction. Therefore, very similar ligand platforms for hydrogen evolving catalysts will be

described. As the reduction of protons is part of the water oxidation reaction, the majority of described catalysis reactions are carried out in water-solvent mixtures.[18]

In the variety of existing catalysts there are several biomimicking complexes. Hydrogenases have either a Fe-Fe or a Fe-Ni active centre. Except the complexes mimicking nitrogenase,[19] there are only a handful of nickel catalysts for hydrogen evolution. The biomimics will not be discussed in this section.

Ni(cyclam) and Ni(biscyclam) (Scheme 2 and 3) have shown reactivity for $CO_2$ reduction as shown in 1.1.1. Hydrogen is observed as a by-product, when the experiments are carried out in a MeCN/$H_2O$ solvent mixture. Catalytic tests without $CO_2$ at higher potentials (-1.26 V vs. SCE; $CO_2$: 1.45 V vs. SCE) showed that both compounds are effective just for hydrogen evolution. The complex with two nickel ions has a higher efficiency probably due to the formation of two nickel hydrides. If cooperation between the nickel ions takes place, was not resolved.

Hydrogen evolution *via* a ligand-centred radical Ni(PDI)$Br_2$ species was discovered by Crabtree, Brudvig and Batista. Mechanistic evaluation by DFT calculations showed that proton coupled electron transfer is the favoured pathway over the thermodynamically unfavoured sequential protonation and reduction. The formation of the hydride v*ia* proton coupled electron transfer includes the reduction of a $Ni^{II}$ ligand radical to form a $Ni^{II}$ hydride with the added proton (Scheme 7).[20-21]

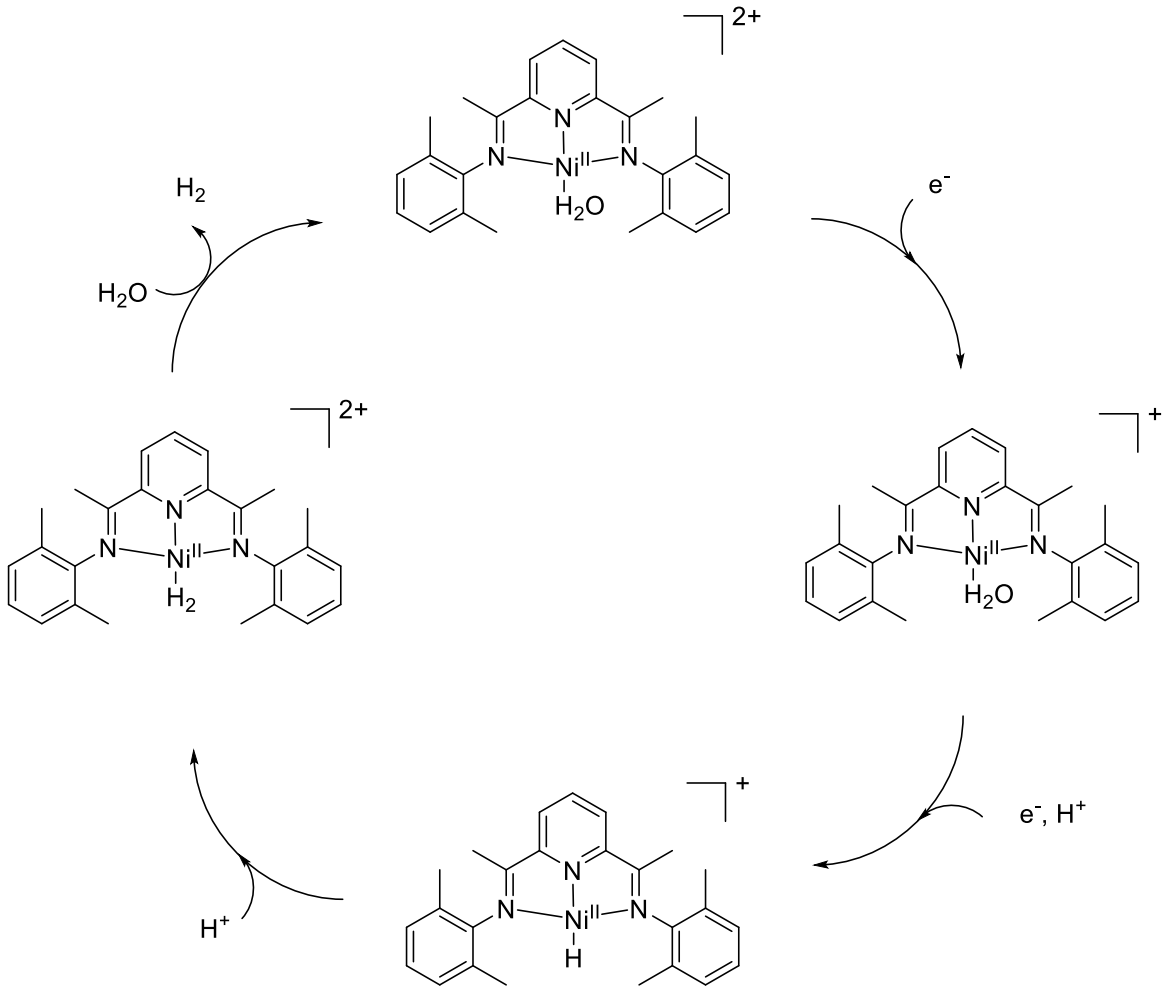


**Scheme 7.** Hydrogen evolution pathway with the catalyst Ni(PDI).

DuBois and co-workers developed the diphosphine catalysts $[Ni(P^{Ph}_2N^{Ph}_2)_2]$ and $[Ni(P^{Ph}_2N^{Ph})_2]$ (Scheme 8).[22-23] The presence of proton relays, amine group, in the second coordination sphere favours the heterolytic mechanism between a proton of the amine and a Ni-H hydride. $[Ni(P^{Ph}_2N^{Ph})_2]$ is an evolution of $[Ni(P^{Ph}_2N^{Ph}_2)_2]$ as mechanistic studies showed that only a part of the intermediates of $[Ni(P^{Ph}_2N^{Ph}_2)_2]$ evolve hydrogen.[22, 24] The formation of bridging protons between amines on one or both sides inhibits the formation of hydrogen. The ligand of $[Ni(P^{Ph}_2N^{Ph})_2]$ possesses only one amine on each side and therefore cannot form inactive intermediates.[22] Both catalyst exhibit high turnover frequencies (up to 1850 and 100000 $s^{-1}$) and can be tuned by substituents on the phenyl groups.[22-23] The active species, before forming the hydride, is a $Ni^0$ compound.

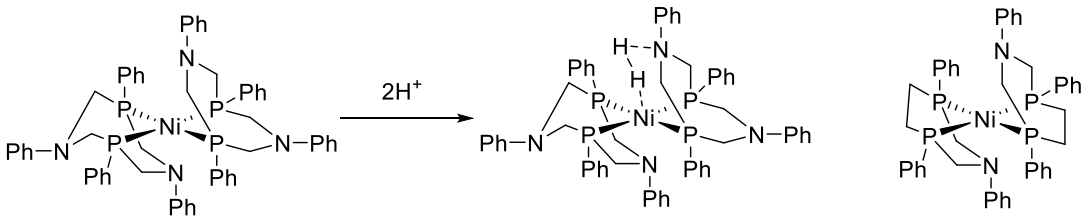


**Scheme 8.** DuBois' diphosphine catalysts for hydrogen production.

Cobalt containing catalysts are probably the most common first row transition metal complexes for hydrogen evolution reactions and several of them are active in aqueous media. Peters' $[Co^{II}N_4H(MeCN)]^{2+}$ (Scheme 2) is an effective $CO_2$ reduction catalyst (-1.54 V vs SCE). The hydrogen evolution catalytic reaction is carried out at a lower potential (-0.94 V vs. SCE) and gives a high faradaic yield (94%). The active species for the hydrogen evolution in the cyclic voltammogram experiments is identified as $Co^{I}$.[25]

A series of cobalt glyoxime complexes (Co(dmgX); Scheme 9) has been established as hydrogen evolution catalysts. At a low overpotential (-0.94 vs SCE and 1.45 vs SCE), the catalysts evolve hydrogen in a high faradaic yield. The instability toward acid is a disadvantage of the cobalt complexes. In theoretical studies, $Co^{II}$-H and $Co^{III}$-H have been identified as possible intermediates in the catalytic reaction.[26-31]

The dithiolene complex (Scheme 9) evolves hydrogen at a potential of -1.0 V (vs. SCE). The active species is a formal $Co^{II}$ ligand radical, where the dianion of the complexes is formed by a two electron reduction of the ligand. The mechanism is not elucidated but a protonation of the ligand is feasible.[32]

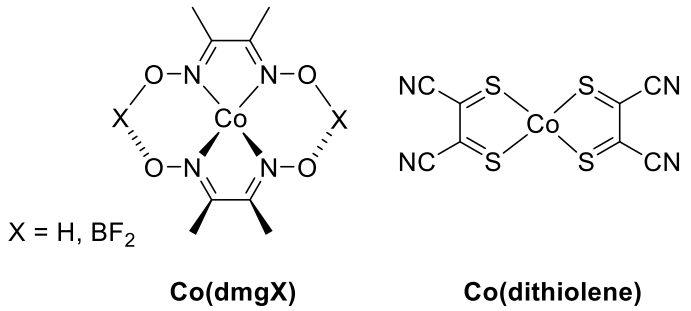


**Scheme 9.** Cobalt containing catalyst for hydrogen evolution reactions.

The photochemical activation of hydrogen evolving catalysts plays an important role in the reduction of protons but would exceed the content of the overview. [33-34]

Overall, the conclusion of this section is that the formation of low-valent complexes and active species is important for the catalytic $CO_2$ reduction and hydrogen evolution reactions. The formation of the low valent forms has to be feasible and therefore, non-innocent ligands have been chosen for some of the catalysts. The advantages of non-innocent ligand scaffolds and cooperation in bimetallic compounds for multi-electron reactions are discussed in the next section.

## 1.2 Mixed valence strategy towards reactivity

Several approaches exist for the development of catalysts capable of facilitating multi electron reactions. An inspiration for the design of the catalysts is taken from metalloenzymes. The metals at the active site and often the surrounding environment work cooperatively by storing electrons or binding protons to activate the substrates. The cooperative bimetallic reactivity might enable transformations inaccessible to single metal ions.[35] Many artificial systems have been developed to imitate the cooperative strategy and the concept of mixed valence is one feasible approach.

Mixed valence is defined by two or more metallic sites whose formal oxidation states differ. A two electron mixed valent compound can be used in a two electron oxidation-reduction reaction.[36] A typical structure of these compounds is $M^n \cdots M^{n+2}$, in which two electron oxidations may be promoted the by $M^{n+2}$ site or the $M^n$ site can promote two electron reduction. The mixed valent strategy has already proven successful in two- and four electron transformation and is therefore a useful strategy for the design of catalysts for multi-electron chemistry.

### 1.2.1 Metal based mixed valence and its reactivity

A challenge of generating metal based two-electron mixed valence compounds is the tendency of the compounds to comproportionate (Scheme 10). Aiming for two metals with different oxidation states and avoiding an intermediate oxidation state, the ligand framework plays an important role.

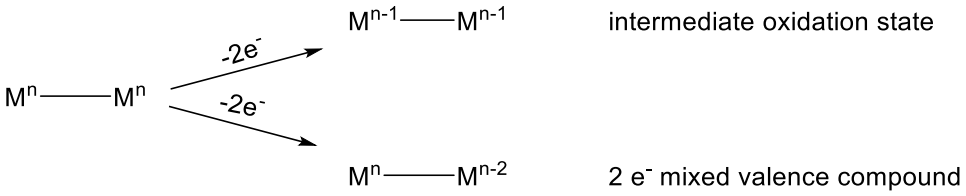


**Scheme 10.** Comproportionation and disproportionation of a 2 $e^-$-reduction.

The first documented compound with a mixed valence state was isolated in 1977 and named “Prussian blue”. The compound incorporates $Fe^{II}$ and $Fe^{III}$ ions in a cubic structure and the intervalence charge transfer between the chemically inequivalent ions causes the blue colour.[37]

Nocera *et al.* reported dirhodium and diiridium based two-electron mixed valence complexes (Figure 1).[38-39]

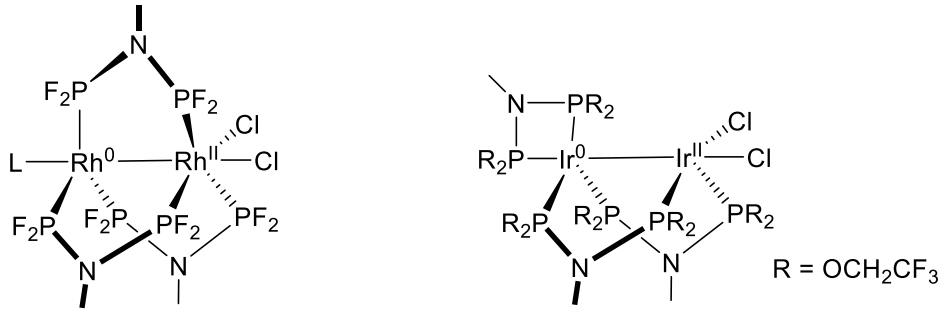


**Figure 1.** Examples of dirhodium and diiridium complexes with the ligand dfpma and tfepma.

The stabilisation of a $M^n \cdots M^{n+2}$ structure was achieved by using dfpma- (bis(difluorophosphino)methylamine) or tfepma- (bis(bis(trifluoroethoxyphosphino)) methylamine) ligands. The ligands have the special characteristic of driving the internal disproportionation of $M^{I,I}$ to $M^{II,0}$. A strong donation of the amine lone pair to the phosphine stabilises the electron deficient $M_b$. A diminishing of the phosphine – $M_b$ $\pi$-backbonding results in phosphines acting as a $\sigma$-donor to maintain the (n+2)-oxidation state. The second phosphine group is a strong π-acceptor and the charge is drawn away from the electron rich $M_a$ to stabilise the n-oxidation state (Figure 2). The stabilisation of the mixed valence state can be explained by a second-order Jahn-Teller instability of the redox-symmetric state.[40] When the bridgehead amine is replaced by a carbon atom and/or the phosphines bind a less electronegative groups, only a dirhodium(I) complex is observed. The electron donation to the phosphines is missing and inverts its binding characterisics.[41]

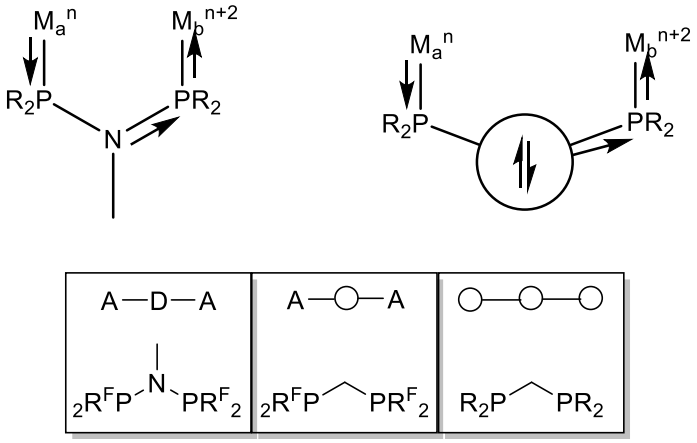


**Figure 2.** Schematic illustration of the distribution of the electron density in the diphosphazane ligand in comparison to non-donating ligands.

Nocera *et al.* reported that the dirhodium compounds are photochemically active.[38, 42] The dirhodium(II) complex $Rh_2(dfpma)_3Br_4$ undergoes a dehalogenation with a two electron reduction when irradiated at a wavelength greater than 436 nm to $Rh_2(dfpma)_3Br_2(L)$, with a $Rh^0Rh^{II}$ bimetallic centre in the presence of a halogen trap. Upon irradiation at wavelengths greater than 335 nm, a four-electron reaction to generate a $Rh^0Rh^0$ compound, $Rh_2(dfpma)_3(L)_2$, is observed (Scheme 11).[42-43]

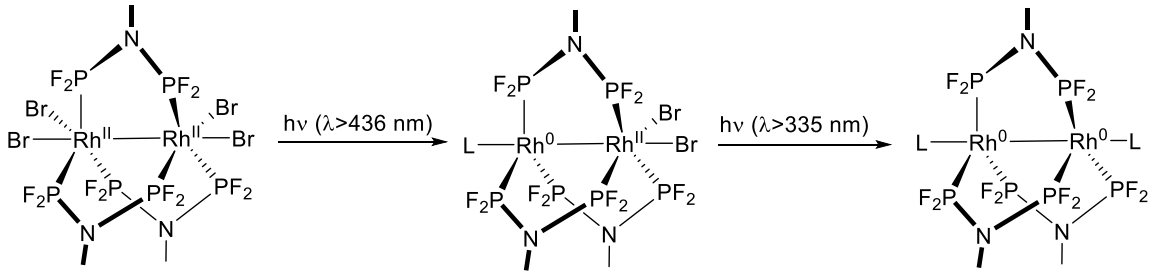


**Scheme 11.** Photochemical reactions of the dirhodium compound $Rh_2(dfpma)_3Br_4$.

In 2001, Nocera *et al.* demonstrated that the two-electron mixed valence rhodium compounds, with dfpma and tfepma as ligands, enable the photocatalytic hydrogen production from hydrohalic solutions (Scheme 13).[41, 44] The dirhodium(0) complex bearing a photolabile CO ligand is irradiated at a wavelength between 300 and 400 nm to release CO. The subsequent reaction with a solution of HX produces a $Rh^{II}Rh^{II}$ dihydride-dihalide intermediate which releases $H_2$. The product, a $Rh^{I}Rh^{I}X_2$ compound is unstable toward disproportionation and the $Rh^0Rh^{II}X_2$ core is obtained *via* the formation of a halide bridge. The catalytic cycle is closed by the photoactivation to eliminate the halogen atoms by a trap

molecule, e.g. THF, dihydroanthracene or 2,3-dimethylbutadiene, to form the dirhodium(0) complex again.

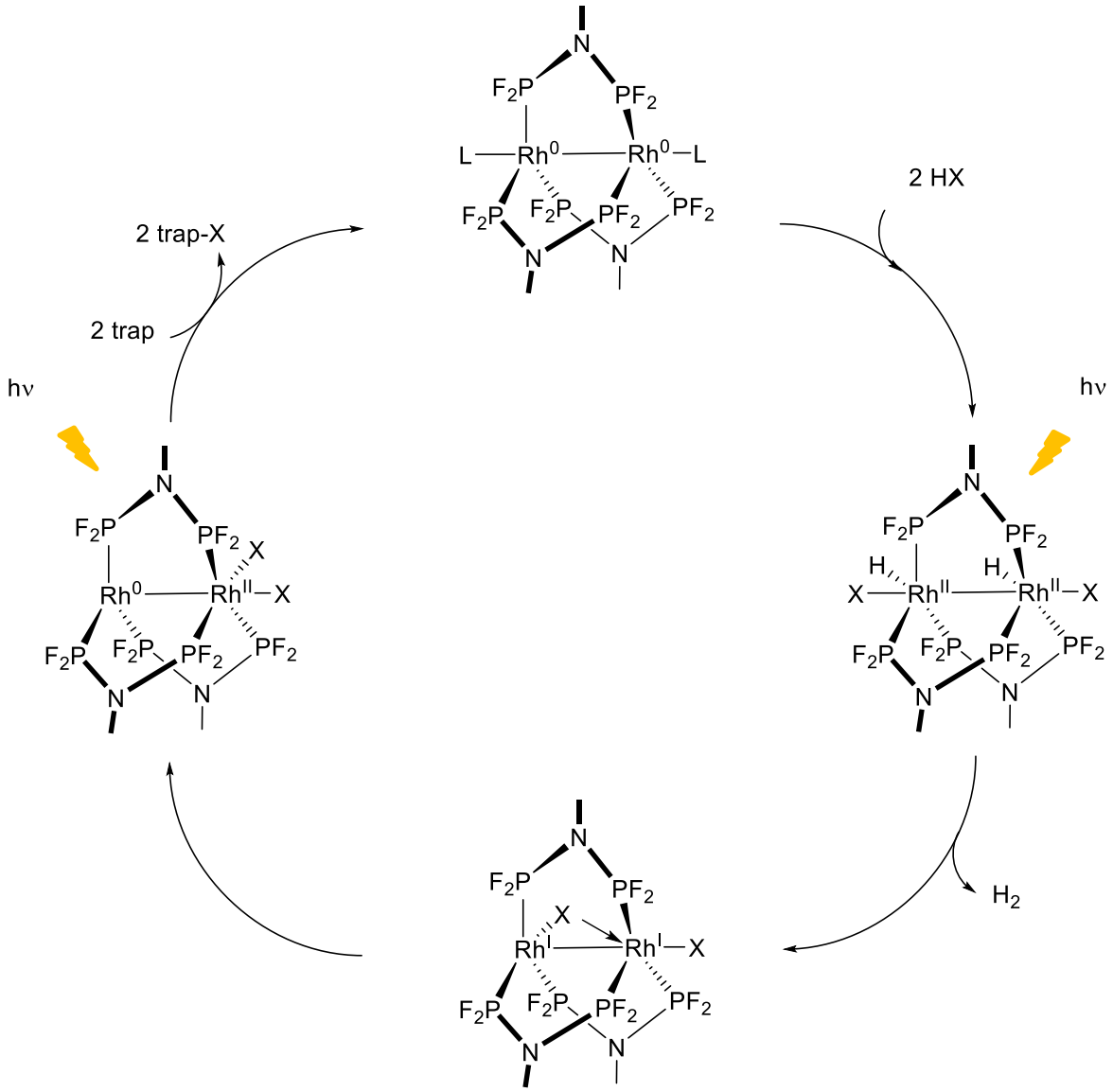


**Scheme 12.** Photocatalytic cycle of proton reduction from HX solutions by a dirhodium catalyst.

The photoelimination is the rate limiting step of the reaction. The release of $H_2$ is expected to happen from a dirhodium compound *via* a reductive elimination. The proposed mechanism is supported by results from experimental and computational studies on the diiridium compound (Scheme 13).[35, 45-46] The hydride on $M_a^{I}$ has to migrate to the $M_b^{III}$ site with a hydride bridge intermediate. The release of $H_2$ reduces the oxidation state of $M_b$ to +2.

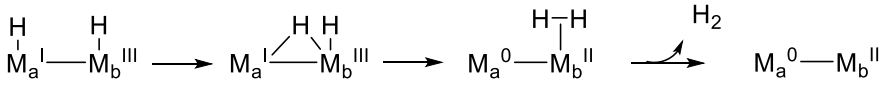

**Scheme 13.** Reductive elimination of hydrogen using a bimetallic two-electron mixed valent complex.

The diiridium compound, $Ir_2(tfepma)_3Cl_2$, is the first complex, in which a reversible $H_2$ addition across a M-M bond has been seen without breaking the M-M bond (Scheme 14).[45] The addition of $H_2$ occurs at the $Ir^{II}$ core. One of the ligands on $M_b$ has to move to an equatorial position to allow a coordination of the hydrogen molecule. The formation of the metal hydrides is the reverse reaction of the reductive elimination. A hydride bridge is formed between $M_a$ and $M_b$ and the metal centres are oxidised by one electron each.

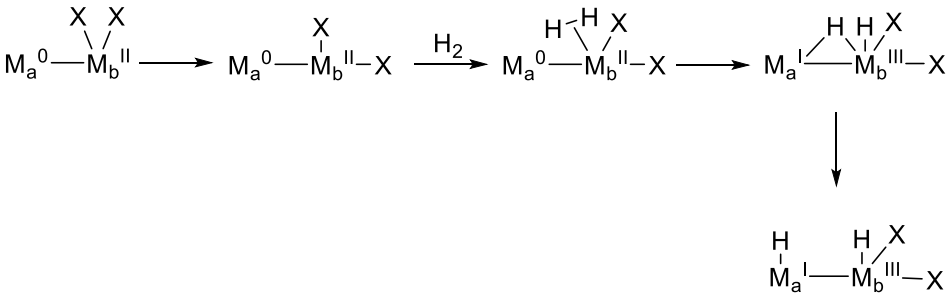

**Scheme 14.** Swing mechanism of hydrogen activation at a bimetallic core.

A mixed valence complex is not only known from reduction chemistry, but also in the oxidation chemistry with diiron compounds. Furthermore, iron is a cheap, abundant metal.

In 2000, Nocera e*t al*. published pacman porphyrins accommodating first row transition metals. The strategy of forming bimetallic complexes with pacman ligand scaffolds was not new, but the group around Nocera overcame the width limitation of the spacer between the cofacial sides by introducing xanthene and dibenzofuran bridges.[47-49] Together with substituents on the porphyrins, they were now able to tune the pocket size and the metal-metal distance (3.5 Å – 8.5 Å).[50-52] While the xanthene bridge has an equal a and b distance between the porphyrin sides (see Figure 3, left), the dibenzofurane bridge has a greater distance on the far side of the complex (b) as the distance next to the bridge molecule (a). Therefore, the angle Θ between the porphyrin planes is wider and the pocket size bigger (Figure 3, right).

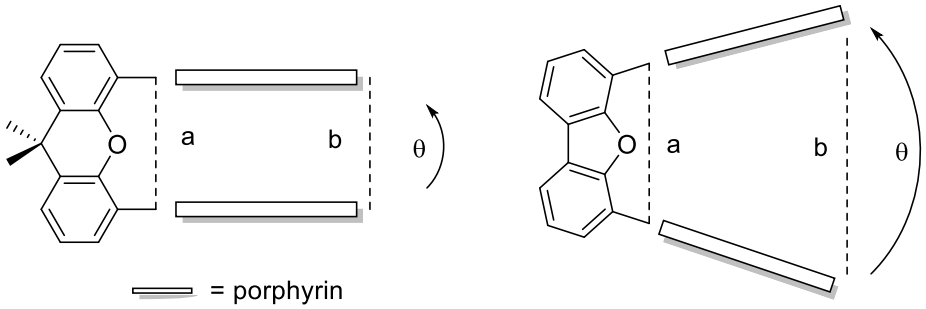


**Figure 3.** Illustration of metal-metal distances in porphyrin pacmans and the angle with different bridge spacer (a, b = distance; Θ = angle).

The reported iron porphyrins are used for oxygen atom transfer reactions induced by photocatalytic activation. With exposure to air, followed by a treatment with basic aluminia the *μ*-oxo bond was formed between the two iron-porphyrin planes. The breakage of the *μ*-oxo bond through light excitation with wavelengths, in the range of the MLCT absorptions, forms a mixed valent intermediate, Fe(II) ⋯Fe(IV)=O, which oxidises electron-rich substrates.[51, 53]

In the early 90s, a mechanism of oxygen activation by porphyrins was stated by Balch and co-workers (Scheme 15).[54-56] The reaction included the formation of a peroxo species in an iron porphyrin dimer which readily disproportionate to an ironoxo species by adding nitrogenous ligands like pyridine and piperidine. The *μ*-oxo iron porphyrin is formed with a second molecule of non-reacted Fe(II) porphyrins. Later on, Richman e*t al.* showed that a photodisproportionation of *μ*-oxo iron diporphyrin enables oxidation chemistry of alkenes.[57-60]

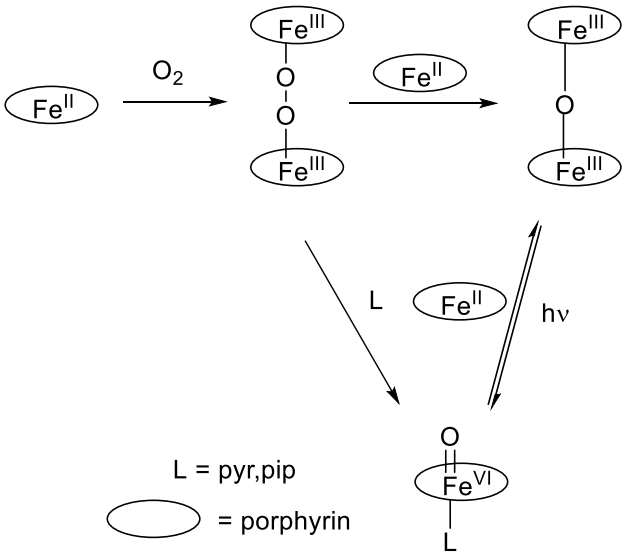


**Scheme 15.** Oxidation of iron porphyrins by the Balch mechanism and their photodisproportionation.

The generation of the oxo species in pacman complexes is modified from the Balch mechanism as shown in Scheme 16. The iron porphyrin compounds, presented by Nocera and co-workers, form the *μ*-oxo species in an intramolecular reaction. The steric hindrance and the angle between the porphyrin planes of the pacman complexes with the dibenzofuran spacer make them “spring loaded”, which increases the distance between the two iron centres. Therefore, the pacman complexes with dibenzofuran spacer are shown be more reactive as the formation of the *μ*-oxo bridge is disrupted after the photoactivation to the oxo-species.[61] The rate of the oxygen atom transfer reaction is higher compared to complexes with a xanthene bridge, which are not sterically hindered. Overall the iron porphyrin pacman complexes offer a platform for two electron mixed valent complexes to drive two electron oxidation reactions under mild photocatalytic conditions with dioxygen as atom sources.

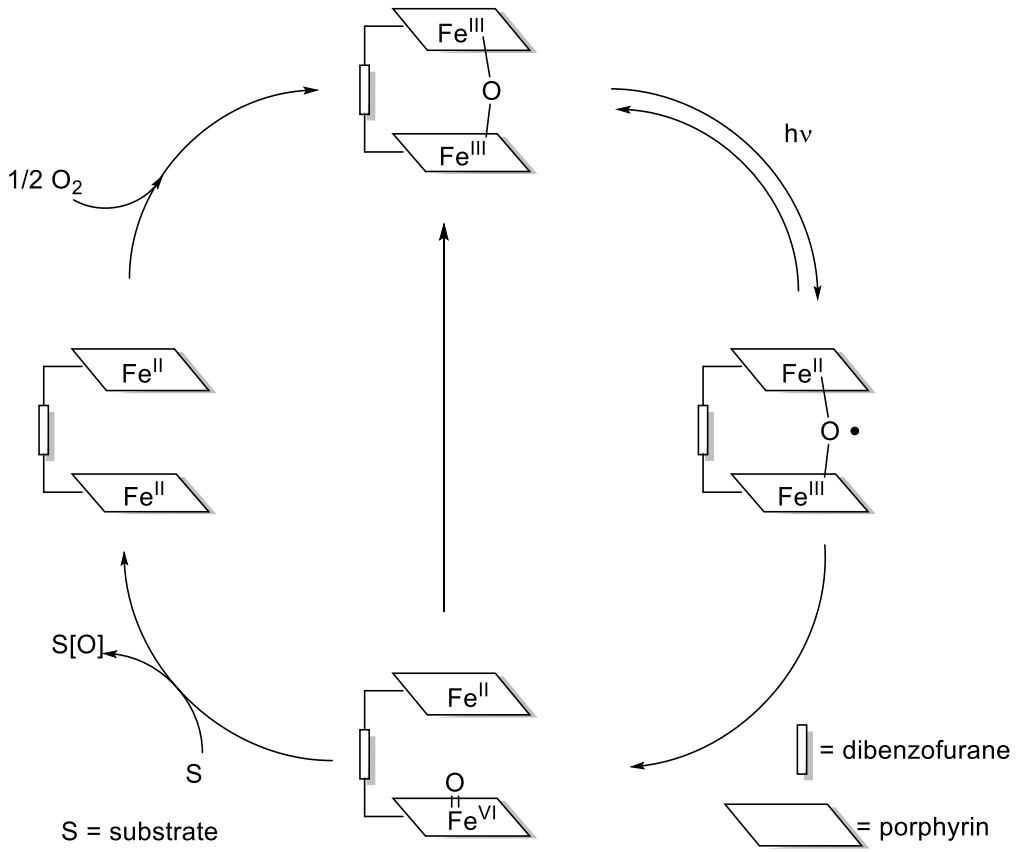


**Scheme 16.** Catalytic cycle of pacman porphyrins in oxygen activation catalysis.

### 1.2.2 Ligand based mixed valence

So far, the described systems are metal centred mixed valent compounds. Ligand based mixed valence complexes contain an uneven distribution of electrons, whereby, in contrast to the metal based complexes, electrons are located at the ligand scaffold. The electron storage at the ligand requires scaffolds which have an accessible redox series and are redox-active.

For earth-abundant metals, like iron or nickel, one electron redox changes are more frequently observed and therefore, are challenging for two electron redox changes. Forming and breaking a bond normally includes a multi-electron step and, therefore, base metal complexes often cannot perform these reactions. To mimic noble metals, the one electron redox process has to be suppressed and as a result redox non-innocent ligands are introduced.[62] The use of non-innocent ligands has opened further new pathways, e.g. the coordination of inert or otherwise unsuitable metals for transformations.[63]

Following these thoughts the properties of non-innocent ligands have to be confined toward reactivity. Bruin *et al.* defined four different possibilities for substrate interaction and the role of the ligand:[64]

1. Increased Lewis acidity on the metal by redox-active ligand
2. Stabilising low energy metal oxidation state (releasing/storing electrons by the ligand)
3. Ligand involved in substrate bond forming/breaking
4. Induced radical-type reactivity on the substrate-ligand

Perhaps the most common application of redox non-innocent ligands in catalysis is their ability to function as electron-reservoirs. Additional electrons can be temporarily stored on (or released from) a redox active ligand, the complex can mediate multi-electron transformations without forcing the metal to adopt an uncommon oxidation state. For two electron reaction, the ligand must donate two electrons (via the metal), and hence the ligand gets oxidised in this process.[64]

The following selected examples show the versatile behaviour of non-innocent ligands.

The interest in porphyrinogens was established in the early 90s, when Rizzoli *et al.* showed, that when two non-hydrogen substituents are binding between the pyrroles, a six-electron oxidation to porphyrin is no longer possible. The modification of the porphyrinogen ended in the formation of one or two spirocyclopropane rings under controlled oxidation with two or four electrons (Scheme 17). The cyclopropane rings are formed by C-C coupling between the *α* – carbons of the neighbouring pyrroles. With the formation of the cyclopropane electrons can be stored in the ligand scaffold.[65-67]

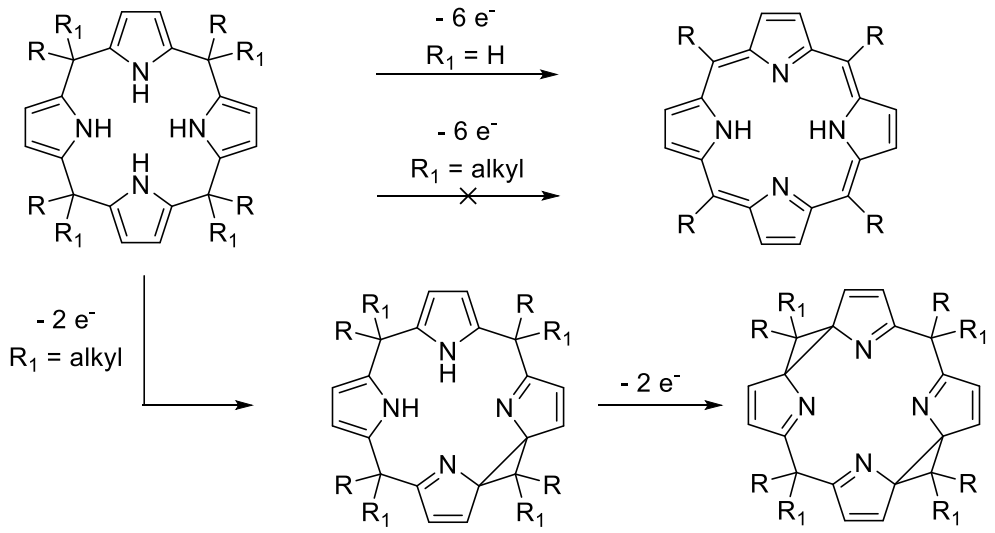


**Scheme 17. Reduction of porphyrinogen to porphyrin and formation of spirocyclopropane rings.**

The porphyrinogen was complexed with metals, but the actual redox activity, which was expected from ligand, was not closely investigated until 2004, when Nocera *et al.* reacted the porphyrinogen with the redox inactive metal zinc.[36] Zinc porphyrinogens serve as frameworks for ligand based mixed valent complexes and the three oxidation states, $[LZn]^{2-}$, $[L^{\Delta}Zn]$ and $[L^{\Delta\Delta}Zn]^{2+}$, have been isolated and spectroscopically as well as structurally characterised (Scheme 18). The occupied orbitals of the oxidised pyrroles in $[L^{\Delta}Zn]$ are energetically lower than the ones of the other pyrroles. The distribution of the orbitals results in a division of the dipyrroles and therefore $[L^{\Delta}Zn]$ is a true two electron mixed valence compound.

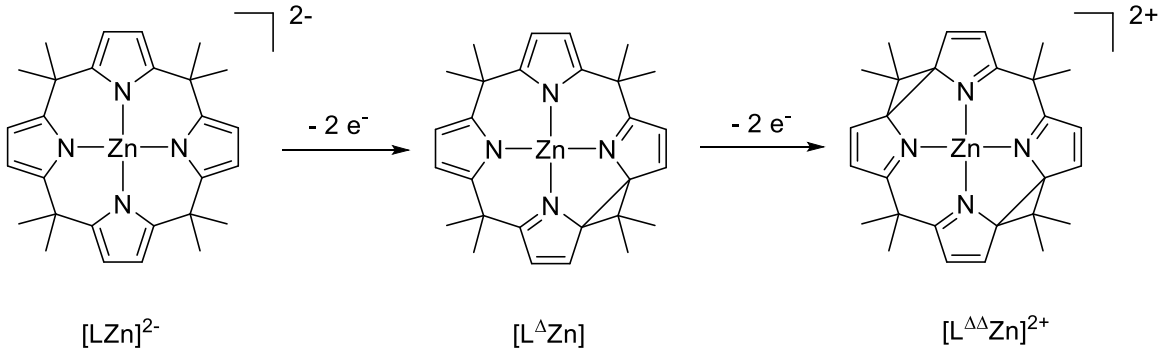


**Scheme 18.Redox series of a ligand based mixed valence Zn-porphyrinogen.**

For the following non-innocent ligands, diimine and pyridine diimine, more details are shown as they are important for this work.

Pyridine diimines (PDI), also bis(imino)pyridines or diiminepyridines, are easily accessible through a condensation reaction of 2,6-diacetylpyrdidine with amines. The majority of the complexes are symmetric with alkyl or aryl substituents but there are several non-symmetric compounds.[68-70]

Toma *et al.* claimed as the first research group that upon reduction of an iron(PDI) compound, ligand radicals are formed.[71] Wieghardt *et al*. intensified the studies on first row transition metals complexed by a PDI to show that a row of redox series for each metal can be created.[72-73] The group around Wieghardt investigated PDI-dimer complexes and tried to isolate the tri-, di- , monocationic and neutral species, not exceeding one electron reduction per ligand.

PDI-ligands have an extended π-system, due to the conjugation of the two imine moieties with the pyridine ring. They have two low-lying π*-orbitals, which are a combination of the two imine π*-orbitals with pyridine proportion. The reduction of the ligand and, with this, a donation of an electron into one of the π*-orbitals, results in elongation of the imine bonds combined with a shortening of the $C_{imine}$-$C_{orthopyr}$-bond.[72]

Diimines can take up to two electrons, PDIs can be reduced by up to four electrons.[74-75] Not only could the aforementioned cationic species be isolated, but also the mono-, di- and trianionic derivatives (Figure 4).

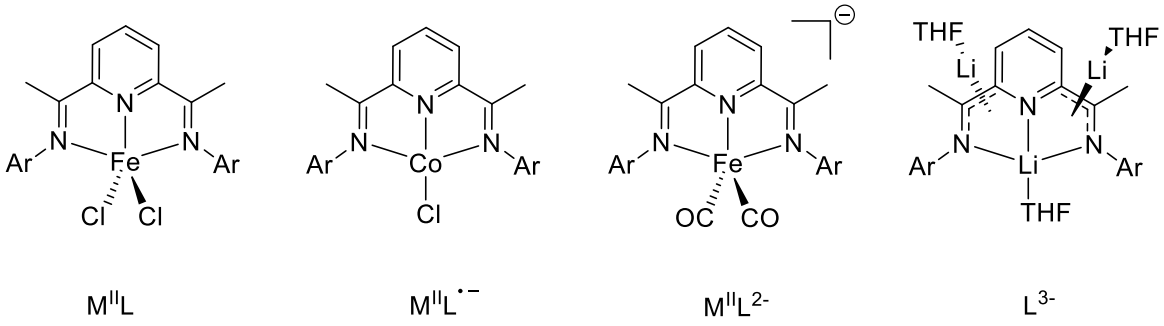


$M^{II}L$ $M^{II}L^{\bullet -}$ $M^{II}L^{2-}$ $L^{3-}$

**Figure 4. Complexes with PDI ligand in their neutral, mono-, di and trianionic form.**

The PDI ligand allows the metal to maintain is stable oxidation state, which does not need to adopt a high energy unstable state. The advantages of the non-innocent ligand scaffolds can be used for earth abundant metal complexes to increase their application possibilities in multi electron reaction. In this work, several metal complexes have been designed and synthesised with the concept of non-innocence.

## 1.3 Conceptual design and aims of the thesis

The aim of the thesis is the creation of metal complexes suitable for multi-electron reactions. The reduction of protons and $CO_2$ can only be managed with earth abundant metals, like iron and nickel, when electron storing on the ligand scaffold is feasible. The concept of redox-active ligands was implemented in our strategy to design ligand scaffolds. Low valent forms of the more abundant metals, like $Fe^0$, which are potentially active species in catalysis, are often unstable as the coordination site has to be adapted to support the oxidation state of the metal. A possible solution is the creation of formal low valent forms by storing electrons on the ligand for obtaining a catalytic active species.

Nocera's work on two-electron mixed valence bimetallic complexes with noble metals was successful in two-electron proton reduction. The two-electron mixed valence compounds are supposed to react in two electron steps and can supply electrons required in multi-electron reactions.

Unsymmetrical ligand scaffolds were designed to favour the formation of two-electron mixed valence species. Therefore, different coordination sites are introduced which allow metal ions in different oxidation states and enable the formation of heterobimetallic compounds.

The formation of bimetallic complexes can favour mechanisms with migration steps, seen in Nocera's work of hydrogen evolution with dirhodium and diiridium compounds. The distance between metal centres, defined by the spacers in the ligand scaffold plays an important role.

The designs of our ligands taking into account all aforementioned features are displayed in Figure 5.

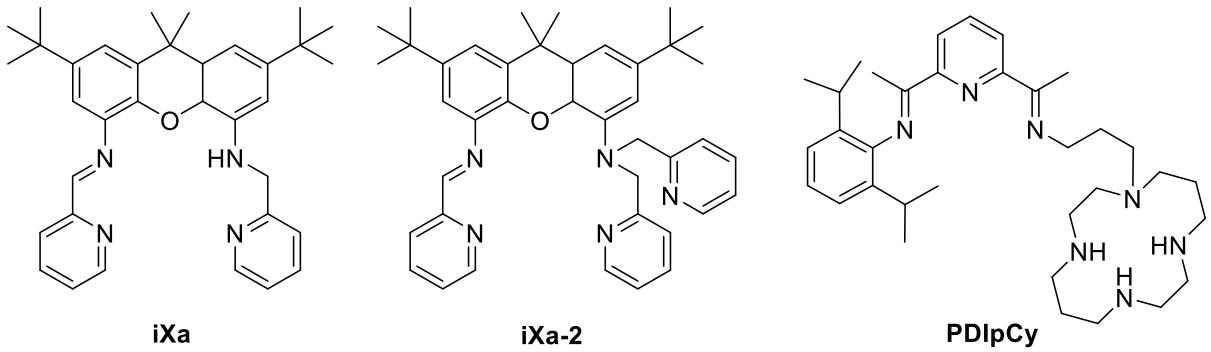


**Figure 5.** Ligand designs.

All unsymmetrical ligand scaffolds offer two coordination sites, with one of them redox-active. The coordination sites are formed by N-donors of the iminopyridine, diiminopyridine, aminopyridine and the cyclam moiety. The coordination of cheap and earth abundant first row transition metals is envisaged. Multi-electron catalysis is feasible due to the electron reservoirs on the ligand scaffolds. The distance between the metals is defined by the xanthene spacer in one design and on the other hand flexible due to the propyl group in the second design.

The complexes formed with the iXa and iXa-2 ligands are presented in Chapter 2. They were designed for reduction processes but show noticeable behaviours in magnetic property studies. The PDIpCy ligand was developed in several stages, which are shown in Chapter 3. The formation of bimetallic compounds with metal ions in distinct coordination sites was carried out with first row transition metals. The characterisation of the electronic structure of the hetero- and homobimetallic complexes was pursued.

## 1.4 References


1. Cook, T. R.; Dogutan, D. K.; Reece, S. Y.; Surendranath, Y.; Teets, T. S.; Nocera, D. G. *Chem. Rev.* **2010,** *110*, 6474-6502.
2. Schwarz, H. A.; Dodson, R. W. **1989,** *93*, 409-414.
3. Benson, E. E.; Kubiak, C. P.; Sathrum, A. J.; Smieja, J. M. *Chem. Soc. Rev.* **2009,** *38*, 89-99.
4. Hinrichsen, K.-O.; Strunk, J. *Nachrichten aus der Chemie* **2006,** *54*, 1080-1084.
5. Lamy, E.; Nadjo, L.; Saveant, J. M. *J. Electroanal. Chem. Interfacial Electrochem.* **1977,** *78*, 403-407.
6. Gennaro, A.; Isse, A. A.; Savéant, J.-M.; Severin, M.-G.; Vianello, E. *J. Am. Chem. Soc.* **1996,** *118*, 7190-7196.
7. Angamuthu, R.; Byers, P.; Lutz, M.; Spek, A. L.; Bouwman, E. *Science* **2010,** *327*, 313-315.
8. Beley, M.; Collin, J.-P.; Ruppert, R.; Sauvage, J.-P. *J. Chem.Soc, Chem. Commun.* **1984**, 1315-1316.
9. Fisher, B. J.; Eisenberg, R. *J. Am. Chem. Soc.* **1980,** *102*, 7361-7363.
10. Froehlich, J. D.; Kubiak, C. P. *J. Am. Chem. Soc.* **2015,** *137*, 3565-3573.
11. Che, C.-M.; Mak, S.-T.; Lee, W.-O.; Fung, K.-W.; Mak, T. C. W. *J. Chem. Soc., Dalton Trans.* **1988**, 2153-2159.
12. Zhang, M.; El-Roz, M.; Frei, H.; Mendoza-Cortes, J. L.; Head-Gordon, M.; Lacy, D. C.; Peters, J. C. *J. Physi. Chem. C* **2015,** *119*, 4645-4654.
13. Costentin, C.; Robert, M.; Saveant, J.-M. *Chem. Soc. Rev.* **2013,** *42*, 2423-2436.
14. Costentin, C.; Robert, M.; Savéant, J.-M. *Acc. Chem. Res.* **2015,** *48*, 2996-3006.
15. Collin, J.-P.; Abdelaziz, J.; Sauvage, J.-P. *Inorg. Chem.* **1988,** *27*, 1986-1988.
16. Chen, L.; Guo, Z.; Wei, X.-G.; Gallenkamp, C.; Bonin, J.; Anxolabéhère-Mallart, E.; Lau, K.-C.; Lau, T.-C.; Robert, M. *J. Am. Chem. Soc.* **2015,** *137*, 10918-10921.
17. Ogden, J. M. *Ann. Rev. of Energy Environ.* **1999,** *24*, 227-279.
18. Thoi, V. S.; Sun, Y.; Long, J. R.; Chang, C. J. *Chem. Soc. Rev.* **2013,** *42*, 2388-2400.
19. Canaguier, S.; Artero, V.; Fontecave, M. *Dalton Trans.* **2008**, 315-325.
20. Luca, O. R.; Konezny, S. J.; Blakemore, J. D.; Colosi, D. M.; Saha, S.; Brudvig, G. W.; Batista, V. S.; Crabtree, R. H. *New J. Chem.* **2012,** *36*, 1149-1152.
21. Luca, O. R.; Konezny, S. J.; Paulson, E. K.; Habib, F.; Luthy, K. M.; Murugesu, M.; Crabtree, R. H.; Batista, V. S. *Dalton Trans.* **2013,** *42*, 8802-7.
22. Helm, M. L.; Stewart, M. P.; Bullock, R. M.; DuBois, M. R.; DuBois, D. L. *Science* **2011,** *333*, 863-866.
23. Kilgore, U. J.; Roberts, J. A. S.; Pool, D. H.; Appel, A. M.; Stewart, M. P.; DuBois, M. R.; Dougherty, W. G.; Kassel, W. S.; Bullock, R. M.; DuBois, D. L. *J. Am. Chem. Soc.* **2011,** *133*, 5861-5872.
24. Dupuis, M.; Chen, S.; Raugei, S.; DuBois, D. L.; Bullock, R. M. *J. Phys. Chem.* **2011,** *115*, 4861-4865.
25. McCrory, C. C. L.; Uyeda, C.; Peters, J. C. *J. Am. Chem. Soc.* **2012,** *134*, 3164-3170.
26. McCrory, C. C. L.; Szymczak, N. K.; Peters, J. C. *Electrocat.* **2015,** *7*, 87-96.
27. Wang, M.; Chen, L.; Sun, L. *Energy Environ. Sci.* **2012,** *5*, 6763-6778.
28. Baffert, C.; Artero, V.; Fontecave, M. *Inorg. Chem.* **2007,** *46*, 1817-1824.
29. Jacques, P.-A.; Artero, V.; Pécaut, J.; Fontecave, M. *Proc. Nat. Ac. Sci.* **2009,** *106*, 20627-20632.
30. Razavet, M.; Artero, V.; Fontecave, M. *Inorg. Chem.* **2005,** *44*, 4786-4795.
31. Hu, X.; Cossairt, B. M.; Brunschwig, B. S.; Lewis, N. S.; Peters, J. C. *Chem. Commun.* **2005**, 4723-4725.
32. McNamara, W. R.; Han, Z.; Alperin, P. J.; Brennessel, W. W.; Holland, P. L.; Eisenberg, R. *J. Am. Chem. Soc.* **2011,** *133*, 15368-15371.
33. Eckenhoff, W. T.; Eisenberg, R. *Dalton Trans.* **2012,** *41*, 13004-13021.
34. Berardi, S.; Drouet, S.; Francas, L.; Gimbert-Surinach, C.; Guttentag, M.; Richmond, C.; Stoll, T.; Llobet, A. *Chem. Soc. Rev.* **2014,** *43*, 7501-7519.

35. Gray, T. G.; Veige, A. S.; Nocera, D. G. *J. Am. Chem. Soc.* **2004,** *126*, 9760-9768.
36. Bachmann, J.; Nocera, D. G. *J. Am. Chem. Soc.* **2004,** *126*, 2829-2837.
37. Buser, H. J.; Schwarzenbach, D.; Petter, W.; Ludi, A. *Inorg. Chem.* **1977,** *16*, 2704-2710.
38. Dulebohn, J. I.; Ward, D. L.; Nocera, D. G. *J. Am. Chem. Soc.* **1988,** *110*, 4054-4056.
39. F. Heyduk, A.; G. Nocera, D. *Chem. Commun.* **1999**, 1519-1520.
40. Gray, T. G.; Nocera, D. G. *Chem. Commun.* **2005**, 1540-1542.
41. Esswein, A. J.; Veige, A. S.; Nocera, D. G. *J. Am. Chem. Soc.* **2005,** *127*, 16641-16651.
42. Heyduk, A. F.; Macintosh, A. M.; Nocera, D. G. *J. Am. Chem. Soc.* **1999,** *121*, 5023-5032.
43. Odom, A. L.; Heyduk, A. F.; Nocera, D. G. *Inorg. Chim. Acta* **2000,** *297*, 330-337.
44. Heyduk, A. F.; Nocera, D. G. *Science* **2001,** *293*, 1639-1641.
45. Heyduk, A. F.; Nocera, D. G. *J. Am. Chem. Soc.* **2000,** *122*, 9415-9426.
46. Veige, A. S.; Gray, T. G.; Nocera, D. G. *Inorg. Chem.* **2005,** *44*, 17-26.
47. Deng, Y.; Chang, C. J.; Nocera, D. G. *J. Am. Chem. Soc.* **2000,** *122*, 410-411.
48. Chang, C. J.; Deng, Y.; Heyduk, A. F.; Chang, C. K.; Nocera, D. G. *Inorg. Chem.* **2000,** *39*, 959-966.
49. Chang, C. J.; Deng, Y.; Shi, C.; Chang, C. K.; Anson, F. C.; Nocera, D. G. *Chem. Commun.* **2000**, 1355-1356.
50. Chng, L. L.; Chang, C. J.; Nocera, D. G. *J. Org. Chem.* **2003,** *68*, 4075-4078.
51. Chang, C. J.; Baker, E. A.; Pistorio, B. J.; Deng, Y.; Loh, Z.-H.; Miller, S. E.; Carpenter, S. D.; Nocera, D. G. *Inorg. Chem.* **2002,** *41*, 3102-3109.
52. Chang, C. J.; Yeh, C.-Y.; Nocera, D. G. *J. Org. Chem.* **2002,** *67*, 1403-1406.
53. Pistorio, B. J.; Chang, C. J.; Nocera, D. G. *J. Am. Chem. Soc.* **2002,** *124*, 7884-7885.
54. Holm, R. H. *Chem. Rev.* **1987,** *87*, 1401-1449.
55. Chin, D.-H.; Del Gaudio, J.; La Mar, G. N.; Balch, A. L. *J. Am. Chem. Soc.* **1977,** *99*, 5486-5488.
56. Chin, D.-H.; La Mar, G. N.; Balch, A. L. *J. Am. Chem. Soc.* **1980,** *102*, 4344-4350.
57. Peterson, M. W.; Richman, R. M. *Inorg. Chem.* **1985,** *24*, 722-725.
58. Peterson, M. W.; Rivers, D. S.; Richman, R. M. *J. Am. Chem. Soc.* **1985,** *107*, 2907-2915.
59. Weber, L.; Haufe, G.; Rehorek, D.; Hennig, H. *Chem. Commun.* **1991**, 502-503.
60. Weber, L.; Hommel, R.; Behling, J.; Haufe, G.; Hennig, H. *J. Am. Chem. Soc.* **1994,** *116*, 2400-2408.
61. Hodgkiss, J. M.; Chang, C. J.; Pistorio, B. J.; Nocera, D. G. *Inorg. Chem.* **2003,** *42*, 8270-8277.
62. Chirik, P. J. *Inorg. Chem.* **2011,** *50*, 9737-9740.
63. Kaim, W. *Eur. J. Inorg. Chem* **2012,** *2012*, 343-348.
64. Lyaskovskyy, V.; de Bruin, B. *ACS Catal.* **2012,** *2*, 270-279.
65. De Angelis, S.; Solari, E.; Floriani, C.; Chiesi-Villa, A.; Rizzoli, C. *J. Am. Chem. Soc.* **1994,** *116*, 5691-5701.
66. De Angelis, S.; Solari, E.; Floriani, C.; Chiesi-Villa, A.; Rizzoli, C. *J. Am. Chem. Soc.* **1994,** *116*, 5702-5713.
67. Crescenzi, R.; Solari, E.; Floriani, C.; Chiesi-Villa, A.; Rizzoli, C. *J. Am. Chem. Soc.* **1999,** *121*, 1695-1706.
68. Small, B. L. *Acc. Chem. Res.* **2015,** *48*, 2599-2611.
69. Delgado, M.; Sommer, S. K.; Swanson, S. P.; Berger, R. F.; Seda, T.; Zakharov, L. N.; Gilbertson, J. D. *Inorg. Chem.* **2015,** *54*, 7239-7248.
70. Delgado, M.; Ziegler, J. M.; Seda, T.; Zakharov, L. N.; Gilbertson, J. D. *Inorg. Chem.* **2016,** *55*, 555-557.
71. Kuwabara, I. H.; Comninos, F. C. M.; Pardini, V. L.; Viertler, H.; Toma, H. E. *Electrochim. Acta* **1994,** *39*, 2401-2406.
72. Budzelaar, P. H. M.; de Bruin, B.; Gal, A. W.; Wieghardt, K.; van Lenthe, J. H. *Inorg. Chem.* **2001,** *40*, 4649-4655.
73. de Bruin, B.; Bill, E.; Bothe, E.; Weyhermüller, T.; Wieghardt, K. *Inorg. Chem.* **2000,** *39*, 2936-2947.

74. Enright, D.; Gambarotta, S.; Yap, G. P. A.; Budzelaar, P. H. M. *Angew. Chem. Int. Ed.* **2002,** *41*, 3873-3876.
75. Reardon, D.; Conan, F.; Gambarotta, S.; Yap, G.; Wang, Q. *J. Am. Chem. Soc.* **1999,** *121*, 9318-9325.

# 2 Synthesis of iXa- and iXa-2-metal complexes and their characterisation

## 2.1 Introduction

The idea behind the design of **iXa** and **iXa-2** is the generation of non-innocent unsymmetrical compounds (Figure 6). Xanthene complexes with iminopyridine functionalities can be found in the literature and accommodate two metal ions.[76-78] The **iXa**- and **iXa-2**-ligand scaffolds present two coordination site possibilities in an unsymmetrical ligand, one formed by an *α*-iminopyridine and the second by either a (2-pyridylmethyl)amino group or a bis(2-pyridylmethyl)amino group. In contrast to the compounds in the literature and the aspired two metal ions in the coordination sites, the coordination of only one iron or zinc metal ion is observed for the ligands **iXa** and **iXa-2**. Nevertheless, especially the seven-coordinate compound of iron, with **iXa,** promises a variety of reactivity and properties.

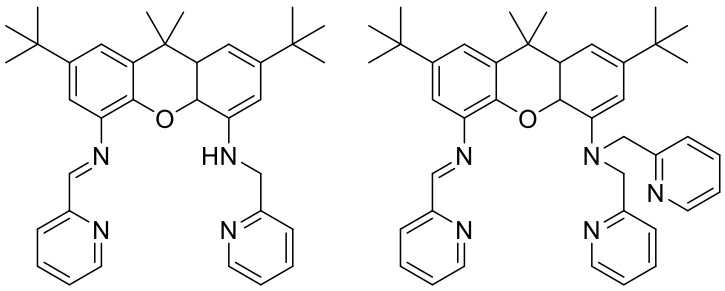


**iXa** **iXa-2**

**Figure 6.** Ligand scaffolds of **iXa** and **iXa-2**.[79]

Complexes with seven-coordinate metal centres represent a minority of structures for transition metal compounds (~1% of ferrous structures, ~1% of zinc containing structures).[80] In nature, only a few enzymes with a seven coordinate metal in the active centre are known and comprise e.g. Mo, Mn, or Cd. In the following, some aspects of seven-coordinate iron compounds will be highlighted.

The structural aspects of synthetic seven-coordinate compounds are in the limelight of many reviews.[81-82] Among the reported examples of seven-coordinate complexes, the pentagonal bipyramidal geometry results from pentadentate chelating ligands, with two additional ligands, like solvent molecules or counterions in the axial position. Less observed

are the geometries, capped octahedral and capped trigonal prismatic for the structural arrangement of seven atoms ligated to a metal centre.

The fluxionality of seven-coordinate compounds toward lower coordinate complexes has been observed. The dynamic equilibrium with five- or six-coordinate products is either a ligand dissociation process or an equilibrium with a geometric reorganisation is observed. The processes are temperature induced for the given iron examples.[83-85] In 1986, Waigel *et. al.* observed a 7-6 equilibrium for their compound $[Fe^{II}L_3(CN)_2]\cdot xH_20$ ($L_3$ = 3,6-dioxaoctane-1,8-diamine) with rising temperature.[84] Britovsek *et. al.* showed in variable temperature (VT) NMR-studies, that a axial ligand loss in their heptacoordinate compound $[Fe(1)](OTf)_2$ (1 = 2,6-bis[(methyl(2-pyridylmethyl)amino)-*N*-methyl]pyridine) is observed, obtaining a five-coordinate complex with rising temperature.[85] In geometry reorganisation processes, lower coordinated intermediates have been observed in NMR-studies. The products are pentagonal bipyramidal or face capped trigonal prismatic and are in equilibrium. During the reorganisation of the ligands one or more ligands weaken or lose their bond to form an intermediate with less than seven coordinating atoms.[86] In addition, seven coordinate complexes are in use as intermediates in associative reactions of six-coordinate complexes or in dissociative reactions of eight-coordinate compounds. The coordination number can affect the electronic structure and as a consequence influence greatly the reactivity.[87]

Some of the seven-coordinate iron compounds show interesting single molecule magnetic behaviour,[88-89] spin crossover[84, 90-92] or exhibit LIESST (light induced spin state trapping) phenomena.[93-94] The magnetic behaviour is so far the best described property of seven coordinate iron compounds. The crossover between high- and low spin, or an intermediate spin, is temperature induced in a constant magnetic field. An activation by light, to change the spin state of the complex, is performed in the LIESST experiment. The activated species can often be trapped at lower temperatures and the life-time of the species is a characteristic feature of the complex.

The imitation of superoxide dismutase activity with complexes like Fe(dapsox) or Mn(dapsox) (dapsox = 2,6-diacetylpyridinebis(semioxamazide) demonstrates that heptacoordinate iron complexes can perform biological related reactions.[95-97] The active centre of iron or manganese superoxide dismutases are six-coordinated, formed by three histidines, one aspartate and one solvent molecule, and differ from the synthetic compounds. Nevertheless, many of the synthetic seven-coordinate iron and manganese compounds are effective superoxide dismutase mimetics. The complexes can deactivate superoxide, although their activity at physiological pH values and in aqueous essays are still limited.[97]

The aforementioned seven coordinate iron complexes show promising properties and reactivities. Furthermore, the **iXa**- and **iXa-2**-ligand are non-innocent due to the *α*-iminopyridine group. Through the low lying *π**-orbitals up to a two-electron reduction is feasible and allows the formation of reduced compounds even with non-redox-active $d^{10}$-metals (see 1.2.2). The redox-active moiety might offer access to a wider range of valence forms. Herein studies on iron, zinc and nickel compounds coordinated by the **iXa**- and **iXa-2**-ligand are presented. The unsymmetrical complexes were studied by cyclic voltammetry, spectroscopic methods, especially by NMR, and by X-ray diffraction. DFT calculations of spin density and molecular orbitals supported our work.

## 2.2 iXa and iXa-2

The syntheses of **iXa** and **iXa-2** are according to strategies developed from former members of the Hess group and therefore will not be described in detail. Both ligands were synthesised in seven steps (see Scheme 19), starting from the commercially available xanthene, 2,7-di-*tert*-butyl-9,9-dimethylxanthene and reacted in a bromination.[98] The dibromide **1** reacted, with the formation of an aryl-lithium intermediate, with $CO_2$ to give the diacid compound **2**.[98] By the hydrolysis of the carbamate, obtained from the reaction with DPPE, $NEt_3$ and BnOH in a Curtius rearrangement, the diamine **3** is formed.[99-100] The bis(2-pyridyl-methyl)amino groups were attached to the mono-BOC-protected **4** by reacting with either one or two equivalents of chloromethylpyridine. The products, aminomethylpyridine **5a** or amino(di(methylpyridine)) **5b**, were separated by column chromatography, followed by the removal of the BOC group in acidic milieu. In the condensation reaction of pyridine carboxaldehyde with the related aminomethylpyridine compounds (**5a** or **5b**) the second coordination site, formed by an iminopyridine moiety, was added to give the unsymmetrical **iXa** and **iXa-2** ligands.[79]

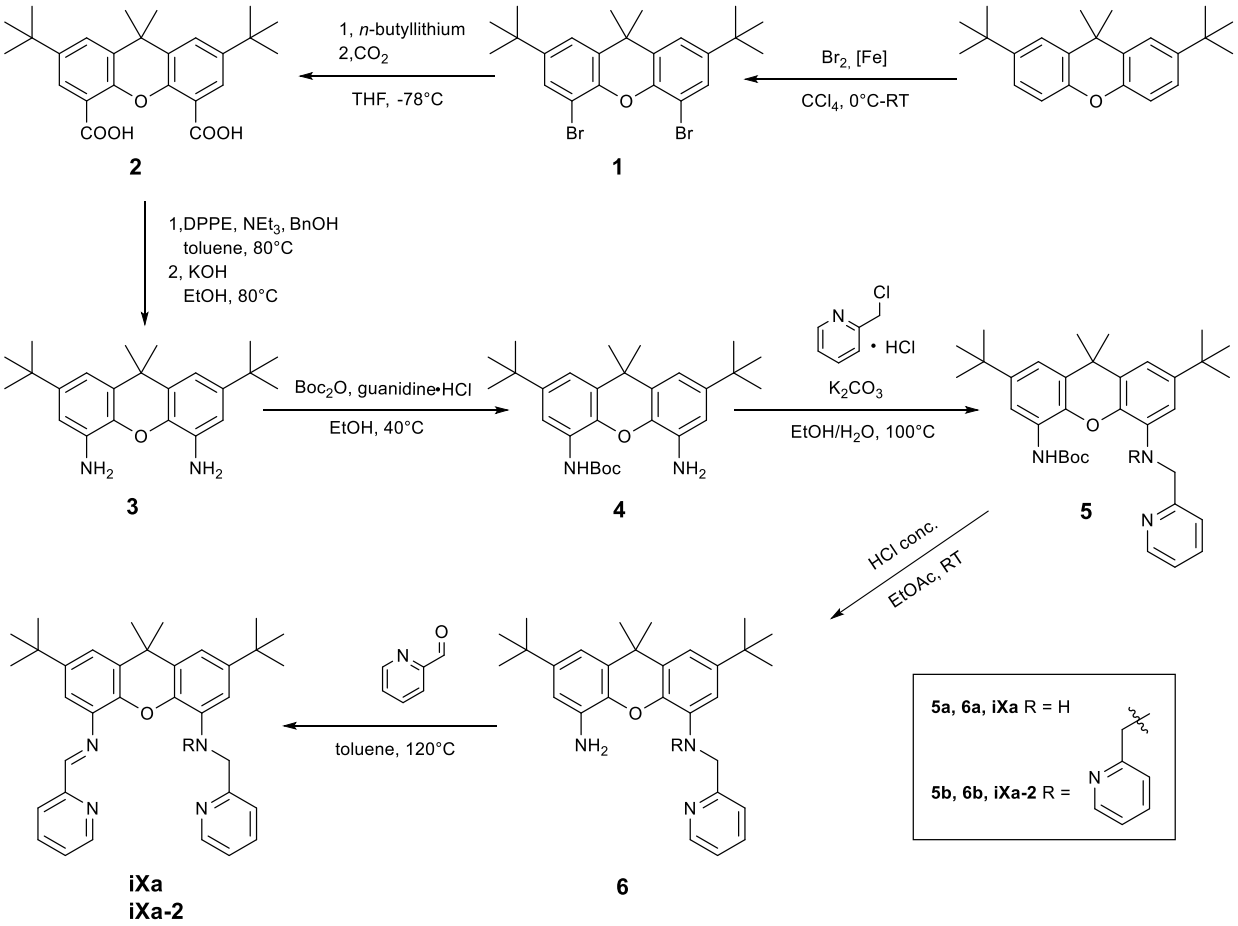


**Scheme 19.** Synthesis of **iXa** and **iXa-2**.

All compounds were characterised by NMR-, IR- and mass spectroscopy to confirm the displayed structures. The characterisation of the final ligands, **iXa** and **iXa-2**, will be presented in detail. The protons of the $^{1}$H-NMR spectra were assigned with the help of $^{13}$C-, COSY-, HSQC- and HMBC-NMR spectra and are shown in the following (Figure 6 and Figure 7).[79]

The asymmetry of the ligand **iXa** causes a splitting of *tert*-butyl group protons ($H_{11}$ and $H_{22}$) into two signals. The 18 protons are, together with the signal of the methyl group, $H_{15}$, the least shifted signals. The singlet at 4.54 ppm represents the protons ($H_{26}$) next to the amino group. A broad signal with an integral of one is assigned to the amine proton ($H_{25}$). The aromatic region is magnified to show the signals in detail. The proton signal of the imine $H_6$ is displayed as a singlet. The xanthene protons, $H_{8,12,19,23}$ cannot couple with any protons on the neighbouring carbon atoms. Due to the aromaticity of the phenyl rings at least small hyperfine coupling values are expected. A coupling of the doublets and triplets of the pyridine protons in the 2D NMR spectra simplifies the assignment of each proton to a pyridine ring. For the final assignments of protons see Figure 7.

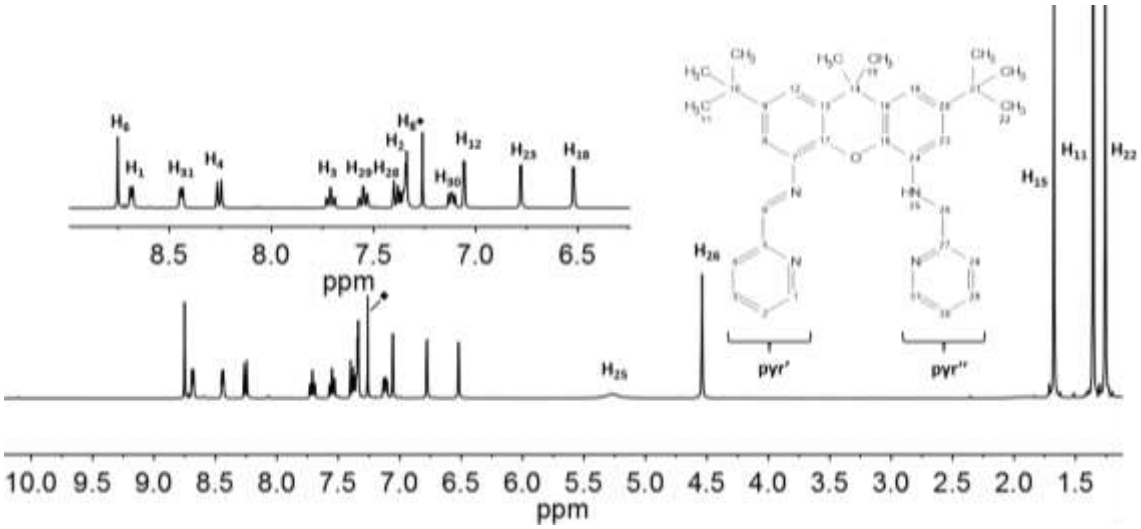


**Figure 7.** $^{1}$H-NMR spectrum of **iXa** (600 MHz, $CDCl_3$) with labelling scheme, magnified aromatic region (inset) and assignment of the protons.

The assignment of **iXa-2** proton signals follows the same strategy as for **iXa**. The methyl ($H_{15}$) and *tert*-butyl ($H_{11}$ and $H_{22}$) group protons are the least shifted signals. The proton signal of $H_{26}$, compared to the corresponding proton in the **iXa** spectrum, is shifted marginally higher to 4.65 ppm due to the electron density influence of two pyridine rings. The assignment of the aromatic multiplet signals to the corresponding protons is easier since the signal integrals of pyr'' are doubled in value compared to **iXa** due to the two identical pyridine rings on the amine side. Several of the signals are located in a narrow range between 7.25 and 7.40 ppm and can be only assigned by their couplings in the 2D-NMR spectra. For detailed assignments refer to Figure 8.

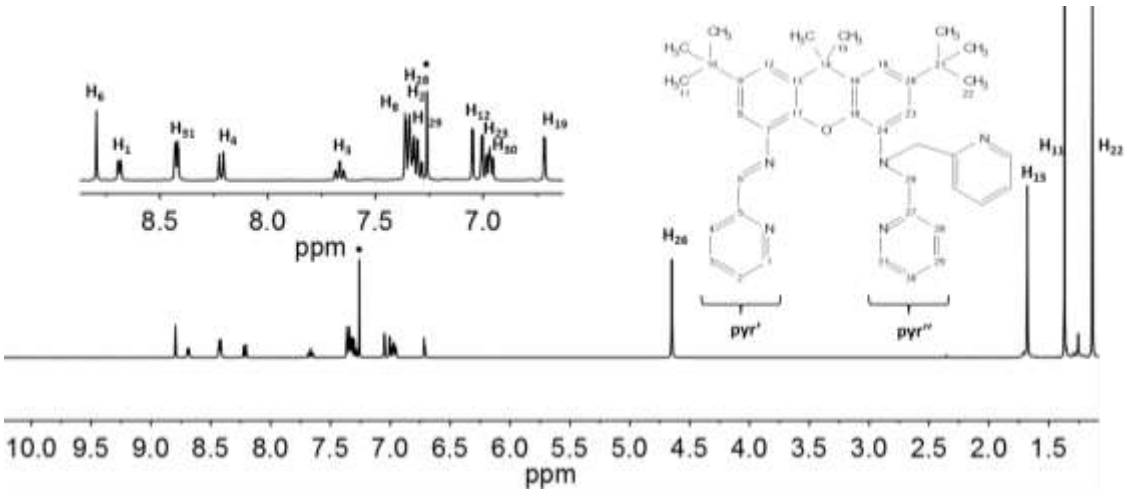


**Figure 8.** $^{1}$H-NMR spectrum of **iXa-2** (600 MHz, $CDCl_3$) with labelling scheme, magnified aromatic region (inset) and assignment of the protons.

The electronic spectra of **iXa** and **iXa-2** (Figure 9) display bands at 298 nm assigned to $\pi$-$\pi^*$-transitions. Further bands are visible as a shoulder with lower intensity at 380 nm ($\varepsilon$ = 4900 $M^{-1}$ $cm^{-1}$).

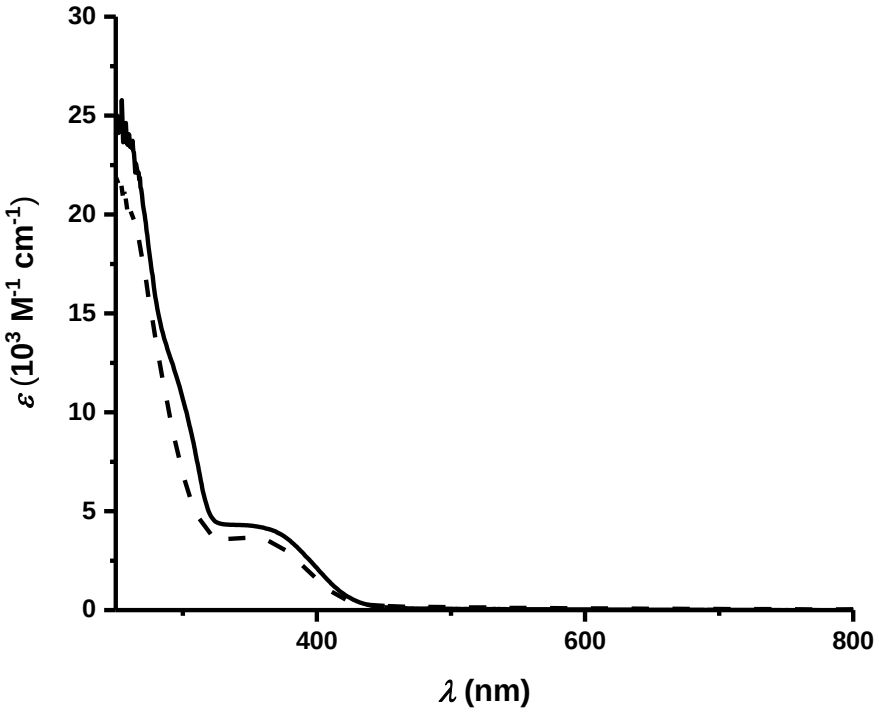


**Figure 9.** Electronic spectra of **iXa** (solid line) and **iXa-2** (dashed line) in MeCN.[79]

The ligands are defined as non-innocent due to the iminopyridine moiety. In 1.2.2, it was shown that the iminopyridine moiety can accept up to two electrons and is redox active. For **iXa** a non-reversible event at -2.2 V was measured, which is probably the one-electron reduction of [iXa] to [$iXa^{\bullet}$]$^-$ (Figure 10). No redox event was observed in the measurement of **iXa-2** at low potentials. Therefore, the cyclic voltammetry measurement of **iXa** confirms the non-innocence of the ligand. As the moiety of the **iXa-2** is similar, a non-innocence is expected as well, but the redox couple is probably at a lower potential. Above 0.2 V an increase of current for **iXa** and **iXa-2** is observed, but none of the observed events is reversible.

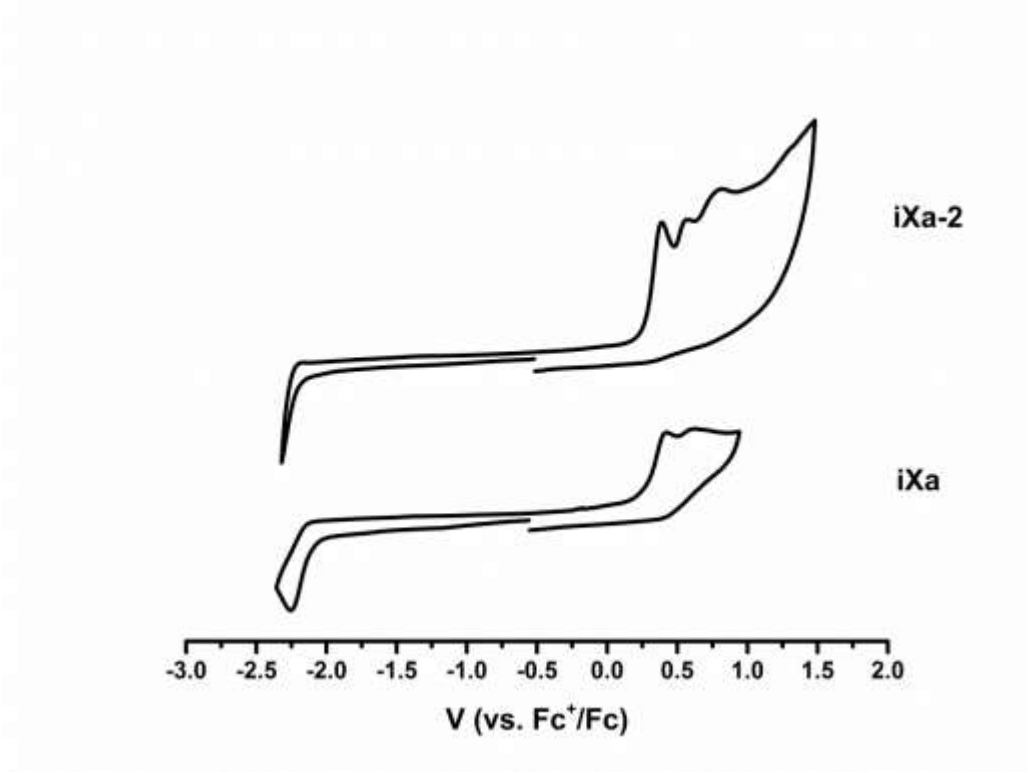


**Figure 10.** Cyclic voltammograms of the ligands, **iXa** and **iXa-2**; MeCN, 0.1 V $s^{-1}$, 0.1 M $[N(n\text{-}Bu)_4]PF_6$.[79]

## 2.3 Iron and zinc compounds of iXa and iXa-2

Metal compounds of **iXa** and **iXa-2** have been synthesised with the metal precursors $[Fe(MeCN)_6](PF_6)_2$ and $Zn(OTf)_2$ to yield $[Fe(iXa)(MeCN)_2](PF_6)_2$ (**7**), $[Zn(iXa)(OTf)_2]$ (**9**), $[Fe(iXa\text{-}2)](PF_6)_2$ (**8**) and $[Zn(iXa\text{-}2)](OTf)_2$ (**10**) (Scheme 20). All reactions were carried out in MeCN at room temperature under inert atmosphere. The purity of the compounds was proven by elemental analysis. A determination of the molecular structure was successful by X-ray diffraction and the compounds were further examined by NMR-, mass- and UVVis-spectroscopy.

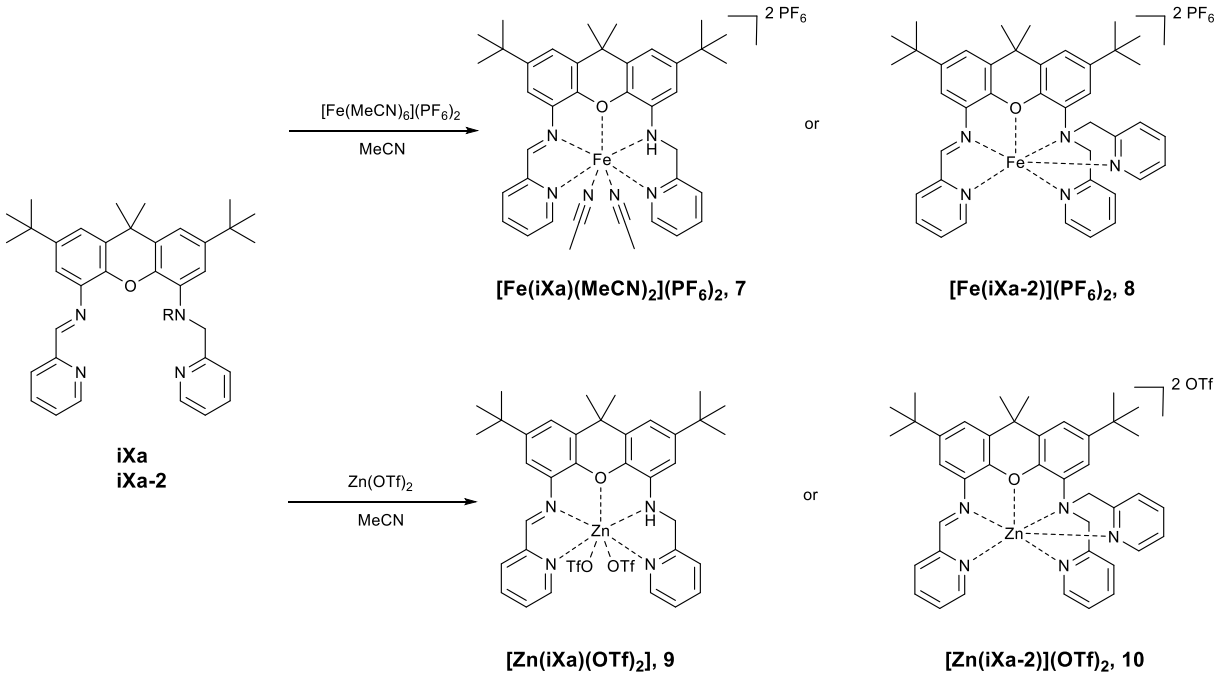


**Scheme 20.** Synthesis of the metal complexes with **iXa** and **iXa-2**.[79]

The complexes of pentadentate **iXa** show a distorted pentagonal bipyramidal geometry in the solid state (Figure 11). Seven-coordinate compounds in a pentagonal bipyramidal geometry are rare for late first row transition metals. The pentagonal plane, N1-N2-O1-N3-N5/O5, is formed by the three nitrogen of the imine (N2), the amino (N3) group and the pyridine nitrogen (N1) in the iminopyridine moiety. The fourth and the fifth bond is between the oxygen (O1) of the xanthene and the metal and either a solvent molecule, in case of the complexed iron an acetonitrile, or the triflate counterion for zinc compounds. While the plane of **7** diverges by 17°, a buckling of the xanthene backbone is noticeable for **9**. The relative rigidity of the xanthene and the iminopyridine moiety, due to the conjugate system, probably prevents the coordination of a second metal ion as the distance between the two coordination sites are too small to accommodate more than one zinc or iron ion. The more flexible aminopyridine moiety would allow a different coordination site as it has been seen with diiminatio and aminoquinoline coordination sites.[101-103] Perpendicular to the plane is the second pyridine nitrogen (N4) of the aminopyridine group and on the opposite the second solvent or counterion molecule. The counterions or the coordinating acetonitrile molecule on the iron compound are in an unusual *cis*-configuration. Up to date no other compound with a *cis*-configuration was reported in the literature to the best of our knowledge.

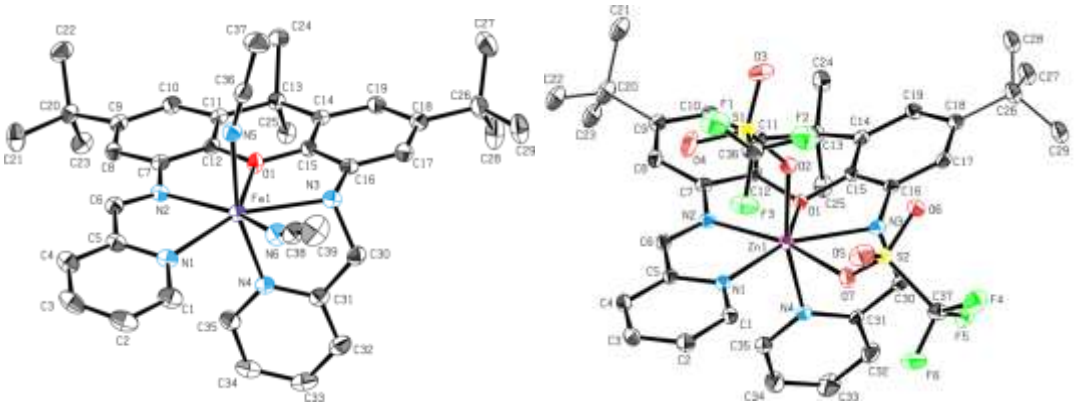

**Figure 11.** Molecular crystal structures of **[Fe(iXa)(MeCN)$_2$](PF$_6$)$_2$** (**7**) and **[Zn(iXa)(OTf)$_2$]** (**9**).

**8** and **10**, comprised by the hexadentate **iXa-2**, are in a six-coordinate geometry (Figure 12). The plane formed by N1-N2-O1-N3 is not from square planar with an angle of 139.37° (expected 90°) between N1-Fe1-N3. Consequently, the structures of **8** and **10** are best described as distorted pentagonal bipyramidal, with one ligand absent in the equatorial pentagon. The nitrogen atoms N4 and N5 of the pyridines, coordinated to the aminomethyl group, take the axial positions. Sterical hindrance probably prevents the coordination of an additional molecule in the free seventh coordination spot. No coordination of solvent molecule or counter ions is observed for the iron and zinc compounds **8** and **10**. The **iXa-2** can accommodate the zinc ion without a buckling of the xanthene.

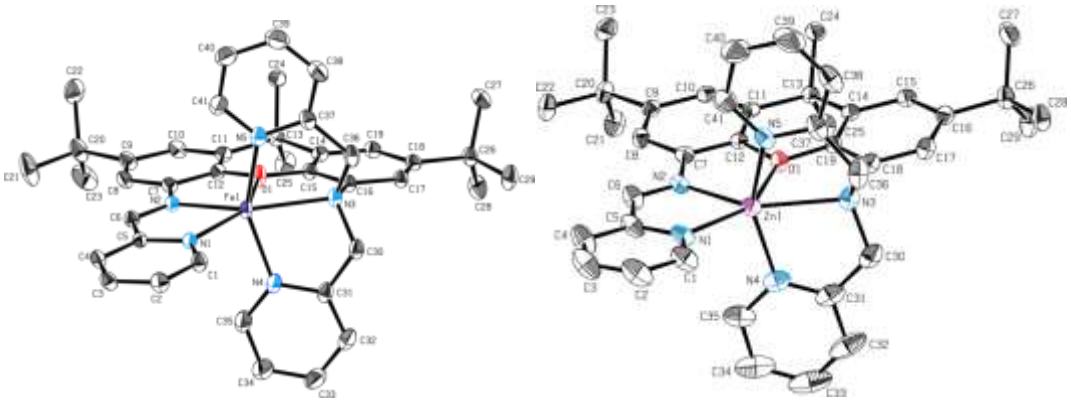

**Figure 12.** Molecular crystal structures of **[Fe(iXa-2)](PF$_6$)$_2$** (**8**) and **[Zn(iXa-2)](OTf)$_2$** (**10**).

The bond lengths of the iron compounds are comparable (see Table 2). The bond lengths of the zinc compounds differ slightly from each other with the bond lengths of the zinc ion to **iXa** are shorter than to **iXa-2**. The metal to oxygen bonds of the xanthene oxygen (O1) is noticeable shorter for the **iXa-2**-compounds. An explanation for this observation could be the buckling of **9**. The average iron-nitrogen bond lengths of **7** and **8** (Fe-N$_{avg}$ = 2.24 Å and Fe-

$N_{avg}$ = 2.17 Å) suggest a high spin configuration. The perfect angle in a pentagon is 72° and the observed angles in the compounds **7** to **10** are in the range between 65°- 77°. The planes of the complexes are close to pentagonal and planar.

**Table 2:** Bond lengths (Å) and angles (°) of **7**, **8**, **9** and **10**.

| M = Fe,Zn | **7** | **8** | **9** | **10** |
|---|---|---|---|---|
| M1-N1 | 2.244(15) | 2.185(11) | 2.136(2) | 2.169(2) |
| M1-N2 | 2.246(14) | 2.152(11) | 2.216(2) | 2.133(2) |
| M1-N3 | 2.335(14) | 2.308(11) | 2.267(2) | 2.379(2) |
| M1-N4 | 2.134(14) | 2.112(14) | 2.096(2) | 2.045(2) |
| M1-N5 | 2.152(15) | 2.103(13) | | 2.057(2) |
| M1-N6 | 2.329(16) | | | |
| M1-O1 | 2.380(11) | 2.212(10) | 2.554(2) | 2.273(2) |
| M1-O2 | | | 2.087(2) | |
| M1-O7 | | | 2.578(2) | |
| N1-M1-N2 | 72.71(5) | 75.62(4) | 76.68(7) | 76.79(7) |
| N2-M1-O1 | 67.26(4) | 71.58(4) | 65.76(6) | 71.18(6) |
| O1-M1-N3 | 68.22(4) | 73.35(4) | 66.73(6) | 70.74(6) |
| N3-M1-N4 | 74.88(5) | 76.14(5) | 78.72(7) | 76.83(8) |
| N4-M1-N5 | 163.74(6) | 150.26(5) | | |
| N4-M1-O2 | | | 165.14(7) | 150.22(8) |
| N5-M1-N6 | 81.91(6) | | | |
| O2-M1-O7 | | | 85.05(5) | |
| N6-M1-N1 | 79.18(5) | | | |
| O7-M1-N1 | | | 80.60(6) | |
| N1-M1-N4 | 93.07(5) | 93.89(5) | 94.78(7) | 99.36(8) |
| N5-M1-O1 | 84.27(5) | 90.75(4) | | |
| O2-M1-O1 | | | 84.27(5) | 91.98(7) |
| N4-M1-O1 | 86.71(5) | 92.97(5) | 76.20(6) | 91.48(7) |
| N4-M1-N6 | 97.02(5) | | | |
| N4-M1-O7 | | | 92.70(6) | |
| N1-M1-N5 | 102.60(5) | 98.81(4) | | |
| N1-M1-O2 | | | 99.32(6) | 93.22(8) |
| N1-M1-N3 | 150.44(5) | 139.37(4) | 150.59(7) | 141.14(7) |

*Electronic spectra*

All four compounds exhibit intense bands at ~330 nm (328, 329, 334 and 340 nm), which are assigned, due to similar bands in the ligand spectra (Figure 9), as *π*-*π**-transitions (Figure 13). Additionally, the spectra of **7** and **8** display weaker absorption bands at 493 nm (**7**) and 548 nm (**8**), which can be assigned to MLCT transitions as they are not present in the spectra of **9** and **10**. The MLCT bands reflect the colours of the compounds, red-brown and green.

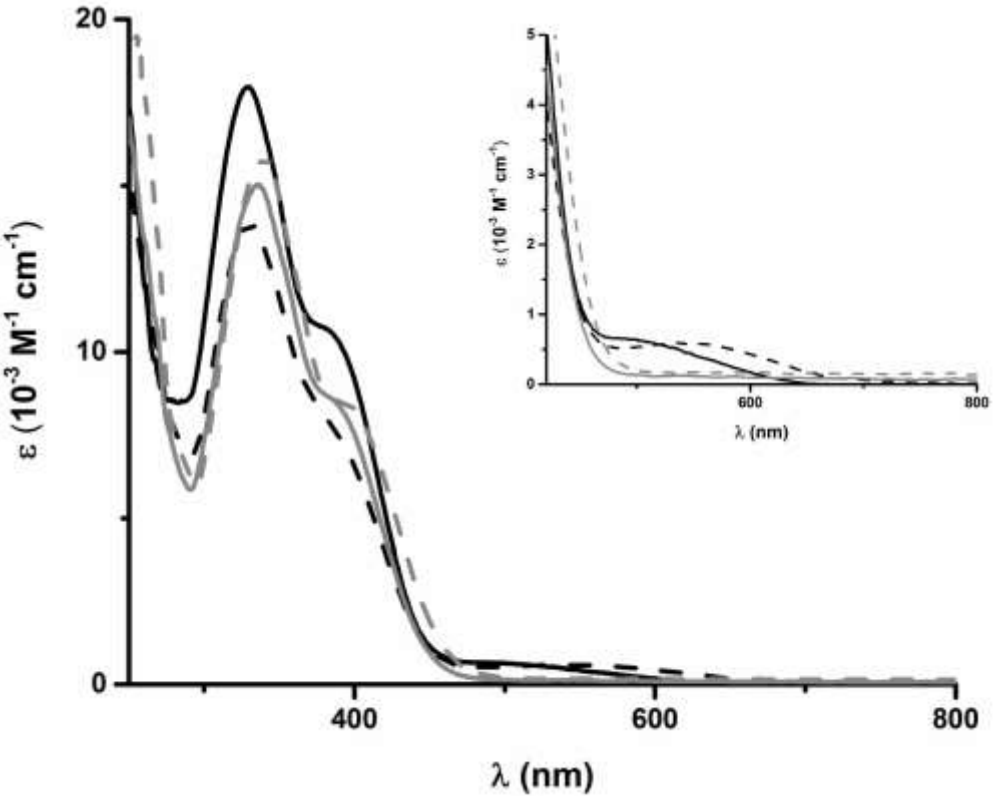


**Figure 13.** Electronic spectra of **7** (black solid line), **8** (black dashed line), **9** (grey solid line) and **10** (grey dashed line) in MeCN. Inset: magnified region from 400 to 800 nm.[79]

*Redox activity*

The non-innocence of the ligands has been shown in Figure 10. The complexation of metal ions increases the possibilities of reduction and oxidation of the compounds. It has to be distinguished between metal-based and ligand-based redox-events.

The first reductive events for the zinc containing compounds **9** and **10** are observed between -1.0 V and -1.2 V (Figure 14). The reduction is assumed to be the ligand centred [iXa]/[iXa$^{\bullet}$]$^{-}$ or [iXa-2]/[iXa-2$^{\bullet}$]$^{-}$ redox couples as Zn$^{II}$ ions are not redox-active and the redox-activity of the iminopyridine group is well-known. In the cyclic voltammograms of the ligands

the potentials of the reduction were significantly lower (-2.2 V and lower). No further events are displayed in the cyclic voltammograms of **9** and **10**, which suggest that the second reduction of the ligands, $[iXa^{\bullet}]^{-}/[iXa]^{2-}$ or $[iXa\text{-}2^{\bullet}]^{-}/[iXa\text{-}2]^{2}$ is at a lower potential. **7** and **8** show their first reductive event at the same potentials as **9** and **10**. The location (-1.2 V and -1.0 V) of the potential leads to the assumption, that the one-electron reduction of the iron compounds is also ligand-based and not the metal-based $Fe^{II}/Fe^{I}$ couple. Upon reduction, the formal $Fe^{I}$ compounds are obtained. At more negative potentials, several smaller events are displayed, but are not caused by a one-electron reduction. Furthermore, **9** exhibits an event in the oxidative region at 1.0 V. In the literature events similar to the observed one, with a splitting to an oxidation curve at 1.0 V and a reduction curve at 0.25 V, are described as one-electron oxidation/reduction process accompanied by a slow geometric rearrangement.[104-105] As the oxidised species was never isolated a rearrangement cannot be confirmed.

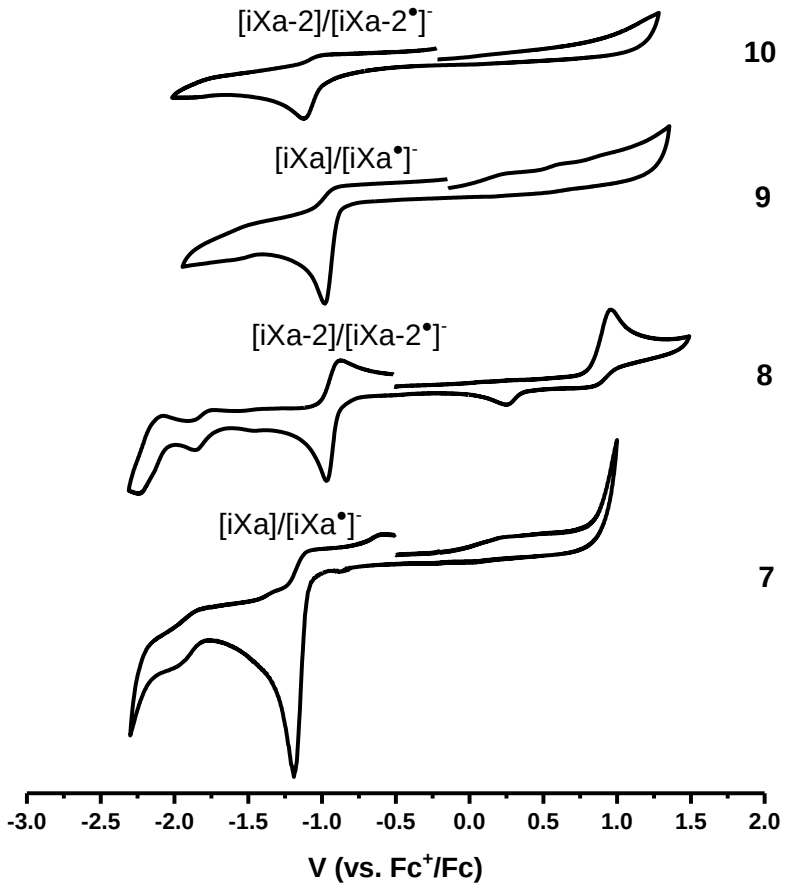


**Figure 14.** Cyclic voltammograms of **7**, **8**, **9** and **10**; MeCN, 0.1 V $s^{-1}$, 0.1 M $[N(n\text{-}Bu)_4]PF_6$.

The first reductive event of each compound was isolated in a measurement to see the reversibility of the redox event. Except for **8**, the reductions are not reversible. The quasi-

reversible reduction of **8** at $E_{pc}$ = -1.011 V with a return oxidation at $E_{pa}$ = -0.922 V, giving E° = -0.97 V (Figure 15), has a peak separation of 0.89 V. A fully reversible one electron redox process is defined as having a peak separation ~ 0.059 V and so the event at -1.0 V can be defined as a one electron transfer.[106]

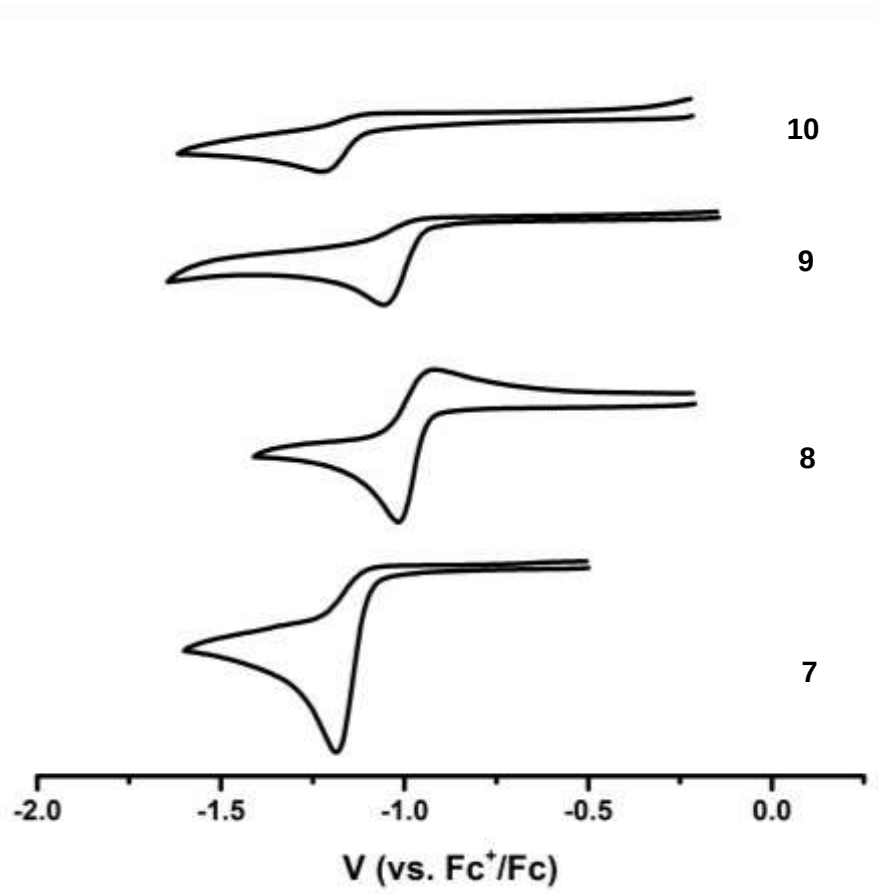


**Figure 15.** Cyclic voltammograms of **7**, **8**, **9** and **10**, showing the first reductive event; MeCN, 0.1 V $s^{-1}$, 0.1 M $[N(n\text{-}Bu)_4]PF_6$.[79]

*DFT calculations*

DFT calculations (B3LYP) were carried out to reveal the spin density distribution in the ferrous complexes (Figure 16). For S = 2 in a high spin configuration a localisation of the density on the Fe centre is expected. The sum of the density roughly adds to four, representing the four unpaired electrons. Only small spin density contributions of the oxygen and nitrogen atoms are observed aside the main spin density on the iron ion. The calculated spin densities play an important role for the calculation of the theoretical contact shifts and the assignment of protons in the NMR spectroscopy part.

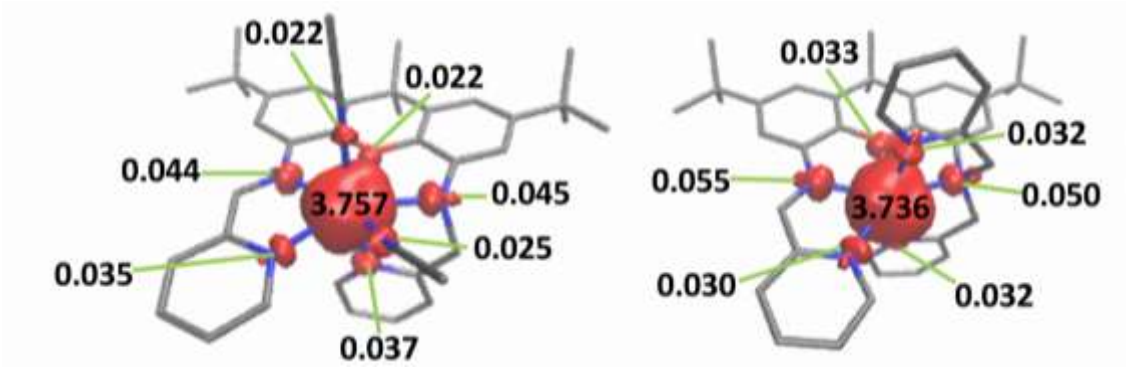


**7** **8**

**Figure 16.** DFT-derived (B3LYP) spin density plots of **7** and **8** based on Löwdin population analysis.[79]

The order of the d-orbitals deviates from a strict pentagonal bipyramidal geometry ($D_{5h}$) because of the unsymmetrical ligand (Figure 17). As a result, the d-orbitals degenerate, although the energy gaps between the orbitals are small. Only the gaps between HOMO and LUMO and HOMO and $d_{x2-y2}$ are bigger. The lowest d-orbital is the $d_{yz}$, doubly occupied, the energetically higher orbitals are singly occupied (SOMOs). For **7**, the orbitals are d-character based and can be described as “non-bonding”. In contrast, $d_{yz}$ orbital of **8** has an overlap with the $\pi^*$-orbitals of the xanthene moiety, which would explain the shorter Fe-O distance in the crystal. The highest occupied molecular orbital (HOMO) is the single occupied $d_{z2}$, as expected for $D_{5h}$. The lowest unoccupied molecular orbital (LUMO) has only a small percentage of d- but a high diimine $\pi^*$-character. The arrangement of the orbitals and the small energy gaps support the assumption that the one electron reductions of compounds can be ligand based. Therefore, the electron has to be placed into the LUMO and not in one of the energetically lower SOMOs.

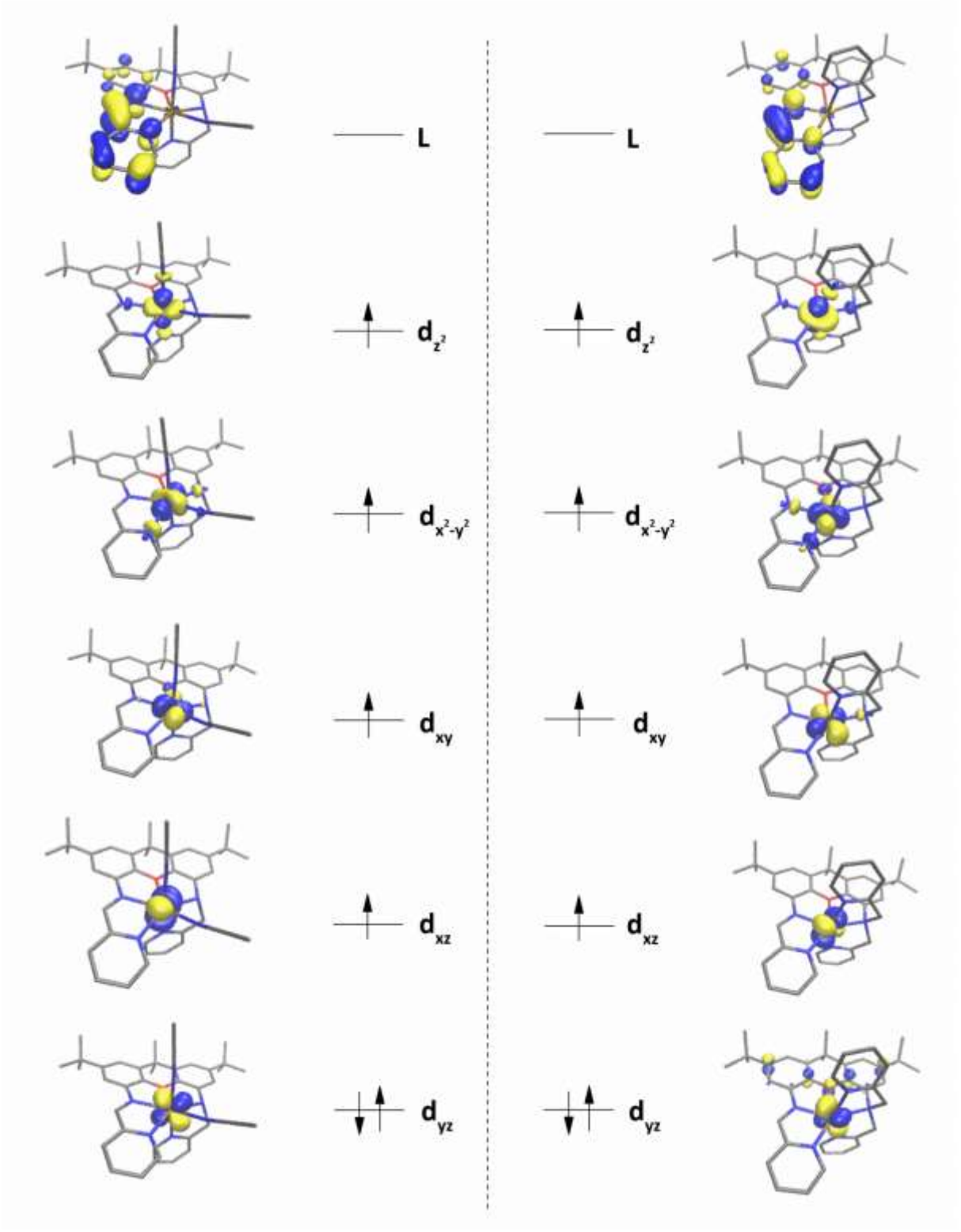


**Figure 17.** DFT-derived (B3LYP) qualitative MO diagrams of **7** and **8**.[79]

*NMR studies*

The compounds **7** to **10** were further studied by NMR spectroscopy. In the literature, geometric reorganisation and equilibria to lower coordinate iron compounds have been observed, as described in 2.1, and followed by NMR-studies. Therefore, detailed studies with VT-NMR spectroscopy have been pursued with the iron compounds **7** and **8**. The proton assignment in the $^{1}$H NMR spectra of **9** and **10** was carried out to determine the diamagnetic shift of the homologues.

The $^{1}$H-NMR spectrum of **9** is shown in Figure 18 and discussed here. For zinc compound **9** the proton signals are shifted slightly higher compared to the uncomplexed ligand. The shift is caused by the higher electron density in the molecule due to the presence of the metal ion. Additionally, more signals are observed than in the spectrum of the **iXa** ligand. Examples for this are the protons of the methyl groups, $H_{15}$ and $H_{15}$', and the methyl protons of the aminopyridine moiety, $H_{26}$ and $H_{26}$'. It is assumed that through the coordination of the zinc ion, the symmetry of the ligand was lowered and the protons are no longer identical. The singlet of proton $H_6$ of the imine group is the signal with the highest shift at 9.46 ppm. The signals of the $H_{26}$- and $H_{26}$'-protons are at 5.13 and 4.40 ppm as a doublet of doublets with coupling constants of 7.0 and 17.0 Hz and a doublet ($J$ = 17.0 Hz). At 5.74 ppm the amine proton ($H_{25}$) signal is located as doublet ($J$ = 7.0 Hz). The coupling constants of the three signals suggest a coupling between the amine proton and the methyl protons. $H_{26}$ is hereby coupling to $H_{26}$' as well as to $H_{25}$, $H_{26}$' is only coupling to its equivalent $H_{26}$ and $H_{25}$ only to $H_{26}$. Further assignments are displayed in Figure 18.

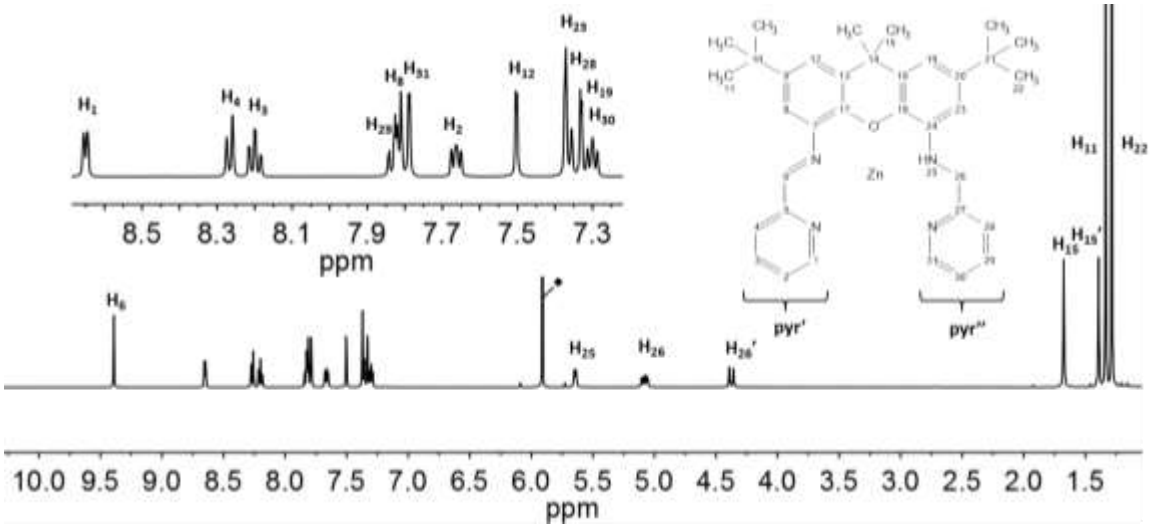


**Figure 18.** $^{1}$H-NMR spectrum of **9** (600 MHz, DCM-$d_2$) with labelling scheme, magnified aromatic region (inset) and assignment of the protons.

The highest shifted proton signal in the spectrum of the zinc compound **10** is the proton $H_6$ of the imine group at 9.84 ppm, as shown in Figure.19. The two protons $H_{26}$ and $H_{26'}$ of the methyl group next to the tertiary amine are displayed as two doublets at 5.10 and 5.06 ppm with a coupling constant of 16.7 Hz. The difference of the shift is less compared to **9 (**0.7 ppm vs 0.05 ppm). An assignment of the aromatic region is shown in the inset; further assignments can be followed in Figure 19.

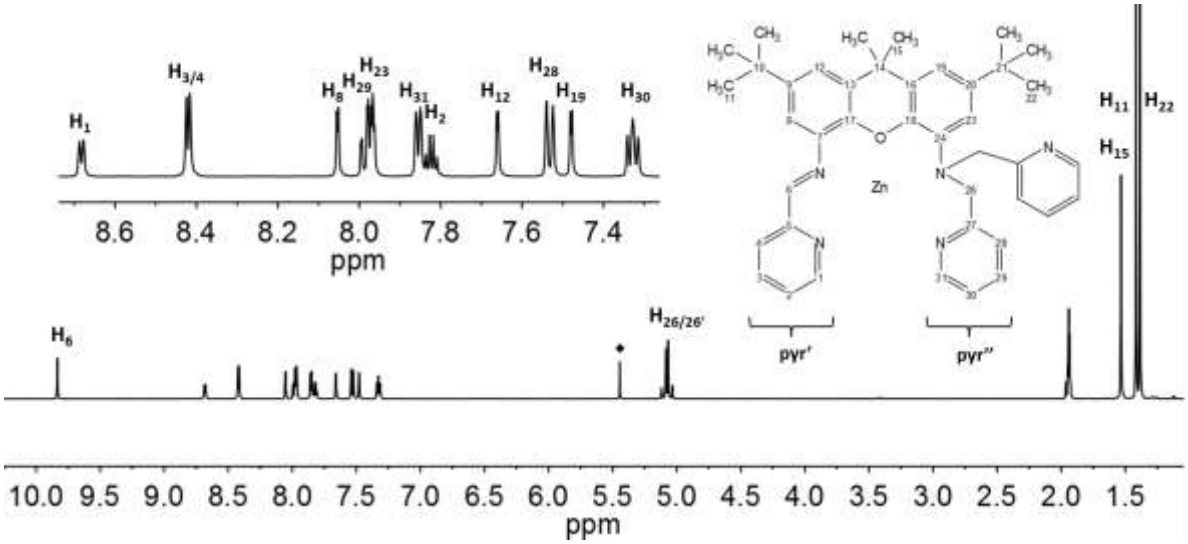


**Figure 19.** $^1$H-NMR spectrum of **10** (600 MHz, DCM-d2) with labelling scheme, magnified aromatic region (inset) and assignment of the protons.

The assignment of **7** and **8** turned out to be more challenging as both are paramagnetic compounds. It required VT NMR studies, which were performed for **7** in TCE-$d_2$ between -20 – 90 °C and for **8** in MeCN-$d_3$ between -20 – 70 °C. The solvent TCE-$d_2$ was chosen to avoid an exchange of solvent molecules, between MeCN and MeCN-$d_3$, in the sample of **7** as the loss of ligands at elevated temperature was examined. **7** is not completely temperature stable, as at higher temperatures, especially in the diamagnetic region, several minor features appear.

DFT calculations (B3LYP) for spin density distribution supported our work in the VT-NMR studies. Small changes of spin density already affect shifts in the NMR spectroscopy and the assignment of protons is based on the mechanism of spin density transfer from the d-orbitals of the metal to the ligand nuclei.[107] The spin causes a pattern of negatively and positively shifted signals corresponding to the sign of the spin density. Additionally, if the ligands would receive spin in their *π*-systems, a typical alternating pattern would be expected. For **7** and **8**, the four SOMOs with a dominant d-orbital character are not only *π*-faced but as well *σ*-faced,

so an alternating pattern is not observed and therefore, less signals experience a negative shift.

Furthermore, the signals are broadened compared to signals in diamagnetic spectra, so that no proton couplings are observed. The broadening of the signals is mainly due to a faster dipolar relaxation, so that signals become broader when Fe···H distance decreases ($\Delta \propto r^{-6}$).[107] The broadening of the half width *Δ* is up to 15 kHz and is more pronounced for **7**.

A combination of spin densities, Fe···H distances, half widths and integrals was used for the assignments. The theoretical shifts, to approximate the experimental shifts, were derived from calculations by converting the calculated spin densities into contact shifts, $\delta_T^{\mathrm{con}}$ , at the measuring temperature *T* and supports the proton assignments.[108-111,112] The contact shift is a component of the experimental shift, $\delta_T^{\mathrm{exp}}$:

**Equation 1:**

$$\delta_T^{exp} = \delta_T^{\mathrm{con}} + \delta_T^{\mathrm{dip}} + \delta^{\mathrm{dia}}$$

$\delta_T^{\mathrm{dip}}$ is the through-space dipolar shift and $\delta^{\mathrm{dia}}$ is the shift of a diamagnetic analogue (here **2_9** and **2_10**). So $\delta_T^{\mathrm{con}}$ can be derived by subtracting the $\delta^{\mathrm{dia}}$ from $\delta_T^{\mathrm{exp}}$, if the $\delta_T^{\mathrm{dip}}$ is small:

**Equation 2:**

$$\delta_T^{\mathrm{con}} = \delta_T^{\mathrm{exp}} - \delta_T^{\mathrm{dip}} - \delta^{\mathrm{dia}}$$

$\delta_T^{\mathrm{dip}}$ can be estimated by following equation (distortion was neglected):[113]

**Equation 3:**

$$\delta_T^{\mathrm{dip}} = \frac{\mu_0}{4\pi}\frac{\beta_{\mathrm{e}}^2}{9k_{\mathrm{B}}T}\, S(S+1)\, \frac{3\cos^2\theta - 1}{r^3}\, \left(g_{\parallel}^2 - g_{\perp}^2\right)\left[1 - \frac{7\left(g_{\parallel}^2 + 0.5g_{\perp}^2\right)}{5(g_{\parallel}^2 - g_{\perp}^2)}\frac{D}{k_{\mathrm{B}}T}\right]$$

(magnetic constant, $\mu_0$, Bohr magneton, $\beta_{\mathrm{e}}$, Boltzmann constant, $k_{\mathrm{B}}$, absolute temperature, *T*, spin quantum number, *S*, vector between a given proton and the iron atom in the crystal, *r*, angle between *r* and the principal magnetic axis, $\theta$, g factors, $g_{\parallel}$ and $g_{\perp}$, zero-field splitting constant, *D*)

The obtained values for $\delta_T^{\mathrm{dip}}$ are relative small (Table A2 and A3) and so can be neglected in most calculation of $\delta_T^{\mathrm{con}}$. Therefore, Equation 2 can be reduced to determine $\delta_T^{\mathrm{con}}$:

**Equation 4:**

$$\delta_T^{\mathrm{con}} \approx \delta_T^{\mathrm{exp}} - \delta^{\mathrm{dia}}$$

A result of the approximation is, that $\delta_T^{\mathrm{exp}}$ is direct proportional to the spin density $\rho$ ($\delta_T^{\mathrm{exp}} \propto \rho$).

$\rho$ is used to determine the theoretical contact shift $\delta_T^{\mathrm{theo}}$:[107]

**Equation 5:**

$$\delta_T^{\mathrm{theor}} = \frac{a_0^3 \mu_0 g_{av}^2 \beta_e^2 (S+1)}{9 k_B T} \rho$$

(Bohr radius, $a_0$, average g factor, $g_{av}$, for further definitions see Equation 3)

A comparison of the obtained values for $\delta_T^{\mathrm{con}}$ from $\rho$ and $\delta_T^{\mathrm{exp}}$ is shown in the appendix (Table A2 and A3). An exception would have to be made for the proton $H_8$ and $H_{29}$ as the protons have a relative large $\delta_T^{\mathrm{dip}}$ compared to the paramagnetic shift and$\delta_T^{\mathrm{dip}}$ cannot be neglected.

The symmetry of **8** in solution is $C_s$ and therefore higher then $C_1$ for **7**, which is why the assignment for **8** is easier and carried out first.

The room temperature $^1$H NMR spectrum of **8** exhibits 18 signals, as observed in the spectrum of the zinc homologue, spanning from -2 – 225 ppm (Figure 20). The signal at 224 ppm is attributed to the imine proton ($H_6$), which has the highest positive spin density. Three other protons, $H_1$, $H_{31}$ and $H_{26}$, in close proximity to the ferrous ion, have as well substantial spin densities, which are assigned to the resonances at 140, 121 and 78 ppm. The structural and therefore electronic inequivalence of the methylene protons next to the amine is shown in two different chemical shifts ($H_{26}$: 78 ppm; $H_{26'}$: 40 ppm). The enormous difference of shift between the protons $H_{26}$ and $H_{26'}$ in the paramagnetic compound **8** compared to **10** is probably due to the electron-nuclear coupling (after correcting for the shielding *via* $\delta^{\mathrm{dia}}$). The coupling v*ia* the pathway Fe-N-C-$H_{26/26'}$ originates from the spin transfer from a component of a π-faced SOMO orbital to the proton in *γ*-position and depends on the angle *Θ* (angle between the C-$H_{26/6'}$ bonds and some *π*-faced metal-centred SOMO component) and the dihedral angle between Fe-N-C-$H_{26/26'}$.The protons $H_3$ and $H_{15}$, appear in the region below 0 ppm, as expected given their negative spin densities. The resonance at 4.4 ppm, which also shows substantial temperature dependence, is attributed to the xanthene H-atom next to the imine, $H_8$. The protons of the xanthene moiety, which have the biggest Fe···H distance and only negligible spin densities, yield the most intense signals in the diamagnetic region. Other signals belonging to the methyl or *tert*-butyl groups could be identified by their integrals and are located in the diamagnetic region, as almost no spin density is located there. All assignment can be found in Figure 20.

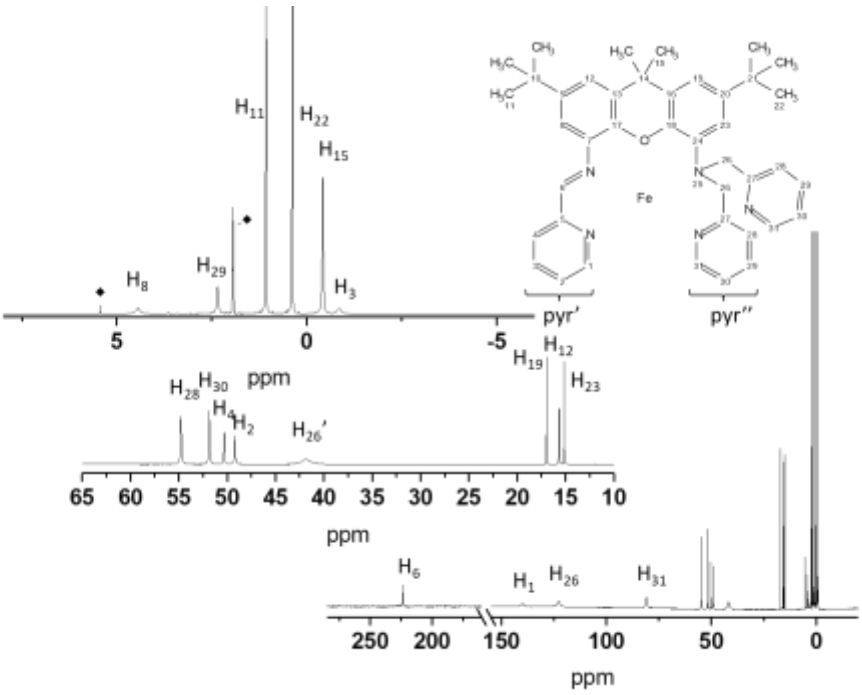


**Figure 20.** $^{1}$H NMR-spectra of **8** (400 MHz, MeCN-$d_3$), with labelling scheme, and magnified regions between 60 and 10 ppm, and 8 and -4 ppm, depicting the individual proton assignments. ◆ = solvent signals: MeCN and DCM.

The proton signals of **7** cover chemical shifts from -50 – 300 ppm at room temperature (Figure 21). A complete assignment was not possible with the existing data and further experiments have to be carried out. The imine proton ($H_6$) again adopts the largest spin density corresponding to the signal at 296 ppm. A signal identified in the opposite region of the spectrum at -57 ppm likely belongs to the amine proton, $H_{25}$ with a significant negative spin density. The half width of the broadest signal at 129 ppm suggests a proton in close proximity to the iron centre, and is assigned to $H_{26}$. The remaining signals from 50 - 150 ppm are likely to comprise the *ortho* and *meta* protons of the pyridine rings. Further, the sharp signals with large integrals at 1.3 and -2.4 can be clearly allocated to the protons of the *tert*-butyl groups, $H_{11}$ and $H_{22}$. The two acetonitrile ligands are either exchangeable or electronically equivalent and cannot be assigned with certainty. The assignment of further protons not mentioned in Figure 21 is also too speculative. Therefore, an answer to the question, that **7** can undergo ligand losses at higher temperature, cannot be given.

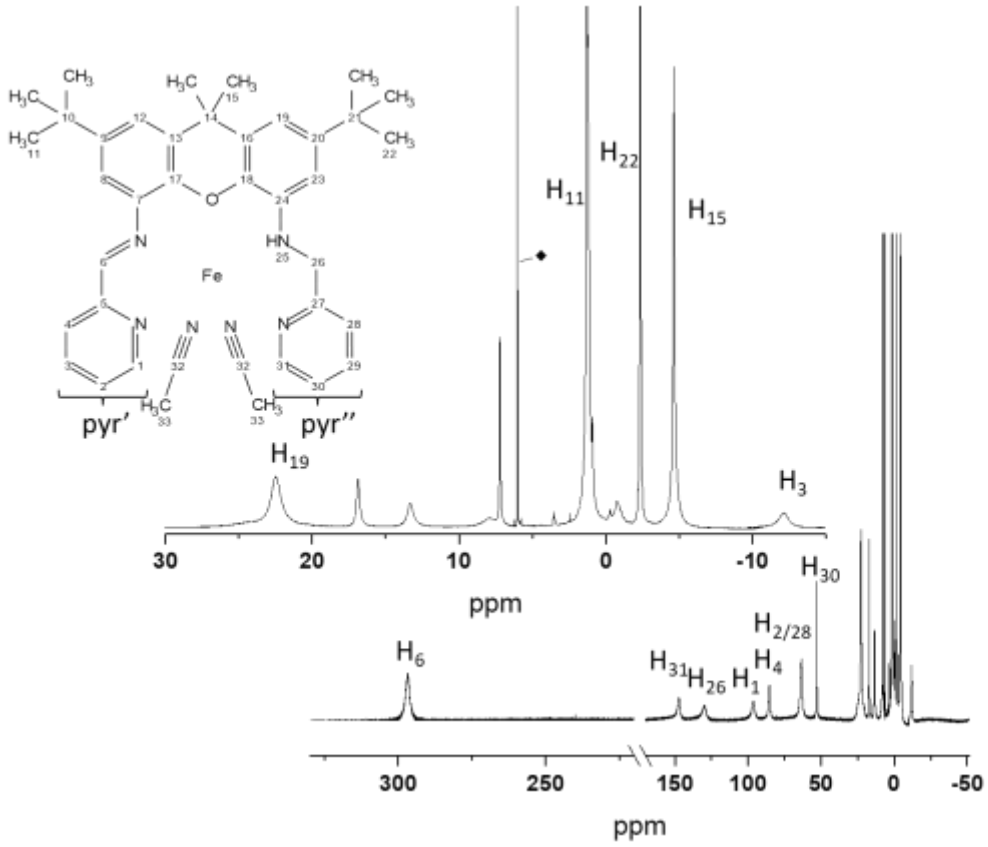


**Figure 21.** $^{1}$H NMR-spectra of **7** (400 MHz, TCE-$d_2$), with labelling scheme and magnified regions between 30 and -15 ppm depicting the individual proton assignments. ◆ = residual solvent signal.

*Magnetic susceptibility*

The solid state measurement of the magnetic susceptibility showed magnetic behaviour (Figure 22), which was not expected for a monometallic iron compound. The obtained magnetic moment at room temperature, 6.1 $\mu_B$ and 5.6 $\mu_B$, confirms the $S$ = 2, high spin configuration for each compound. A total spin of S = 2 suggests that four of six electrons remain unpaired. The theoretical value of a S = 2, high spin is 4.9 $\mu_B$, which fits better than a triplet high spin configuration (2 $\mu_B$) or a singlet, low spin configuration (0 $\mu_B$). At temperatures below 100 K an increase of the magnetic susceptibility up to 7 $\mu_B$ and 6.1 $\mu_B$ was observed. The magnetic susceptibility values can be simulated by assuming a multimetallic iron compound and suggest a long range ordering in the compounds at lower temperatures. Therefore, the determination of the magnetic susceptibility was carried out in solution, to distinguish between an intra- and intermolecular effect. In solution, intermolecular effects are not expected as the distance between the molecules is too big, due to the dilution, to allow an interaction. Intramolecular effects, like spin transitions, would be still displayed in a change of the magnetic susceptibility.

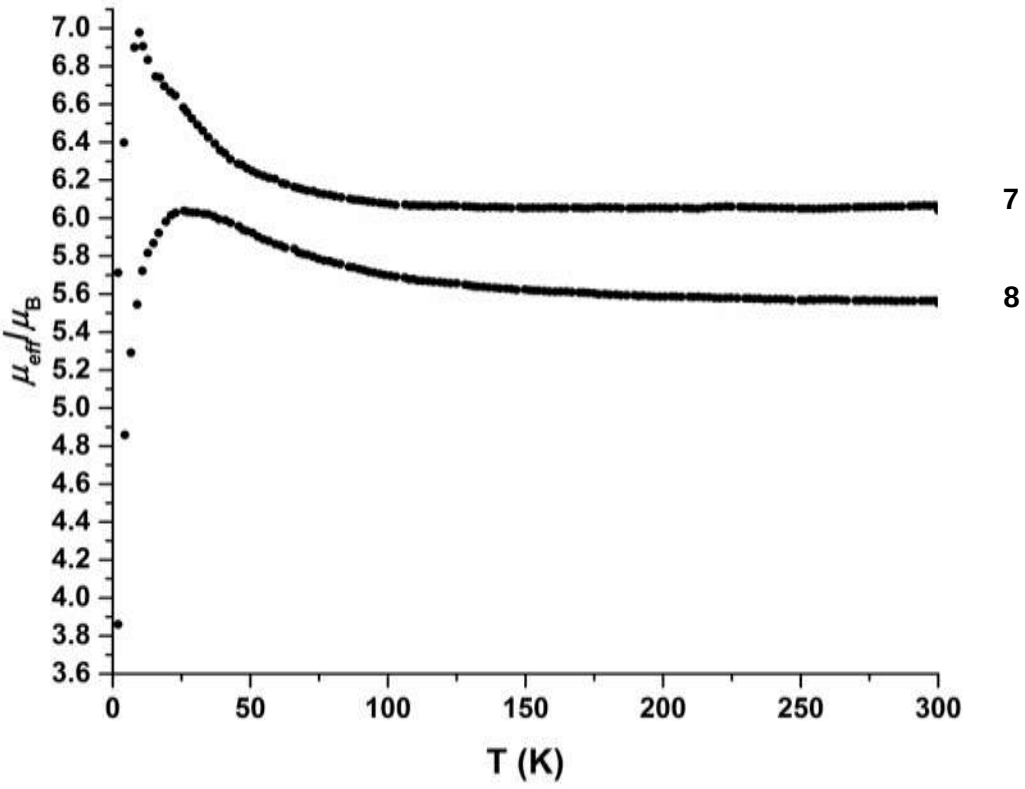


**Figure 22.** Temperature dependence of the magnetic moment $\mu_{eff}$ of **7** and **8**. from 4 K to 300 K (solid state).[79]

For the measurement of the magnetic susceptibility in frozen solution (Figure 23), a solution of ~ 6 mM compound in MeCN was prepared. The data showed no significant increase of the magnetic susceptibility above the room temperature value. An intramolecular effect can be excluded since it would be still visible in a diluted system and leaves the intermolecular interactions as only possible explanation for the observed high magnetic susceptibility values below 100 K in the solid state measurements. At temperatures around 200 K, melting effects disturbed the measurements. The lower magnetic moments (4.2 $\mu_B$ and 3.7 $\mu_B$) compared to the measurements of the solid are due to solvent corrections applied in the measurement. For **7** (graphic on the left), the best fit was achieved at 1 T with $g_1$ = 1.7, $|D_1|$ = 4.95 $cm^{-1}$, $E/D_1$ = 0 and TIP = 24657 × $10^{-6}$ emu and for **8** , $g_1$ = 1.5, $|D_1|$ = 5 $cm^{-1}$, $E/D_1$ = 0 and TIP = 36000 × $10^{-6}$ emu.

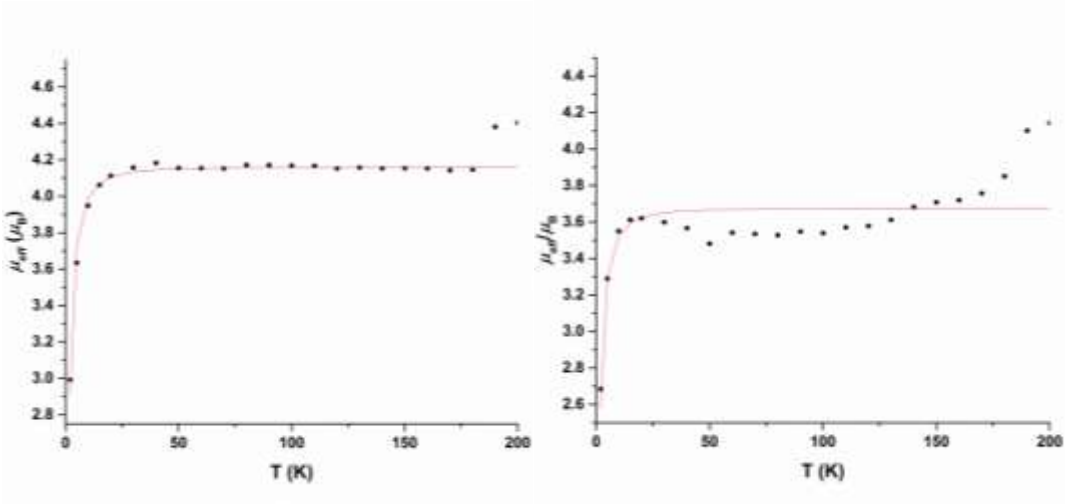


**Figure 23.** Temperature dependence of the magnetic moment $\mu_{eff}$ of **7** (left) and **8** (right) from 4 K to 200 K (frozen solution); black dots: experimental data, red line: simulated data.[79]

Intermolecular exchange interactions are detectable in the crystal structure. The shortest Fe-Fe distances in the packing are 11.010 and 11.179 Å. The distance between the metal centres preclude an interaction without a pathway (bridging molecule), which is not given in our complexes. There is no obvious $\pi$-stacking of the pyridine or of the xanthene rings, so a connection between the iron centres cannot account for intermolecular exchanges. An analysis of the crystal measurement data with the Hirshfeld surface analysis technic was used to visualise interaction. In the Hirshfeld surface analysis technic, electrostatic potentials and thereby, the interactions of adjacent molecules in the crystal are mapped on Hirshfeld surfaces.[114-115] One of the $PF_6$ counterions was investigated in detail and, following the green dashes in Figure 24, shows close contact over the pyridine and xanthene part between the molecules. The contact could be a pathway for the mediation between the complexes. A contact over counterions has been observed in the literature before and would explain the magnetic data of our compounds.[116]

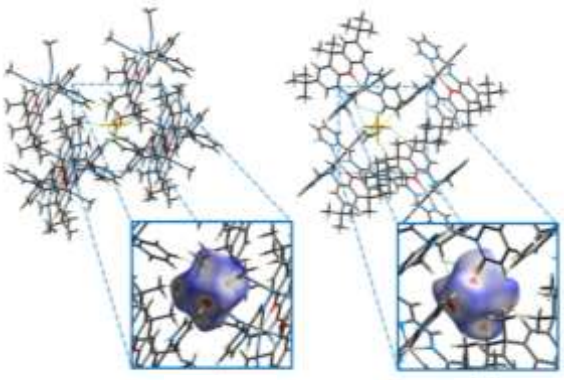

**7** **8**

**Figure 24.** Hirshfeld surface analysis.[79]

To verify the statement, that the contact between the counterions and the conjugated system of the ligands could be a pathway for the mediation between the complexes, the $^{31}$P NMR spectra in solid and solution state was measured (Figure 25). In solution, the expected septets are found at -144.62 and -144.30 ppm. The signals are sharp and not influenced by spin density transfer of a paramagnetic metal centre. In the solid state, the signals are broadened and shifted to higher frequency due to the influence of the paramagnetic iron centre, which is consistent with spin density transfer through interactions from the cation to the anion. The obtained results are similar to the results observed in literature.[116]

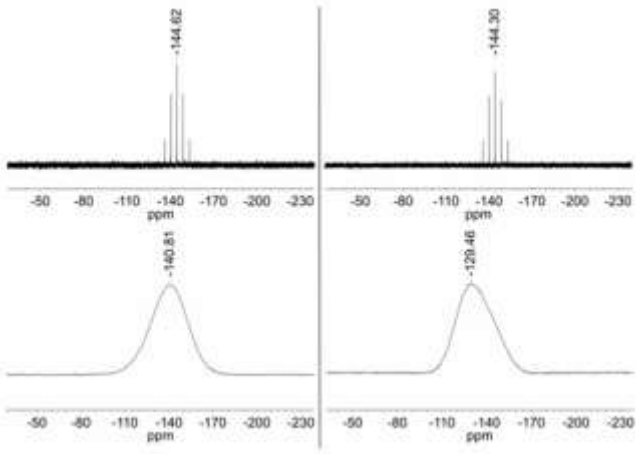


**Figure 25.** Top: $^{31}$P NMR (162 MHz, $CD_3CN$) spectra of **7** and **8**. Bottom: $^{31}$P MAS NMR (121 MHz) spectra of **7** and **8**.[79]

The data of the measurements in solution (SQUID and $^{31}$P NMR spectroscopy) confirm, that an interaction between molecules can be observed in the solid state. The obtained results explain the observed high magnetic susceptibilities values below 100 K and the shifted broadened and shifted signals in the $^{31}$ P NMR spectra. In solution, the dilution causes a breakage of the interaction pathway between the counterions and the cation. The magnetic susceptibilities values are not raised above the room temperature value.

## 2.4 Experiments with nickel and iXa

The complexations of the ligands **iXa** and **iXa-2** were performed with further metal precursors. Already known from preceding work in the Hess group, both ligands can

accommodate $Co^{II}$ ions. The iron compounds in 2.3 were synthesised among other things for oxidation chemistry, but due to the accessible low valent forms by the non-innocence of the ligand, as well proton and $CO_2$ reduction could be pursued. In 1.1.2, nickel compounds with non-innocent ligands, used for proton reduction, are shown. The mentioned nickel complexes, for example Ni(PDI), also show a high efficiency for $CO_2$ reductions compared to other complexes based on abundant metals. As the storage of the electrons for the reduction is a key point for the reactivity, our scaffolds may be suitable in the reductive catalysis. Furthermore, the ionic radius of $Ni^{II}$ ions is smaller compared to $Fe^{II}$ and $Zn^{II}$ ions. The iXa-scaffold already showed that a buckling of the xanthene backbone is necessary to accommodate the zinc ion. Therefore, a coordination of more than one ion might be feasible. Furthermore, seven coordinate nickel compounds, which are not cluster like, are very rare as the $Ni^{II}$ ions prefer a octahedral or tetrahedral geometry. In the following, the attempts to coordinate nickel ions are shown.

**iXa** was complexed with $NiBr_2$(dme), yielding an orange solid (Scheme 21). The NMR of the crude material already suggested a paramagnetic substance; hence a XRD measurement was performed for confirming the structural composition. The result of the XRD measurement showed that the $Ni^{II}$ ion is coordinated in an octahedral geometry structure with a modified iXa-ligand.

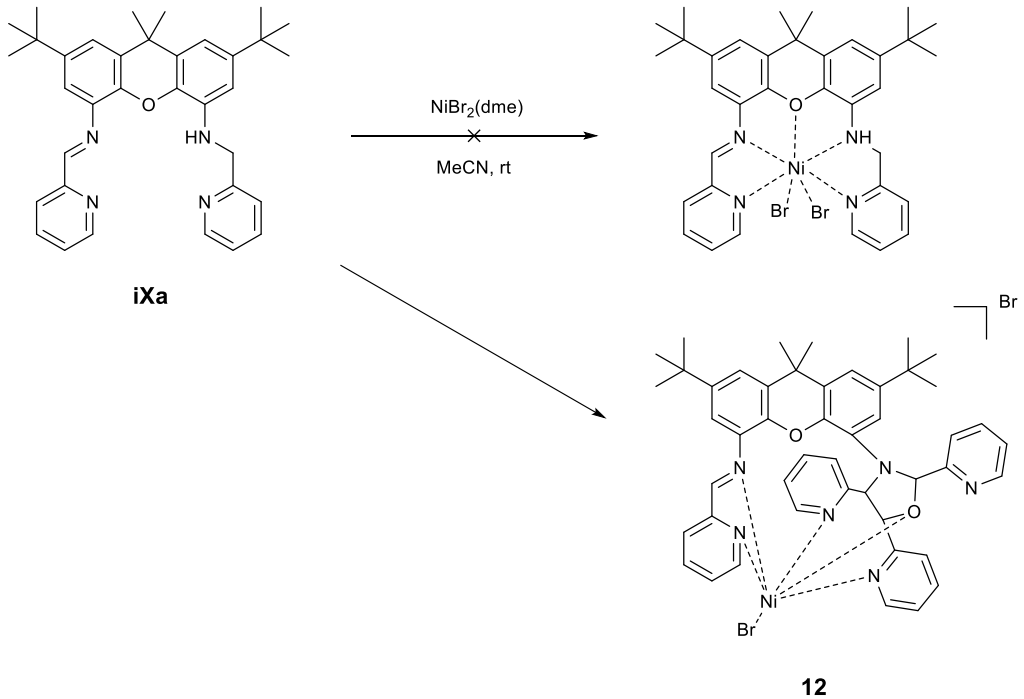


**Scheme 21.** Reaction of iXa with $NiBr_2$(dme).

The ligand was modified in the complexation reaction and only the iminopyridine and the xanthene moiety are still intact in the complex **12**, compared to the **iXa** (Figure 26). The peculiar rearrangement could be explained by the size of the iXa binding site being too large for the accommodation of only one nickel ion or the unfavoured pentadentate coordination. Instead of a methylpyridine group on the amine, a 5-membered ring was formed around the amine, containing an oxygen atom. On the three carbon atoms, pyridine rings are attached. Two of the pyridine nitrogens, N3 and N5, the oxygen atom O2, the two nitrogen of the iminopyridine moiety (N1 and N4) and one of the bromide ions form the octahedral environment of the nickel. The xanthene oxygen (O1), as well as the amine (N2), is not included in the complexation, hence the binding pocket is different from the above mentioned iron and zinc complexes. Nickel-ions and $Ni^0$ catalyse a wide range of organic reactions.[117] The reorganisation of the ligand probably happens *via* a reductive coupling, catalysed by $Ni^{II}$ ions and involves one of the reagents of the ligand synthesis, 2-pyridine carboxaldehyde. Also normally a high conversion in our ligand synthesis is observed, traces of 2-pyridine carboxaldehyde or a reverse condensation reaction of the ligand due to water traces in the solvent cannot be excluded. The imine moiety is still intact in the complex as the C=N bond length is with 1.28 Å in the range of an imine bond. A mechanism of the reaction still has to be determined.

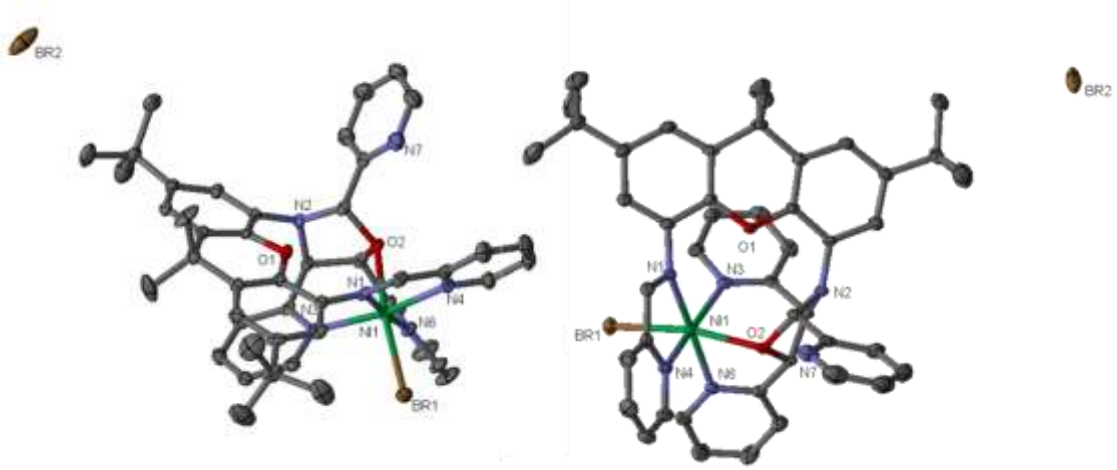


**Figure 26.** Preliminary molecular crystal structure of **12** displayed in different perspectives.

As the one nickel ion is likely either to be too small to be enfolded by the xanthene pocket or prefers a different coordination geometry, the nickel ion does not coordinate in the same binding pocket as iron-, zinc- or cobalt ions, the original idea of a bimetallic compound was picked up. Two equivalents of nickel precursor were added with the aim to get one nickel atom in the iminopyridine-, the other one into the aminopyridine-moiety. Additionally, the attempt was made to insert a $Ni^0$ precursor, $Ni(cod)_2$, to get to a formally $Ni^0$ species, a

reduced species. The comproportionation reactions were also taken into account by inserting $Ni^{II}$ and $Ni^{0}$ precursors simultaneously. As one experiment lead to another, different ratios of the nickel salts were tested in the reactions, which are shown in Table 3.

**Table 3.** Coordination experiments with $NiCl_2$ and $Ni(cod)_2$.

| Experiment | eq. $NiCl_2$ | eq. $Ni(cod)_2$ |
|---|---|---|
| 1 | 2 | 0 |
| 2 | 1 | 1 |
| 3 | 0 | 2 |
| 4 | 1 | 2 |
| 5 | 4 | 0 |
| 6 | 0 | 4 |

From experiment 2 (see Table 3) a crystal was obtained forming the trimetallic compound **13**, shown as molecular structure in Figure 27.

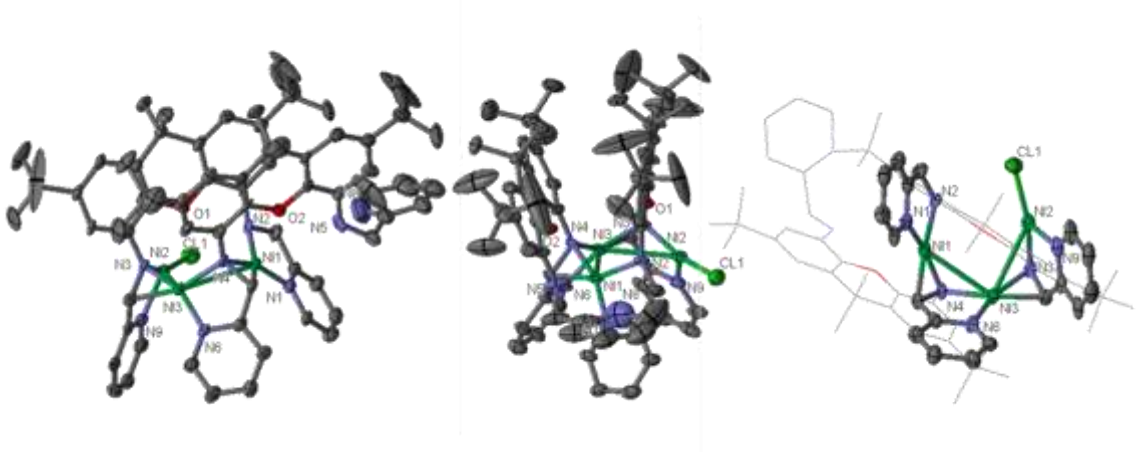


**Figure 27**. Preliminary molecular crystal structure of **13** in different perspectives.

To support the trimetallic structure the ligand deploys a dimer, with one amine moiety not coordinated, which gave rise to the idea that the formation of a tetramer would be feasible. The oxidation states of the nickel ions in dimeric compound remain unclear. Only one chloride counterion can be detected and the overall charge is 0. Noticeably, the imine bond is elongated to 1.44 Å by a back donation of the nickel but has still nearly the character of a double bond as described by Budzlaar and Poffenberger e*t al*.[118-119] All bond lengths and angles of their compounds are comparable with the obtained bond length and angles in the crystal of **13** (bond length are shown in Table 4). The formal $Ni^{0}$ atoms (Ni1 and Ni3)

coordinate in a distorted square planar geometry with on one site the imine and on the other site an amino-pyridine moiety.[120] The environment of Ni2 is best described as trigonal planar with the chloride counterion coordinated. Trigonal planar geometry for $Ni^{I}$ (formed by a comproportionation between $Ni^{II}$ and $Ni^{0}$) is rare but not unknown in the literature.[121] More examples for trigonal planar geometry can be found for $Ni^{0}$ species, but due to the chloride counterion it is unlikely to be $Ni^{0}$.[122-123] The overall Ni-N bond length between Ni2 and N3 or N9 (1.9 -2.0 Å) are too short for a $Ni^{II}$ but too long for a $Ni^{I}$ and in the range of the other observed $Ni^{0}$-N bond length. The distances between the Ni centres of 3 Å is too long for an actual bond but still could allow metal-metal interaction. A charge distribution over the three nickel centres is possible and would explain the intermediate bond length. Therefore, a true oxidation state of each nickel atom cannot be given for sure.

**Table 4:** Bond lengths (Å) of **13**.

| bond | | bond | |
|---|---|---|---|
| Ni1-N1 | 2.021 | Ni3-N3 | 1.881 |
| Ni1-N2 | 1.892 | Ni3-N4 | 1.989 |
| Ni1-N4 | 1.883 | Ni3-N6 | 1.895 |
| Ni1-C58 | 1.969 | Ni3-C27 | 1.923 |
| Ni2-Cl1 | 2.171 | Ni1-Ni3 | 3.038 |
| Ni2-N3 | 1.960 | Ni2-Ni3 | 3.002 |
| Ni2-N9 | 1.950 | Ni1-Ni2 | 3.988 |
| C27-N3 | 1.417 | C58-N4 | 1.435 |

The ligand framework of **iXa** is susceptible to ligand modifications with $Ni^{0}$ and $Ni^{II}$ ions. The high reactivity of the imine bonds, so far one of the outstanding properties of this compound due to non-innocence, is now target of reaction with nickel. Both experiments have to be repeated as the aspects of the reaction still need to be investigated. Especially for the formation of **12** the experiment needs to be performed in thoroughly dried solvents and a high conversion in the ligand synthesis needs to be obtained.

## 2.5 Conclusion

The synthesis of **iXa** and **iXa-2** was in place before this work started and is very well reproducible. A closer examination of the ligands by cyclic voltammetry unveil that both have

a very low (< -2 V) reduction potential. Hence, the ligands are belonging to the group of non-innocent ligands, which can take up at least one electron.

The coordination of only one iron or zinc metal ion was not expected, as data in the literature suggested the coordination of two ions is feasible. The formation of a dimeric structure, to complex more than one metal ion, or a coordination in the outer sphere of the ligand was not observed for iron and zinc. Nickel ions were coordinated in a different binding pocket due to the unfavoured seven-coordinate geometry and forms octahedral compounds. $Ni^0$ forms a cluster like complex with a dimeric structure. The formation of bimetallic complexes is still aim of further studies. A modification of the ligand to increase the space between the imino- and aminopyridine might be feasible by either exchanging the xanthene for a larger backbone or remove the iminopyridine and replace it by a more flexible arm.

The coordination sites of **7** and **8** are in pentagonal bipyramidal geometry. The data obtained for the zinc complexes in the NMR spectroscopy was used to evaluate the iron containing compounds. A loss of ligands with rising temperature for **7**, as described in 2.1, could not be confirmed with the carried out experiments. Further studies, for example the measurement and assignment of the carbon atoms by NMR spectroscopy, have to be performed, which might help to assign the remaining protons, especially protons of MeCN, in the spectra of **7**.

The reduction of the iron containing compounds is probably not reversible for **7**. The first reductive event of the iron compounds is ligand based and cannot be further reversible reduced. The oxidative region is inconclusive but **7** and **8** might be accessible for oxidation reactions. As reported in the introduction not many reactions are noted for seven coordinate iron complexes, but oxo and nitrene reactivity is known.[124-125] The reactivity in the described compounds proceed *via* a labile axial ligand. **8** might be limited in reactivity as the steric hindrance of the pyridines, which does not allow a solvent molecule to coordinate in the seventh binding site, might be too big to allow any molecule to coordinate. In contrast, **7** coordinates two solvent molecules but the lability of the acetonitrile molecules could not be confirmed in NMR experiments. The *cis*-arrangement otherwise could be advantageous for reactivity, as the substrates would bind in close proximity. Furthermore, in comparison to compounds described in the 1.1, the reactivity of the low valent forms can be tested for $CO_2$ and proton reduction. The isolations of reduced or oxidised compounds have to be further pursued as it was not part of this work.

Meanwhile, the intermolecular interactions mediated by the counterions gave interesting low-temperature magnetic behaviour. That is to the best of our knowledge a unique example as the exchange coupling in seven coordinate compounds are normally induced by hydrogen

bonds or covalently linked bridging molecules.[82, 88, 126-128] The compounds are probably not suitable as spin-crossover materials. Because of the interaction of the molecules at low temperature, no change from a low spin to a high spin state was observed. Its use as single-molecule magnetic material is more realistic. Two coupling heptacoordinate $Fe^{II}$ centres have been described by Sutter *et al*. as single-ion magnets and show a slow magnetisation relaxation.[88] Further studies have to be made with **iXa** and **iXa-2** compounds to test them as magnetic materials.

## 2.6 Experimentals

Chemicals were purchased from Sigma Aldrich and used as received unless otherwise noted. Metal compounds were synthesised in an inert atmosphere glove box ($N_2$), using anhydrous solvents. Solvents were dried by passage over activated alumina columns from MBraun and stored over 3 Å (acetonitrile) or 4 Å molecular sieves. $[Fe(CH_3CN)_6](PF_6)_2$,[129] 4,5-Dibromo-2,7-di-*tert*-butyl-9,9-dimethylxanthene (**1**),[130] 2,7-Di-*tert*-butyl-9,9-dimethyl-4,5-xanthene dicarboxylic acid (**2**) [130] and 2,7-Di-*tert*-butyl-9,9-dimethyl-4,5-xanthene diamine (**3**) [131] were prepared as described in the literature. Additionally, the experimental procedures below are described as in the publication of Hess *et al*.[79]

Solution state NMR spectra were recorded on Bruker Avance-400 or Bruker Avance Ultrashield (400 MHz $^1H$, 100 MHz $^{13}C$, 162 MHz $^{31}P$), Bruker Avance Ultrashield (500 MHz $^1H$, 126 MHz $^{13}C$), Varian VNMRS-600 (600 MHz $^1H$, 151 MHz $^{13}C$) or Varian VNMRS-500 (500 MHz $^1H$, 126 MHz $^{13}C$) spectrometers. Solid state NMR spectra for $^{31}P$ were recorded using a Bruker Avance 300 (121 MHz $^{31}P$) spectrometer equipped with a 2.5 mm BBMAS probe head at a rotation frequency of 20 kHz and referenced to $(NH_4)H_2PO_4$ ($\delta$ ($^{31}P$) = 1.1 ppm) as an external standard at 298 K. $ZrO_2$ rotors of 2.5 mm were packed under argon and sealed with Kel-F caps. The FIDs were sampled after applying single pulses. Electronic spectra were recorded on an Agilent Cary 60 UV-visible spectrophotometer. ESI mass spectra were measured using a Waters TQD instrument or on a Xevo QToF for high-resolution spectra (atmospheric pressure solids analysis probe ionization experiments (ASAP)). Microanalyses were carried out at the London Metropolitan University or at the Technische Universität München. Electrochemical measurements were carried out using an $EmStat^{3+}$ potentiostat using a three-electrode cell equipped with a glassy carbon working electrode and Pt wire as counter and reference electrodes. Potentials are reported with reference to an internal standard of ferrocenium/ferrocene ($Fc^{+/0}$).

Magnetic susceptibility data collected on solid samples were recorded using a MPMS XL 5 (Quantum Design) superconducting quantum interference device (SQUID) magnetometer with liquid Helium cooling in a temperature range of 1.8 – 300 K and magnetic field of 0.1 T. The samples were placed in a calibrated gelatine capsule, fixed in the centre of a plastic straw.

Magnetic susceptibility data (2−290 K) for solution samples were recorded using a SQUID magnetometer (MPMS7, Quantum Design) in a 1 T external field. Data were corrected for underlying diamagnetism using tabulated Pascal's constants, a solvent correction was applied, and the data fit using julX (Dr E. Bill, MPI for Energy Conversion). The samples were dissolved in acetonitrile (~ 0.5 mM) and sealed in glass tubes under Argon.

Crystallographic data were collected on an X-ray single crystal diffractometer equipped with a CCD detector (Bruker APEX II, κ-CCD), a rotating anode (Bruker AXS, FR591) with $MoK_\alpha$ radiation (λ = 0.71073 Å) and a MONTEL mirror optic by using the APEX software package.[132] The measurements were performed on a single crystal coated with perfluorinated ether. The crystal was fixed on top of a glass fiber and transferred to the diffractometer. The crystal was frozen under a stream of cold nitrogen. A matrix scan was used to determine the initial lattice parameters. Reflections were merged and corrected for Lorenz and polarisation effects, scan speed, and background using SAINT.[133] Absorption corrections, including odd and even ordered spherical harmonics were performed using SADABS.[133] Space group assignments were based upon systematic absences, E statistics, and successful refinement of the structures. Structures were solved by direct methods with the aid of successive difference Fourier maps, and were refined against all data using SHELXLE[134] in conjunction with SHELXL-2014[135]. Hydrogen atoms were assigned to ideal positions and refined using a riding model with an isotropic thermal parameter 1.2 times that of the attached carbon atom (1.5 times for methyl hydrogen atoms). If not mentioned otherwise, non-hydrogen atoms were refined with anisotropic displacement parameters. Full-matrix least-squares refinements were carried out by minimising $\Sigma w(F_o^2-F_c^2)^2$ with SHELXL-97[136] weighting scheme. Neutral atom scattering factors for all atoms and anomalous dispersion corrections for the non-hydrogen atoms were taken from International Tables for Crystallography.[137] Images of the crystal structures were generated by PLATON.[138-139]

Density Functional Theory (DFT) calculations were performed with the ORCA program package.[140] Geometry optimizations of the complexes were performed at the B3LYP[141-143] level of DFT. The all-electron Gaussian basis sets were those developed by Ahlrich's group.[144-145] Triple-ζ quality basis sets were TZV(P) with one set of polarization functions on the metals and on the atoms directly coordinated to the metal centre was used.[145] For the

carbon and hydrogen atoms, slightly smaller polarized split-valence SV(P) basis sets were used that were of double-ζ quality in the valence region and contained a polarizing set of d functions on the non-hydrogen atoms. Auxiliary basis sets used to expand the electron density in the resolution-of-the-identity (RI) approach were chosen,[146-147] where applicable, to match the orbital basis. SCF calculations were tightly converged ($1 \times 10^{-8}$ $E_h$ in energy, $1 \times 10^{-7}$ $E_h$ in the density change, and $1 \times 10^{-7}$ $E_h$ in maximum element of the DIIS error vector). Geometry optimizations for all complexes were carried out in redundant internal coordinates without imposing symmetry constraints. In all cases the geometries were considered converged after the energy change was less than $5 \times 10^{-6}$ $E_h$, the gradient norm and maximum gradient element were smaller than $1 \times 10^{-4}$ and $3 \times 10^{-4}$ $E_h$ $Bohr^{-1}$, respectively, and the root-mean square and maximum displacements of all atoms were smaller than $2 \times 10^{-3}$ and $4 \times 10^{-3}$ Bohr, respectively. For **4**, the acetonitrile ligands were constrained in the geometry optimizations. Single-point calculations on the non-optimised structures, using the coordinates obtained crystallographically, also were carried out using the B3LYP functional, for comparison. Orbital and spin density plots were created using VMD.[148]

***tert*-butyl (5-amino-2,7-di-*tert*-butyl-9,9-dimethyl-xanthen-4-yl)carbamate, 4**

di-*tert*-butylcarbonate (1.1 g, 4.9 mmol) and guanidine·HCl (60 mg, 0.6 mmol) was added to a solution of 2,7-Di-*tert*-butyl-9,9-dimethyl-4,5-xanthene diamine (**3**) (1.4 g, 4.1 mmol) in ethanol (250 mL) at 40 °C and stirred for 1 h. The solvent was removed in vacuo. The crude product was purified by column chromatography (ethyl acetate:hexane = 1:4, $R_f$ = 0.45) to give a colourless solid (1.2 g, 63% yield). $^1$H NMR $\delta$ (400 MHz, $CDCl_3$) 7.95 (s, 1H), 7.10 (d, *J* = 2.2 Hz, 1H), 6.91 (s, 1H), 6.86 (d, *J* = 2.2, 1H), 6.72 (d, *J* = 2.2 Hz, 1H), 3.87 (s, 2H), 1.62 (s, 6H), 1.56 (s, 9H), 1.35 (s, 9H), 1.31 (s, 9H); $^{13}$C NMR $\delta$ (100 MHz, $CDCl_3$) 153.0, 146.2, 145.6, 137.5, 136.4, 133.6, 129.9, 129.4, 125.7, 116.5, 115.0, 112.7, 111.5, 80.7, 34.9, 34.8, 34.6, 32.1, 31.7, 31.6, 31.1, 28.6; IR ($cm^{-1}$, neat) 3360, 2962, 1688, 1626, 1494, 1429, 1359, 1285, 1227, 1159, 1063, 856, 768; LRMS ($ESI^+$) *m/z*: 453.24 $[M + H]^+$, 475.14 $[M + Na]^+$; HRMS ($ESI^+$) *m/z*: 453.2410 $[M + H]^+$.

***tert*-butyl (2,7-di-*tert*-butyl-9,9-dimethyl-5-((pyridin-2-ylmethyl)amino)-xanthen-4-yl), 5a and *tert*-butyl (5-(bis(pyridin-2-ylmethyl)amino)-2,7-di-*tert*-butyl-9,9-dimethyl-xanthen-4-yl)carbamate, 5b**

(2-Chloromethyl)pyridine hydrochloride (2.2 g, 13.2 mmol)) were added to a suspension of **4** (2.0 g, 4.4 mmol) and $K_2CO_3$ (2.4 g, 17.6 mmol in a 1:2 ethanol/water mixture (45 mL). The reaction mixture was heated to 100 °C for 4 h. The suspension was cooled to room temperature. The reaction mixture was filtered over celite and the residue washed with ethyl acetate. The solvent was removed in vacuo and the crude product purified by column

chromatography (ethyl acetate:hexane = 1:2 → 1:1, **5b** $R_f$ (ethyl acetate:hexane = 1:2) = 0.41, **5a** $R_f$ (ethyl acetate:hexane = 1:1) = 0.39) to give the two products as light yellow solids (**5a**: 1.7 g, 86%; **5b**: 0.4 g, 14%). **5a:** $^1$H NMR $\delta$ (400 MHz, $CDCl_3$) 8.69 (d, *J* = 4.5 Hz, 1H), 7.96 (s, 1H), 7.67 (td, *J* = 7.7 Hz, *J* = 1.8 Hz, 1H), 7.38 (d, *J* = 7.8 Hz, 1H), 7.20 (t, *J* = 5.9 Hz, 2H), 7.11 (d, *J* = 2.2 Hz, 1H), 6.81 (d, *J* = 2.1 Hz, 1H), 6.60 (d, *J* = 2.1 Hz, 1H), 4.57 (s, 2H), 1.63 (s, 6H), 1.56 (s, 9H), 1.36 (s, 9H), 1.29 (s, 9H); $^{13}$C NMR $\delta$ (100 MHz, $CDCl_3$) 158.3, 153.3, 149.3, 146.2, 145.5, 137.9, 136.9, 136.4, 135.9, 129.7, 129.0, 125.8, 122.2, 121.9, 116.5, 115.4, 110.9, 107.5, 80.5, 49.7, 34.90, 34.88, 34.80, 32.0, 31.72, 31.68, 28.6; IR ($cm^{-1}$, neat) 3456, 2963, 1732, 1626, 1537, 1422, 1364, 1283, 1224, 1151, 1075, 999, 884, 770; LRMS ($ESI^+$) *m/z*: 544.4 $[M + H]^+$, 566.3 $[M + Na]^+$; HRMS ($ESI^+$) *m/z*: 544.3539 $[M + H]^+$. **5b**: $^1$H NMR $\delta$ (400 MHz, $CDCl_3$) 8.56–8.58 (m, 2H), 8.34 (s, 1H), 7.99 (d, *J* = 1.8 Hz, 1H), 7.52 (td, *J* = 7.7 Hz, *J* = 1.8 Hz, 2H), 7.29 (d, *J* = 7.8 Hz, 2H), 7.07–7.10 (m, 3H), 7.03 (d, *J* = 2.2 Hz, 1H), 6.86 (d, *J* = 2.2 Hz, 1H), 4.51 (s, 4H), 1.62 (s, 6H), 1.50 (s, 9H), 1.37 (s, 9H), 1.16 (s, 9H); $^{13}$C NMR $\delta$ (100 MHz, $CDCl_3$) 158.8, 153.7, 149.3, 145.7, 145.3, 142.6, 138.4, 137.8, 136.4, 130.6, 130.0, 126.6, 123.1, 122.0, 118.4, 116.5, 115.7, 115.4, 80.2, 59.1, 35.2, 35.0, 34.7, 31.8, 31.49, 31.46, 28.6; IR ($cm^{-1}$, neat) 3455, 2965, 1618, 1534, 1435, 1364, 1231, 1159, 1066, 981, 866, 732; LRMS ($ESI^+$) *m/z*: 635.4 $[M + H]^+$, 657.4 $[M + Na]^+$; HRMS ($ESI^+$) *m/z*: 635.3978 $[M + H]^+$.

**2,7-di-*tert*-butyl-9,9-dimethyl-*N*-(pyridin-2-ylmethyl)-xanthene-4,5-diamine, 6a**

Concentrated HCl (10.0 mL) was added slowly to a solution of **5a** (171 mg, 0.31 mmol) in ethyl acetate (10.0 mL). The resultant white suspension was stirred at room temperature for 1 h, after which time the mixture turned clear. The solution was basified (pH 14) by slowly adding 10% aqueous NaOH solution (200 mL). The product was extracted with ethyl acetate (3 × 20 mL). The combined organic layers were washed with brine (30 mL), dried over $MgSO_4$ and the solvent removed in vacuo to give a brown oil. (140 mg, 98% yield) **6a**: $^1$H NMR $\delta$ (400 MHz, $CDCl_3$) 8.60 (d, *J* = 4.2 Hz, 1H), 7.64 (td, *J* = 7.7 Hz, *J* = 1.7 Hz, 1H), 7.38 (d, *J* = 7.8 Hz, 1H), 7.17–7.20 (m, 1H), 6.85 (d, *J* = 2.2 Hz, 1H), 6.79 (d, *J* = 2.1 Hz, 1H), 6.71 (d, *J* = 2.2 Hz, 1H), 6.54 (d, *J* = 2.1 Hz, 1H), 4.57 (s, 2H), 1.63 (s, 6H), 1.31 (s, 9H), 1.26 (s, 9H); $^{13}$C NMR $\delta$ (100 MHz, $CDCl_3$) 159.0, 149.3, 145.7, 145.6, 136.9, 136.8, 136.5, 135.8, 133.7, 130.0, 128.9, 122.2, 121.8, 112.5, 111.2, 110.9, 107.0, 49.7, 34.9, 34.8, 34.6, 32.0, 31.69, 31.68; $R_f$ (EtOAc:hexane = 1:1) 0.32; IR ($cm^{-1}$, neat) 3349, 2952, 1632, 1520, 1494, 1445, 1422, 1360, 1286, 1224, 1167, 1093, 1046, 858, 840, 738; LRMS ($ESI^+$) *m/z*: 444.3 $[M + H]^+$, 466.1 $[M + Na]^+$; HRMS ($ESI^+$) 444.3014 $[M + H]^+$.

**2,7-di-*tert*-butyl-9,9-dimethyl-*N*,*N*-bis(pyridin-2-ylmethyl)-xanthene-4,5-diamine, 6b**

was prepared from **5b** according to a procedure similar to that described for the synthesis of **6a. 6b** was obtained as a yellow-brown oil in 98% yield. $^{1}$H NMR $\delta$ (400 MHz, $CDCl_3$) 8.52–8.54 (m, 2H), 7.55 (td, *J* = 7.6 Hz, *J* = 1.8 Hz, 2H), 7.49 (d, *J* = 7.8 Hz, 2H), 7.07–7.11 (m, 2H), 7.00 (d, *J* = 2.2 Hz, 1H), 6.85 (d, *J* = 2.2 Hz, 1H), 6.80 (d, *J* = 2.2 Hz, 1H), 6.65 (d, *J* = 2.2 Hz, 1H), 4.58 (s, 4H), 1.62 (s, 6H), 1.30 (s, 9H), 1.14 (s, 9H); $^{13}$C NMR $\delta$ (100 MHz, $CDCl_3$) 159.4, 149.2, 145.9, 144.6, 142.2, 137.1, 136.7, 136.6 , 134.4, 130.4, 130.0, 122.6, 122.0, 117.2, 116.1, 111.4, 110.8, 59.0, 35.0, 34.6, 34.5, 32.0, 31.7, 31.4; $R_f$ (EtOAc) 0.49; IR ($cm^{-1}$, neat) 3324, 2962, 1625, 1591, 1474, 1432, 1361, 1279, 1211, 1162, 999, 909, 852, 756, 730; LRMS ($ESI^+$) *m/z*: 535.3 $[M + H]^+$, 557.3 $[M + Na]^+$; HRMS ($ESI^+$) *m/z*:, 535.3426 $[M + H]^+$.

**2,7-di(*tert*-butyl)-9,9-dimethyl-*N*-(pyridin-2-ylmethyl)-5-((pyridin-2-ylmethylene) amino)-xanthen-4-amine, iXa**

2-Pyridine carboxaldehyde (0.1 mL, 1.0 mmol) was added to a solution of **6a** (443 mg, 1.0 mmol) in toluene (10 mL) over molecular sieves (4 Å). The reaction mixture was heated at 120 °C for 5 h. The solution was filtered and the solvent was evaporated to give a yellow solid (0.522 g, 98% yield). $^{1}$H NMR $\delta$ (600 MHz, $CDCl_3$) 8.75 (s, 1H, $H_6$), 8.69 (d, *J* = 4.5 Hz, 1H, $H_1$), 8.44 (d, *J* = 4.3 Hz, 1H, $H_{31}$), 8.26 (d, *J* = 7.9 Hz, 1H, $H_4$), 7.71 (td, *J* = 7.7 Hz, *J* = 1.3 Hz, 1H, $H_3$), 7.55 (td, *J* = 7.7 Hz, *J* = 1.7 Hz, 1H $H_{29}$), 7.39 (d, *J* = 7.8 Hz, 1H, $H_{28}$), 7.34–7.37 (m, 2H, $H_{2/8}$), 7.12 (dd, *J* = 6.0 Hz, *J* = 1.5 Hz, 1H, $H_{30}$), 7.06 (d, *J* = 2.2 Hz, 1H, $H_{12}$), 6.78 (d, *J* =2.0 Hz, 1H, $H_{23}$), 6.52 (d, *J* = 2.0 Hz, 1H, $H_{18}$), 5.27 (s, 1H, $H_{25}$), 4.54 (s, 2H, $H_{26}$), 1.68 (s, 6H, $H_{15}$), 1.36 (s, 9H, $H_{11}$), 1.26 (s, 9H, $H_{22}$); $^{13}$C NMR $\delta$ (151 MHz, $CDCl_3$) 161.7 ($C_6$), 159.5 ($C_{27}$), 155.2 ($C_5$), 149.7 ($C_4$), 149.2 ($C_{31}$), 146.0 ($C_{18}$), 145.7 ($C_{17}$), 141.6 ($C_9$), 138.8 ($C_7$), 136.8 ($C_3$), 136.6 ($C_{29}$), 136.5 ($C_{20}$), 136.1 ($C_{24}$), 131.3 ($C_{13}$), 128.8 ($C_{16}$), 125.1 ($C_2$), 121.9 ($C_{30}$), 121.5 ($C_{28}$), 120.8 ($C_8$), 115.3 ($C_{12}$), 110.1 ($C_{23}$), 106.6 ($C_{19}$), 50.0 ($C_{26}$), 35.1 ($C_{14}$), 34.8 ($C_{10}$), 34.8 ($C_{21}$), 31.7 ($C_{15}$), 31.6 ($C_{11/22}$); IR ($cm^{-1}$, neat) 3412, 2962, 1622, 1584, 1519, 1477, 1425, 1362, 1246, 1218, 1148, 1117, 1092, 998, 863, 778, 753; LRMS ($ESI^+$) *m/z:* 533.16 $[M + H]^+$, 554.98 $[M + Na]^+$; HRMS (ASAP) *m/z:* 533.3260 $[M + H]^+$.

**2,7-di(*tert*-butyl)-9,9-dimethyl-*N*,*N*-bis(pyridin-2-ylmethyl)-5-((pyridin-2-ylmethylene) amino)-xanthen-4-amine, iXa-2**

The synthesis of **iXa-2** from **6b** was as described for the preparation of **iXa.** Yield 91%. $^{1}$H NMR $\delta$ (600 MHz, $CDCl_3$) 8.79 (s, 1H, $H_6$), 8.69 (d, *J* = 4.5 Hz, 1H, $H_1$), 8.43 (ddd, *J* = 4.9 Hz, *J* = 1.6 Hz, *J* = 0.9 Hz, 1H, $H_{31}$), 8.21 (d, *J* = 7.9 Hz, *J* = 0.9 Hz, 1H, $H_4$), 7.67 (tdd, *J* = 7.7 Hz, *J* = 1.6 Hz, *J* = 0.5 Hz, 1H, $H_3$), 7.28–7.36 (m, 6H, $H_{8/28/2/29}$), 7.05 (d, *J* = 2.3 Hz, 1H, $H_{12}$),

7.01 (d, *J* = 2.2 Hz, 1H, $H_{23}$), 6.97 (tdd, *J* = 6.0 Hz, *J* = 1.9 Hz, *J* = 1.4 Hz, 2H, $H_{30}$), 6.71 (d, *J* = 2.2 Hz, 1H, $H_{19}$), 4.65 (s, 4H, $H_{26}$), 1.68 (s, 6H, $H_{15}$), 1.37 (s, 9H, $H_{11}$), 1.14 (s, 9H $H_{22}$); $^{13}$C NMR $\delta$ (151 MHz, $CDCl_3$) 161.7 ($C_6$), 159.6 ($C_{27}$), 155.0 ($C_5$), 149.6 ($C_1$), 148.8 ($C_{31}$), 145.9 ($C_{17}$), 145.2 ($C_{18}$), 142.5 ($C_{20}$), 141.9 ($C_9$), 139.3 ($C_7$), 137.2 ($C_{24}$), 136.9 ($C_3$), 136.1 ($C_{29}$), 131.3 ($C_{13}$), 130.2 ($C_{19}$), 125.1 ($C_2$) 122.9 ($C_4$), 121.9 ($C_{29}$), 121.6 ($C_{30}$), 120.5 ($C_8$), 119.0 ($C_{19}$), 115.7 ($C_{23}$), 115.4 ($C_{12}$), 58.4 ($C_{26}$), 35.2 ($C_{14}$), 34.9 ($C_{10}$), 34.6 ($C_{21}$), 31.9 ($C_{15}$), 31.7 ($C_{11/22}$), 31.5; IR ($cm^{-1}$, neat) 3060, 2958, 1587, 1488, 1456, 1275, 1261; LRMS ($ESI^+$) *m/z*: 624.3 $[M + H]^+$; HRMS (ASAP) *m/z*: 624.3719$[M + H]^+$.

**[Fe(iXa)($CH_3CN$)$_2$]($PF_6$)$_2$, 7**

$Fe(CH_3CN)_6(PF_6)_2$ (119 mg, 0.20 mmol) was added to a solution of **iXa** (102 mg, 0.19 mmol) in acetonitrile (5 mL) and stirred for 72 h at room temperature. Single crystals were obtained by slow diffusion of diethyl ether into a concentrated solution of **7**, yielding red-brown crystals (140 mg, 81%). Anal. Calcd. for $C_{39}H_{46}F_{12}FeN_6OP_2$:C, 48.76; H, 4.83; N, 8.75. Found: C, 48.69; H, 4.93; N, 8.87; UV/VIS $\lambda_{max}$ ($CH_3CN$)/nm 328, 381 and 493 ($\varepsilon/M^{-1}cm^{-1}$ 18,960, 10,700 and 650).

**[Fe(iXa-2)]($PF_6$)$_2$, 8**

The compound was prepared according to a procedure similar to that described for **7,** yielding green crystals of **8**. Yield: 74%; Anal. Calcd. for $C_{43}H_{48}F_{12}FeN_6OP_2$:C, 50.79; H, 4.68; N, 7.22. Found: C, 50.65; H, 4.64; N, 7.27; UV/VIS $\lambda_{max}$ ($CH_3CN$)/nm 329, 377 and 548 ($\varepsilon/M^{-1}cm^{-1}$ 13,880, 8,250 and 600), LRMS ($ESI^+$ *m/z*) $[M]^{2+}$ 339.96.

**[Zn(iXa)($OTf$)$_2$], 9**

$Zn(OTf)_2$ (68 mg, 0.19 mmol) was added to a solution of **iXa** (100 mg, 0.19 mmol) in acetonitrile (5 mL) and stirred for 4 h at room temperature. Single crystals were obtained by slow diffusion of pentane into a concentrated solution of **9** in dichloromethane, yielding light yellow crystals (95 mg, 56%). Anal. Calcd. for $C_{37}H_{40}F_6N_4O_7S_2Zn$:C, 49.59; H, 4.50; N, 6.25. Found: C, 49.66; H, 4.48; N, 6.27; UV/VIS $\lambda_{max}$ ($CH_3CN$)/nm 334 and 388 ($\varepsilon/M^{-1}cm^{-1}$ 14,960 and 8,450), $^1$H NMR $\delta$ (500 MHz, $C_2D_2Cl_4$) 9.39 (s, 1H, $H_6$), 8.66 (d, *J* = 4.9 Hz, 1H, $H_1$), 8.27 (d, *J* = 7.7 Hz, 1H, $H_4$), 8.20 (td, *J* = 7.7 Hz, *J* = 1.4 Hz, 1H, $H_3$), 7.83 (d, *J* = 7.8 Hz, 1H, $H_{29}$), 7.81 (d, *J* =1.8 Hz, 1H, $H_8$), 7.79 (d, *J* = 5.3 Hz, 1H, $H_{31}$), 7.66 (td, *J* = 6.0 Hz, *J* = 0.7 Hz, 1H, $H_2$), 7.50 (d, *J* = 1.7 Hz, 1H, $H_{12}$), 7.37-7.33 (m, 3H, $H_{23/28/19}$), 7.30 (t, *J* = 6.5 Hz, 1H, $H_{30}$), 5.65 (d, *J* = 7.6 Hz, 1H, $H_{25}$), 5.08 (dd, *J* = 7.6 Hz, *J* = 17.0 Hz, 1H, $H_{26}$), 4.38 (d, *J* = 17.0 Hz, 1H, $H_{26'}$), 1.68 (s, 3H, $H_{15}$), 1.39 (s, 1H, $H_{15'}$), 1.34 (s, 9H, $H_{11}$), 1.29 (s, 9H, $H_{22}$); $^{13}$C NMR $\delta$ (126 MHz, $C_2D_2Cl_4$) 154.68 ($C_6$), 154.48 ($C_{27}$), 150.36 ($C_4$), 149.74 ($C_9$), 149.31 ($C_{20}$), 147.28 ($C_5$), 146.87 ($C_{28}$), 142.73, 142.00 ($C_3$), 141.69 ($C_{29}$), 141.43, 132.84, 131.73 ($C_{24}$), 131.72,

130.18 ($C_2$), 129.77 ($C_1$), 128.70 ($C_7$), 126.08 ($C_{12}$), 125.96 ($C_{31}$), 124.49 ($C_{30}$), 122.26 ($C_{19}$), 122.01 ($C_{23}$), 113.61 ($C_8$), 55.22 ($C_{26}$), 36.15 ($C_{14}$), 35.54 ($C_{10}$), 35.29 ($C_{21}$), 32.22 ($C_{15}$), 31.70 ($C_{22}$), 31.60 ($C_{11}$), 28.37 ($C_{15}$).

**[Zn(iXa-2)](OTf$_6$)$_2$, 10**

The synthesis, using **iXa-2** and Zn(OTf)$_2$, was analogous to the procedure described for **9**. Slow diffusion of pentane into a concentrated solution of **10** in dichloromethane yielded yellow crystals. Yield: 46%; Anal. Calcd. for $C_{43}H_{45}F_6N_5O_7S_2Zn$:C, 52.31; H, 4.59; N, 7.09. Found: C, 52.20; H, 4.69; N, 7.03; UV/VIS $\lambda_{max}$ ($CH_3CN$)/nm 340 and 394 ($\varepsilon/M^{-1}cm^{-1}$ 15,860 and 8,470), $^1$H NMR $\delta$ (500 MHz, $CD_3CN$) 9.83 (s, 1H, $H_6$), 8.69 (d, *J* = 4.9 Hz, 1H, $H_1$), 8.42 (m, 2H, $H_{3/4}$), 8.06 (d, *J* = 2.0 Hz, 1H, $H_8$), 8.00-7.96 (m, 3H, $H_{29/23}$), 7.86 (d, *J* = 5.2 Hz, 2H, $H_{31}$), 7.83 (q, *J* = 4.7 Hz, 1H, $H_2$), 7.66 (d, *J* = 1.9 Hz, 1H, $H_{12}$), 7.53 (d, *J* = 7.9 Hz, 2H, $H_{28}$), 7.48 (d, *J* = 2.1 Hz, 1H, $H_{19}$), 7.33 (t, *J* = 6.5 Hz, 2H, $H_{30}$), 5.11 (d, *J* = 16.7 Hz, 2H, $H_{26}$), 5.06 (d, *J* = 16.7 Hz, 2H, $H_{26'}$), 1.53 (s, 6H, $H_{15}$), 1.42 (s, 9H, $H_{11}$), 1.39 (s, 9H, $H_{22}$); $^{13}$C NMR $\delta$ (126 MHz, $CD_3CN$) 159.74 ($C_6$), 156.25 ($C_{27}$), 151.34 ($C_1$), 150.67 ($C_{20}$), 149.34 ($C_9$), 148.62 ($C_5$), 148.45 ($C_{31}$), 143.30 ($C_4$), 142.98 ($C_{30}$), 141.54, 140.84, 137.11 ($C_{24}$), 132.05, 131.36 ($C_2$), 131.25 ($C_3$), 129.25 ($C_7$), 127.87 ($C_{12}$), 126.47 ($C_{29}$), 125.63 ($C_{28}$), 124.70 ($C_{19}$), 122.62 ($C_{23}$), 115.12 ($C_8$), 63.99 ($C_{26}$), 35.96 ($C_{21}$), 35.94 ($C_{10}$), 35.90 ($C_{14}$), 32.14 ($C_{15}$), 31.40 ($C_{22}$), 31.39 ($C_{11}$).

## 2.7 References


76. Panunzi, A.; Giordano, F.; Orabona, I.; Ruffo, F. *Inorg. Chim. Acta* **2005,** *358*, 1217-1224.
77. Bheemaraju, A.; Beattie, J. W.; Danylyuk, Y.; Rochford, J.; Groysman, S. *Eur. J. Inorg. Chem.* **2014,** *2014*, 5865-5873.
78. Takano, S.; Takeuchi, D.; Osakada, K.; Akamatsu, N.; Shishido, A. *Angew. Chem. Int. Ed.* **2014,** *53*, 9246-9250.
79. Haas, R. M.; Arshad, M.; Anthony, J.; Altmann, P. J.; Pothig, A.; Kohler, F. H.; Hess, C. R. *Inorganic Chemistry Frontiers* **2016,** *3*, 616-629.
81. Casanova, D.; Alemany, P.; Bofill, J. M.; Alvarez, S. *Chem.– Eur. J.* **2003,** *9*, 1281-1295.
82. Drahoš, B.; Herchel, R.; Trávníček, Z. *Inorg. Chem.* **2015,** *54*, 3352-3369.
83. Villafañe, F. *Coord. Chem. Rev.* **2014,** *281*, 86-99.
84. Nelson, S. M.; McIlroy, P. D. A.; Stevenson, C. S.; Konig, E.; Ritter, G.; Waigel, J. *J. Chem. Soc., Dalton Trans.* **1986**, 991-995.
85. Grau, M.; England, J.; Torres Martin de Rosales, R.; Rzepa, H. S.; White, A. J. P.; Britovsek, G. J. P. *Inorg. Chem.* **2013,** *52*, 11867-11874.
86. Lonnon, D. G.; Ball, G. E.; Taylor, I.; Craig, D. C.; Colbran, S. B. *Inorg. Chem.* **2009,** *48*, 4863-4872.
87. Hoffmann, R.; Beier, B. F.; Muetterties, E. L.; Rossi, A. R. *Inorg. Chem.* **1977,** *16*, 511-522.
88. Bar, A. K.; Pichon, C.; Gogoi, N.; Duhayon, C.; Ramasesha, S.; Sutter, J.-P. *Chem. Commun.* **2015,** *51*, 3616-3619.
89. Craig, G. A.; Barrios, L. A.; Costa, J. S.; Roubeau, O.; Ruiz, E.; Teat, S. J.; Wilson, C. C.; Thomas, L.; Aromi, G. *Dalton Trans.* **2010,** *39*, 4874-4881.
90. Morgenstern-Badarau, I.; Lambert, F.; Philippe Renault, J.; Cesario, M.; Maréchal, J.-D.; Maseras, F. *Inorg. Chim. Acta* **2000,** *297*, 338-350.
91. Koenig, E.; Ritter, G.; Dengler, J.; Nelson, S. M. *Inorg. Chem.* **1987,** *26*, 3582-3588.
92. Bonhommeau, S.; Guillon, T.; Lawson Daku, L. M.; Demont, P.; Sanchez Costa, J.; Létard, J.-F.; Molnár, G.; Bousseksou, A. *Angew. Chem. Int. Ed.* **2006,** *45*, 1625-1629.
93. Hayami, S.; Gu, Z.-z.; Einaga, Y.; Kobayasi, Y.; Ishikawa, Y.; Yamada, Y.; Fujishima, A.; Sato, O. *Inorg. Chem.* **2001,** *40*, 3240-3242.
94. Costa, J. S.; Balde, C.; Carbonera, C.; Denux, D.; Wattiaux, A.; Desplanches, C.; Ader, J.-P.; Gütlich, P.; Létard, J.-F. *Inorg. Chem.* **2007,** *46*, 4114-4119.
95. Zhang, D.; Busch, D. H.; Lennon, P. L.; Weiss, R. H.; Neumann, W. L.; Riley, D. P. *Inorg. Chem.* **1998,** *37*, 956-963.
96. Gutman, C. T.; Brunold, T. C. *Inorg. Chem.* **2012,** *51*, 12729-12737.
97. Liu, G.-F.; Filipović, M.; Heinemann, F. W.; Ivanović-Burmazović, I. *Inorg. Chem.* **2007,** *46*, 8825-8835.
98. Nowick, J. S.; Ballester, P.; Ebmeyer, F.; Rebek, J. *J. Am. Chem. Soc.* **1990,** *112*, 8902-8906.
99. Bühlmann, P.; Nishizawa, S.; Xiao, K. P.; Umezawa, Y. *Tetrahedron* **1997,** *53*, 1647-1654.
100. Hamann, B. C.; Branda, N. R.; Rebek, J. *Tetrahedron Letters* **1993,** *34*, 6837-6840.
101. Haack, P.; Limberg, C.; Ray, K.; Braun, B.; Kuhlmann, U.; Hildebrandt, P.; Herwig, C. *Inorg. Chem.* **2011,** *50*, 2133-2142.
102. Siewert, I.; Limberg, C., A Xanthene-based Ligand with Two Adjacent Malonate Binding Sites. In *Z. Naturfor. B*, 2007; Vol. 62, p 1251.
103. McQuade, L. E.; Lippard, S. J. *Inorg. Chem.* **2010,** *49*, 7464-7471.
104. Barcena, H. S.; Liu, B.; Mirkin, M. V.; Canary, J. W. *Inorg. Chem.* **2005,** *44*, 7652-7660.
105. Medlycott, E. A.; Hanan, G. S. *Chem. Commun.* **2007**, 4884-4886.
106. Kissinger, P. T.; Heineman, W. R. *J. Chem. Edu.* **1983,** *60*, 702.
107. Köhler, F. H., Probing Spin Densities by Use of NMR Spectroscopy. In *Magnetism: Molecules to Materials I*, Wiley-VCH Verlag GmbH & Co. KGaA: 2003; pp 379-430.
108. Vaara, J. *Phys. Chem. Chem. Phys.* **2007,** *9*, 5399-5418.

109. Aquino, F.; Pritchard, B.; Autschbach, J. *J. Chem. Theory Comput.* **2012,** *8*, 598-609.
110. Rastrelli, F.; Bagno, A. *Chem. – Eur. J.* **2009,** *15*, 7990-8004.
111. Kaupp, M.; Köhler, F. H. *Coord. Chem. Rev.* **2009,** *253*, 2376-2386.
113. Acerete, R.; Casan-Pastor, N.; Bas-Serra, J.; Baker, L. C. W. *J. Am. Chem. Soc.* **1989,** *111*, 6049-6056.
114. Turner, M. J.; McKinnon, J. J.; Wolff, S. K.; Grimwood, D. J.; Spackman, P. R.; Jayatilaka, D.; Spackman, M. A. *CrystalExplorer15*, 2015.
115. McKinnon, J. J.; Spackman, M. A.; Mitchell, A. S. *Acta Crystal. B* **2004,** *60*, 627-668.
116. Heise, H.; Köhler, F. H.; Herker, M.; Hiller, W. *J. Am. Chem. Soc.* **2002,** *124*, 10823-10832.
117. Tasker, S. Z.; Standley, E. A.; Jamison, T. F. *Nature* **2014,** *509*, 299-309.
118. Sepelak, D. J.; Pierpont, C. G.; Barefield, E. K.; Budz, J. T.; Poffenberger, C. A. *J. Am. Chem. Soc.* **1976,** *98*, 6178-6185.
119. Zhu, D.; Thapa, I.; Korobkov, I.; Gambarotta, S.; Budzelaar, P. H. M. *Inorg. Chem.* **2011,** *50*, 9879-9887.
120. Blanchard, S.; Neese, F.; Bothe, E.; Bill, E.; Weyhermüller, T.; Wieghardt, K. *Inorg. Chem.* **2005,** *44*, 3636-3656.
121. Norman, N. C.; Orpen, A. G.; Quayle, M. J.; Whittell, G. R. *Acta Crystal. C* **2002,** *58*, m160-m161.
122. Iluc, V. M.; Miller, A. J. M.; Hillhouse, G. L. *Chem. Commun.* **2005**, 5091-5093.
123. Proft, B.; Pörschke, K.-R.; Lutz, F.; Krüger, C. *Chem. Berichte* **1994,** *127*, 653-655.
124. Tong, G. S. M.; Che, C.-M. *Eur. J. Inorg. Chem.* **2010,** *2010*, 5113-5123.
125. Soo, H. S.; Sougrati, M. T.; Grandjean, F.; Long, G. J.; Chang, C. J. *Inorg. Chim. Acta* **2011,** *369*, 82-91.
126. Venkatakrishnan, T. S.; Sahoo, S.; Bréfuel, N.; Duhayon, C.; Paulsen, C.; Barra, A.-L.; Ramasesha, S.; Sutter, J.-P. *J. Am. Chem. Soc.* **2010,** *132*, 6047-6056.
127. Slep, L. D.; Calvo, R.; Nascimento, O. R.; Baggio, R.; Garland, M. T.; Peña, O.; Perec, M. *Inorg. Chim. Acta* **2007,** *360*, 2911-2916.
128. Larionova, J.; Kahn, O.; Golhen, S.; Ouahab, L.; Clérac, R. *Inorg. Chem.* **1999,** *38*, 3621-3627.
129. Barbour, C. J.; Cameron, J. H.; Winfield, J. M. *J. Chem. Soc. Dalton* **1980**, 2001-2005.
130. Nowick, J. S.; Ballester, P.; Ebmeyer, F.; Rebek, J. *J. Am. Chem. Soc.* **1990,** *112*, 8902 - 8906.
131. Bühlmann, P.; Nishizawa, S.; Xiao, K. P.; Umezawa, Y. *Tetrahedron* **1997,** *53*, 1647-1654.
132. *APEX suite of crystallographic software, APEX 2, version 2008.4.*, Bruker AXS Inc., Madison, Wisconsin, USA (2008).
133. *SAINT, version 7.56a, SADABS, version 2008.1*, Bruker AXS Inc., Madison, Wisconsin, USA (2008).
134. Hübschle, C. B.; Sheldrick, G. M.; Dittrich, B. *SHELXLE, J. Appl. Crystallogr.* **2011,** *44*, 1281-1284.
135. Sheldrick, G. M. *SHELXL-2014*, University of Göttingen, Göttingen, Germany (2014).
136. Sheldrick, G. M. *SHELXL-97*, University of Göttingen, Göttingen, Germany (1998).
137. Wilson, A. J. C. *International Tables for Crystallography*, Dordrecht, The Netherlands, Kluwer Academic Publishers (1992).
138. Spek, A. L. *J. Appl. Cryst.* **2003,** *36*, 7-13.
139. Spek, A. L. *Acta Cryst.* **2009,** *D65*, 148-155.
140. Neese, F. *An Ab initio, DFT and Semiempirical SCF-MO Package*, Max Plank Institute for Bioinorganic Chemistry, Mühlheim an der Ruhr, Germany, Jan 2012.
141. Becke, A. D. *J. Chem. Phys.* **1986,** *84*, 4524-4529.
142. Becke, A. D. *J. Chem. Phys.* **1993,** *98*, 5648-5652.
143. Lee, C. T.; Yang, W. T.; Parr, R. G. *Phys. Rev. B* **1988,** *37*, 785-789.
144. Schäfer, A.; Horn, H.; Ahlrichs, R. *J. Chem. Phys.* **1992,** *97*, 2571-2577.
145. Schäfer, A.; Huber, C.; Ahlrichs, R. *J. Chem. Phys.* **1994,** *100*, 5829-5835.
146. Eichkorn, K.; Treutler, O.; Ohm, H.; Häser, M.; Ahlrichs, R. *Chem. Phys. Lett.* **1995,** *240*, 283-290.

147. Eichkorn, K.; Treutler, O.; Ohm, H.; Häser, M.; Ahlrichs, R. *Chem. Phys. Lett.* **1995,** *242*, 652-660.
148. Humphrey, W.; Dalke, A.; Schulten, K. *J. Molec. Graphics* **1996,** *14*, 33-38.

# 3 A three generation ligand, PDIpCy, and the metal complexes thereof – exploring the possibilities

## 3.1 Introduction

Synergistic cooperative activation can be often found in metalloenzymes. The efficiency and selectivity in the reactivity of the enzymes can be obtained by holding the included moieties in optimal geometry through non-covalent bonding interactions or simultaneously activating multiple reacting species.[149] The metal-metal separation plays a crucial role as well for designed complexes. The arrangement of the metal centres in close proximity (3.6- 6 Å) is probably the key to success.[150] Even if there is no direct interaction between the metal ions, the metals are still close enough to interact with the substrate with both metals or to bind two reactants in close proximity. Dinucleating ligands can be divided into two classes:[151]

(a) Ligands which form complexes in which the metal ions are sharing at least one donor atom. The ligands contain adjacent sites in which the central donor moiety provides a bridge between the metals.

(b) Ligands in which the donor sets are isolated and form complexes in which donor atoms are not shared.

It should be noted that the two metals in the dinuclear complexes can be the homobimetallic or heterobimetallic. The metal variety can be extended from transition row metals to alkali metal, alkaline earth elements or lanthanide.[70, 152-158] The second metal, which is often referred to as secondary coordination sphere, can effect a wide range of functions, *e.g.* the modulation of physical properties, like redox potentials, migration and removal of products.[157]

Hence, one of the biggest challenges is the design of the complex. The coordination sites have to be able to accommodate different combinations of metal ions in various oxidation states and allow proximity of the metal centres. The reactivity shown by some select complexes, where the influence of a second metals has been proven, has been promising already. [157-160]

Asymmetry becomes an important factor when enantioriched compounds have to be synthesised.[149] Further, unsymmetrical complexes might as well promote an electron separation toward mixed valent complexes.

One example stands out of the unsymmetrical complexes as it follows a similar design as we approached for our ligands. A PDI-based ligand, accommodating alkali metals in a crown ether, was reported by Gilbertson e*t. al*.[70] The secondary coordination sphere, the crown ether, contains a redox-inactive Lewis acid, which shall enhance the reactivity and move the reduction potential to more positive values.[161-162] In contrast, our ligand design combines two coordination sites for transition metals to support redox reactivity at both coordination sites (Figure 28). The distinct binding sites are hereby formed by pyridine diimine (PDI) and tetraazacyclodecane (cyclam). Coordination complexes of both ligands, PDI and cyclam are well known[163-167] and have demonstrated promising results for reactions including $CO_2$ reduction, $H_2$ evolution and olefin epoxidation.[26, 168-173] The pyridine diimine (PDI) was chosen as a non-innocent moiety, where storage of up to three electrons is possible. To form the second coordination site, various groups such as azamacrocyclo- and bidentate diamine frameworks have been chosen. The coordination sites are separated by a spacer, which connects the two coordination site frameworks *via* a carbon chain. To create the flexible M-M-distance propyl groups are chosen as spacer. The synthesis of symmetric and unsymmetrical compounds is shown in this chapter.

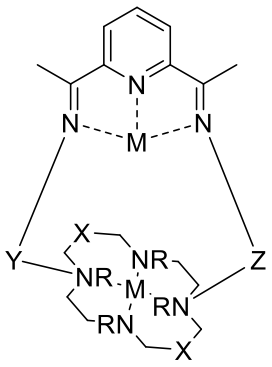


R = H, Me

X = $CH_2$, /

Y = $(CH_2)_3$, /

Z = $(CH_2)_3$

**Figure 28.** Structural design of the three generations.

## 3.2 Development of the PDIpCy

The ligand PDIpCy was developed in three stages. The first generation “basket ligands” was developed by a former member of the Hess group and used in complexation experiments with iron. In this work only some subsequent works were carried out. Therefore, only a brief description of the synthesis and complexation will be given. In Figure 29, the three generations of the ligands are displayed.

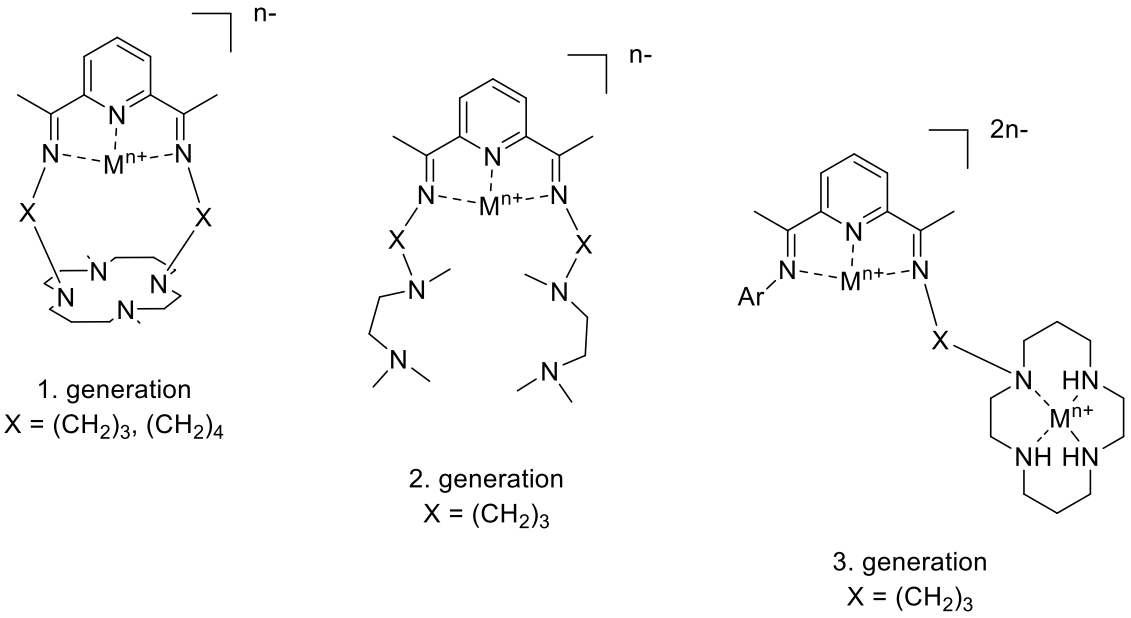


**Figure 29.** The three generations.

*First generation* – The “basket ligands” were designed to form a cavity for substrates in the shape of a basket. The two coordination sites are a pyridine diimine moiety and a cyclam. The schematic synthesis of the ligands parts and the metal complexes are shown in Scheme 22.

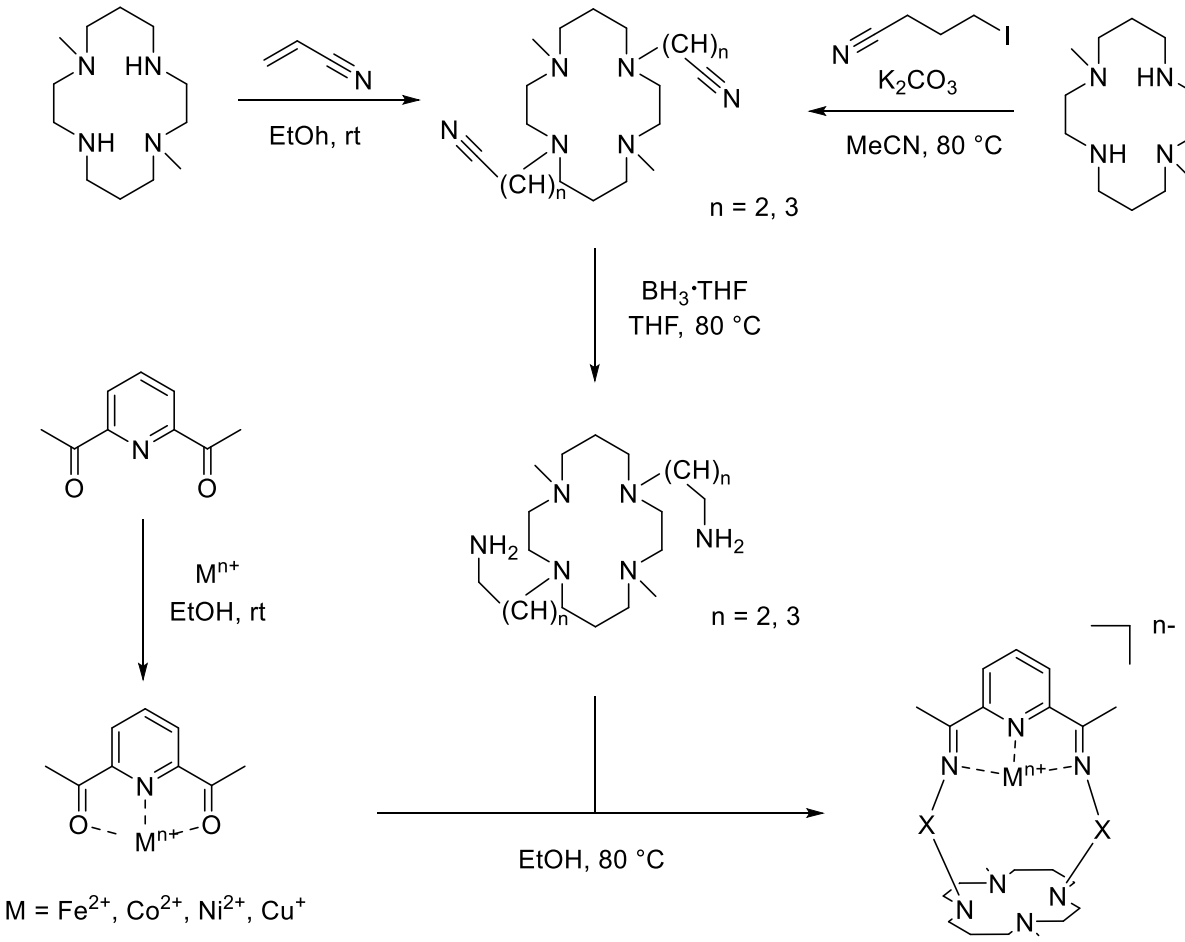


**Scheme 22.** Synthesis of the "basket ligands" and metal complexes.

For the synthesis, a precursor was formed of diacetylpyridine and a metal salt as it has been used in Schiff base condensation reactions.[174] The metal, complexed in the diacetylpyridine, promotes the condensation by polarising the carbonyl bond for nucleophilic attacks and kinetic and thermodynamical template effects.[174] The formed precursor subsequently reacts in a Schiff base condensation reaction with the diamine cyclam compound. The reaction requires a very slow addition of both components into a highly diluted reaction mixture to avoid polymerisation reactions. Several different metal salts ($[Fe(MeCN)_6](PF_6)_2$, $FeCl_2$, $[Co(MeCN)_6](PF_6)_2$, $CoCl_2$, $Ni(OAc)_2$) were used for the complexation reaction. Except the iron salts, none of the metal salts have been used before in the condensation reactions to form the "basket ligand" complexes. The obtained products in the condensation reactions were insoluble in most solvents and only slightly soluble in DMF, MeCN, water and alcohols. Crystallisation attempts never gave monocrystalline solids suitable for x-ray diffraction.

Two different paths were pursued to form a bimetallic compound. The formed monometallic iron compounds were stirred with a second metal salt in the attempt to form a

bimetallic compound. No data could be gathered, which would indicate a reaction with the second metal, as the metal salt was recovered. A hindrance of the reaction is probably the insolubility of the monometallic compounds. The second path was the addition of a precursor formed by the cyclam and a metal salt to the condensation reaction, but the products could never be identified as bimetallic complexes. No product was identified by mass and NMR spectroscopy in the condensation reaction of the diacetylpyridine with the cyclam amine without a metal complexed in the diacetylpyridine. Due the insolubility of the compounds, the analytical data was difficult to collect. Hence, the ligand scaffold was adapted to enhance the solubility of the complexes resulting in the second generation of complexes.

*Second generation* – Especially the solubility was supposed to be enhanced in the second generation of the ligand. The rigidity of the closed basket ligand was broken down on the cyclam side to achieve better solubility and was replaced by two bidentate ethylene diamines to form the "open basket ligand". The synthesis and analytical data for the ligand and the metal compounds will be given in the next section (3.3). It has to be anticipated, that these compounds are better soluble. Further studies with benzylic linker carried out in our group showed that the second binding site, the diamine, probably does not accommodate a metal due to steric reasons. Therefore, the next ligand generation was designed bearing a more distinct second binding site.

*Third generation* – For the third generation, the motifs of PDI and cyclam were combined in a ligand scaffold, linked by a propyl spacer. The second acetyl group of the diacetylpyridine was reacted with an aryl group. The ligand was named PDIpCy, according to an abbreviation of the two moieties. PDI and Cy represent pyridine diimine and cyclam respectively and p stands for the propyl group linking the two moieties. The ligand and its metal complexes will be described in 3.4.

## 3.3 Synthesis of the "open basket ligand" and its metal complexes

The synthesis of the "open basket ligand" with a propyl spacer started with the *N,N,N'*-trimethylethylenediamine, which reacted in a Michael-Addition with acrylonitrile, to give **11** in 98% yield (Scheme 23). The signals in the NMR spectra were identified as product signals and the mass confirmed by ESI mass spectroscopy. The product was used without further purification in the subsequent reduction with $LiAlH_4$. The pure product **12** was obtained by distillation (46% yield). The analytical data is in good agreement with the literature.[175] The synthesis in a pressure tube at 80 °C in toluene without an acidic catalyst gave the highest

conversion. The pressure tube was needed as in preceding test the amine proved to be relatively volatile. To further overcome the volatility issue and shift the condensation equilibrium, an excess of amine, (2.1 equivalents) was used. The reaction mixture was stirred over molecular sieves to remove the formed water molecules and therefore, shift the equilibrium of the condensation reactions further to the product side. The condensation reaches a conversion of ≥ 99% and the excess of **12** is removed *in vacuo*.

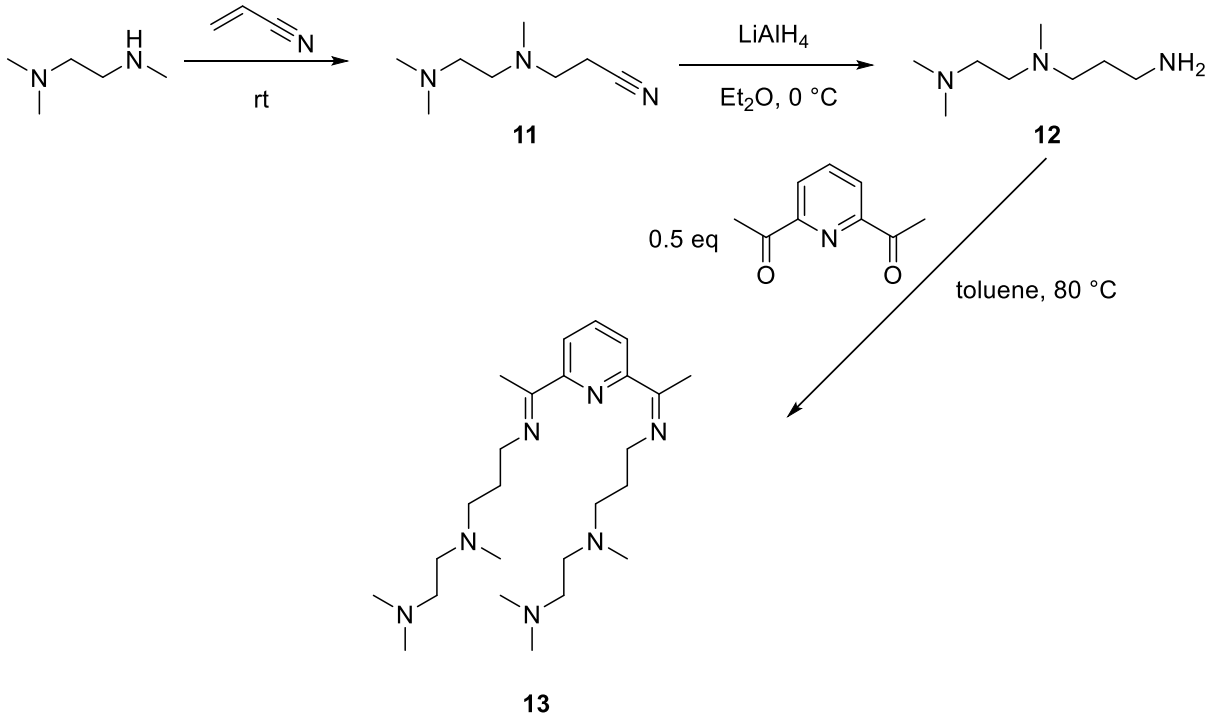


**Scheme 23.** Synthesis of **13**.

The NMR spectrum of the ligand was examined more closely and the protons assigned. The ligand is symmetric and therefore, the signals are equivalent on both side arms of the pyridine diimine. The three singlets at 2.37, 2.20 and 2.13 ppm represent the eight methyl groups on the diamine and pyridine diimine. The signal of the four protons $H_6$ is highfield shifted to 3.53 ppm, due to the electronegative nitrogen atoms of the imines, and displayed as a triplet. The proton signals of $H_8$, $H_9$ and $H_{10}$, neighbouring the amines, and the methyl group with the protons $H_{11}$ form the multiplet with 18 protons. For further assignments refer to Figure 30.

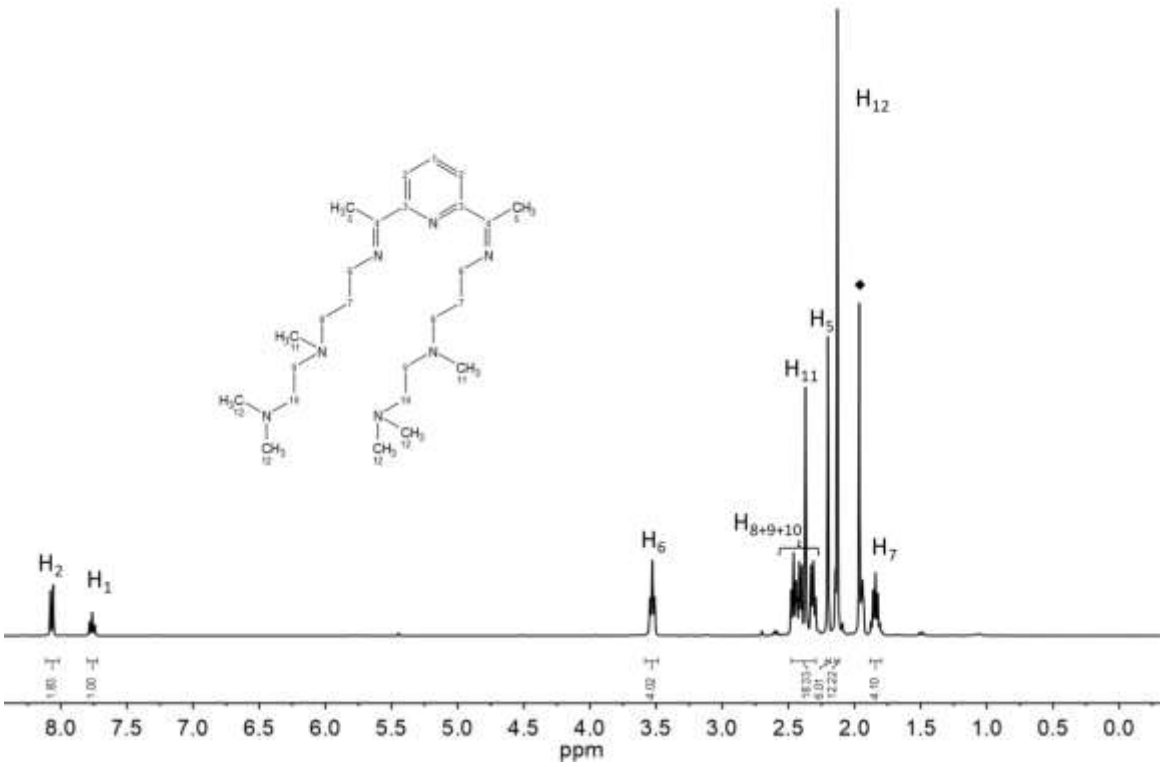


**Figure 30.** $^{1}$H NMR spectrum of **13** (400 MHz, in MeCN-$d_3$) with labelling scheme and assignment of the protons (◆ = residual solvent signal).

The electronic spectrum of **13** exhibits $\pi$-$\pi^*$-transition bands at 283 nm with $\varepsilon$ = 7400 $M^{-1}$ $cm^{-1}$ (Figure 31).

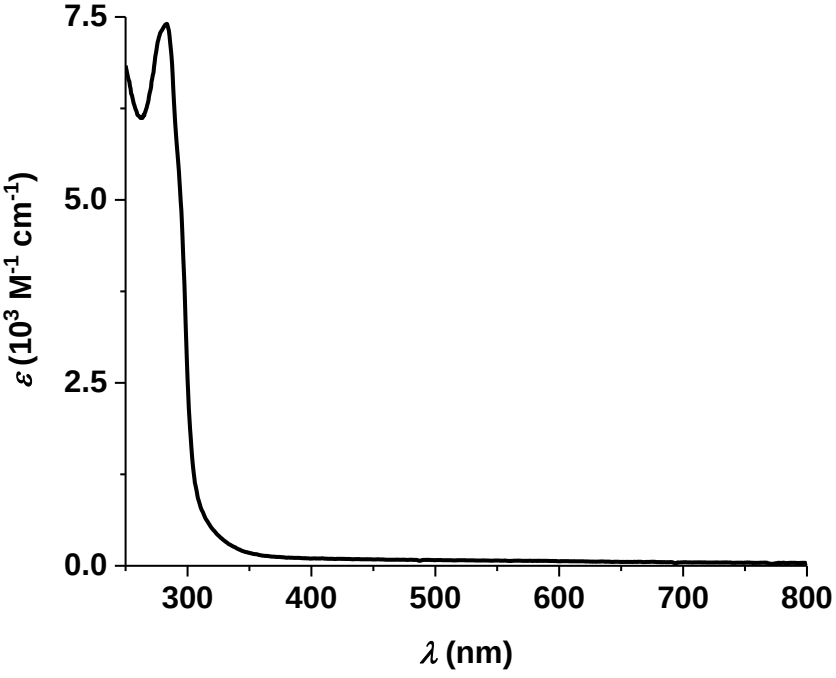


**Figure 31.** Electronic spectra of **13** in MeCN.

The complexation of **13** was carried out with a variety of late first row transition metal salts, including iron, cobalt, nickel, copper and zinc. All experiments were conducted with two equivalents of metal salt and the counter ions were varied. The metal salts used for the reactions are listed in Table 5 along with the colours of the products in the respective solvent.

**Table 5.** Complexation experiments conducted with **13**.

| experiment | metal | counterion | colour |
|---|---|---|---|
| 1 | Fe | $PF_6$ | purple (MeCN) |
| 2 | $Ni^{II}$ | OAc | brown (MeCN) |
| 3 | Co | $PF_6$ | red (MeCN, DCM) |
| 4 | $Zn^{II}$ | OTf | yellow-orange (MeCN) |

For each metal, the electronic spectrum of a compound is provided below. All identified bands of the four metal complexes are in good agreement with data of similar metal-PDI complexes in the literature.[176-181] Therefore, the coordination of a metal in the PDI moiety can be confirmed. The absorption bands of metal-amine compounds are weaker and are assigned, for example, to MLCT- or d-d transitions. It was envisaged, that the metal in the second coordination site is enfolded by four amines. A coordination similar to a metal-cyclam complex is expected and a comparison of the bands with metal-cyclam complex absorption bands has been made. However, the coordination of only two amines by only one linker arm would be possible as well.

The spectrum of the iron compound exhibits intense bands between 490 and 600 nm, one band with less intensity at 370 nm and a $\pi$-$\pi$*-transition band at 302 nm with higher intensity. Comparable bands of iron amine compounds, like Fe(cyclam) absorption bands, are located at 370 nm and 500 to 700 nm.[182-183] The spectrum in Figure 32 displays a shoulder at 370 nm, which can be assigned to an iron amine complex and is probably a MLCT transition band. The absorption bands between 500 and 700 nm are in the same range as the expected bands of the Fe(PDI) complexes.[179-180] The bands between 490 and 600 nm are assigned as well to MLCT bands, as no bands are observed in the ligand spectrum (Figure 31) or the spectrum of the zinc containing compound (Figure 33) in this region. Furthermore, they are too intense for forbidden d-d transition.

The spectrum of the cobalt complex shows a $\pi$-$\pi$*-transition band at 295 nm, with a shoulder at 365 nm, and two minor features at 476 and 548 nm. The absorption bands higher than 350 nm are likely to be MLCT bands as in the ligand spectrum only $\pi$-$\pi$*-transition are

observed at a smaller wavelength than 350 nm (Figure 32). According to the literature, a Co(cyclam) complex spectrum exhibits bands around 481 and 358 nm.[184-185] The absorption bands are in a similar range as the bands observed for Co(PDI) complexes. Therefore, a coordination of a second metal ion in the amine side cannot be fully elucidated.

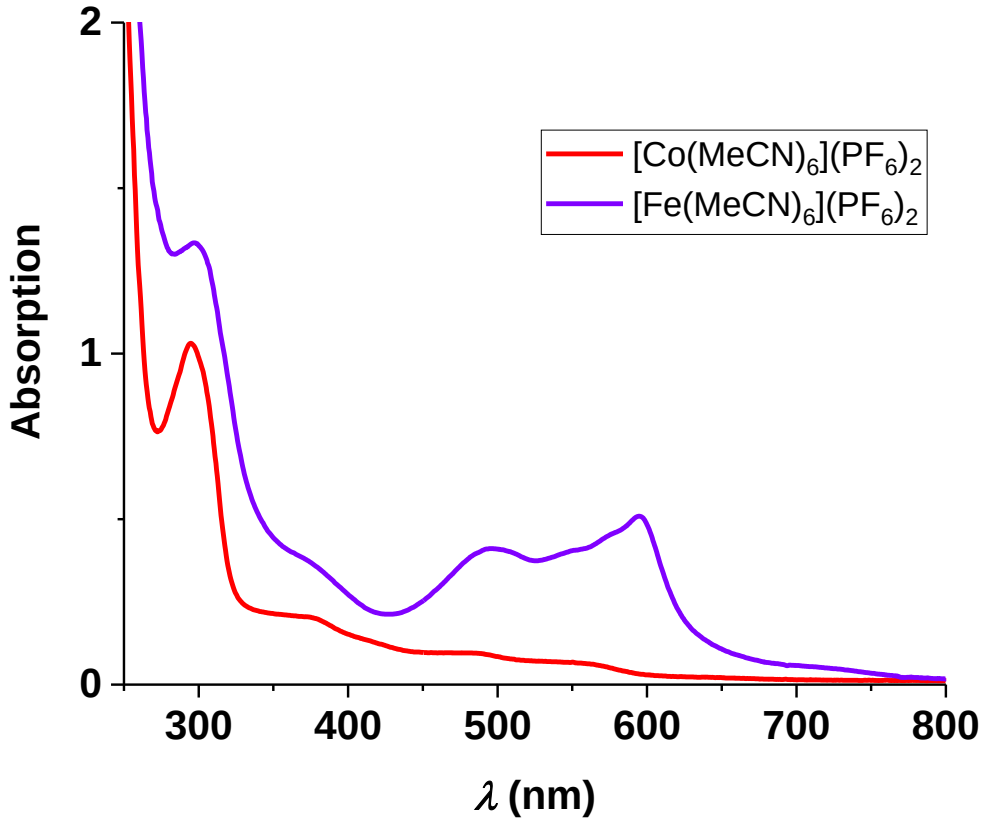


**Figure 32.** Electronic spectra of the products of the reactions with the metal precursors $[Fe(MeCN)_6](PF_6)_2$ and $[Co(MeCN)_6](PF_6)_2$.

The spectrum of the zinc compound displays *π*-*π**-transition bands at 290 (Figure 33). The zinc compound spectrum does not exhibit further bands than the *π*-*π**-transition bands. For zinc-amine compounds, no absorption bands are expected and the coordination of a second metal cannot be proven by UVVis spectroscopy for zinc.

In the spectrum of the nickel complex, a *π*-*π**-transition bands at 283 nm is observed. A feature around 680 nm, with low intensity, is displayed and additionally, there is a slight absorption till 800 nm. The bands around 680 nm of the Ni containing compounds are likely to be MLCT bands due to the same reason as mentioned for the iron and cobalt compounds. For Ni(PDI) compounds, also bands above 800 nm are reported, which would explain the slight absorption till 800 nm.[178, 180-181, 186] Ni(cyclam) compounds exhibit significant bands at longer wavelengths ($\lambda_{max}$ = 369, 461 nm).[187-189] None of the bands around 369 and 461 nm

are observed in the spectrum of our nickel compound, which makes a coordination of a second metal ion unlikely for nickel.

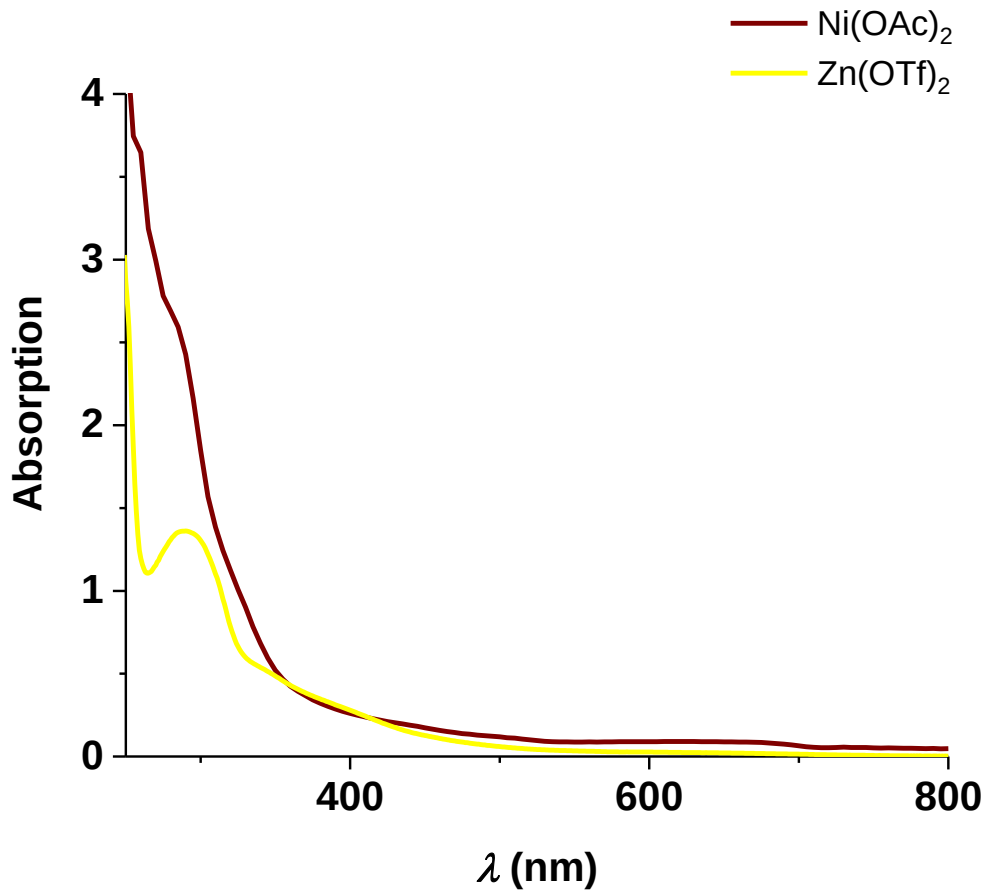


**Figure 33.** Electronic spectra of the products of the reactions with the metal precursors $Ni(OTf)_2$ and $Zn(OTf)_2$.

Titration experiments were performed to elucidate, whether a coordination of a metal ion to the second coordination site formed by the amines is feasible. The dissolved metal precursors $[Fe(MeCN)_6](PF_6)_2$ and $[Co(MeCN)_6](PF_6)_2$ are titrated to a solution with a known concentration of **13**. The metal precursors were added in 0.5 eq steps and the experiment monitored by UVVis spectroscopy (Figure 34).

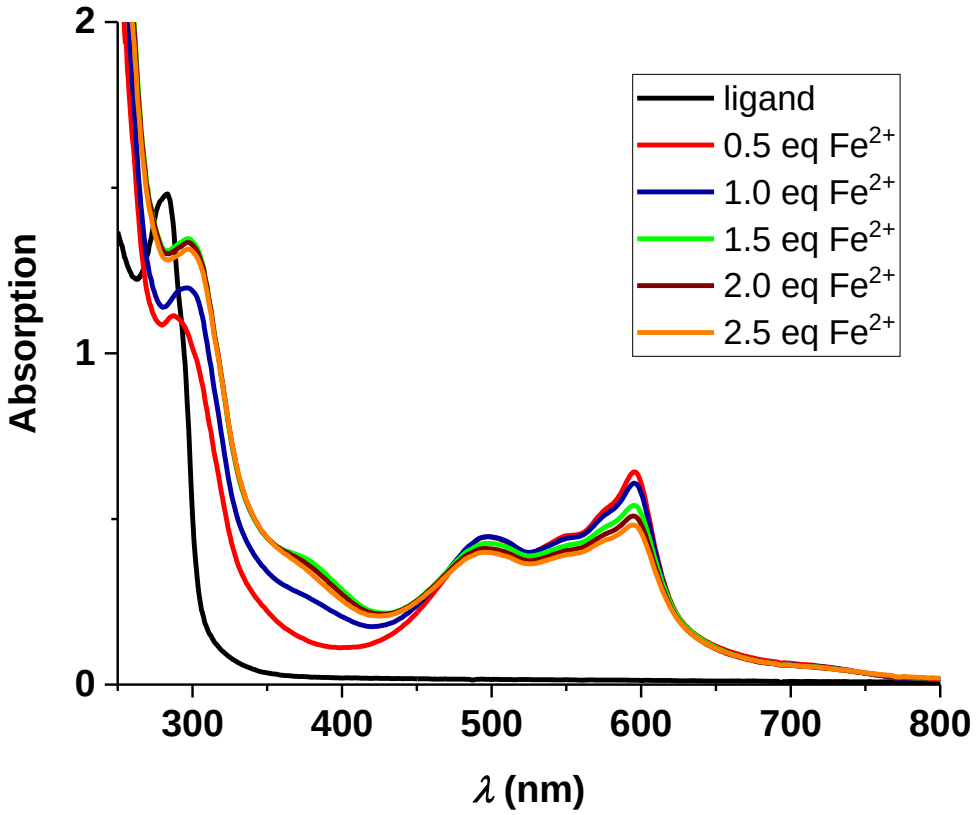


**Figure 34.** Electronic spectra of titration experiment with 0.5-2.5 eq $[Fe(MeCN)_6](PF_6)_2$ in to a solution of **13** in MeCN.

The titration experiment was performed with the assumption, that one coordination site is preferred over the other. With the addition of 0.5 eq of $[Fe(MeCN)_6](PF_6)_2$ (red spectrum) the *π*-*π**-transition band at 283 nm shifts to a higher wavelength (294 nm) and the bands between 490 and 600 nm form. The bands can be related to observed absorption bands of Fe(PDI) compounds. No band can be observed at 370 nm. A band at 370 nm would indicate an occupation of the amine coordination site, so the iron ions are only coordinated to the PDI moiety at this step. The reaction of further 0.5 eq $[Fe(MeCN)_6](PF_6)_2$ (in total 1.0 eq; blue spectrum) causes a shift of the *π*-*π**-transition band to 302 nm, a wavelength which is observed in the spectrum with 2 eq of metal precursor (Figure 32) as well and the band at 370 nm forms. The addition of up to 2.0 eq of metal precursor intensifies the *π*-*π**-transition bands and the band at 370 nm. The spectra are not dilution corrected, but from the spectra of 2.0 eq (brown) to 2.5 eq (orange) it is obvious that the dilution effect is marginal.

Noticeable is, that the bands between 490 and 600 nm, assigned as MLCT bands of the Fe(PDI), are very intense in the red spectrum and do not intensify with the addition of further

equivalents. Following the Lambert-Beer'sche law and when the PDI moiety is the preferred coordination site of the metal ions, absorption of half the value of the final complex is expected. If no coordination site is preferred, even less absorption is expected as the PDI moiety is less occupied. In the literature, dimers have been observed for PDI-ligands and metals of the first transition row with two ligand molecules encapsulating one metal ion.[71, 73] The absorption of the ligand-dimer-complexes are higher compared to compounds with only one ligand coordinated to the metal ion. Our observation of bands, which are not intensifying in absorption with further metal ions, might lead to the assumption, that dimers are observed as well in our titration experiment. Further studies have to be carried out to prove the dimerization. Due to the formation of the dimer the spectra are more complicated to evaluate. The coordination of two metals is very likely as stated before, as bands corresponding to transitions of both metal compounds are observed. Furthermore, the PDI site seems to be slightly preferred as the feature at 370 nm, assigned to iron amine compounds, does not form with 0.5 eq of metal precursor.

A titration experiment with the same procedure was performed with the metal salt $[Co(MeCN)_6](PF_6)_2$ (Figure 35). With the addition of the first 0.5 eq of metal precursor the $\pi$-$\pi$*-transition band marginally shifts to higher wavelength (ligand: 283 nm, red spectrum: 287 nm). The only band, which is not observed compared to the spectrum with 2.0 eq metal precursor, is the shoulder at 365 nm. With the addition of further equivalents a feature at 365 nm forms and the $\pi$-$\pi$*-transition bands shift to 295 nm. The absorption of the spectrum of 0.5 eq of metal salt is noticeably more intense than in the following spectra. The intense $\pi$-$\pi$*-transition absorption could be caused by the formation of a dimer as mentioned in the iron titration experiment. After the addition of 1.0 eq the bands are decreasing because of the dilution. In the titration experiment, no change, except dilution, of the bands was observed after the addition of 1.0 eq of metal salt. A coordination of a cobalt ion in the PDI is preferred and probably no cobalt ion is complexed by the amines.

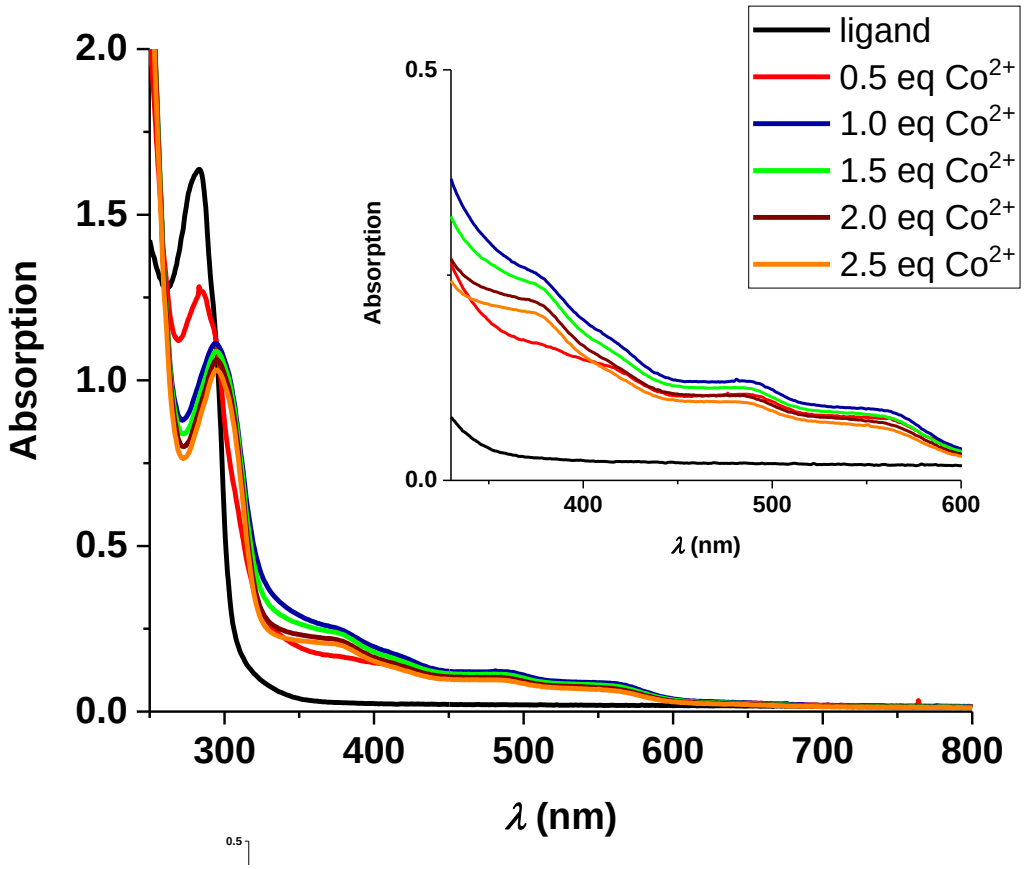


**Figure 35.** Electronic spectra of titration experiment with 0.5-2.5 eq $[Co(MeCN)_6](PF_6)_2$ to a solution of **13**.

With UVVis spectroscopy, the coordination of iron and cobalt ions with the ligand **13** was elucidated. As already mentioned above, the accommodation of zinc ions by the amines cannot be followed by UVVis spectroscopy. Therefore, NMR spectroscopy experiments were performed with $Zn(OTf)_2$ and, as a second example, the reaction with $[Cu(MeCN)_4]PF_6$ metal salt was chosen to be monitored by NMR spectroscopy.

Two equivalent of respective metal salt were added to a solution of **13** in MeCN-$d_3$ in one equivalent steps and the reaction was followed by NMR spectroscopy.

With the addition of the first equivalent of $[Cu(MeCN)_4]PF_6$ a lowfield shift for all signals close to the PDI moiety can be observed (Figure 36). The two signals ($H_1$ and $H_2$) in the aromatic region merge to one signal and the signal for $H_6$ shifts to lowfield. Signals assigned to the diamine groups and the linker protons closer to the amines seem to be not affected by the copper ion. The coordination of the $Cu^+$ ion to the PDI-moiety is more likely and only one species is formed. After the addition of the second equivalent of metal salt a significant shift of the signal of the aromatic proton $H_1$, forming the triplet, is visible. All proton signals,

belonging to PDI-moiety, linker and diamine groups, experience a lowfield shift. With each equivalent a change in the spectrum is observed, suggesting that the coordination of two $Cu^+$ ions is feasible, but a preferred coordination site cannot be determined as with the second equivalent as well changes in shift of proton signals, belonging to the PDI-moiety, are observed.

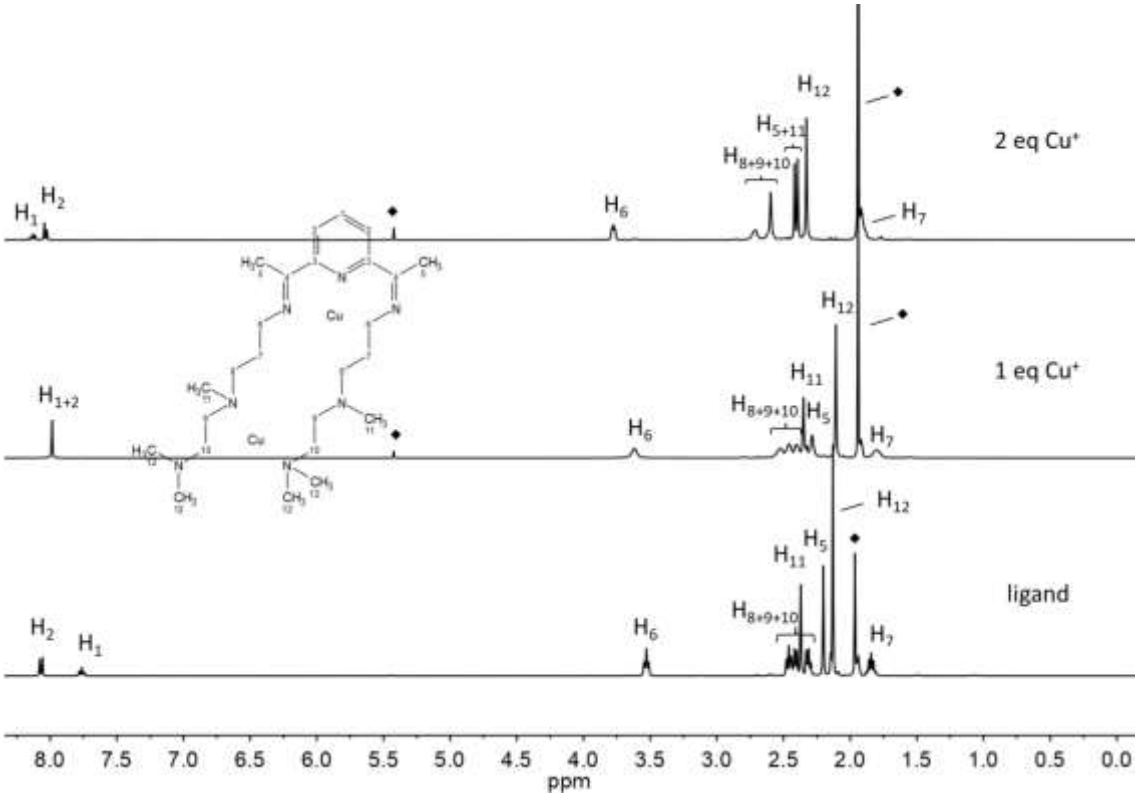


**Figure 36.** Stacked NMR spectra of titration of **13** with $[Cu(MeCN)_4]PF_6$ in MeCN-$d_3$ (◆ = residual solvent signal).

An experiment with the same procedure was conducted with $Zn(OTf)_2$ in MeCN-$d_3$ (Figure 37). After the addition of the first equivalent, two species are formed in a 2:1 ration (defined by the aromatic region, where two triplets and two duplets can be located; the second species is labelled with $H_{x'}$). Signals of free ligand are not observed in the spectrum. The compound, with the lower percentage, seems to have a lower symmetry class as a splitting of the $H_{6'}$ protons is observed. Therefore, an assignment of protons is more difficult and could only be carried out partially. The four signals in the aromatic region are highfield shifted compared to the corresponding ligand signals, while $H_6$ shifts to a lower value and $H_{6'}$ are highfield shifted. The same behaviour is observed for $H_7$ and $H_{7'}$. The rest of the signals of two compounds cannot be assigned for sure. All protons are affected upon addition of the metals salts. The formation of a monometallic coexisting with bimetallic compound would be possible but with the addition of the second equivalent only on product would be observed.

The addition of the second equivalent causes mainly changes in the highfield and there are still two species in the reaction mixture. The coordination of zinc ions is more difficult to elucidate and a definite answer to the preferred coordination site and the accommodation of two zinc ions cannot be given.

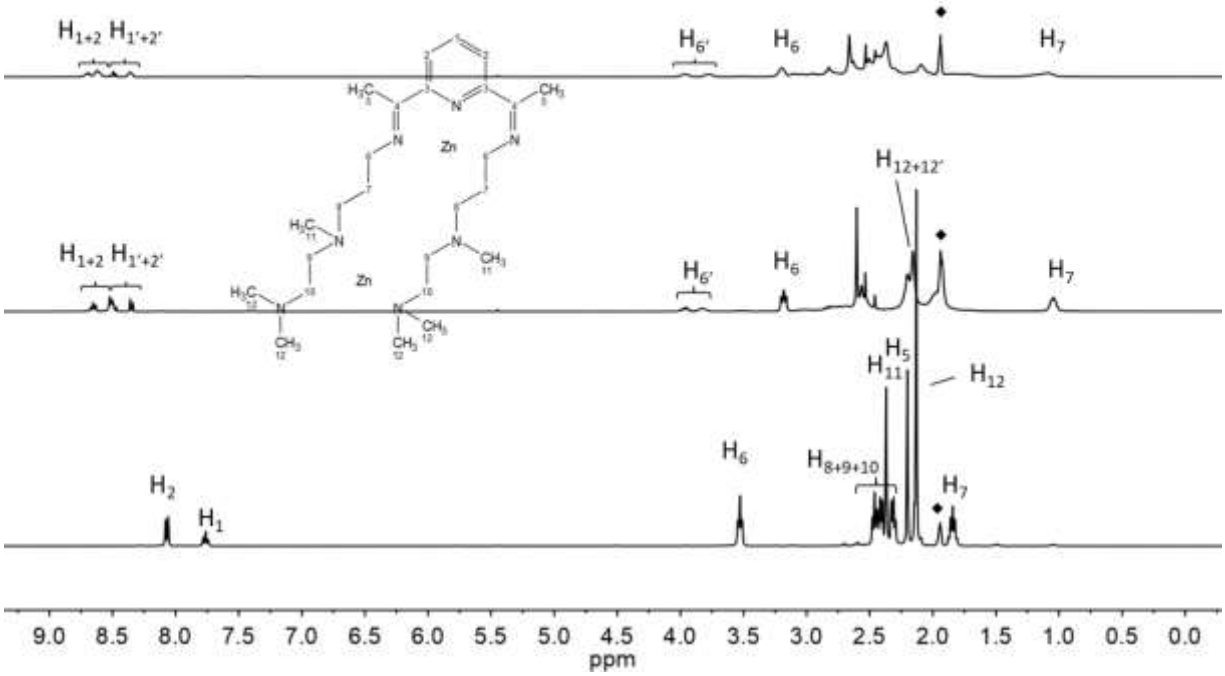


**Figure 37.** Stacked NMR spectra of titration of **13** with $Zn(OTf)_2$ in MeCN-$d_3$ (◆ = residual solvent signal).

The conclusion of the titration experiments by UVVis and NMR is that the ligand **13** probably does not support a bimetallic compound for every metal species. There are some hints that the formation of bimetallic compounds with $Fe^{II}$ and $Cu^{I}$ is feasible, but a final answer can only be given with a structural proof. The flexible linkers of the compound probably inhibit the single crystal growth, wherefore structural proof is missed. As the formation of bimetallic complexes is still the aim of this work, the ligand was adapted with a second distinct coordination site. The results are shown in the following.

## 3.4 Synthesis of PDIpCy

The third attempt to establish a ligand with two distinct coordination sites, one innocent and one non-innocent, was pursued with the synthesis of the PDIpCy (Figure 38). A further highlight of the ligand is the asymmetry of the scaffold, compared to the two generations aforementioned, and the flexibility of the linker. In addition, several sites in this ligand can be modified: linker, substituents at the cyclam- and at the PDI-moiety. The modification can change the solubility, the metal-metal distance and the potentials of oxidation and reduction.

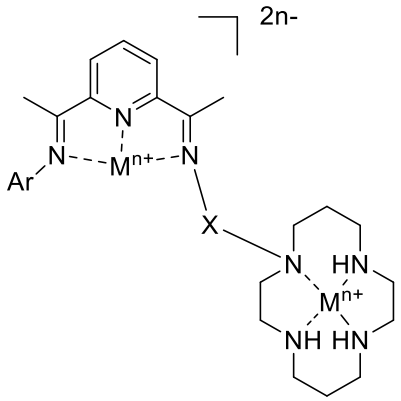


**Figure 38.** PDIpCy-metal complexes.

For the ligand synthesis, the coordination sites were prepared separately and were combined by a condensation reaction (Scheme 24). The reactions, except the second condensation to form the PDIpCy, are literature known, but were in case of the cyclam precursors modified to obtain better yields.[190-191] 1,4,8,11-tetraazacyclotetradecane reacted in a Michael-Addition with acrylonitrile to **14**. The side products were separated from the product by column chromatography and identified as multiple substituted propionitrile cyclam compounds and cyclam by mass spectroscopy. The nitrile group of **14** was reduced using Raney-Nickel and purified by distillation to yield **15**. The yields were improved to 60% and 80% compared to 40% in the literature.[190] The second precursor for the ligand synthesis was prepared in a condensation reaction of 2,6-diacetylpyridine with 2,6-di*iso*propylaniline to form **16**, which was obtained in literature yield. Both precursors were reacted in a condensation reaction in MeOH with 70% conversion. The ligand **PDIpCy** was isolated upon recrystallization in MeCN at -30 °C.

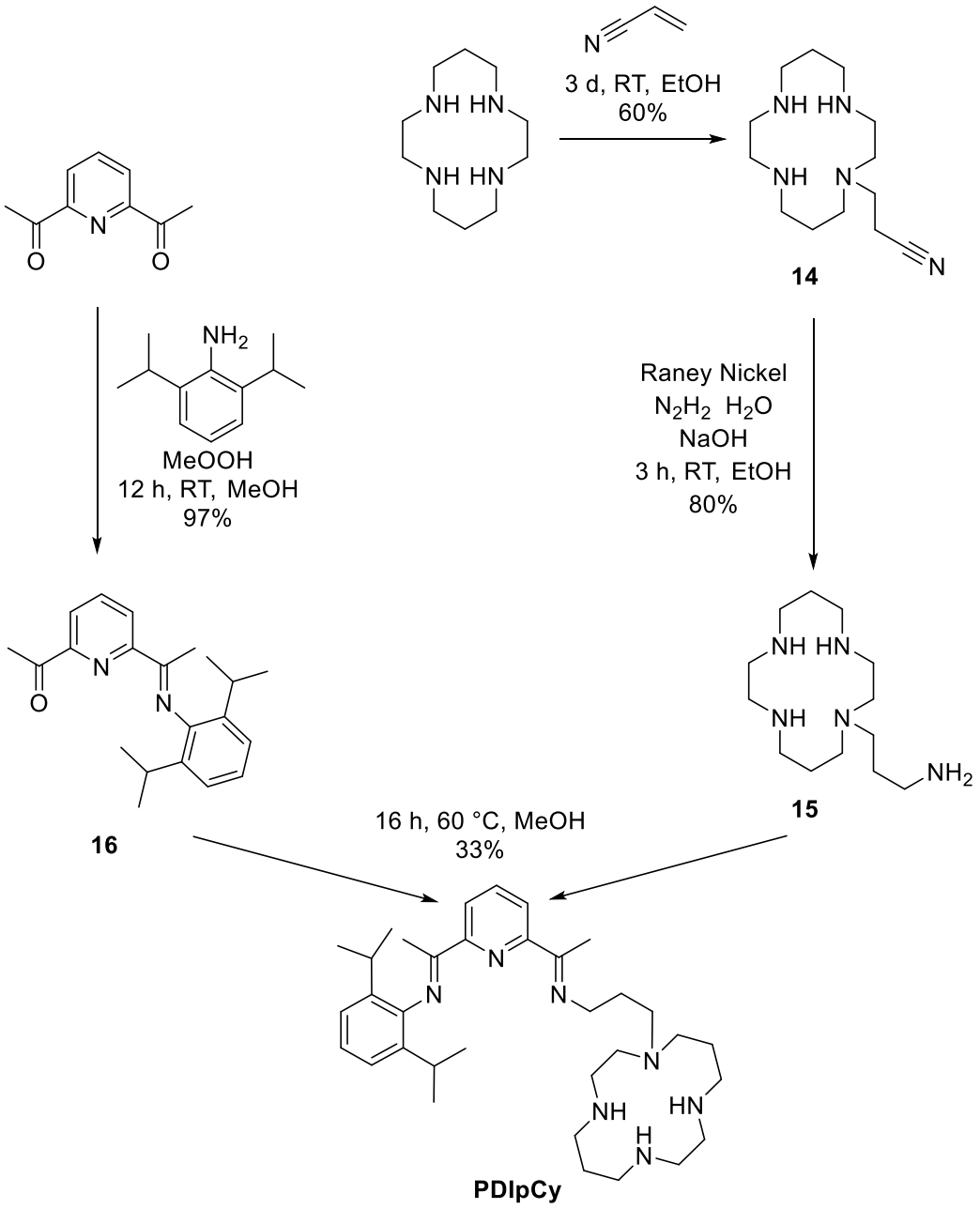


**Scheme 24.** Synthesis of **PDIpCy**.

The products were identified by NMR and mass spectroscopy and compared with the literature. [190-191] The protons of the ligand were assigned in the $^{1}$H NMR spectrum (Figure 39). In the aromatic region in total five signals are shown. The signals of the protons in *meta* position to the pyridine nitrogen are shifted differently due to the unsymmetrical substitution of the pyridine. The protons of the linker can be found as a triplet at 3.55 ppm ($H_9$) and a triplet of triplet at 1.91 ppm ($H_{10}$). $H_{11}$ is in the multiplet at 2.78 – 2.50 ppm. For the cyclam ring, only the protons $H_{13}$ could be assigned individually to the signals at 1.72 and 1.65 ppm. For further assignments refer to Figure 38.

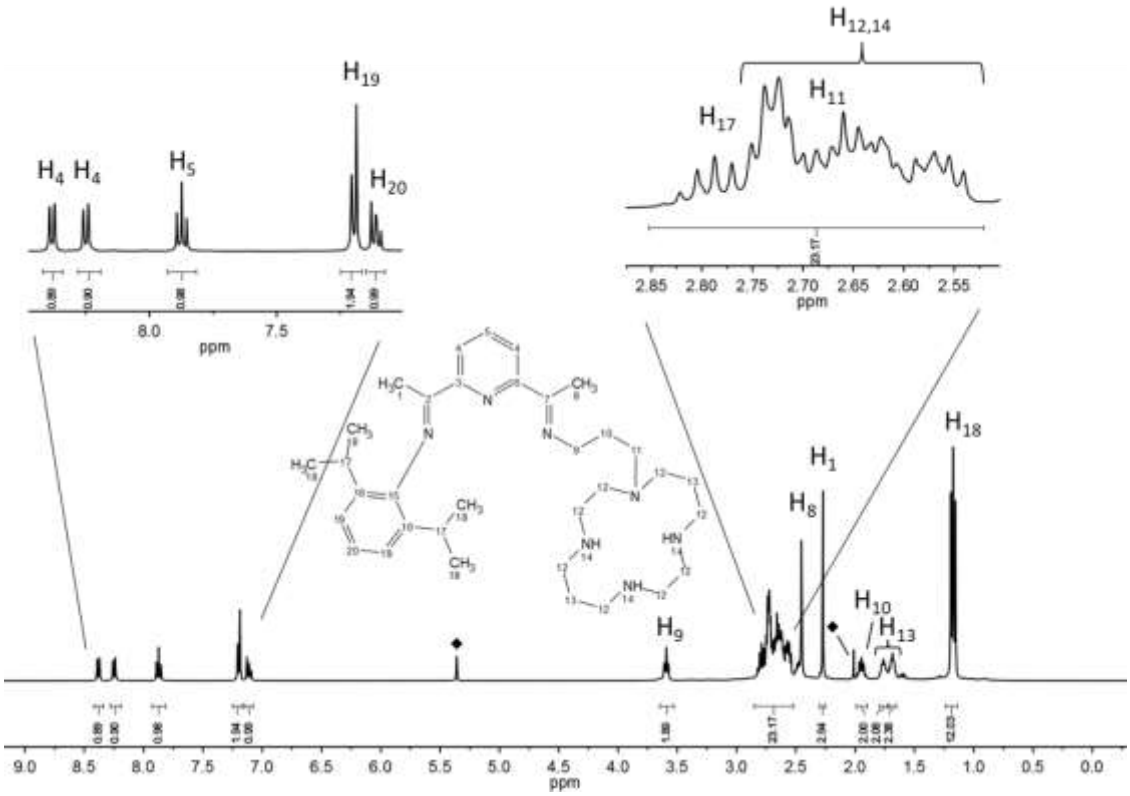


**Figure 39.** $^{1}$H-NMR spectrum of **PDIpCy** (400 MHz, DCM-$d_2$), with labelling scheme (Magnified: aromatic region and 2.5 – 2.9 ppm; ◆ = residual solvent signal) and assignment of the protons.[192]

The electronic spectrum of the **PDIpCy** in the UV and visible region exhibits two bands assigned to $\pi$-$\pi^*$-transition at 281 and 297 nm with 9910 and 6450 $M^{-1}$ $cm^{-1}$ (Figure 40).

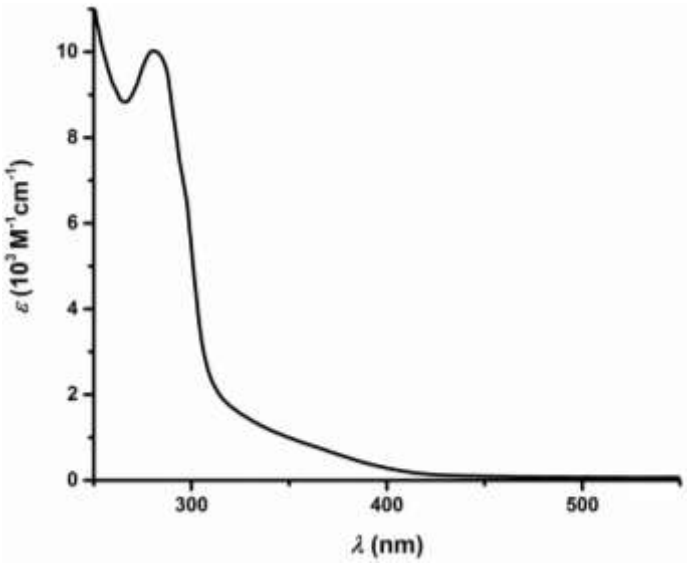


**Figure 40.** Electronic spectrum of **PDIpCy** in THF.[192]

In the spectrum of the infra-red region, the formation of the imine bond, which has its vibration band below 1700 $cm^{-1}$, can be confirmed (Figure 41). The bands of C=C bond and pyridine bond vibrations, between 1644 – 1567 $cm^{-1}$ are in close proximity and can be distinguished from the imine bands. Above 3000 $cm^{-1}$, there are the weak stretching vibrations of the amines and the aryl-H bonds, below 3000 $cm^{-1}$ the bands are assigned to C-H vibrations.

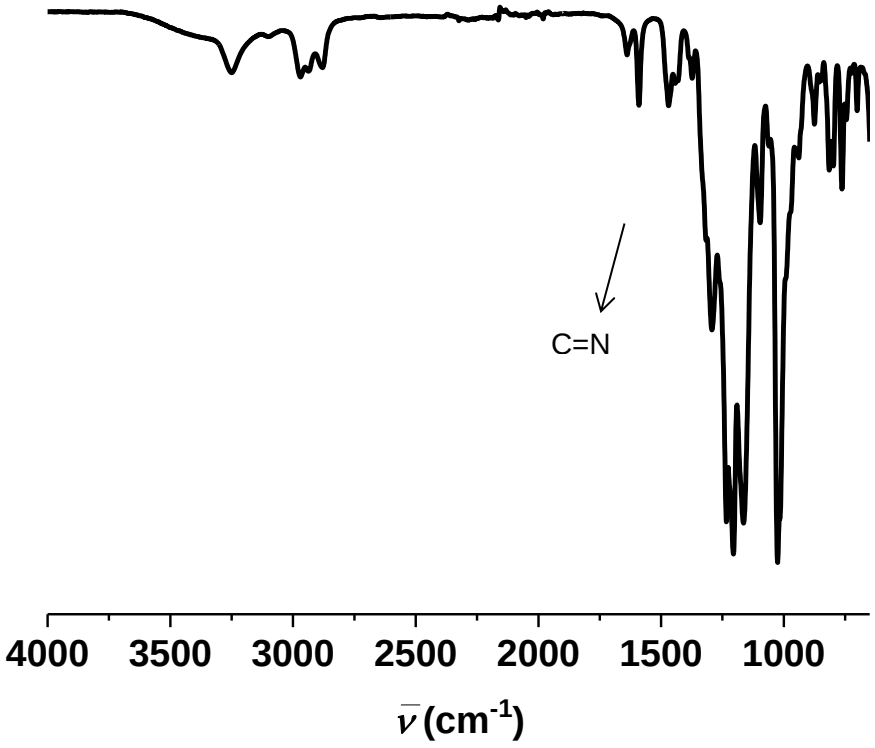


**Figure 41.** Infrared spectrum of **PDIpCy** (neat).[192]

The analytical data shows that the synthesis of an unsymmetrical ligand scaffold with two distinct coordination sites in close proximity was successful and the ligand can be isolated cleanly.

## 3.5 Metal complexes of PDIpCy with nickel and zinc

The ligand **PDIpCy**, with its two coordination sites, offers now the opportunity to react it with metal salts of the first transition metal row. The formation of homo- and heterobimetallic complexes will be now examined and in the following section, analytical data of nickel and zinc containing complexes will be shown.

The synthesis of **17**, the bimetallic zinc complex was carried out in MeCN at room temperature with two equivalents of the metal precursor $Zn(OTf)_2$. The synthesis of **18** and **19** required heat to form the homo- and heterobimetallic complexes in EtOH. The metal precursors $Zn(OTf)_2$ and $Ni(OTf)_2$ were added simultaneously in the reaction to form **19** (Scheme 25).

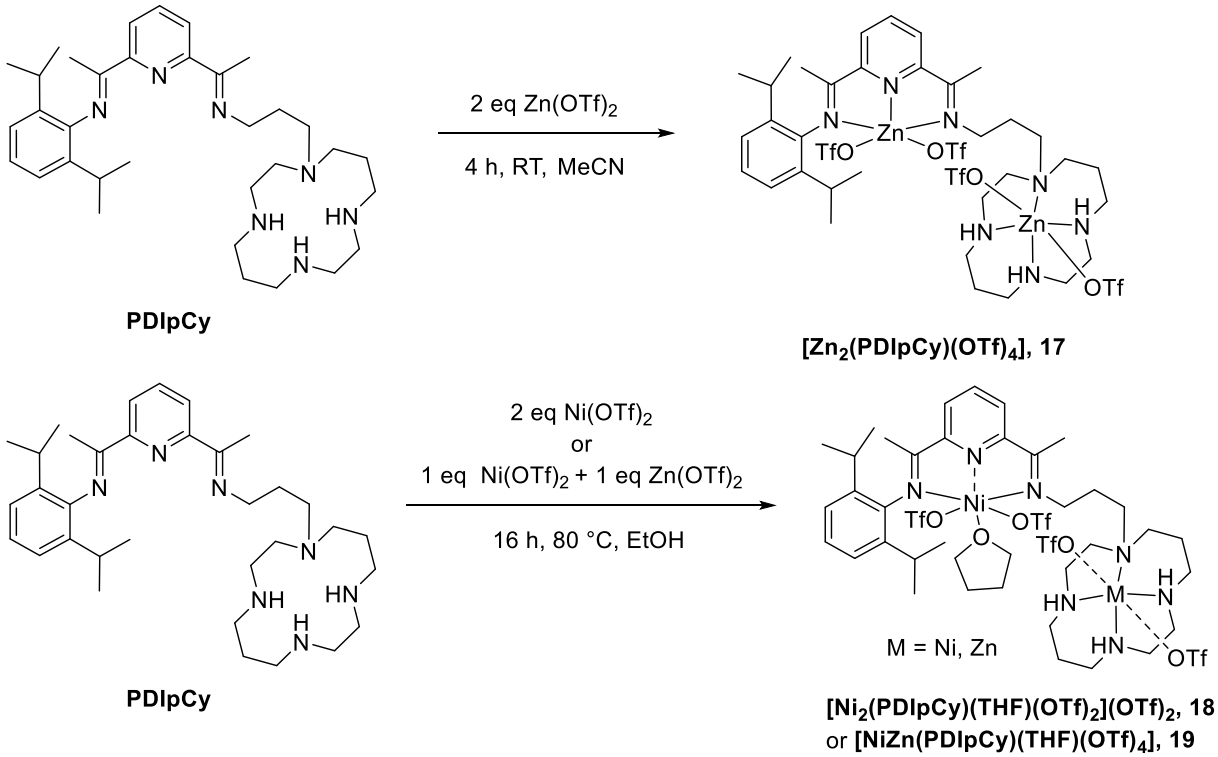


**Scheme 25.** Synthesis of **17, 18** and **19**.[192]

The compounds were crystallised and the molecular formula confirmed by elemental analysis. The LIFDI mass spectra showed that the only formed species in the reaction are the desired metal complexes (Figure A1). Especially for **19**, the proof of the formation of only the heterobimetallic complex is important. A formation of only zinc or only nickel containing complexes aside the heterobimetallic compound is not observed. The biggest detected fragment in the spectra is $[M\text{-}(THF+OTf)]^+$.

The crystal structure of **17**, **18** and **19** are displayed in Figure 42. The metal centres of **17**, **18** and **19** are separated by 8 Å. The coordination sites of **17** are in a six coordinate pseudo octahedral geometry with the planes formed by the nitrogen atoms of the cyclam or the PDI moiety and a THF molecule. The axial positions are occupied by the triflate counterions in a *trans*-arrangement, binding with the metal-oxygen distance of $Zn_{PDI}\cdots O_{avg}$ ~ 2.16 Å and $Zn_{cy}\cdots O_{avg}$ ~ 2.32 Å. The molecular structure of **18** has a similar geometry as **17**, except the coordination of the triflate counterion to the cyclam moiety. The triflate counterions of the $Ni_{cy}$

are only orientated towards the metal centre, but are not bound to it ($Ni_{Cy}\cdots O_{avg}$ ~ 2.7 Å), so that the cyclam moiety is best described as square planar.

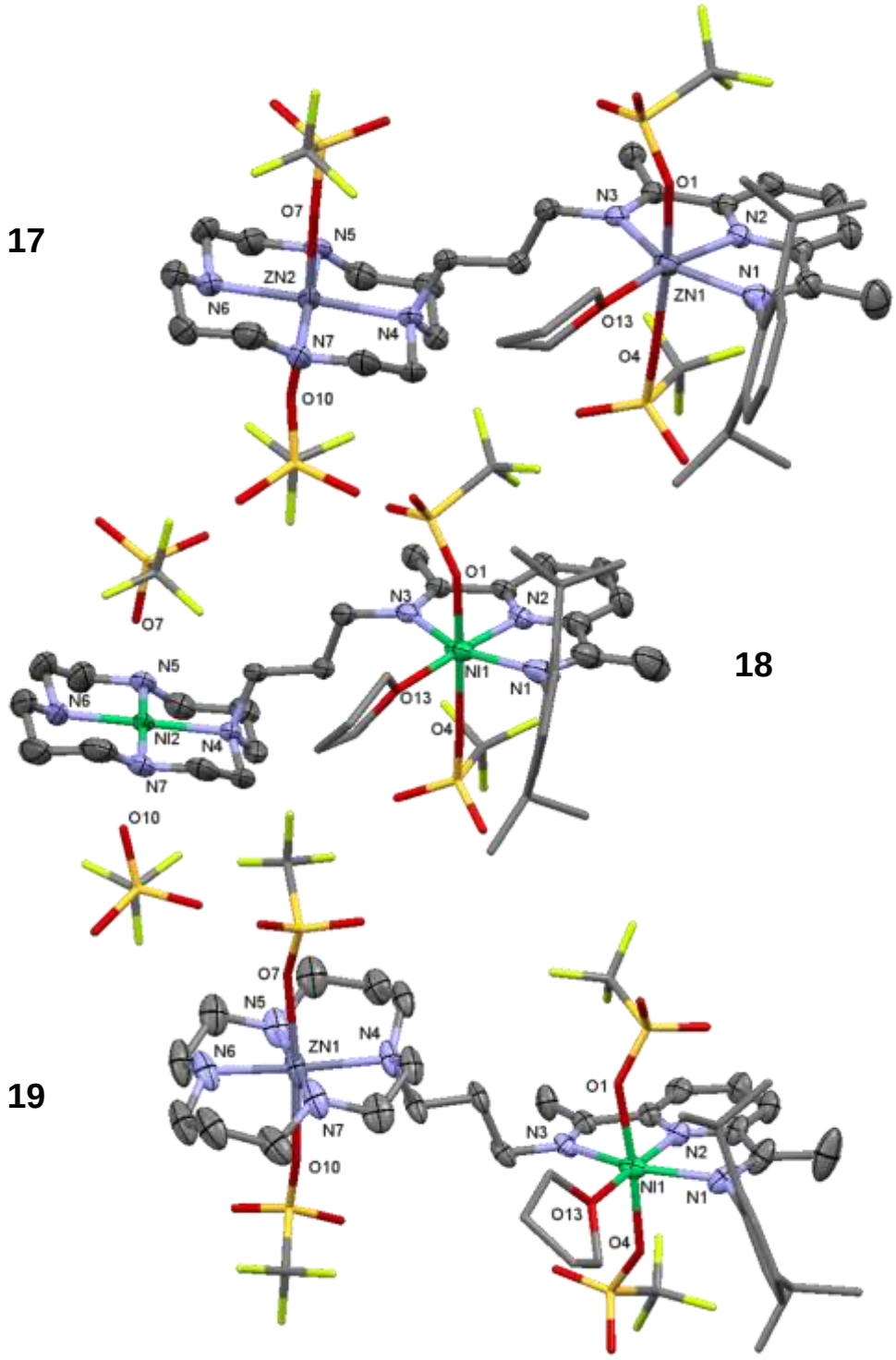


**Figure 42.** Molecular structures of **17, 18** and **19** (50% probability ellipsoids). Hydrogen and solvent molecules are omitted for clarity.

The limited quality of the crystal is reflected in the high R-value and several disorders in the structure, but the close environment around the metal ions can be discussed. Overall the Ni-N bond length are shorter compared to the Zn-N bonds due to the bigger $Ni^{II}$ ionic radius. For both complexes, the metal-ligand bond distances are in agreement with literature values for related mononuclear PDI and cyclam compounds. [193-199] The molecular structure of **19** shows a preferred coordination of the $Ni^{II}$ ion to the PDI site, whereas the $N_4$-macrocycle is occupied by the zinc atom. The assignment is confirmed by crystallographic parameters (R-values) and comparative data of **17** and **18** in terms of bond lengths (Table 6).

**Table 6.** Selected bond lengths (Å) and angles (°) for **17**, **18** and **19**.

| | **17** | **18** | **19** |
|---|---|---|---|
| M1-N1 | 2.259(4) | 2.195(5) | 2.193(6) |
| M1-N2 | 2.043(4) | 1.971(4) | 1.964(5) |
| M1-N3 | 2.146(4) | 2.107(4) | 2.095(5) |
| M1-O13 | 2.034(4) | 2.094(12) | 2.043(5) |
| M1-O1 | 2.088(4) | 2.065(9) | 2.139(5) |
| M1-O4 | 2.233(10) | 2.114(10) | 2.073(5) |
| M2-N4 | 2.153(4) | 1.975(4) | 2.157(5) |
| M2-N5 | 2.088(6) | 1.957(5) | 2.090(6) |
| M2-N6 | 2.096(6) | 1.947(5) | 2.076(6) |
| M2-N7 | 2.079(6) | 1.942(6) | 2.077(6) |
| M2-O7 | 2.249(4) | - | 2.382(5) |
| M2-O10 | 2.390(4) | - | 2.222(5) |
| N1-M1-N2 | 75.36(16) | 77.88(17) | 77.5(2) |
| N2-M1-N3 | 77.19(16) | 78.23(15) | 79.0(2) |
| N4-M2-N5 | 94.14 (19) | 92.9(2) | 94.0(2) |
| N5-M2-N6 | 85.4 (2) | 86.1(2) | 84.8(3) |
| N6-M2-N7 | 94.2 (2) | 93.1(2) | 94.8(2) |
| N7-M2-N4 | 86.00 (19) | 87.8(2) | 86.0(2) |

*NMR spectroscopy*

**17** can be easily examined with NMR-spectroscopy ($^{1}H$, $^{13}C$, COSY, HMBC, HSQC) since it is diamagnetic. The nickel containing compounds **18** and **19** are both paramagnetic.

The $^{1}$H-NMR spectrum of the diamagnetic **17** indicates that no THF is present (Figure 43). The solvent molecule THF, seen in the solid state structure (Figure 42), seems to substitutionally labile. Upon treating the solid under vacuum the solvent molecule is removed. A molecule without THF has been confirmed by the results of the elemental analysis fitting to the molecular formula without THF. The NMR spectrum shows a slight upfield shift of all proton resonances, compared to the ligand, due to the coordination of the zinc ions. Several resonances exhibit more complex splitting patterns, indicating an overall loss of symmetry upon coordination of the zinc ion. The signals of the protons $H_9$ appear as triplet of doublets at 4.06 and 3.91 ppm. Amine protons could not be detected as isolated signals but are in the multiplet from 3.26 ppm to 2.55 ppm. The amine protons are estimated to be underneath the multiplet of $H_{11+12+14+17}$. For further assignments refer to Figure 43.

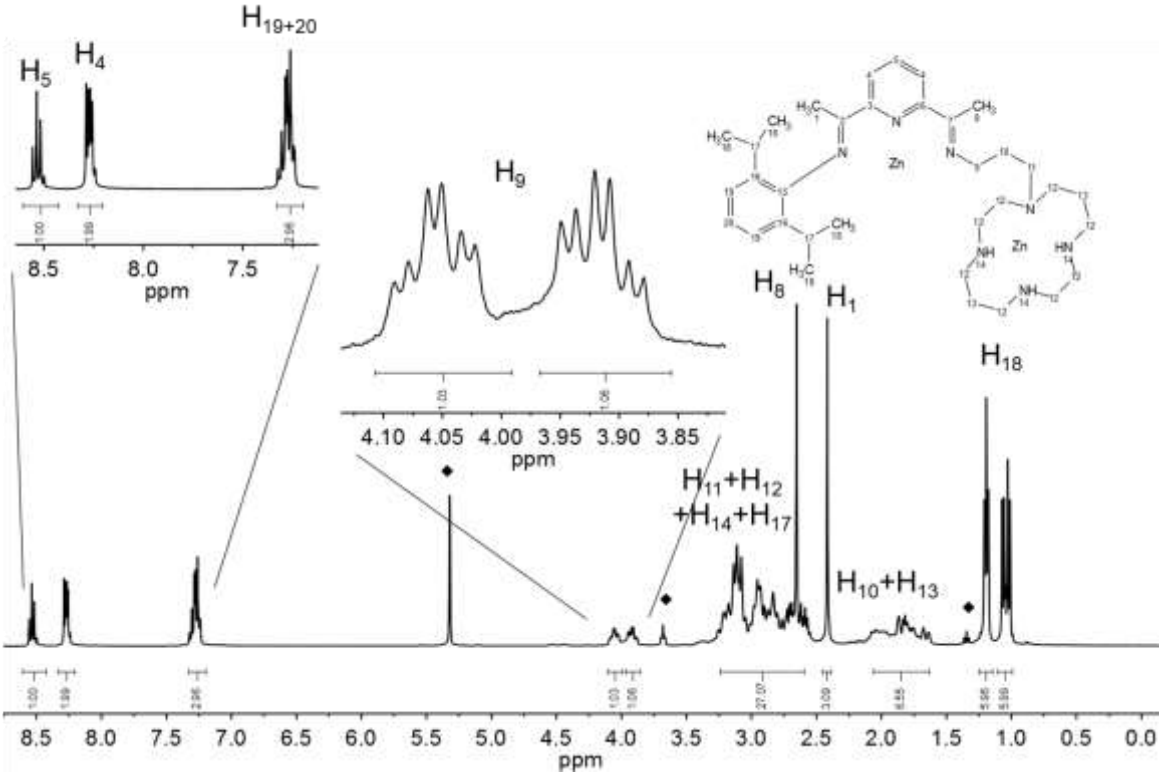


**Figure 43.** $^{1}$H-NMR spectrum of **17** (400 MHz, DCM-$d_2$) with labelling scheme (magnified: aromatic region and 3.80 – 4.15 ppm; ◆ = residual solvent signal) and assignment of the protons.[192]

The resonances for **18** are in a broad range from 210 – -7 ppm. The largest shifts and a broadening of the signals are expected for the protons next to the $Ni_{PDI}$ (see 2.2 for explanation). For **18**, an assignment has been carried out for the protons of the ring atoms, the methyl groups and one of the bridge atoms according to Ni(PDI) compounds in the literature and the integrals. [21, 200] Spin density calculations for an exact assignment were not

carried out. The assignments are displayed in Figure 44. The spectrum of **19** is more complex. The signals are in a range from 160 – -5 ppm. Further studies and calculations have to be made to make further assignments.

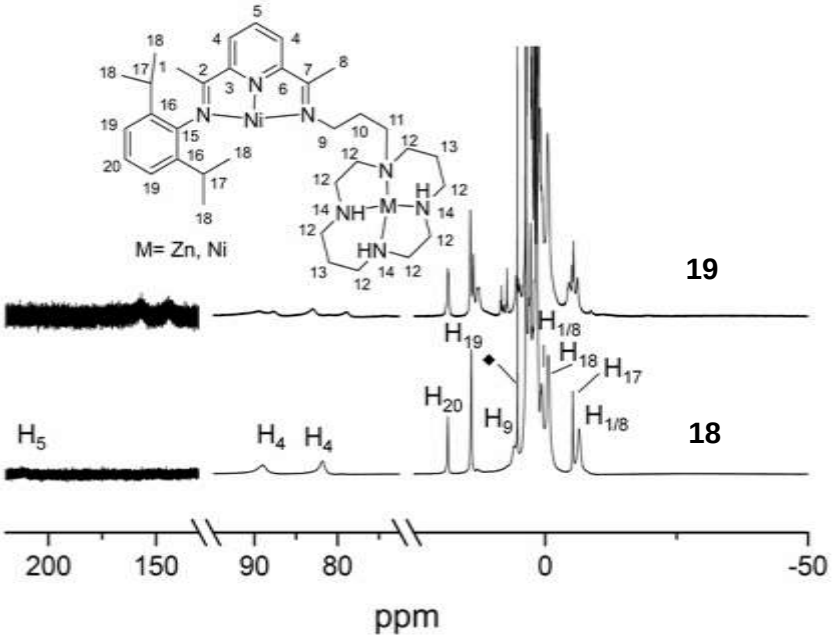


**Figure 44.** $^{1}$H-NMR spectrum of **18** and **19** (400 MHz, DCM-$d_2$) with labelling scheme (◆ = residual solvent signal) and assignment of the protons.

Evan's magnetic susceptibility measurements yielded a magnetic moment of 3.2 $\mu_B$ for **18** and **19**. The magnetic moment is consistent with an $S$ = 1 $Ni^{II}$ ion in the PDI and a $Zn^{II}$ or a square planar, diamagnetic $Ni^{II}$ ion in the cyclam. The signals of the cyclam protons in the $^{1}$H NMR spectrum of **18** (Figure 44) are not significantly shifted compared to the diamagnetic shifts of **17**. Therefore, the $Ni^{II}$ ion in the cyclam moiety is in a low spin configuration and has only low amounts of spin density due to the high-spin configuration of the $Ni^{II}$ ion in the PDI moiety

Electronic spectra

The electronic spectra (Figure 45) exhibit bands around 300 nm for all three compounds and are assigned as $\pi$-$\pi^*$-transitions, compared to the literature. [69, 178, 181, 201] **17** has additionally a shoulder at 352 nm, assigned as well to the Zn-PDI unit. For the Zn-cyclam moiety no transitions are expected, therefore, the $\pi$-$\pi^*$-transitions band are the only bands observed in the spectrum of **17**. The spectrum of **18** features further absorptions at longer

wavelengths ($\lambda_{max}$ = 369, 461 nm), as observed among Ni-cyclam complexes.[187-189] The bands are probably due to MLCT transitions as the absorption coefficient fit to MLCT bands and $\pi$-$\pi^*$-transitions are not expected. The transition bands are not present in the visible region in the spectrum of **19**. Below 350 nm, the spectrum of **19** is superimposable with **18** confirming the nickel coordination to the PDI unit in the heterobimetallic complex. The Ni-containing compounds additionally exhibit broad bands in the NIR region, with $\lambda_{max}$ = 948 (**18**) and 960 (**19**) nm (Figure A2). The absorption coefficients of the bands are small ($\varepsilon$ = 40 (**18**) and 25 (**19**) and therefore, these bands are probably due to d-d transitions.

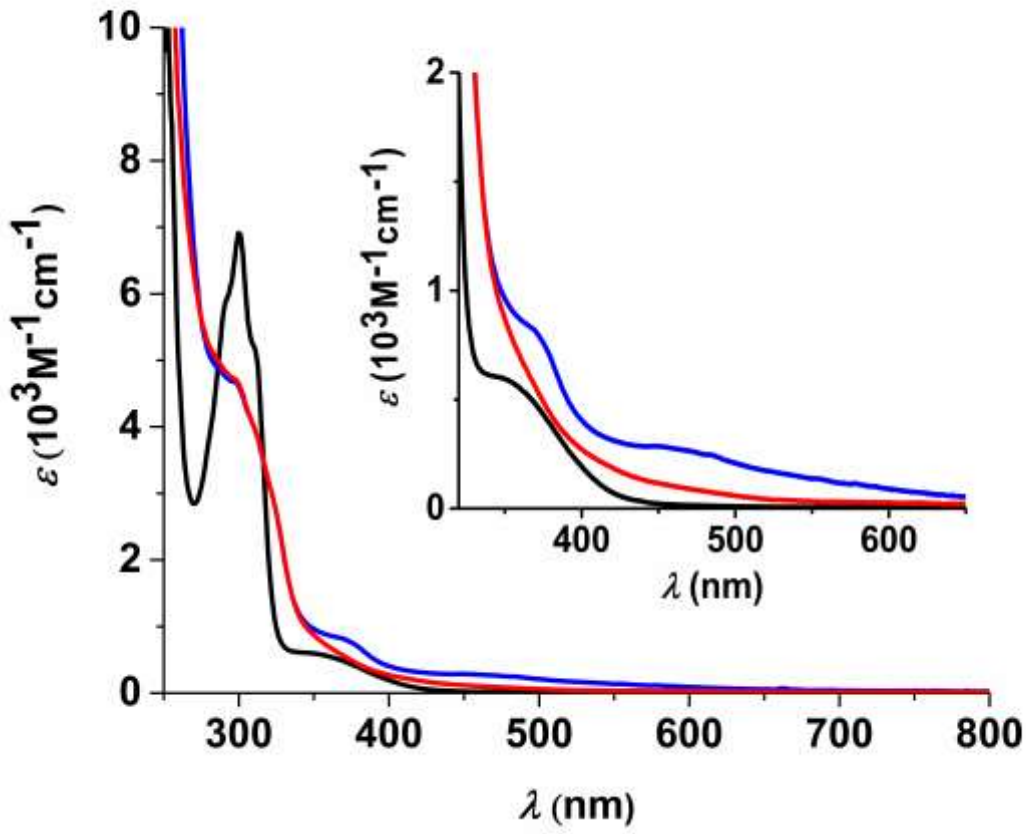


**Figure 45.** Electronic spectra of **17** (black), **18** (blue) and **19** (red) in THF (Inset: magnified region from 325 nm – 650 nm).[192]

*Redox activity*

The ligand scaffold was designed to support a wide range of oxidation states in both coordination sites. Furthermore, a non-innocent moiety was incorporated to generate low-valent forms, as well with metals like zinc. The low-valent forms are the active species in desired catalytic reactions, like $CO_2$ reduction (see 1.1.1). The redox-active PDI in the framework gives access to ligand-centred redox-processes and can accept up to four

electrons in its diimine $\pi^*$-orbitals. Therefore, a reduction of the dizinc complex **17** is feasible.[74-75] The first reduction event in the cyclic voltammogram is at a potential of -1.3 V (Figure 46) and fully reversible. It was assigned to the $PDI^0/PDI^{\bullet-}$ couple. With the second reduction at -1.7 V a dianionic $PDI^{2-}$ is formed, which is quasi-reversible. Both reductions are one-electron reduction processes. Compound **18** has additionally metal-centred processes. In the oxidative region a reversible $Ni^{III/II}$ couple at +0.8 V was detected and at lower potentials, -0.9, -1.4 and -1.6 V three reversible events are observed. The cyclic voltammograms of **19** and **17** help to elucidate the processes in the cyclic voltammograms of **18** and the assignment of cyclam based or PDI based redox couples can be carried out. In the cyclic voltammogram of **19** only two events at -0.9 and -1.4 V are observed. The reductive processes have to be Ni(PDI) based as the Zn(cyclam) is redox-inert. The events are assigned to the formation of the formally $Ni^{I}$ and $Ni^0$ compounds. The two other processes in the cyclic voltammogram of **3_8** are cyclam based and are the oxidation to $Ni^{III}$ (+0.8 V) and the redox couple $Ni^{II/I}$ (-1.6 V) of the cyclam ligated nickel ion. The potential for one-electron reduction of mononuclear cyclam compounds is highly dependent on the nature of additional ligands, but similar values in the literature support our assignments.[202-204] In comparison to the potentials of **17,** the first events of **18** and **19** are at a lower potential than the first potential of **17**. Thus the first reduction is probably metal based, while the second reduction of **18** and **19** is at a similar potential as the reduction to $PDI^{\bullet-}$ and therefore probably ligand based. Nevertheless, ligand- and metal-centered one-electron reduced Ni-PDI complexes are described in the literature and a final conclusion of metal-based or ligand based reduction can be drawn from the EPR data of the reduced compounds.[178, 205]

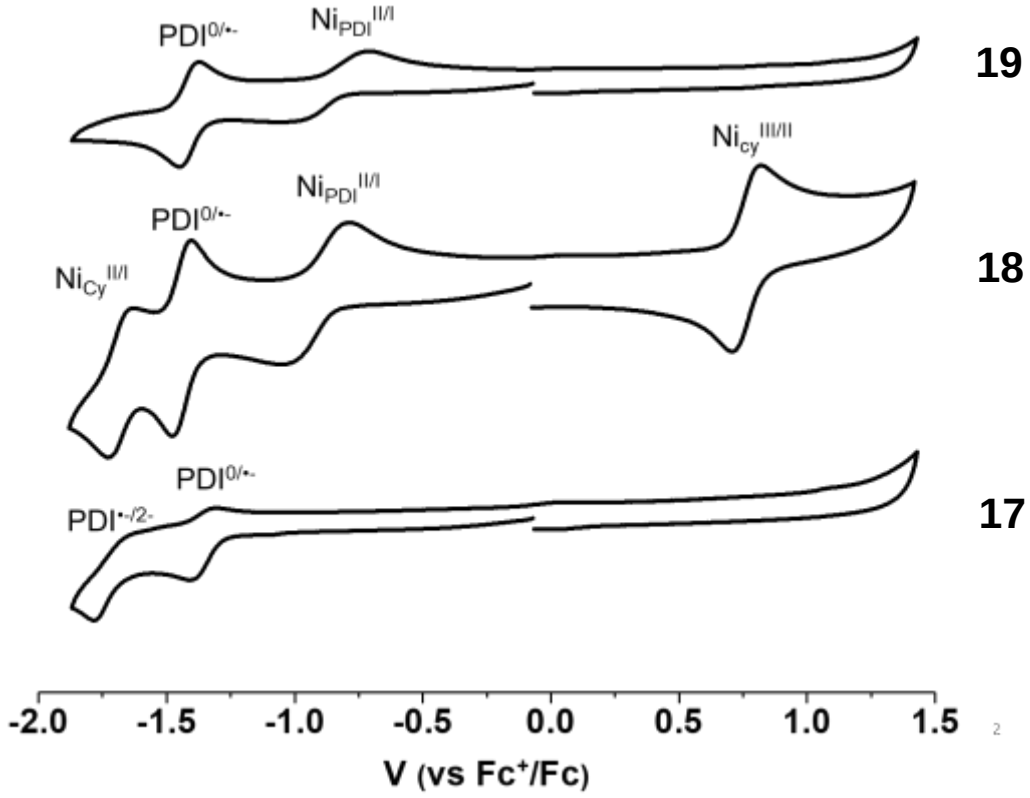


**Figure 46.** Cyclic voltammograms of **17, 18** and **19**; MeCN, 0.1 V $s^{-1}$, 0.1 M $[N(n\text{-}Bu)_4]PF_6$.[192]

## 3.6 Reduced forms of nickel and zinc complexes

The active species in catalytic reactions are often a low valent form of the actual complex as summarised in 1.1. The elucidation of the mechanism in catalytic studies is often difficult as the intermediates cannot be easily isolated. Therefore, the chemical generation of low valent forms is desirable.

The chemical generation of the one-electron reduced complexes is straightforward (Scheme 26). **17** was reduced with one equivalent of decamethylcobaltocene in THF yielding a bright orange compound (yield after crystallisation: 46%). The reduction of **18** and **19** occurs at a lower potential and was carried out with cobaltocene to give dark-blue compounds (yield after crystallisation: 2**1** 56%; **22** 37%). The results of the elemental analysis data of **20** suggest a THF solvent molecule in the molecular structure.

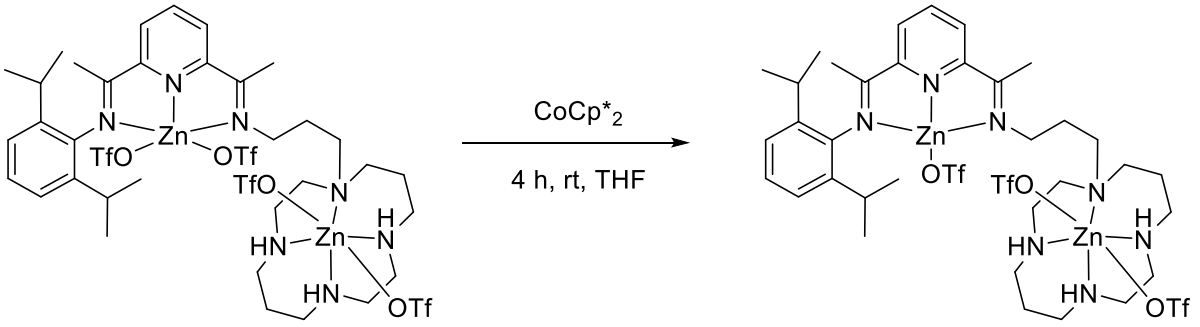


**[$Zn_2$(PDIpCy)(OTf)$_4$], 17**

**[$Zn_2$(PDIpCy)(OTf)$_3$], 20**

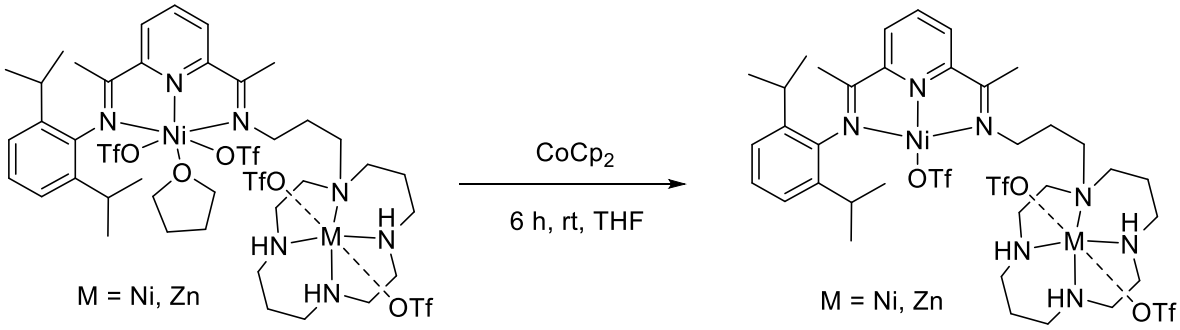


**[$Ni_2$(PDIpCy)(THF)(OTf)$_2$](OTf)$_2$, 18**
or **[NiZn(PDIpCy)(THF)(OTf)$_4$], 19**

**[$Ni_2$(PDIpCy)(OTf)](OTf)$_2$, 21**
or **[NiZn(PDIpCy)(OTf)$_3$], 22**

**Scheme 26.** Synthesis of **20, 21** and **22**.[192]

*Electronic spectra*

The electronic spectra of **20, 21** and **22** were measured in THF (Figure 47). The *π*-*π**-transition bands of **20** are shifted to lower wavelength (284 nm) compared to the non-reduced compound. Additionally, the dizinc compound exhibits two charge transfer bands at 367 and 500 nm in the visible region with an absorption coefficient of 3980 and 3270 $M^{-1}$ $cm^{-1}$ of presumably *π*-*π**-character and several bands in the NIR region from 800 – 2200 nm (*ε* = 230 and 630 $M^{-1}$ $cm^{-1}$). A red-shift in bands has been observed in the literature as well.[73] Compound **21** and **22** display several bands in the visible and NIR region between 400 – 1600 nm with intensities between 1010 – 1610 $M^{-1}$ $cm^{-1}$ and 790 – 1520 $M^{-1}$ $cm^{-1}$. The wavelength values of the absorption maxima are similar and are comparable with data in the literature.[178, 205-206] All three compounds display several bands in the same region, e.*g.* at 500 and 1100 nm. Therefore, the character of the bands is probably *π*-*π**-transition based as the bands of the **20** are *π*-*π**-transition bands. The character of the other bands cannot be assigned for sure but MLCT bands are one possibility. A comparison of the absorption bands

with data in the literature shows no difference between ligand- or metal-centred reduced Ni(PDI) compounds.

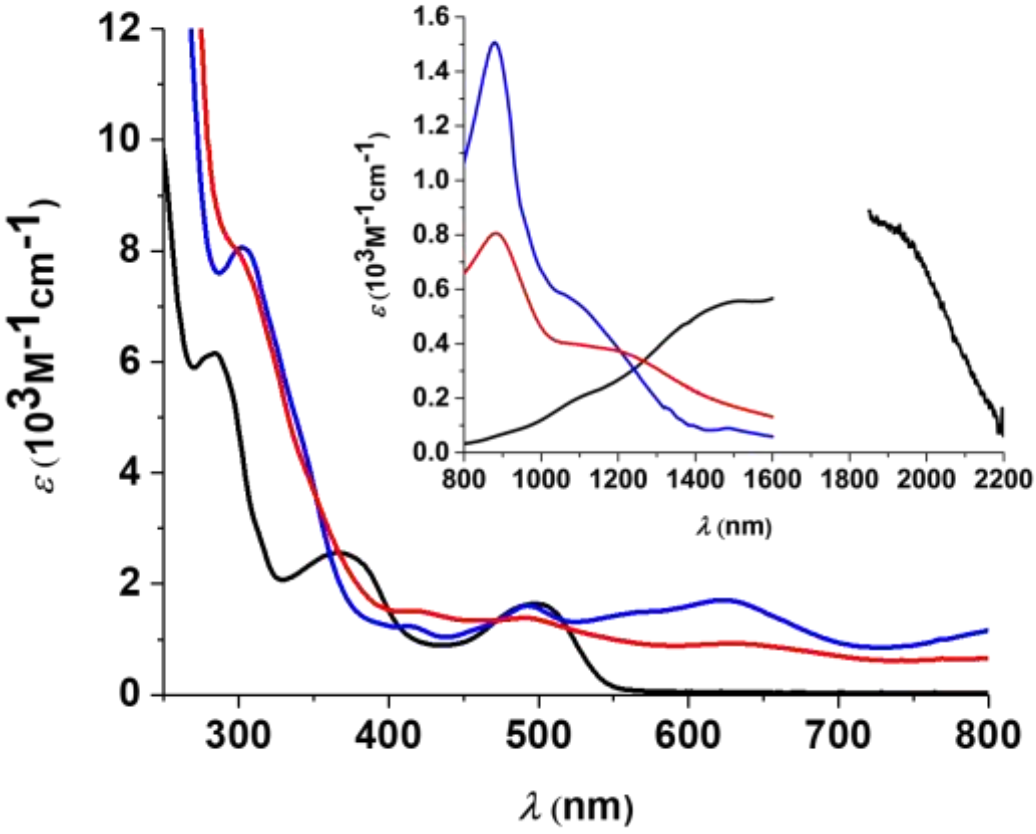


**Figure 47.** Electronic spectra of **20** (black), **21** (blue) and **22** (red) in THF (Inset: magnified region from 800 nm – 2200 nm).[192]

*Electron paramagnetic resonance*

The electronic structure of the reduced compounds is a ligand radical for **20** and the reduction of the nickel containing species **21** and **22** is assumed to be metal-based. The assumptions are taken from the cyclic voltammetry measurements of the non-reduced compounds (Figure 46). As for the Ni(PDI) compounds metal-based and ligand-based reduction exist in the literature, EPR measurements are pursued to determine the electronic structure of the compounds. [178, 205] For the measurement and the interpretation of the spectra we were supported by Dr. Stephen Sproules (University of Glasgow).

The EPR spectrum of **20** displays a signal corresponding to an organic radical (Figure 48). The *g*-values confirm a ligand-centred radical, confined in the PDI-moiety, in a near anisotropic spectrum ($g$ = (2.0105, 2.0060, 2.0005)). The assignment to a ligand radical supports our assignments in the cyclic voltammetry measurements and is expected for a

non-redox active zinc ion in a non-innocent ligand. The *g*-value is comparable with a value measured for a Zn(PDI) in the literature.[207]

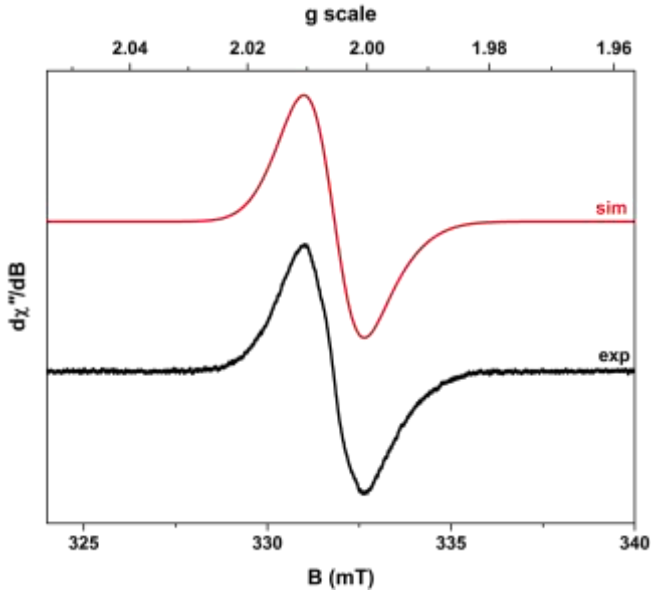


**Figure 48.** X-band EPR spectrum of **20** in THF at 140 K. Experimental data are shown by the black line; simulation depicted by the red trace (experimental conditions: frequency, 9.3174 GHz; modulation, 0.5 mT; power, 0.63 mW).[192]

The EPR spectrum of **21** in frozen THF at 140 K features several signals (Figure 49). The pattern of the features cannot be explained with one reduced nickel species. One of the features (highlighted in Figure 49) can be assigned as a ligand radical and has a similar *g*-value as it was observed in the measurement of **20**. The other features cannot be explained with only one $Ni^{I}$ species as the integrated spectrum do not fit to one $Ni^{I}$ species. At least two species, probably one three-, the other four coordinate, cause the pattern of the signal. To elucidate the exact ratio and the reasons for coexisting species further studies, for example temperature depending studies and measurements in different solvents, have to be carried out.

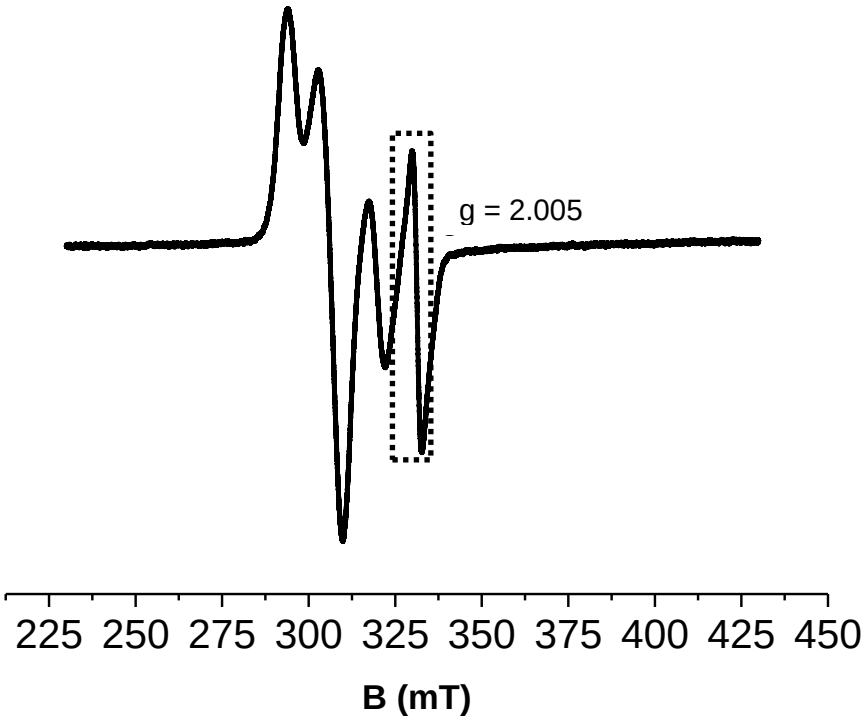


**Figure 49.** X-band EPR spectra of **21**. (THF at 140 K; experimental conditions: frequency, 9.264 GHz; modulation, 0.4 mT; power, 0.63 mW). Box highlights the position of the ligand radical signal.

The electronic structure of **21** and **22** are confirmed as a $d^9$ paramagnetic centre by the room temperature spectra and the frozen glass (140 K) solution spectra recorded in MeCN/toluene (Figure 50). The isotropic room temperature spectra display signals with *g*-values of 2.1512 (**21**) and 2.1510 (**22**). Both compounds give as well similar spectra for the frozen glass measurements at 140 K, with *g* = (2.2363, 2.1310, 2.0858) for **21**, and *g* = (2.2336, 2.1412, 2.0901) for **22,** and are the mixed-valent compounds $[Ni^{I}Ni^{II}(PDIpCy)]^{3+}$ and $[Ni^{I}Zn^{II}(PDIpCy)]^{3+}$. The $Ni^{I}$ ion of PDI site is probably four-coordinate in a square planar geometry and no other species is observed in the spectra, in contrast to the spectrum measured in THF for **21**. As the structural evidence of the compounds is missed, no elucidation of the coordination is feasible. The values and geometry are in good agreement with metal-based reduced Ni(PDI) sites in the literature.[200, 205, 208]

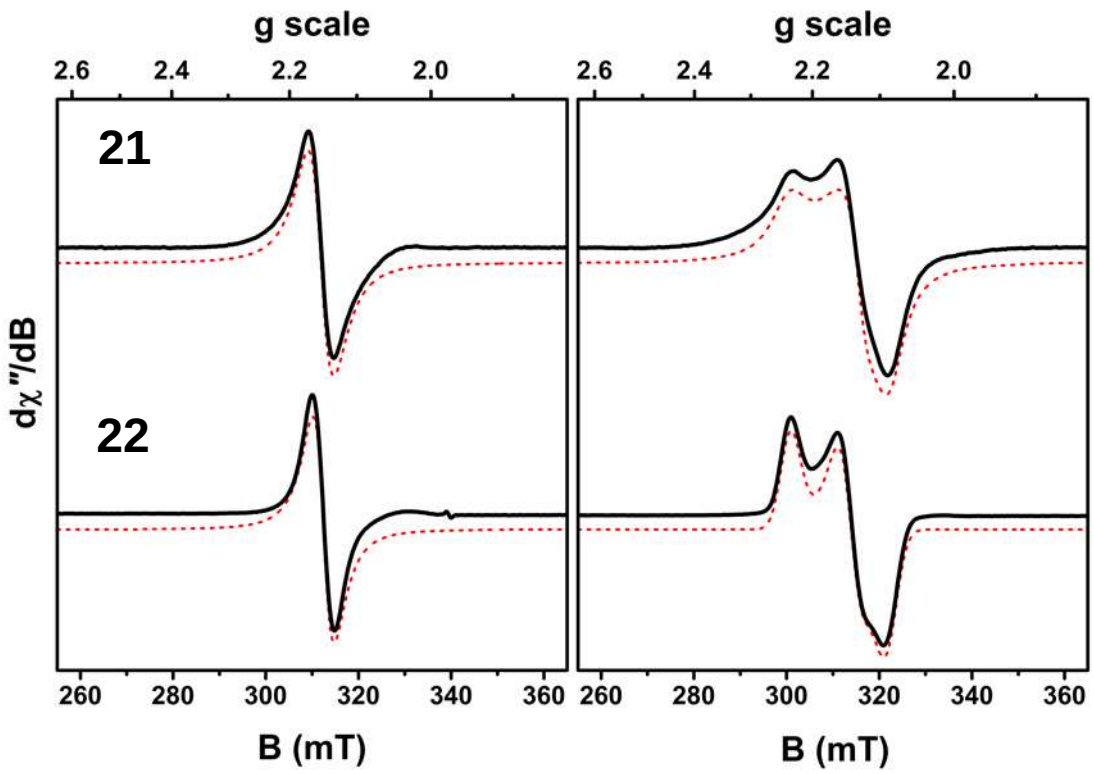


**Figure 50.** X-band EPR spectra of **21** and **22.** (left: MeCN/toluene at room temperature; right: MeCN/toluene frozen glass at 140 K. Experimental data are shown by the solid line; simulation depicted by the dashed trace; experimental conditions: frequency, 9.410 GHz; modulation, 0.5 mT; power, 0.63 mW).[192]

*Results of further reduction experiments*

The second reduction of **20** and **21** has been conducted as well, but only preliminary results are collected so far (Scheme 27). The reduction of the zinc containing compound to a $PDI^{2-}$ species, with two equivalents of sodium or decamethylcobaltocene, was so far not successful. Stabilisation of the two times reduced species with 4-(dimethylamino)-pyridine, as it is done in literature, did not lead to the product either.[207] The reduction to a formal $Ni^0$ compound, $Ni^I$ ligand radical, as assumed from the cyclic voltammetry experiment, is feasible with decamethylcobaltocene. The reduced species seems to be only short lived at room temperature and therefore, is handled at temperatures below -30 °C.

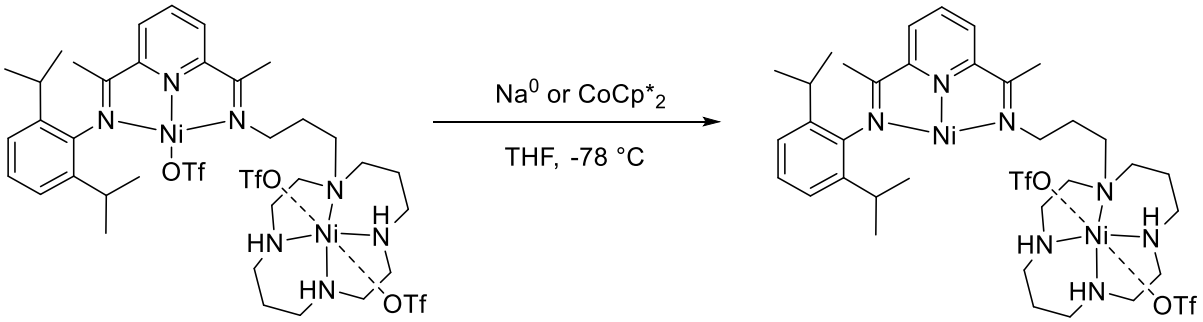


**[Ni$_2$(PDIpCy)(OTf)](OTf)$_2$, 21** **[Ni$_2$(PDIpCy)(OTf)](OTf)$_2$, 23**

**Scheme 27.** Synthesis of **23.**

So far no structural data exists for **23**. The absorption bands of the UVVis measurement have been compared with the literature (Figure 51).[178] The compound features several bands at 436, 477 and 700 nm and *π*-*π**-transition bands at 279 nm (Figure 53). Wieghardt *et al.* showed in their work that for their $[Ni(L)]^{n+}$ (L = 2,12-dimethyl-3,7,11,17-tetraazabicyclo[11.3.1]-heptadeca-1(17),2,11,13,15-pentane) compounds the two-electron reduced species has similar bands, two bands below 500 nm and another band at 750 nm. It has to be taken into account that the PDI in **23** has different substituents and therefore, the absorption can be observed at slightly different wavelength. Additional data has to be collected to confirm the generation of a formal $Ni^0$ compound and consequently the formation of a two-electron mixed valence compound.

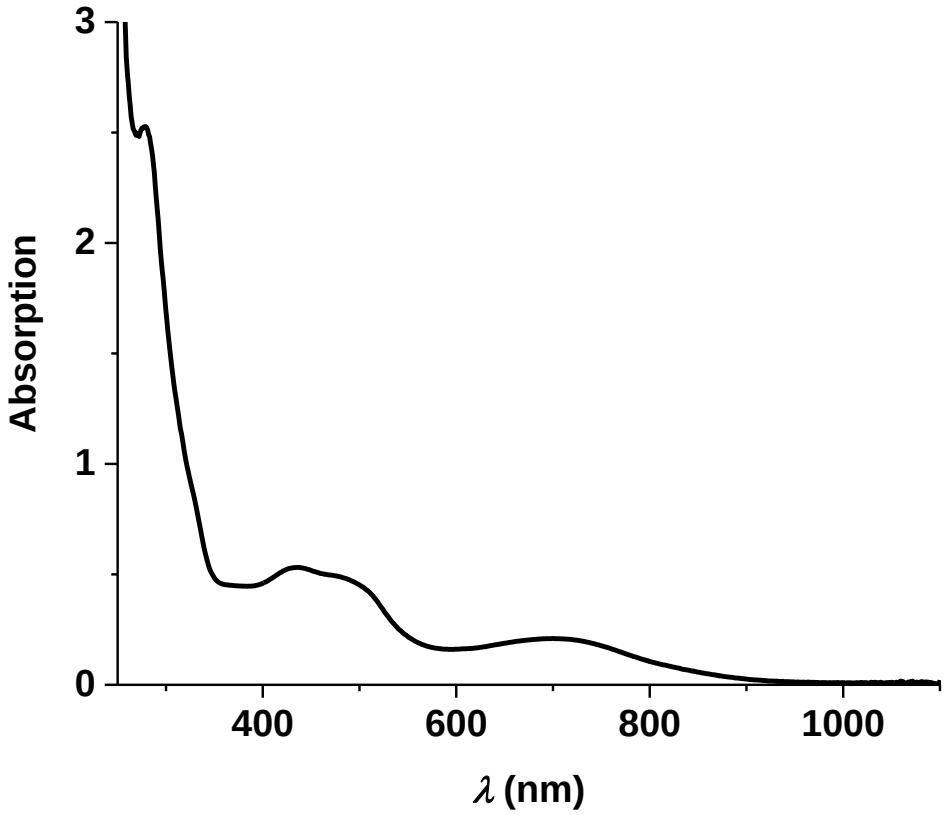


**Figure 51.** Electronic spectra of **23** in THF.

## 3.7 Metal complexes with iron

The compounds with nickel and zinc have already been carefully examined and low-valent forms isolated. Diiron compounds are forming interesting *μ*-oxo bridged compounds which are used in oxidation reactions (see 1.2.2). Furthermore, iron compounds can be used in $CO_2$ reduction, where iron porphyrins compounds already showed promising results (see 1.1.1). Therefore, the next attempt was to synthesise a diiron complex.

The synthesis of the three iron complexes with the counterions chloride, triflate and hexafluorophosphate are carried out in MeCN at room temperature to give blue (chloride) and red (triflate, hexafluorophosphate) compounds (Scheme 28). The molecular formula, as suggested in Scheme 28, is not ensured due to the possibilities of coordinating solvent molecules. Structural evidence could not be obtained so far. A coordination of solvent molecules, especially for the weak or non-coordinating counterions, is highly likely as for the compound **25** and **26** a colour change to purple is observed upon dissolving in THF.

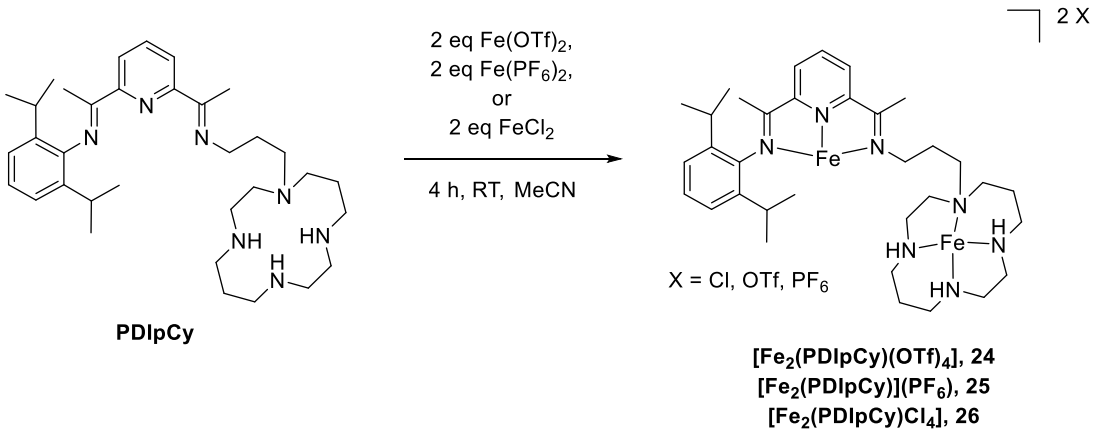


**Scheme 28.** Synthesis of **24, 25** and **26.**

The electronic spectra of **24** and **26** are shown in Figure 54. The bands of **25** are identical with **24** and therefore not displayed in Figure 52, but shown later in Figure 53. While in THF **26** has one broad absorption band between 450 and 650 nm displaying the purple colour, the compound in MeCN exhibits bands at 445 and 494 nm explaining the red colour. The maximum of the *π*-*π**-transitions are around 300 nm in the spectra. The blue complex **24** has an absorption band at 660 nm. The bands at higher wavelength are probably due to MLCT transitions as the no bands are observed in spectrum of **20** in this region.

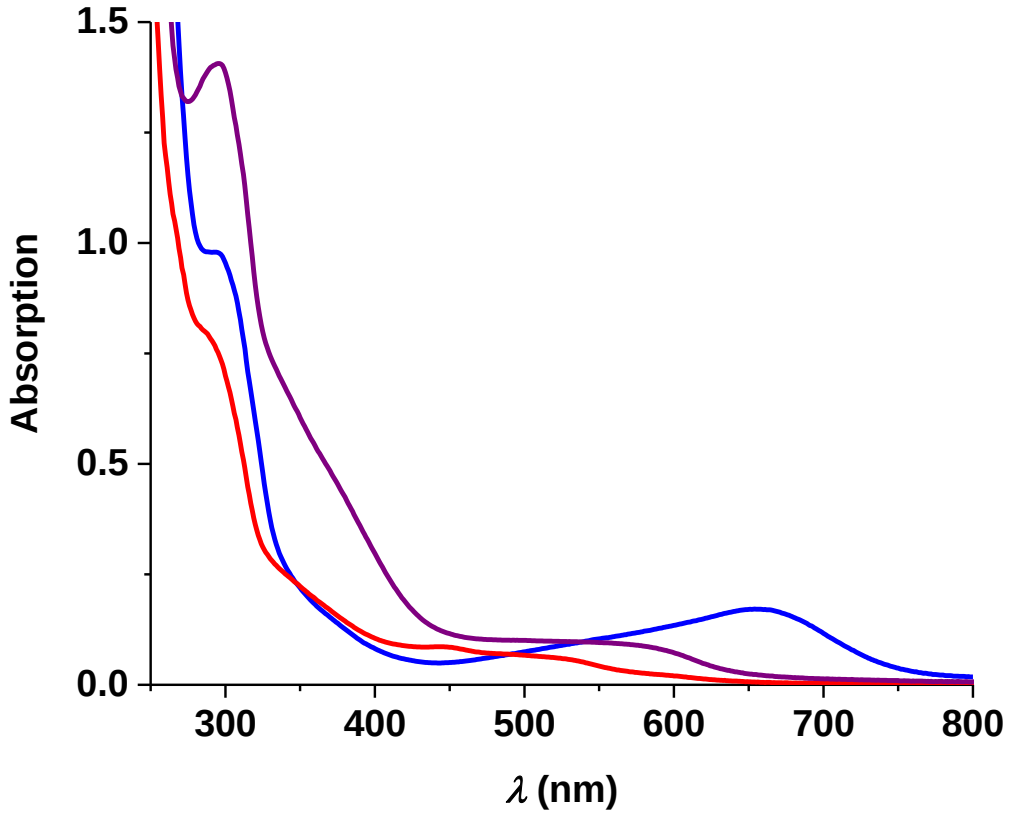


**Figure 52.** Electronic spectra of **24** in THF (purple), **24** in MeCN (red) and **26** in MeCN (blue).

The bands identified in the electronic spectra are assigned to bands of the PDI moiety as the absorption of the Fe(cyclam) is weak and is located at 370 nm and 500 to 700 nm.[69, 182-183] A coordination of the second metal cannot be proven with the spectra of **24** and **26**, therefore, a titration experiment was performed with the soluble $Fe^{II}$ precursor $[Fe(MeCN)_6](PF_6)_2$ in MeCN (Figure 53). The spectrum is not dilution corrected. With the first equivalent no shift of the $\pi$-$\pi^*$-transition bands compared to the ligand is observed, but a band at ~350 nm rise. In literature, weak bands for Fe(cyclam) compounds are described at these wavelengths. [182-183] With addition of the second equivalent an effect on the $\pi$-$\pi^*$-transitions bands is observed and the bands shift to a higher wavelength. The band between 450 and 650 nm intensifies as well. The observation of the consecutive rising bands leads to the conclusion that the iron ion coordinates to the cyclam first and the second equivalent of iron ions is accommodated by the PDI moiety. Therefore, a coordination of two iron ions is feasible.

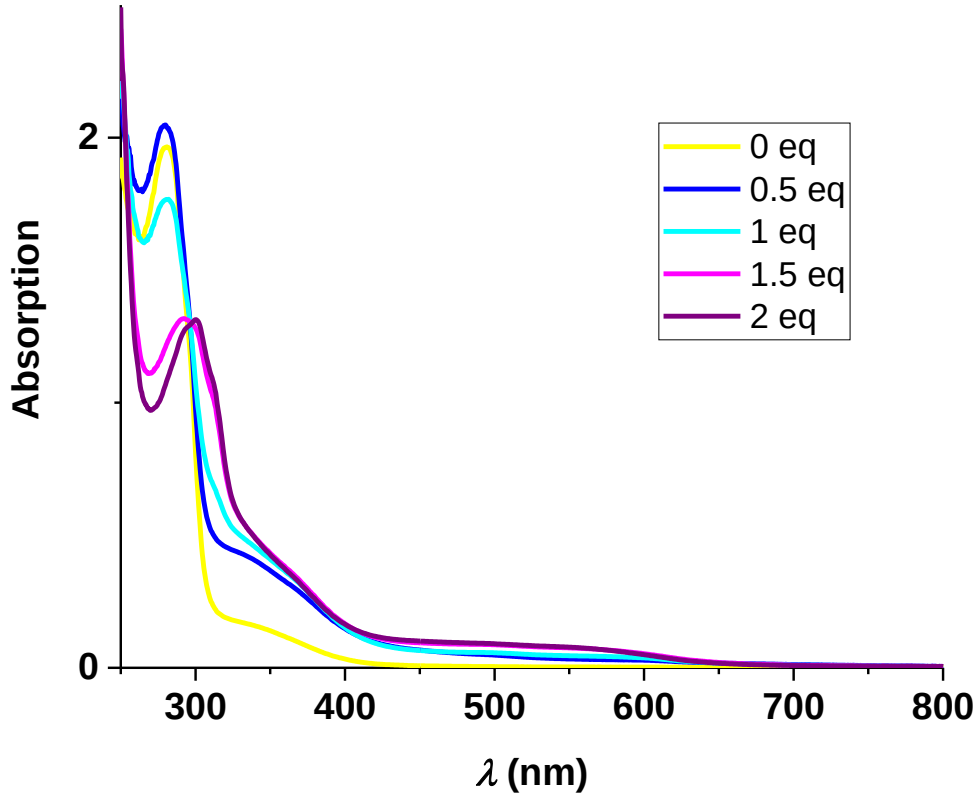


**Figure 53.** Electronic spectra of titration experiment with 0.5-2.0 eq $[Fe(MeCN)_6](PF_6)_2$ into a solution of **PDIpCy** in MeCN.

Further reinforcing of the statement of the coordination of two iron ions is done by FAB mass analytic. The FAB mass spectroscopy is a destructive method and so for only fragments are detected. The biggest detected fragment for **26** and **24** are 776.7 m/z and 1117.7 m/z fitting to the fragments $[Fe_2(PDIpCy(-3H))(Cl)_3]$ and $[Fe_2(PDIpCy(-3H))(OTf)_3]$.

*Future work*

The Fe(cyclam) compounds have been object of several oxidation studies as it supports several iron-oxo species and is a good oxidation catalyst.[164, 173] Some preliminary studies have been made with the Fe(PDIpCy) compounds and the stability in air tested.

A crystal was obtained from slow diffusion of air into a solution of **27** in DCM/pentane and the preliminary molecular structure is shown in Figure 56. The ligand scaffold and the coordination sites are intact after exposure to air. Both iron ions have the oxidation state +3 and are connected *via* a *μ*-oxo bridge. The complex is charged +2. An interesting feature of

the crystal is that it shows the flexibility of the linker. The two iron ions are 3.6 Å apart, which is noticeable shorter than 8 Å observed for **17**, **18** and **19**. The Fe – O distance is 1.8 Å and is in the range of *μ*-oxo bonds observed for Fe(PDI)-(*μ*-oxo)-Fe(PDI) and Fe(cyclam)-(*μ*-oxo)-Fe(cyclam).[209-210] The angle Fe1 – O – Fe2 is 167° and close to linear. Furthermore, the Fe – N distances fit as well to $Fe^{III}$ ions, so a mixed valence species $Fe^{II}Fe^{III}$ with a (*μ*-hydroxo)-bridge is not likely. For (*μ*-hydroxo)-bridges, longer Fe – O distances (~2 Å) and more bended angles are observed compared to (*μ*-oxo) as well. [209-212] The mechanism for the formation of the *μ*-oxo bridge is more difficult to elucidate. A similar mechanism as the Balch mechanism (Scheme 16) is imaginable, but would include a reductant (*e.g.* $Fe^{II}$ ions) in the reaction. The homolytic splitting of the, with oxygen, formed diiron-peroxo-species $Fe^{II}$ ion is as well a pathway as a reaction of an iron-peroxo-species with protons, originating from water molecules, and the release of a hydroxyl group. Both pathways include the reaction with a $Fe^{II}$ to form a *μ*-oxo bridge. None of these described pathways have been proven and further studies have to be carried out for the elucidation of the mechanism.

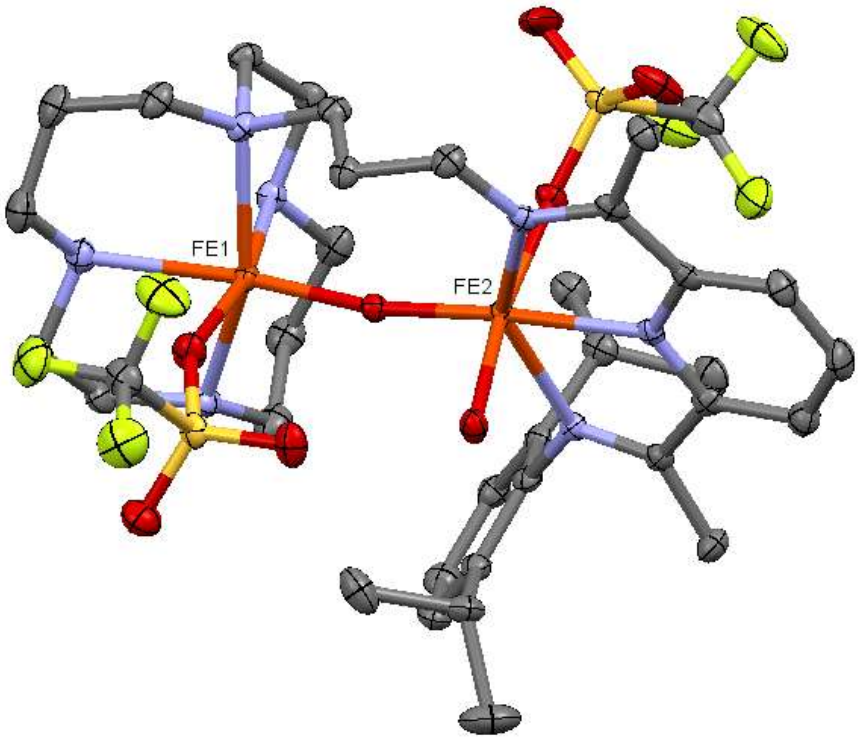


**Figure 54.** Preliminary molecular structures of the oxidised **27** (50% probability ellipsoids). Hydrogen, non-coordinated counter ions and solvent molecules are omitted for clarity.

## 3.8 Conclusion

The first and the second generation of the “basket ligands” formed already promising complexes. In the first generation, the solubility of the monometallic complexes and consequently the formation of a bimetallic complex was the reason to adapt the ligand scaffold. For continuing studies the solubility of the complexes with the ligands of the first generation has to be enhanced, as well to be suitable for homogenous catalysis, by adding functional groups.

The synthesis of the “open basket ligand”, the second generation, and the metal complexes already gave promising results for bimetallic complexes. The coordination of a second metal in ligand scaffold **3_3** is not feasible for every metal ion. Complexes with iron are so far the most promising complexes as the coordination of two metals is likely. The coordination geometry is not revealed as a molecular structure is missing, which would be especially interesting for the innocent site, formed by the amines.

With the PDIpCy ligand an unsymmetrical ligand scaffold with great potential was established. Homo- and heterobimetallic compounds are accessible in a one-pot synthesis. The metal ions in the PDIpCy ligand are only physically connected *via* the propyl linker, but concluding from the NMR studies are not electronically coupled as otherwise the cyclam protons would be more effected by the paramagnetic Ni ion in the PDI moiety. The flexible linker along with the possible configuration of the cyclam (in our molecular structure only the R,S,S,R configuration is observed) interferes with the crystal growing which is seen in the rest electron density in the crystal structure, but nonetheless, a crystal was successfully grown to determine the molecular structure of **17, 18** and **19**. The formation of bimetallic complexes for catalysis can enhance reaction rates, as shown in 1.1, by cooperative interactions between the metals (see 3.1). Heterobimetallic compounds may help to elucidate the mechanism and the role of the second metal in catalysis.

Furthermore, the synthesis of the ligand-based reduced compound **20** and the metal based reduced compounds **21** and **22** was successful. The reduced compounds are a step toward elucidating the reactivity of the compounds and the mechanism of catalytic cycles. Especially the role of the second metal will be interesting. The metal ions as Lewis acid would be conceivable, in particular for the non-redox-active zinc ion, but as well for the nickel ions. [213-214] On the other reactions including migration of substrates, as seen in the diiridium complex of Nocera’s group should be feasible. The described pathways for hydrogen production or $CO_2$ activation include two-electron processes. Therefore, the generation and isolation of the formally $Ni^0$ species in the PDI moiety, a two-electron mixed valent

compound, is the next goal. Additionally, the ligand scaffold offers amine protons. In several examples amines have shown to enhance the effectivity of catalysts as they can be protonated. A pending proton can favour the heterolytic mechanism for hydrogen production.[22-23, 215-217]

The structural proof of the diiron compounds **24**, **25** and **26** is one of the missing parts in the iron PDIpCy project. Chirik *et al.* showed several applications for Fe(PDI) compounds, in the reduced and non-reduced version, *e.g.* hydrogenation and N-N-bond cleavage.[167, 171-172] The role of the second metal in the cyclam moiety has to be defined in reactivity experiments. On the other side, the cyclam is known in the oxidation chemistry. The preliminary structure of the Fe-*μ*-oxo-Fe compound has not only shown the flexibility of the ligand scaffold, but as well that in the presence of a suitable substrate or bridging atoms cooperative interactions might be possible through the connection of the metal ions. The reactivity of Fe-*μ*-oxo-Fe compound in oxidation reactions has to be pursued as well, since Fe(cyclam) compounds are known to perform as catalysts in oxidation reactions. The active species in iron cyclams is often described a $Fe^{IV}$=O intermediate.[61, 164] The activation of the *μ*-oxo group, as seen in Nocera's experiment with Fe(porphyrin)-compounds by photoactivation, could be a key point in the reactivity.

Overall the formation of additional homo and heterobimetallic compounds have to be further pursued and the reactivity explored. [216, 218]

## 3.9 Experimentals

Chemicals were purchased from Sigma Aldrich and used as received unless otherwise noted. Solvents were dried by passage over activated alumina columns from MBraun and stored over 3 Å (MeCN, EtOH) or 4 Å molecular sieves. 1-(6-(1-((2,6-diisopropylphenyl)imino) ethyl)pyridin-2-yl)ethan-1-one (**16**) [191] was prepared as described in the literature, additionally the experimental procedures below are described as in the publication of Hess *et al*.[192]

Solution state NMR spectra were recorded on a Bruker Avance Ultrashield (400 MHz $^{1}$H, 100 MHz $^{13}$C). Electronic spectra were recorded on an Agilent Cary 60 UV-visible spectrophotometer, equipped with a UNISOKU CoolspeK cell for low temperature measurements. Electronic spectra for the NIR region were recorded with a Shimadzu

UV3600 Plus. ESI (electrospray ionization) mass spectra were measured using a LCQ fleet (solvent: MeCN + 0.1% formic acid, flow rate 0.35 ml/min and UV-detector at 220 and 280 nm). LIFDI (liquid injection field desorption ionization) mass spectra were measured with a Waters LCT; special ionization cell obtained from Linden CMS GmbH, Leeste, Germany. IR measurements were performed on a PerkinElmers FT IR Frontiers spectrometer with a ZnSe ATR unit. Microanalyses were carried out at the Technische Universität München. Electrochemical measurements were carried out using an EmStat3+ potentiostat using a three-electrode cell equipped with glassy carbon electrodes as counter and working electrodes and $Ag/AgNO_3$ as reference electrode. Potentials are reported with reference to an internal standard of ferrocenium/ferrocene ($Fc^{+/0}$). X-band EPR spectra were collected on a Bruker ELEXSYS E500 spectrometer or a JEOL JES-FA 200 and simulations were performed using Bruker's Xsophe software package.[219]

Crystallographic data were collected on an X-ray single crystal diffractometer equipped with a CMOS detector (Apex III, κ-CMOS), an IMS microsource with $CuK_\alpha$ radiation ($\lambda = 1.54178$ Å) and a Helios optic using the Apex III software package.[132] The measurements were performed on a single crystal coated with perfluorinated ether. The crystal was fixed on top of a glass fiber and transferred to the diffractometer. The crystal was frozen under a stream of cold nitrogen. A matrix scan was used to determine the initial lattice parameters. Reflections were merged and corrected for Lorenz and polarization effects, scan speed, and background using SAINT.[133] Absorption corrections, including odd and even ordered spherical harmonics were performed using SADABS.[133] Space group assignments were based upon systematic absences, E statistics, and successful refinement of the structures. Structures were solved by direct methods with the aid of successive difference Fourier maps, and were refined against all data using SHELXLE[134] in conjunction with SHELXL-2014.[135] Hydrogen atoms were assigned to ideal positions and refined using a riding model with an isotropic thermal parameter 1.2 times that of the attached carbon atom (1.5 times for methyl hydrogen atoms). If not mentioned otherwise, non-hydrogen atoms were refined with anisotropic displacement parameters. Due to the limited quality of the crystal and multiply positional disordered residues and solvent/anion molecules, multiple restraints (DELU, RIGU, SAME) and constraints (EADP) had to be used in the final model. Full-matrix least-squares refinements were carried out by minimizing $\Sigma w(F_o^2-F_c^2)^2$ with SHELXL-97[136] weighting scheme. Neutral atom scattering factors for all atoms and anomalous dispersion corrections for the non-hydrogen atoms were taken from International Tables for Crystallography.[137] Images of the crystal structures were generated by Mercury.

**3-((2-(dimethylamino)ethyl)(methyl)amino)propanenitrile, 11**

Trimethylethylenediamine (1.4 g, 13.7 mmol, 1.0 eq) was dissolved in 25 ml EtOH and acrylonitrile (2.8 g, 54.8 mmol, 4.0 eq) was added. The solution was stirred at room temperature for 16 h. The solution was concentrated in vacuo to give a colourless liquid (2.2 g, 13.6 mmol, 98%). $^{1}$H NMR δ (400 MHz, $CDCl_3$) 2.76 (t, *J* = 7.1 Hz, 2H), 2.52 (t, *J* = 6.5 Hz, 2H), 2.48 (t, *J* = 7.1 Hz, 2H), 2.39 (t, *J* = 7.1 Hz, 2H), 2.30 (s, 3H), 2.23 (s, 6H); $^{13}$C NMR δ (100 MHz, $CDCl_3$) 119.1, 57.4, 55.2, 53.4, 46.0, 42.0, 16.; LRMS ($ESI^+$) *m/z*: 155.99 $[M + H]^+$; HRMS ($ESI^+$) *m/z*: 156.1493 $[M + H]^+$.

**N-(2-(dimethylamino)ethyl)-N-methylpropane-1,3-diamine, 12**

**11** (2.2 g, 14 mmol, 1.0 eq) was added slowly to a suspension of $LiAlH_4$ (560 mg, 15 mmol, 1.05 eq) in 8 ml $Et_2O$ at 0 °C. The suspension was stirred for 3 h at room temperature and alternately quenched with 560 µl $H_2O$, 560 µl aq. NaOH (15%) and 1.68 ml $H_2O$. The suspension was filtered and the solvent removed before purification by distillation (30 °C, 9 x $10^{-2}$ bar) to give a colourless oil (1.03 g, 6.5 mmol, 46%). $^{1}$H NMR (400 MHz, $CDCl_3$) δ 2.72 (t, *J* = 6.8 Hz, 2H), 2.52 (m, 6H), 2.23 (s, 9H), 1.16 (q, *J* = 7.0 Hz, 2H), 1.45 (s. 2H); $^{13}$C NMR (100 MHz, $CDCl_3$) δ 57.6, 56.1, 55.9, 46.0, 42.8, 40.8, 31.2; LRMS ($ESI^+$) *m/z*: 160.02 $[M + H]^+$; HRMS ($ESI^+$) *m/z*: 160.1808 $[M + H]^+$.

***N*,*N*-(((pyridine-2,6-diylbis(ethan-1-yl-1-ylidene))bis(azaneylylidene))bis(propane-3,1-diyl))bis(*N*,*N*,*N*-trimethylethane-1,2-diamine) 13**

A solution of **12** (1.0g, 6.3 mmol, 2.1 eq) and diacetylpyridine (488 mg, 3.0 mmol, 1.0 eq) in 10 ml toluene was heated to 80 °C for 40 h over 4 Å molecular sieves in a pressure tube. The solution was filtered and the excess of **12** and solvent removed to give **13** as a yellow oil (1.03 g, 2.3 mmol, 77%). $^{1}$H NMR δ (400 MHz, MeCN-$d_3$) 8.07 (d, *J* = 7.7 Hz, 2H), 7.76 (t, *J* = 7.8 Hz, 1H), 3.53 (t, *J* = 6.9 Hz, 4H), 2.44 (dt, *J* = 17.2, 7.3 Hz, 8H), 2.37 (s, 6H), 2.31 (dd, *J* = 8.1, 5.9 Hz, 4H), 2.20 (s, 6H), 2.13 (s, 12H), 1.84 (p, *J* = 6.9 Hz, 4H), LRMS ($ESI^+$) *m/z*: 445.96 $[M + H]^+$; HRMS ($ESI^+$) *m/z*: 446.3964 $[M + H]^+$.

**3-(1,4,8,11-tetraazacyclotetradecan-1-yl)propanenitrile, 14** was prepared according to literature procedure with minor modification.[220] 1,4,8,11-tetraazacyclotetradecane (0.5 g, 2.5 mmol, 1.2 eq) and acrylonitrile (110 mg, 136 µL, 2.1 mmol, 1.0 eq) was dissolved in 30 mL of EtOH. The mixture was stirred at RT for 86 h. The solvent was removed and the product was purified by column chromatography ($CHCl_3$:MeOH:*i*-$PrNH_2$ = 10:1:1; $R_f$ = 0.31) to give a white solid (320 mg, 1.3 mmol, 60%). $^{1}$H NMR δ (400 MHz, $CDCl_3$) 2.78 (t, *J* = 7.0 Hz, 2H, $H_4$), 2.76-2.73 (m, 6H, $H_{6,6'}$), 2.70 (t, *J* = 5.5 Hz, 2H, $H_{6'}$), 2.66-2.64 (m, 4H, $H_6$), 2.58-2.55 (m, 4H, $H_{6,6'}$), 2.53 (t, *J* = 7.0 Hz, 2H, $H_3$), 2.41 (br s, 3H, $H_7$), 1.76 (quint, *J* = 5.5 Hz, 2H, $H_8$), 1.71

(quint, *J* = 5.2 Hz, 2H, $H_8$); $^{13}$C (100 MHz, $CDCl_3$) 119.12 ($C_2$), 54.77, 52.78, 51.28, 49.60, 48.78, 48.36 ($C_4$), 47.89, 47.44, 28.83, 28.81 ($C_8$), 26.38 ($C_8$), 15.42 ($C_3$); LRMS (ESI$^+$) *m/z*: 254.29 $[M+H]^+$; HRMS (ESI$^+$) *m/z*: 254.2338 $[M+H]^+$; IR (cm$^{-1}$, neat): 3331(m), 3280(m), 3263(m),3171(w), 2933(m), 2890(m), 2809(s), 2737(m), 2656(w), 2249(w),1656(w), 1460(s), 1381(w), 1366(w), 13498(w), 1334(w), 1300(w), 1276(m), 1259(m), 1235(w), 1225(w), 1211(m), 1190(w), 1168(w), 1131(s), 1122(s), 1111(s), 1084(m), 10738(m), 1044(s), 1006(s), 955(m), 929(m), 886(m), 868(w), 829(s), 816(s), 777(s), 750(s).

**3-(1,4,8,11-tetraazacyclotetradecan-1-yl)propan-1-amine, 15**

**14** (320 mg, 1.3 mmol, 1.0 eq) and NaOH (120 mg, 3.0 mmol, 2.3 eq) were dissolved in 25 mL EtOH. Hydrazine monohydrate (64-65%, 1.0 mL, 19.5mmol, 15.0 eq) and Raney Nickel (400 mg) were added alternately to the mixture. The reaction mixture was subsequently stirred for 3 h at RT. The suspension was filtered over celite and the solvent removed in vacuo. The residue was dissolved in hot hexane and the solvent removed before purification of the product by distillation (250 °C, 1 x 10$^{-3}$ bar) to give a white solid (268 mg, 1.0 mmol, 80 %). $^1$H NMR δ (400 MHz, $CDCl_3$) 2.76-2.64 (m, 14H, $H_4$+$H_6$), 2.54-2.46 (m, 6H, $H_6$), 2.27 (br s, 5H, $H_1$+$H_7$), 1.79-1.70 (m, 4H, $H_8$), 1.62 (quint, *J* = 7.3 Hz, 2H, $H_3$); $^{13}$C (100 MHz, $CDCl_3$) 54.49 ($C_6$), 54.10 ($C_6$), 51.42 ($C_3$), 50.26 ($C_6$), 49.83 ($C_6$), 49.73 ($C_6$), 48.93 ($C_6$), 48.15 ($C_6$), 47.78 ($C_6$), 42.43 ($C_6$), 40.47 ($C_4$), 30.00 ($C_2$), 28.82 ($C_8$), 26.27 ($C_8$), the data is in good agreement with the compound synthesized by a different method;[221] LRMS (ESI$^+$) *m/z*: 258.33 $[M+H]^+$; HRMS (ESI$^+$) *m/z*: 258.2651 $[M+H]^+$; IR (cm$^{-1}$, neat): 3266(m), 3184(m), 3001(w), 2922(m), 2865(s), 2800(s), 2731(m), 2656(w), 1596(w), 1519(w), 1475(s), 1462(s), 1451(s), 1432(m), 1374(w), 1332(m), 1279(m), 1253(w), 1206(m), 1121(s), 1069(s), 990(w), 966(s), 937(m), 910(m), 894(m), 881(m), 828(s), 792(s), 745(s).

***N*-(3-(1,4,8,11-tetraazacyclotetradecan-1-yl)propyl)-1-(6-(1-((2,6-diisopropylphenyl) imino)ethyl)pyridin-2-yl)ethan-1-imine (PDIpCy)**

**15** (520 mg, 2.0 mmol, 1.0 eq) and **16** (652 mg, 2.0 mmol, 1.0 eq) was of anhydrous MeOH were dissolved in 5 mL. The mixture was heated to 60 °C for 16 h, cooled to -78 °C and filtered. The filtrate was concentrated *in vacuo* and the product purified by recrystallization in MeCN at -30 °C to give a yellow solid (370 mg, 0.65 mmol, 33%). $^1$H NMR δ (400 MHz, DCM-$d_2$) 8.34 (d, *J* = 7.7 Hz, 1H, $H_4$), 8.21 (d, *J* = 7.2 Hz, 1H, $H_4$), 7.83 (t, *J* = 7.8 Hz, 1H, $H_5$), 7.16 (d, *J* = 7.4 Hz, 2H, $H_{19}$), 7.07 (dd, *J* = 8.3 Hz, *J* = 6.9 Hz, 1H, $H_{20}$), 3.55 (t, *J* = 6.9 Hz, 2H, $H_9$), 2.78-2.50 (m, 23H, $H_{11}$+$H_{12}$+$H_{14}$+$H_{17}$), 2.41 (s, 3H, $H_8$), 2.23 (s, 3H, $H_1$), 1.91 (tt, *J* = 7.1 Hz, *J* = 7.1 Hz, 2H, $H_{10}$), 1.72 (tt, *J* = 5.6 Hz, *J* = 5.6 Hz, 2H, $H_{13}$), 1.65 (tt, *J* = 5.5 Hz, *J* = 5.5 Hz, 2H, $H_{13}$) 1.19-1.16 (m, 12 H, $H_{18}$); $^{13}$C (100 MHz, DCM-$d_2$) 167.72 ($C_2$), 166.56 ($C_7$), 157.20 ($C_6$), 155.35 ($C_3$), 147.18 ($C_{15}$), 137.12 ($C_5$), 136.35 ($C_{16}$), 124.02

($C_{20}$), 123.49 ($C_{19}$), 122.15 ($C_4$), 121.76 ($C_4$), 51.36, 51.17, 51.08 ($C_9$), 49.56, 49.46, 49.29, 48.26, 48.25, 48.51, 28.81 ($C_{13}$+$C_{17}$), 27.62 ($C_{10}$), 26.79 ($C_{13}$), 23.54 ($C_{18}$), 23.12 ($C_{18}$), 17.49 ($C_1$), 14.00 ($C_8$); UV/Vis, $\lambda_{max}$ (THF)/nm 297 and 281 ($\varepsilon$/$M^{-1}$ $cm^{-1}$ 6450, 9910); LRMS (LIFDI) *m/z*: 562.7 [M]; IR ($cm^{-1}$, neat):3280(w), 3194(w), 3063(w), 2959(m), 2925(m), 2868(m), 2800(m), 1701(m), 1645(s), 1578(m), 1568(m), 1459(s), 1437(m), 1381(m),1363(s), 1331(m), 1318(m), 1299(m), 1253(m), 1238(m), 1192(m), 1120(s), 1078((m), 1044(m), 1020(w), 994(m), 956(w), 935(w), 883(w), 847(w), 824(s), 791(s), 760(s), 741(s), 705(m).

**[$Zn_2$(PDIpCy)$(OTf)_4$], 17**

**PDIpCy** (100 mg, 0.17 mmol, 1.0 eq) was dissolved in 15 mL MeCN and $Zn(OTf)_2$ (129 mg, 0.34 mmol, 2.0 eq) was added. The mixture was stirred for 4 h. After the solvent was removed, slow diffusion of pentane into a concentrated solution of the product in THF yielded yellow crystals of **17** (112 mg, 0.09 mmol, 51%) Anal. calcd. for $C_{38}H_{55}F_{12}N_7O_{12}S_4Zn_2$: C, 35.41; H, 4.30; N, 7.61. Found: C, 35.34; H, 4.33; N, 7.61; UV/Vis $\lambda_{max}$ (THF)/nm 352, 311sh, 300 and 297sh ($\varepsilon$/$M^{-1}$ $cm^{-1}$ 591, 5080, 6880, 5750); $^1$H NMR δ (400 MHz, DCM-$d_2$) 8.54 (t, *J* = 7.9 Hz, 1H, $H_5$), 8.29-8.24(m, 2H, $H_4$), 7.32-7.24 (m, 3H, $H_{19}$+ $H_{20}$), 4.06 (td, *J* = 11.3 Hz, *J* = 4.7 Hz, 1H, $H_9$), 3.91 (td, *J* = 11.5 Hz, *J* = 5.0 Hz, 1H, $H_{9'}$), 3.26-2.55 (m, 24H, $H_{11}$ + $H_{12}$ + $H_{14}$ + $H_{17}$), 2.65 (s, 3H, $H_8$), 2.42 (s, 3H, $H_1$), 2.08-1.64 (m, 6H, $H_{10}$ + $H_{13}$), 1.21-1.19 (m, 3H, $H_{18}$), 1.07-1.01 (m, 3H, $H_{18}$); $^{13}$C (100 MHz, DCM-$d_2$) 168.90 ($C_2$) , 167.33 ($C_7$), 148.54 ($C_6$), 146.45 ($C_3$) , 145.65 ($C_5$), 141.11 ($C_{15}$) , 139.56 ($C_{17}$), 139.29($C_{17}$), 127.71 ($C_{20}$), 126.66 ($C_4$), 126.59 ($C_4$), 125.80 ($C_{19}$), 124.64 ($C_{19}$), 121.48 ($C_{16}$), 118.95 ($C_{16}$), 52.49, 51.59, 50.22 ($C_9$), 50.46, 49.69, 49.38, 49.00, 47.20, 45.92, 45.81 ($C_{12}$), 28.87($C_{11}$), 26.10 ($C_{18}$), 24.18 ($C_{18}$), 23.67 ($C_{13}$), 23.46 ($C_{13}$), 20.10 ($C_{10}$), 18.79 ($C_1$), 15.60 ($C_8$); LRMS (LIFDI) *m/z*: 1138.46 [M-(OTf)$^+$] ; IR ($cm^{-1}$, neat): 3250(w), 2970(w), 2880(w), 1639(w), 1590(w), 1470(w), 1373(w), 1293(m), 1234(s), 1205(s), 1164(s), 1096(m), 1025(s), 939(w), 875(w), 815(w), 798(w), 763(m), 745(w), 701(w).

**[$Ni_2$(PDIpCy)(THF)$(OTf)_2$]$(OTf)_2$, 18**

**PDIpCy** (80 mg, 0.14 mmol, 1.0 eq) and $Ni(OTf)_2$ (102 mg, 0.28 mmol, 1.0 eq) were dissolved in 5 ml of EtOH. The reaction mixture was stirred for 16 h at 80 °C to give a brown solution. The solvent was removed *in vacuo*. The crude product was dissolved in THF and brown crystals of **18** were obtained by slow diffusion of pentane into the solution (84 mg, 0.06 mmol, 45%). Anal. calcd. for $C_{42}H_{63}F_{12}N_7Ni_2O_{13}S_4$: C,37.43; H,4.71; N,7.28. Found: C, 37.08; H, 4.81; N, 7.45 ; UV/Vis, $\lambda_{max}$ (THF)/nm ($\varepsilon$/$M^{-1}$ $cm^{-1}$) 948, 461, 369, 323sh, 311sh and 297 (40, 280, 820, 2890, 3920 and 4590); $^1$H NMR δ (400 MHz, DCM-$d_2$) 210.81, 88.94, 81.97, 18.52, 14.09, 5.93, 3.64, 3.33, 3.09, 2.79, 2.48, 2.25, 2.04, 1.87, 1.56, 0.88, 0.66, -0.55, -5.26, -6.49; LRMS (LIFDI) *m/z*: 1123.87 [M-(OTf+THF)]$^+$, 975.11 [M-(2OTf+THF)]$^+$,

487.85 [M-(2OTf+THF)]$^{2+}$; IR (cm$^{-1}$, neat): 3176(w), 2967(w), 2880(w), 1637(w), 1590(w), 1469(w), 1374(s), 1213(s), 1160(s), 1102(m), 1025(s), 937(w), 880(w), 817(w), 799(w), 760(m), 702(w).

**[NiZn(PDIpCy)(THF)(OTf)$_4$], 19**

**PDIpCy** (70 mg, 0.12 mmol, 1.0 eq), Ni(OTf)$_2$ (44 mg, 0.12 mmol, 1.0 eq) and Zn(OTf)$_2$ (45 mg, 0.12 mmol, 1.0 eq) were dissolved in 5 ml of EtOH. The reaction mixture was stirred for 16 h at 80 °C to give a brown solution. The solvent was removed *in vacuo*, the crude product was dissolved in THF and brown to yellow crystals of **19** were obtained by slow diffusion of pentane into the solution (68 mg, 0.05 mmol, 42%). Anal. calcd. for $C_{42}H_{63}F_{12}N_7NiO_{13}S_4Zn$: C, 37.25; H, 4.69; N, 7.24. Found: C, 37.20; H, 4.84; N, 7.22; UV/Vis, $\lambda_{max}$ (THF)/nm ($\varepsilon$/M$^{-1}$ cm$^{-1}$) 960, 323, 311 and 297 (25, 2830, 3840 and 4540); $^1$H NMR δ (400 MHz, DCM-d$_2$) 157.20, 143,33, 89.51, 87.71, 83.02, 78.86, 18.51, 18.35, 14.21, 13.60, 12.92, 12.61, 5.49, 4.78, 3.38, 3.23, 3.12, 2.98, 2.87, 2.79, 2.63, 2.40, 2.03, 1.69, 1.30, 1.20, 1.05, 1.00, 0.86, 0.67, -0.45, -4.51, -5.11, -5.35, -6.17; LRMS (LIFDI) *m/z*: 1130.17 [M-(OTf+THF)]$^+$; IR (cm$^{-1}$, neat): 3245(w), 2968(w), 2878(w), 1635(w), 1589(w), 1469(w), 1374(w), 1287(m), 1234(s), 1211(s), 1160(s), 1097(w), 1025(s), 939(w), 876(w), 814(w), 799(w), 759(w), 702(w).

**[Zn$_2$(PDIpCy)(OTf)$_3$], 20**

**17** (30 mg, 0.02 mmol, 1.0 eq) was dissolved in 4 ml THF and decamethylcobaltocene (8 mg, 0.02 mmol, 1.0 eq) was added. The reaction mixture was stirred for 4 h at rt. Decamethylcobaltocenium triflate was removed by filtration and the solvent was removed from the filtrate *in vacuo*. The crude product was dissolved in THF. The compound was obtained by slow diffusion of pentane into the THF solution to give the orange crystalline **20** (12 mg, 0.01 mmol, 46%) Anal. calcd. for $C_{37}H_{55}F_9N_7O_9S_3Zn_2$·THF: C, 40.63; H, 5.24; N, 8.09. Found: C, 40.39; H, 5.21; N, 8.04; UV/Vis, $\lambda_{max}$ (THF)/nm ($\varepsilon$/M$^{-1}$ cm$^{-1}$) 1523, 1104, 500, 367 and 284 (630, 230, 3270, 3980 and 8140).

**[Ni$_2$(PDIpCy)(OTf)](OTf)$_2$, 21**

**18** (50 mg, 0.04 mmol, 1.0 eq) was dissolved in 4 ml THF and cobaltocene (7 mg, 0.04 mmol, 1.0 eq) was added. The reaction mixture was stirred for 6 h at rt. Cobaltocenium triflate was removed by precipitation with pentane. The solvent was removed from the filtrate *in vacuo* and the crude product was dissolved in THF. The compound was recrystallized by slow diffusion of pentane into the THF solution to give dark blue crystals of **21** (21 mg, 0.02 mmol, 50%) Anal. calcd. for $C_{37}H_{55}F_9N_7Ni_2O_9S_3$: C, 39.45; H, 4.92; N, 8.70. Found: C, 39.52;

H, 5.03; N, 8.34; UV/Vis, $\lambda_{max}$ (THF)/nm ($\varepsilon$/$M^{-1}$ $cm^{-1}$), 1075, 880, 624, 560, 492, 413 and 300 (550, 1510, 1610, 1350, 1420, 1010 and 7850); LRMS (ESI) *m/z*: 1124.02 $[M]^+$.

**[NiZn(PDIpCy)(OTf)$_3$], 22**

**19** (50 mg, 0.04 mmol, 1.0 eq) was dissolved in 4 ml THF and cobaltocene (7 mg, 0.04 mmol, 1.0 eq) was added. The reaction mixture was stirred for 6 h at rt. Cobaltocenium triflate was removed by precipitation with pentane. The solvent was removed from the filtrate *in vacuo* and the crude product was dissolved in THF. The compound was recrystallized by slow diffusion of pentane into the THF solution to give the dark blue crystalline **22** (16 mg, 0.01mmol, 37%) Anal. calcd. for $C_{37}H_{55}F_9N_7NiO_9S_3Zn$: C, 39.22; H, 4.89; N, 8.65. Found: C, 39.07; H, 4.79; N, 8.31; UV/Vis, $\lambda_{max}$ (THF)/nm ($\varepsilon$/$M^{-1}$ $cm^{-1}$), 1099, 884, 627, 494, 412 and 294 (380, 790, 960, 1410, 1520, and 8500); LRMS (ESI) *m/z*: 1130.10 $[M]^+$.

## 3.10 References


21. Luca, O. R.; Konezny, S. J.; Paulson, E. K.; Habib, F.; Luthy, K. M.; Murugesu, M.; Crabtree, R. H.; Batista, V. S. *Dalton Trans.* **2013,** *42*, 8802-7.
22. Helm, M. L.; Stewart, M. P.; Bullock, R. M.; DuBois, M. R.; DuBois, D. L. *Science* **2011,** *333*, 863-866.
23. Kilgore, U. J.; Roberts, J. A. S.; Pool, D. H.; Appel, A. M.; Stewart, M. P.; DuBois, M. R.; Dougherty, W. G.; Kassel, W. S.; Bullock, R. M.; DuBois, D. L. *J. Am. Chem. Soc.* **2011,** *133*, 5861-5872.
26. McCrory, C. C. L.; Szymczak, N. K.; Peters, J. C. *Electrocat.* **2015,** *7*, 87-96.
61. Hodgkiss, J. M.; Chang, C. J.; Pistorio, B. J.; Nocera, D. G. *Inorg. Chem.* **2003,** *42*, 8270-8277.
69. Delgado, M.; Sommer, S. K.; Swanson, S. P.; Berger, R. F.; Seda, T.; Zakharov, L. N.; Gilbertson, J. D. *Inorg. Chem.* **2015,** *54*, 7239-7248.
70. Delgado, M.; Ziegler, J. M.; Seda, T.; Zakharov, L. N.; Gilbertson, J. D. *Inorg. Chem.* **2016,** *55*, 555-557.
71. Kuwabara, I. H.; Comninos, F. C. M.; Pardini, V. L.; Viertler, H.; Toma, H. E. *Electrochim. Acta* **1994,** *39*, 2401-2406.
73. de Bruin, B.; Bill, E.; Bothe, E.; Weyhermüller, T.; Wieghardt, K. *Inorg. Chem.* **2000,** *39*, 2936-2947.
74. Enright, D.; Gambarotta, S.; Yap, G. P. A.; Budzelaar, P. H. M. *Angew. Chem. Int. Ed.* **2002,** *41*, 3873-3876.
75. Reardon, D.; Conan, F.; Gambarotta, S.; Yap, G.; Wang, Q. *J. Am. Chem. Soc.* **1999,** *121*, 9318-9325.
132. *APEX suite of crystallographic software, APEX 2, version 2008.4.*, Bruker AXS Inc., Madison, Wisconsin, USA (2008).
133. *SAINT, version 7.56a, SADABS, version 2008.1*, Bruker AXS Inc., Madison, Wisconsin, USA (2008).
134. Hübschle, C. B.; Sheldrick, G. M.; Dittrich, B. *SHELXLE, J. Appl. Crystallogr.* **2011,** *44*, 1281-1284.
135. Sheldrick, G. M. *SHELXL-2014*, University of Göttingen, Göttingen, Germany (2014).
136. Sheldrick, G. M. *SHELXL-97*, University of Göttingen, Göttingen, Germany (1998).
137. Wilson, A. J. C. *International Tables for Crystallography*, Dordrecht, The Netherlands, Kluwer Academic Publishers (1992).
149. Park, J.; Hong, S. *Chem. Soc. Rev.* **2012,** *41*, 6931-6943.
150. van den Beuken, E. K.; Feringa, B. L. *Tetrahedron* **1998,** *54*, 12985-13011.
151. Vigato, P. A.; Tamburini, S.; Fenton, D. E. *Coord. Chem. Rev.* **1990,** *106*, 25-170.
152. Zhang, H.; Dechert, S.; Maurer, J.; Linseis, M.; Winter, R. F.; Meyer, F. *J. Organomet. Chem.* **2007,** *692*, 2956-2964.
153. Wang, D.; Lindeman, S. V.; Fiedler, A. T. *Inorg. Chim. Acta* **2014,** *421*, 559-567.
154. Roth, A.; Buchholz, A.; Rudolph, M.; Schütze, E.; Kothe, E.; Plass, W. *Chem. Eur. J* **2008,** *14*, 1571-1583.
155. Roth, A.; Spielberg, E. T.; Plass, W. *Inorg. Chem.* **2007,** *46*, 4362-4364.
156. Lin, P.-H.; Takase, M. K.; Agapie, T. *Inorg. Chem.* **2015,** *54*, 59-64.
157. Cook, S. A.; Borovik, A. S. *Acc. Chem. Res.* **2015,** *48*, 2407-2414.
158. Connor, G. P.; Holland, P. L. *Catal. Today* **2017,** *286*, 21-40.
159. Cammarota, R. C.; Clouston, L. J.; Lu, C. C. *Coord. Chem. Rev.* **2017,** *334*, 100-111.
160. Krogman, J. P.; Bezpalko, M. W.; Foxman, B. M.; Thomas, C. M. *Dalton Trans.* **2016,** *45*, 11182-11190.
161. Herbert, D. E.; Lionetti, D.; Rittle, J.; Agapie, T. *J. Am. Chem. Soc.* **2013,** *135*, 19075-19078.
162. Morimoto, Y.; Kotani, H.; Park, J.; Lee, Y.-M.; Nam, W.; Fukuzumi, S. *J. Am. Chem. Soc.* **2011,** *133*, 403-405.
163. Barefield, E. K. *Coord. Chem. Rev.* **2010,** *254*, 1607-1627.
164. Cho, J.; Sarangi, R.; Nam, W. *Acc. Chem. Res.* **2012,** *45*, 1321-1330.

165. Chirik, P. J., Electronic Structures of Reduced Manganese, Iron, and Cobalt Complexes Bearing Redox-Active Bis(imino)pyridine Pincer Ligands. In *Pincer and Pincer-Type Complexes: Applications in Organic Synthesis and Catalysis,*, Szabo, K. J.; Wendt, O. F., Eds. Wiley-VCH Verlag GmbH & Co. KGaA: 2014; pp 189-212.
166. Ren, T. *Chem. Commun.* **2016,** *52*, 3271-3279.
167. Tondreau, A. M.; Milsmann, C.; Lobkovsky, E.; Chirik, P. J. *Inorg. Chem.* **2011,** *50*, 9888-9895.
168. Chen, L.; Chen, G.; Leung, C.-F.; Yiu, S.-M.; Ko, C.-C.; Anxolabéhère-Mallart, E.; Robert, M.; Lau, T.-C. *ACS Catal.* **2015,** *5*, 356-364.
169. Schneider, J.; Jia, H.; Kobiro, K.; Cabelli, D. E.; Muckerman, J. T.; Fujita, E. *Energ. & Environ. Sci.* **2012,** *5*, 9502-5910.
170. Lee, D.; Bang, H.; Suh, M. P. *J. Mol. Cat. A* **2000,** *151*, 71-78.
171. Chirik, P. J. *Acc. Chem. Res.* **2015,** *48*, 1687-1695.
172. Russell, S. K.; Lobkovsky, E.; Chirik, P. J. *J. Am. Chem. Soc.* **2009,** *131*, 36-37.
173. Wang, B.; Lee, Y.-M.; Clémancey, M.; Seo, M. S.; Sarangi, R.; Latour, J.-M.; Nam, W. *J. Am. Chem. Soc.* **2016,** *138*, 2426-2436.
174. Beckmann, U.; Brooker, S. *Coord. Chem. Rev.* **2003,** *245*, 17-29.
175. Somin, I. N. *Zhurnal Organicheskoi Khimii* **1968,** *4*, 122-125, 128-133.
176. Davis, R. N.; Tanski, J. M.; Adrian Jr, J. C.; Tyler, L. A. *Inorg. Chim. Acta* **2007,** *360*, 3061-3068.
177. Blake, A. J.; Lavery, A. J.; Hyde, T. I.; Schröder, M. *J. Chem. Soc., Dalton Trans.* **1989**, 965-970.
178. Ghosh, M.; Weyhermüller, T.; Wieghardt, K. *Dalton Trans.* **2010,** *39*, 1996-2007.
179. Britovsek, G. J. P.; Gibson, V. C.; Spitzmesser, S. K.; Tellmann, K. P.; White, A. J. P.; Williams, D. J. *J. Chem. Soc., Dalton Trans.* **2002**, 1159-1171.
180. Nelson, S. M.; McCann, M.; Stevenson, C.; Drew, M. G. B. *J. Chem. Soc., Dalton Trans.* **1979**, 1477-1481.
181. Krüger, H.-J.; Holm, R. H. *J. Am. Chem. Soc.* **1990,** *112*, 2955-2963.
182. Hua, W. S.; Ajiboye, S. I.; Haining, G.; McGhee, L.; Peacock, R. D.; Peattie, G.; Siddique, R. M.; Winfield, J. M. *J. Chem. Soc., Dalton Trans.* **1995**, 3837-3841.
183. Rohde, J.-U.; Que, L. *Angew. Chem. Int. Ed.* **2005,** *44*, 2255-2258.
184. Kofod, P. *Inorg. Chem.* **1995,** *34*, 2768-2770.
185. Hull, E. A.; West, A. C.; Pestovsky, O.; Kristian, K. E.; Ellern, A.; Dunne, J. F.; Carraher, J. M.; Bakac, A.; Windus, T. L. *Dalton Trans.* **2015,** *44*, 3811-3816.
186. Blake, A. J.; Lavery, A. J.; Hyde, T. I.; Schröder, M. *J. Chem. Soc. Dalton Trans.* **1989**, 965-970.
187. Boiocchi, M.; Fabbrizzi, L.; Foti, F.; Vazquez, M. *Dalton Trans.* **2004**, 2616-2620.
188. Craig, C. A.; Spreer, L. O.; Otvos, J. W.; Calvin, M. *J. Phys. Chem.* **1990,** *94*, 7957-7960.
189. Ciampolini, M.; Fabbrizzi, L.; Licchelli, M.; Perotti, A.; Pezzini, F.; Poggi, A. *Inorg. Chem.* **1986,** *25*, 4131-4135.
190. Ferreira, K. Q.; Doro, F. G.; Tfouni, E. *Inorg. Chim. Acta* **2003,** *355*, 205-212.
191. Bianchini, C.; Mantovani, G.; Meli, A.; Migliacci, F.; Zanobini, F.; Laschi, F.; Sommazzi, A. *Eur. J. Inorg. Chem.* **2003,** *2003*, 1620-1631.
192. Haas, R. M.; Hern, Z.; Sproules, S.; Hess, C. R. *Inorganic Chemistry* **2017,** *accepted*.
193. Baidya, N.; Olmstead, M. M.; Mascharak, P. K. *J. Am. Chem. Soc.* **1992,** *114*, 9666-9668.
194. Coggin, D. K.; Gonzalez, J. A.; Kook, A. M.; Stanbury, D. M.; Wilson, L. J. *Inorg. Chem.* **1991,** *30*, 1115-1125.
195. Davis, R. N.; Tanski, J. M.; Adrian, J. C.; Tyler, L. A. *Inorg. Chim. Acta* **2007,** *360*, 3061-3068.
196. Crick, I. S.; Gable, R. W.; Hoskins, B. F.; Tregloan, P. A. *Inorg. Chim. Acta* **1986,** *111*, 35-38.
197. Hambley, T. W. *J. Chem. Soc. Dalton Trans.* **1986**, 565-569.
198. Kim, J. C.; Lough, A. J.; Park, H.; Kang, Y. C. *Inorg. Chem. Commun.* **2006,** *9*, 514-517.
199. Kannappan, R.; Rousselin, Y.; Jabri, R. Z.; Goze, C.; Brandès, S.; Guilard, R.; Zrineh, A.; Denat, F. *Inorg. Chim. Acta* **2011,** *373*, 150-158.
200. Marganian, C. A.; Vazir, H.; Baidya, N.; Olmstead, M. M.; Mascharak, P. K. *J. Am. Chem. Soc.* **1995,** *117*, 1584-1594.

201. Hartle, M. D.; Delgado, M.; Gilbertson, J. D.; Pluth, M. D. *Chem. Commun.* **2016,** *52*, 7680-7682.
202. Blake, A. J.; Gould, R. O.; Hyde, T. I.; Schröder, M. *J. Chem. Soc., Chem. Commun.* **1987**, 431-433.
203. El Ghachtouli, S.; Cadiou, C.; Déchamps-Olivier, I.; Chuburu, F.; Aplincourt, M.; Turcry, V.; Le Baccon, M.; Handel, H. *Eur. J. Inorg. Chem.* **2005,** *2005*, 2658-2668.
204. Barefield, E. K.; Freeman, G. M.; Van Derveer, D. G. *Inorg. Chem.* **1986,** *25*, 552-558.
205. Lewis, J.; Schröder, M. *Dalton Trans.* **1982**, 1085-1089.
206. Manuel, T. D.; Rohde, J.-U. *J. Am. Chem. Soc.* **2009,** *131*, 15582-15583.
207. Chu, T.; Belding, L.; Poddutoori, P. K.; van der Est, A.; Dudding, T.; Korobkov, I.; Nikonov, G. I. *Dalton Trans.* **2016,** *45*, 13440-13448.
208. Ciszewski, J. T.; Mikhaylov, D. Y.; Holin, K. V.; Kadirov, M. K.; Budnikova, Y. H.; Sinyashin, O.; Vicic, D. A. *Inorg. Chem.* **2011,** *50*, 8630-8635.
209. Hubin, T. J.; McCormick, J. M.; Collinson, S. R.; Alcock, N. W.; Clase, H. J.; Busch, D. H. *Inorg. Chim. Acta* **2003,** *346*, 76-86.
210. Fleischer, E.; Hawkinson, S. *J. Am. Chem. Soc.* **1967,** *89*, 720-721.
211. Hess, C. R.; Weyhermüller, T.; Bill, E.; Wieghardt, K. *Inorg. Chem.* **2010,** *49*, 5686-5700.
212. Shakya, R.; Powell, D. R.; Houser, R. P. *Eur. J. Inorg. Chem* **2009,** *2009*, 5319-5327.
213. **!!! INVALID CITATION !!! {}**.
214. Zhanaidarova, A.; Steger, H.; Reineke, M. H.; Kubiak, C. P. *Dalton Trans.* **2017,** *46*, 12413-12416.
215. Costamagna, J.; Ferraudi, G.; Matsuhiro, B.; Campos-Vallette, M.; Canales, J.; Villagrán, M.; Vargas, J.; Aguirre, M. J. *Coord. Chem. Rev.* **2000,** *196*, 125-164.
216. Dempsey, J. L.; Esswein, A. J.; Manke, D. R.; Rosenthal, J.; Soper, J. D.; Nocera, D. G. *Inorg. Chem.* **2005,** *44*, 6879-6892.
217. Bernhardt, P. V.; Jones, L. A. *Inorg. Chem.* **1999,** *38*, 5086-5090.
218. Rosenthal, J.; Bachman, J.; Dempsey, J. L.; Esswein, A. J.; Gray, T. G.; Hodgkiss, J. M.; Manke, D. R.; Luckett, T. D.; Pistorio, B. J.; Veige, A. S.; Nocera, D. G. *Coord. Chem. Rev.* **2005,** *249*, 1316-1326.
219. Hanson, G. R.; Gates, K. E.; Noble, C. J.; Griffin, M.; Mitchell, A.; Benson, S. *J. Inorg. Biochem.* **2004,** *98*, 903-916.
220. Stewart, C. A.; Dickie, D. A.; Kemp, R. A. *Inorganica Chimica Acta* **2012,** *392*, 268-276.
221. Ferreira, K. Q.; Doro, F. G.; Tfouni, E. *Inorg. Chim. Acta* **2003,** *355*, 205-212.

# 4 References


1. Cook, T. R.; Dogutan, D. K.; Reece, S. Y.; Surendranath, Y.; Teets, T. S.; Nocera, D. G. *Chem. Rev.* **2010,** *110*, 6474-6502.
2. Schwarz, H. A.; Dodson, R. W. **1989,** *93*, 409-414.
3. Benson, E. E.; Kubiak, C. P.; Sathrum, A. J.; Smieja, J. M. *Chem. Soc. Rev.* **2009,** *38*, 89-99.
4. Hinrichsen, K.-O.; Strunk, J. *Nachrichten aus der Chemie* **2006,** *54*, 1080-1084.
5. Lamy, E.; Nadjo, L.; Saveant, J. M. *J. Electroanal. Chem. Interfacial Electrochem.* **1977,** *78*, 403-407.
6. Gennaro, A.; Isse, A. A.; Savéant, J.-M.; Severin, M.-G.; Vianello, E. *J. Am. Chem. Soc.* **1996,** *118*, 7190-7196.
7. Angamuthu, R.; Byers, P.; Lutz, M.; Spek, A. L.; Bouwman, E. *Science* **2010,** *327*, 313-315.
8. Beley, M.; Collin, J.-P.; Ruppert, R.; Sauvage, J.-P. *J. Chem.Soc, Chem. Commun.* **1984**, 1315-1316.
9. Fisher, B. J.; Eisenberg, R. *J. Am. Chem. Soc.* **1980,** *102*, 7361-7363.
10. Froehlich, J. D.; Kubiak, C. P. *J. Am. Chem. Soc.* **2015,** *137*, 3565-3573.
11. Che, C.-M.; Mak, S.-T.; Lee, W.-O.; Fung, K.-W.; Mak, T. C. W. *J. Chem. Soc., Dalton Trans.* **1988**, 2153-2159.
12. Zhang, M.; El-Roz, M.; Frei, H.; Mendoza-Cortes, J. L.; Head-Gordon, M.; Lacy, D. C.; Peters, J. C. *J. Physi. Chem. C* **2015,** *119*, 4645-4654.
13. Costentin, C.; Robert, M.; Saveant, J.-M. *Chem. Soc. Rev.* **2013,** *42*, 2423-2436.
14. Costentin, C.; Robert, M.; Savéant, J.-M. *Acc. Chem. Res.* **2015,** *48*, 2996-3006.
15. Collin, J.-P.; Abdelaziz, J.; Sauvage, J.-P. *Inorg. Chem.* **1988,** *27*, 1986-1988.
16. Chen, L.; Guo, Z.; Wei, X.-G.; Gallenkamp, C.; Bonin, J.; Anxolabéhère-Mallart, E.; Lau, K.-C.; Lau, T.-C.; Robert, M. *J. Am. Chem. Soc.* **2015,** *137*, 10918-10921.
17. Ogden, J. M. *Ann. Rev. of Energy Environ.* **1999,** *24*, 227-279.
18. Thoi, V. S.; Sun, Y.; Long, J. R.; Chang, C. J. *Chem. Soc. Rev.* **2013,** *42*, 2388-2400.
19. Canaguier, S.; Artero, V.; Fontecave, M. *Dalton Trans.* **2008**, 315-325.
20. Luca, O. R.; Konezny, S. J.; Blakemore, J. D.; Colosi, D. M.; Saha, S.; Brudvig, G. W.; Batista, V. S.; Crabtree, R. H. *New J. Chem.* **2012,** *36*, 1149-1152.
21. Luca, O. R.; Konezny, S. J.; Paulson, E. K.; Habib, F.; Luthy, K. M.; Murugesu, M.; Crabtree, R. H.; Batista, V. S. *Dalton Trans.* **2013,** *42*, 8802-7.
22. Helm, M. L.; Stewart, M. P.; Bullock, R. M.; DuBois, M. R.; DuBois, D. L. *Science* **2011,** *333*, 863-866.
23. Kilgore, U. J.; Roberts, J. A. S.; Pool, D. H.; Appel, A. M.; Stewart, M. P.; DuBois, M. R.; Dougherty, W. G.; Kassel, W. S.; Bullock, R. M.; DuBois, D. L. *J. Am. Chem. Soc.* **2011,** *133*, 5861-5872.
24. Dupuis, M.; Chen, S.; Raugei, S.; DuBois, D. L.; Bullock, R. M. *J. Phys. Chem.* **2011,** *115*, 4861-4865.
25. McCrory, C. C. L.; Uyeda, C.; Peters, J. C. *J. Am. Chem. Soc.* **2012,** *134*, 3164-3170.
26. McCrory, C. C. L.; Szymczak, N. K.; Peters, J. C. *Electrocat.* **2015,** *7*, 87-96.
27. Wang, M.; Chen, L.; Sun, L. *Energy Environ. Sci.* **2012,** *5*, 6763-6778.
28. Baffert, C.; Artero, V.; Fontecave, M. *Inorg. Chem.* **2007,** *46*, 1817-1824.
29. Jacques, P.-A.; Artero, V.; Pécaut, J.; Fontecave, M. *Proc. Nat. Ac. Sci.* **2009,** *106*, 20627-20632.
30. Razavet, M.; Artero, V.; Fontecave, M. *Inorg. Chem.* **2005,** *44*, 4786-4795.
31. Hu, X.; Cossairt, B. M.; Brunschwig, B. S.; Lewis, N. S.; Peters, J. C. *Chem. Commun.* **2005**, 4723-4725.
32. McNamara, W. R.; Han, Z.; Alperin, P. J.; Brennessel, W. W.; Holland, P. L.; Eisenberg, R. *J. Am. Chem. Soc.* **2011,** *133*, 15368-15371.
33. Eckenhoff, W. T.; Eisenberg, R. *Dalton Trans.* **2012,** *41*, 13004-13021.

34. Berardi, S.; Drouet, S.; Francas, L.; Gimbert-Surinach, C.; Guttentag, M.; Richmond, C.; Stoll, T.; Llobet, A. *Chem. Soc. Rev.* **2014,** *43*, 7501-7519.
35. Gray, T. G.; Veige, A. S.; Nocera, D. G. *J. Am. Chem. Soc.* **2004,** *126*, 9760-9768.
36. Bachmann, J.; Nocera, D. G. *J. Am. Chem. Soc.* **2004,** *126*, 2829-2837.
37. Buser, H. J.; Schwarzenbach, D.; Petter, W.; Ludi, A. *Inorg. Chem.* **1977,** *16*, 2704-2710.
38. Dulebohn, J. I.; Ward, D. L.; Nocera, D. G. *J. Am. Chem. Soc.* **1988,** *110*, 4054-4056.
39. F. Heyduk, A.; G. Nocera, D. *Chem. Commun.* **1999**, 1519-1520.
40. Gray, T. G.; Nocera, D. G. *Chem. Commun.* **2005**, 1540-1542.
41. Esswein, A. J.; Veige, A. S.; Nocera, D. G. *J. Am. Chem. Soc.* **2005,** *127*, 16641-16651.
42. Heyduk, A. F.; Macintosh, A. M.; Nocera, D. G. *J. Am. Chem. Soc.* **1999,** *121*, 5023-5032.
43. Odom, A. L.; Heyduk, A. F.; Nocera, D. G. *Inorg. Chim. Acta* **2000,** *297*, 330-337.
44. Heyduk, A. F.; Nocera, D. G. *Science* **2001,** *293*, 1639-1641.
45. Heyduk, A. F.; Nocera, D. G. *J. Am. Chem. Soc.* **2000,** *122*, 9415-9426.
46. Veige, A. S.; Gray, T. G.; Nocera, D. G. *Inorg. Chem.* **2005,** *44*, 17-26.
47. Deng, Y.; Chang, C. J.; Nocera, D. G. *J. Am. Chem. Soc.* **2000,** *122*, 410-411.
48. Chang, C. J.; Deng, Y.; Heyduk, A. F.; Chang, C. K.; Nocera, D. G. *Inorg. Chem.* **2000,** *39*, 959-966.
49. Chang, C. J.; Deng, Y.; Shi, C.; Chang, C. K.; Anson, F. C.; Nocera, D. G. *Chem. Commun.* **2000**, 1355-1356.
50. Chng, L. L.; Chang, C. J.; Nocera, D. G. *J. Org. Chem.* **2003,** *68*, 4075-4078.
51. Chang, C. J.; Baker, E. A.; Pistorio, B. J.; Deng, Y.; Loh, Z.-H.; Miller, S. E.; Carpenter, S. D.; Nocera, D. G. *Inorg. Chem.* **2002,** *41*, 3102-3109.
52. Chang, C. J.; Yeh, C.-Y.; Nocera, D. G. *J. Org. Chem.* **2002,** *67*, 1403-1406.
53. Pistorio, B. J.; Chang, C. J.; Nocera, D. G. *J. Am. Chem. Soc.* **2002,** *124*, 7884-7885.
54. Holm, R. H. *Chem. Rev.* **1987,** *87*, 1401-1449.
55. Chin, D.-H.; Del Gaudio, J.; La Mar, G. N.; Balch, A. L. *J. Am. Chem. Soc.* **1977,** *99*, 5486-5488.
56. Chin, D.-H.; La Mar, G. N.; Balch, A. L. *J. Am. Chem. Soc.* **1980,** *102*, 4344-4350.
57. Peterson, M. W.; Richman, R. M. *Inorg. Chem.* **1985,** *24*, 722-725.
58. Peterson, M. W.; Rivers, D. S.; Richman, R. M. *J. Am. Chem. Soc.* **1985,** *107*, 2907-2915.
59. Weber, L.; Haufe, G.; Rehorek, D.; Hennig, H. *Chem. Commun.* **1991**, 502-503.
60. Weber, L.; Hommel, R.; Behling, J.; Haufe, G.; Hennig, H. *J. Am. Chem. Soc.* **1994,** *116*, 2400-2408.
61. Hodgkiss, J. M.; Chang, C. J.; Pistorio, B. J.; Nocera, D. G. *Inorg. Chem.* **2003,** *42*, 8270-8277.
62. Chirik, P. J. *Inorg. Chem.* **2011,** *50*, 9737-9740.
63. Kaim, W. *Eur. J. Inorg. Chem* **2012,** *2012*, 343-348.
64. Lyaskovskyy, V.; de Bruin, B. *ACS Catal.* **2012,** *2*, 270-279.
65. De Angelis, S.; Solari, E.; Floriani, C.; Chiesi-Villa, A.; Rizzoli, C. *J. Am. Chem. Soc.* **1994,** *116*, 5691-5701.
66. De Angelis, S.; Solari, E.; Floriani, C.; Chiesi-Villa, A.; Rizzoli, C. *J. Am. Chem. Soc.* **1994,** *116*, 5702-5713.
67. Crescenzi, R.; Solari, E.; Floriani, C.; Chiesi-Villa, A.; Rizzoli, C. *J. Am. Chem. Soc.* **1999,** *121*, 1695-1706.
68. Small, B. L. *Acc. Chem. Res.* **2015,** *48*, 2599-2611.
69. Delgado, M.; Sommer, S. K.; Swanson, S. P.; Berger, R. F.; Seda, T.; Zakharov, L. N.; Gilbertson, J. D. *Inorg. Chem.* **2015,** *54*, 7239-7248.
70. Delgado, M.; Ziegler, J. M.; Seda, T.; Zakharov, L. N.; Gilbertson, J. D. *Inorg. Chem.* **2016,** *55*, 555-557.
71. Kuwabara, I. H.; Comninos, F. C. M.; Pardini, V. L.; Viertler, H.; Toma, H. E. *Electrochim. Acta* **1994,** *39*, 2401-2406.
72. Budzelaar, P. H. M.; de Bruin, B.; Gal, A. W.; Wieghardt, K.; van Lenthe, J. H. *Inorg. Chem.* **2001,** *40*, 4649-4655.

73. de Bruin, B.; Bill, E.; Bothe, E.; Weyhermüller, T.; Wieghardt, K. *Inorg. Chem.* **2000,** *39*, 2936-2947.
74. Enright, D.; Gambarotta, S.; Yap, G. P. A.; Budzelaar, P. H. M. *Angew. Chem. Int. Ed.* **2002,** *41*, 3873-3876.
75. Reardon, D.; Conan, F.; Gambarotta, S.; Yap, G.; Wang, Q. *J. Am. Chem. Soc.* **1999,** *121*, 9318-9325.
76. Panunzi, A.; Giordano, F.; Orabona, I.; Ruffo, F. *Inorg. Chim. Acta* **2005,** *358*, 1217-1224.
77. Bheemaraju, A.; Beattie, J. W.; Danylyuk, Y.; Rochford, J.; Groysman, S. *Eur. J. Inorg. Chem.* **2014,** *2014*, 5865-5873.
78. Takano, S.; Takeuchi, D.; Osakada, K.; Akamatsu, N.; Shishido, A. *Angew. Chem. Int. Ed.* **2014,** *53*, 9246-9250.
79. Haas, R. M.; Arshad, M.; Anthony, J.; Altmann, P. J.; Pothig, A.; Kohler, F. H.; Hess, C. R. *Inorganic Chemistry Frontiers* **2016,** *3*, 616-629.
80. current status in CCDC on the Oct 2nd 2017
81. Casanova, D.; Alemany, P.; Bofill, J. M.; Alvarez, S. *Chem.– Eur. J.* **2003,** *9*, 1281-1295.
82. Drahoš, B.; Herchel, R.; Trávníček, Z. *Inorg. Chem.* **2015,** *54*, 3352-3369.
83. Villafañe, F. *Coord. Chem. Rev.* **2014,** *281*, 86-99.
84. Nelson, S. M.; McIlroy, P. D. A.; Stevenson, C. S.; Konig, E.; Ritter, G.; Waigel, J. *J. Chem. Soc., Dalton Trans.* **1986**, 991-995.
85. Grau, M.; England, J.; Torres Martin de Rosales, R.; Rzepa, H. S.; White, A. J. P.; Britovsek, G. J. P. *Inorg. Chem.* **2013,** *52*, 11867-11874.
86. Lonnon, D. G.; Ball, G. E.; Taylor, I.; Craig, D. C.; Colbran, S. B. *Inorg. Chem.* **2009,** *48*, 4863-4872.
87. Hoffmann, R.; Beier, B. F.; Muetterties, E. L.; Rossi, A. R. *Inorg. Chem.* **1977,** *16*, 511-522.
88. Bar, A. K.; Pichon, C.; Gogoi, N.; Duhayon, C.; Ramasesha, S.; Sutter, J.-P. *Chem. Commun.* **2015,** *51*, 3616-3619.
89. Craig, G. A.; Barrios, L. A.; Costa, J. S.; Roubeau, O.; Ruiz, E.; Teat, S. J.; Wilson, C. C.; Thomas, L.; Aromi, G. *Dalton Trans.* **2010,** *39*, 4874-4881.
90. Morgenstern-Badarau, I.; Lambert, F.; Philippe Renault, J.; Cesario, M.; Maréchal, J.-D.; Maseras, F. *Inorg. Chim. Acta* **2000,** *297*, 338-350.
91. Koenig, E.; Ritter, G.; Dengler, J.; Nelson, S. M. *Inorg. Chem.* **1987,** *26*, 3582-3588.
92. Bonhommeau, S.; Guillon, T.; Lawson Daku, L. M.; Demont, P.; Sanchez Costa, J.; Létard, J.-F.; Molnár, G.; Bousseksou, A. *Angew. Chem. Int. Ed.* **2006,** *45*, 1625-1629.
93. Hayami, S.; Gu, Z.-z.; Einaga, Y.; Kobayasi, Y.; Ishikawa, Y.; Yamada, Y.; Fujishima, A.; Sato, O. *Inorg. Chem.* **2001,** *40*, 3240-3242.
94. Costa, J. S.; Balde, C.; Carbonera, C.; Denux, D.; Wattiaux, A.; Desplanches, C.; Ader, J.-P.; Gütlich, P.; Létard, J.-F. *Inorg. Chem.* **2007,** *46*, 4114-4119.
95. Zhang, D.; Busch, D. H.; Lennon, P. L.; Weiss, R. H.; Neumann, W. L.; Riley, D. P. *Inorg. Chem.* **1998,** *37*, 956-963.
96. Gutman, C. T.; Brunold, T. C. *Inorg. Chem.* **2012,** *51*, 12729-12737.
97. Liu, G.-F.; Filipović, M.; Heinemann, F. W.; Ivanović-Burmazović, I. *Inorg. Chem.* **2007,** *46*, 8825-8835.
98. Nowick, J. S.; Ballester, P.; Ebmeyer, F.; Rebek, J. *J. Am. Chem. Soc.* **1990,** *112*, 8902-8906.
99. Bühlmann, P.; Nishizawa, S.; Xiao, K. P.; Umezawa, Y. *Tetrahedron* **1997,** *53*, 1647-1654.
100. Hamann, B. C.; Branda, N. R.; Rebek, J. *Tetrahedron Letters* **1993,** *34*, 6837-6840.
101. Haack, P.; Limberg, C.; Ray, K.; Braun, B.; Kuhlmann, U.; Hildebrandt, P.; Herwig, C. *Inorg. Chem.* **2011,** *50*, 2133-2142.
102. Siewert, I.; Limberg, C., A Xanthene-based Ligand with Two Adjacent Malonate Binding Sites. In *Z. Naturfor. B*, 2007; Vol. 62, p 1251.
103. McQuade, L. E.; Lippard, S. J. *Inorg. Chem.* **2010,** *49*, 7464-7471.
104. Barcena, H. S.; Liu, B.; Mirkin, M. V.; Canary, J. W. *Inorg. Chem.* **2005,** *44*, 7652-7660.
105. Medlycott, E. A.; Hanan, G. S. *Chem. Commun.* **2007**, 4884-4886.

106. Kissinger, P. T.; Heineman, W. R. *J. Chem. Edu.* **1983,** *60*, 702.
107. Köhler, F. H., Probing Spin Densities by Use of NMR Spectroscopy. In *Magnetism: Molecules to Materials I*, Wiley-VCH Verlag GmbH & Co. KGaA: 2003; pp 379-430.
108. Vaara, J. *Phys. Chem. Chem. Phys.* **2007,** *9*, 5399-5418.
109. Aquino, F.; Pritchard, B.; Autschbach, J. *J. Chem. Theory Comput.* **2012,** *8*, 598-609.
110. Rastrelli, F.; Bagno, A. *Chem. – Eur. J.* **2009,** *15*, 7990-8004.
111. Kaupp, M.; Köhler, F. H. *Coord. Chem. Rev.* **2009,** *253*, 2376-2386.
112. The theoretical shifts were determined together with Prof. Frank H. Köhler and supported the assignments.
113. Acerete, R.; Casan-Pastor, N.; Bas-Serra, J.; Baker, L. C. W. *J. Am. Chem. Soc.* **1989,** *111*, 6049-6056.
114. Turner, M. J.; McKinnon, J. J.; Wolff, S. K.; Grimwood, D. J.; Spackman, P. R.; Jayatilaka, D.; Spackman, M. A. *CrystalExplorer15*, 2015.
115. McKinnon, J. J.; Spackman, M. A.; Mitchell, A. S. *Acta Crystal. B* **2004,** *60*, 627-668.
116. Heise, H.; Köhler, F. H.; Herker, M.; Hiller, W. *J. Am. Chem. Soc.* **2002,** *124*, 10823-10832.
117. Tasker, S. Z.; Standley, E. A.; Jamison, T. F. *Nature* **2014,** *509*, 299-309.
118. Sepelak, D. J.; Pierpont, C. G.; Barefield, E. K.; Budz, J. T.; Poffenberger, C. A. *J. Am. Chem. Soc.* **1976,** *98*, 6178-6185.
119. Zhu, D.; Thapa, I.; Korobkov, I.; Gambarotta, S.; Budzelaar, P. H. M. *Inorg. Chem.* **2011,** *50*, 9879-9887.
120. Blanchard, S.; Neese, F.; Bothe, E.; Bill, E.; Weyhermüller, T.; Wieghardt, K. *Inorg. Chem.* **2005,** *44*, 3636-3656.
121. Norman, N. C.; Orpen, A. G.; Quayle, M. J.; Whittell, G. R. *Acta Crystal. C* **2002,** *58*, m160-m161.
122. Iluc, V. M.; Miller, A. J. M.; Hillhouse, G. L. *Chem. Commun.* **2005**, 5091-5093.
123. Proft, B.; Pörschke, K.-R.; Lutz, F.; Krüger, C. *Chem. Berichte* **1994,** *127*, 653-655.
124. Tong, G. S. M.; Che, C.-M. *Eur. J. Inorg. Chem.* **2010,** *2010*, 5113-5123.
125. Soo, H. S.; Sougrati, M. T.; Grandjean, F.; Long, G. J.; Chang, C. J. *Inorg. Chim. Acta* **2011,** *369*, 82-91.
126. Venkatakrishnan, T. S.; Sahoo, S.; Bréfuel, N.; Duhayon, C.; Paulsen, C.; Barra, A.-L.; Ramasesha, S.; Sutter, J.-P. *J. Am. Chem. Soc.* **2010,** *132*, 6047-6056.
127. Slep, L. D.; Calvo, R.; Nascimento, O. R.; Baggio, R.; Garland, M. T.; Peña, O.; Perec, M. *Inorg. Chim. Acta* **2007,** *360*, 2911-2916.
128. Larionova, J.; Kahn, O.; Golhen, S.; Ouahab, L.; Clérac, R. *Inorg. Chem.* **1999,** *38*, 3621-3627.
129. Barbour, C. J.; Cameron, J. H.; Winfield, J. M. *J. Chem. Soc. Dalton* **1980**, 2001-2005.
130. Nowick, J. S.; Ballester, P.; Ebmeyer, F.; Rebek, J. *J. Am. Chem. Soc.* **1990,** *112*, 8902 - 8906.
131. Bühlmann, P.; Nishizawa, S.; Xiao, K. P.; Umezawa, Y. *Tetrahedron* **1997,** *53*, 1647-1654.
132. *APEX suite of crystallographic software, APEX 2, version 2008.4.*, Bruker AXS Inc., Madison, Wisconsin, USA (2008).
133. *SAINT, version 7.56a, SADABS, version 2008.1*, Bruker AXS Inc., Madison, Wisconsin, USA (2008).
134. Hübschle, C. B.; Sheldrick, G. M.; Dittrich, B. *SHELXLE, J. Appl. Crystallogr.* **2011,** *44*, 1281-1284.
135. Sheldrick, G. M. *SHELXL-2014*, University of Göttingen, Göttingen, Germany (2014).
136. Sheldrick, G. M. *SHELXL-97*, University of Göttingen, Göttingen, Germany (1998).
137. Wilson, A. J. C. *International Tables for Crystallography*, Dordrecht, The Netherlands, Kluwer Academic Publishers (1992).
138. Spek, A. L. *J. Appl. Cryst.* **2003,** *36*, 7-13.
139. Spek, A. L. *Acta Cryst.* **2009,** *D65*, 148-155.
140. Neese, F. *An Ab initio, DFT and Semiempirical SCF-MO Package*, Max Plank Institute for Bioinorganic Chemistry, Mühlheim an der Ruhr, Germany, Jan 2012.
141. Becke, A. D. *J. Chem. Phys.* **1986,** *84*, 4524-4529.

142. Becke, A. D. *J. Chem. Phys.* **1993,** *98*, 5648-5652.
143. Lee, C. T.; Yang, W. T.; Parr, R. G. *Phys. Rev. B* **1988,** *37*, 785-789.
144. Schäfer, A.; Horn, H.; Ahlrichs, R. *J. Chem. Phys.* **1992,** *97*, 2571-2577.
145. Schäfer, A.; Huber, C.; Ahlrichs, R. *J. Chem. Phys.* **1994,** *100*, 5829-5835.
146. Eichkorn, K.; Treutler, O.; Ohm, H.; Häser, M.; Ahlrichs, R. *Chem. Phys. Lett.* **1995,** *240*, 283-290.
147. Eichkorn, K.; Treutler, O.; Ohm, H.; Häser, M.; Ahlrichs, R. *Chem. Phys. Lett.* **1995,** *242*, 652-660.
148. Humphrey, W.; Dalke, A.; Schulten, K. *J. Molec. Graphics* **1996,** *14*, 33-38.
149. Park, J.; Hong, S. *Chem. Soc. Rev.* **2012,** *41*, 6931-6943.
150. van den Beuken, E. K.; Feringa, B. L. *Tetrahedron* **1998,** *54*, 12985-13011.
151. Vigato, P. A.; Tamburini, S.; Fenton, D. E. *Coord. Chem. Rev.* **1990,** *106*, 25-170.
152. Zhang, H.; Dechert, S.; Maurer, J.; Linseis, M.; Winter, R. F.; Meyer, F. *J. Organomet. Chem.* **2007,** *692*, 2956-2964.
153. Wang, D.; Lindeman, S. V.; Fiedler, A. T. *Inorg. Chim. Acta* **2014,** *421*, 559-567.
154. Roth, A.; Buchholz, A.; Rudolph, M.; Schütze, E.; Kothe, E.; Plass, W. *Chem. Eur. J* **2008,** *14*, 1571-1583.
155. Roth, A.; Spielberg, E. T.; Plass, W. *Inorg. Chem.* **2007,** *46*, 4362-4364.
156. Lin, P.-H.; Takase, M. K.; Agapie, T. *Inorg. Chem.* **2015,** *54*, 59-64.
157. Cook, S. A.; Borovik, A. S. *Acc. Chem. Res.* **2015,** *48*, 2407-2414.
158. Connor, G. P.; Holland, P. L. *Catal. Today* **2017,** *286*, 21-40.
159. Cammarota, R. C.; Clouston, L. J.; Lu, C. C. *Coord. Chem. Rev.* **2017,** *334*, 100-111.
160. Krogman, J. P.; Bezpalko, M. W.; Foxman, B. M.; Thomas, C. M. *Dalton Trans.* **2016,** *45*, 11182-11190.
161. Herbert, D. E.; Lionetti, D.; Rittle, J.; Agapie, T. *J. Am. Chem. Soc.* **2013,** *135*, 19075-19078.
162. Morimoto, Y.; Kotani, H.; Park, J.; Lee, Y.-M.; Nam, W.; Fukuzumi, S. *J. Am. Chem. Soc.* **2011,** *133*, 403-405.
163. Barefield, E. K. *Coord. Chem. Rev.* **2010,** *254*, 1607-1627.
164. Cho, J.; Sarangi, R.; Nam, W. *Acc. Chem. Res.* **2012,** *45*, 1321-1330.
165. Chirik, P. J., Electronic Structures of Reduced Manganese, Iron, and Cobalt Complexes Bearing Redox-Active Bis(imino)pyridine Pincer Ligands. In *Pincer and Pincer-Type Complexes: Applications in Organic Synthesis and Catalysis,*, Szabo, K. J.; Wendt, O. F., Eds. Wiley-VCH Verlag GmbH & Co. KGaA: 2014; pp 189-212.
166. Ren, T. *Chem. Commun.* **2016,** *52*, 3271-3279.
167. Tondreau, A. M.; Milsmann, C.; Lobkovsky, E.; Chirik, P. J. *Inorg. Chem.* **2011,** *50*, 9888-9895.
168. Chen, L.; Chen, G.; Leung, C.-F.; Yiu, S.-M.; Ko, C.-C.; Anxolabéhère-Mallart, E.; Robert, M.; Lau, T.-C. *ACS Catal.* **2015,** *5*, 356-364.
169. Schneider, J.; Jia, H.; Kobiro, K.; Cabelli, D. E.; Muckerman, J. T.; Fujita, E. *Energ. & Environ. Sci.* **2012,** *5*, 9502-5910.
170. Lee, D.; Bang, H.; Suh, M. P. *J. Mol. Cat. A* **2000,** *151*, 71-78.
171. Chirik, P. J. *Acc. Chem. Res.* **2015,** *48*, 1687-1695.
172. Russell, S. K.; Lobkovsky, E.; Chirik, P. J. *J. Am. Chem. Soc.* **2009,** *131*, 36-37.
173. Wang, B.; Lee, Y.-M.; Clémancey, M.; Seo, M. S.; Sarangi, R.; Latour, J.-M.; Nam, W. *J. Am. Chem. Soc.* **2016,** *138*, 2426-2436.
174. Beckmann, U.; Brooker, S. *Coord. Chem. Rev.* **2003,** *245*, 17-29.
175. Somin, I. N. *Zhurnal Organicheskoi Khimii* **1968,** *4*, 122-125, 128-133.
176. Davis, R. N.; Tanski, J. M.; Adrian Jr, J. C.; Tyler, L. A. *Inorg. Chim. Acta* **2007,** *360*, 3061-3068.
177. Blake, A. J.; Lavery, A. J.; Hyde, T. I.; Schröder, M. *J. Chem. Soc., Dalton Trans.* **1989**, 965-970.
178. Ghosh, M.; Weyhermüller, T.; Wieghardt, K. *Dalton Trans.* **2010,** *39*, 1996-2007.
179. Britovsek, G. J. P.; Gibson, V. C.; Spitzmesser, S. K.; Tellmann, K. P.; White, A. J. P.; Williams, D. J. *J. Chem. Soc., Dalton Trans.* **2002**, 1159-1171.

180. Nelson, S. M.; McCann, M.; Stevenson, C.; Drew, M. G. B. *J. Chem. Soc., Dalton Trans.* **1979**, 1477-1481.
181. Krüger, H.-J.; Holm, R. H. *J. Am. Chem. Soc.* **1990,** *112*, 2955-2963.
182. Hua, W. S.; Ajiboye, S. I.; Haining, G.; McGhee, L.; Peacock, R. D.; Peattie, G.; Siddique, R. M.; Winfield, J. M. *J. Chem. Soc., Dalton Trans.* **1995**, 3837-3841.
183. Rohde, J.-U.; Que, L. *Angew. Chem. Int. Ed.* **2005,** *44*, 2255-2258.
184. Kofod, P. *Inorg. Chem.* **1995,** *34*, 2768-2770.
185. Hull, E. A.; West, A. C.; Pestovsky, O.; Kristian, K. E.; Ellern, A.; Dunne, J. F.; Carraher, J. M.; Bakac, A.; Windus, T. L. *Dalton Trans.* **2015,** *44*, 3811-3816.
186. Blake, A. J.; Lavery, A. J.; Hyde, T. I.; Schröder, M. *J. Chem. Soc. Dalton Trans.* **1989**, 965-970.
187. Boiocchi, M.; Fabbrizzi, L.; Foti, F.; Vazquez, M. *Dalton Trans.* **2004**, 2616-2620.
188. Craig, C. A.; Spreer, L. O.; Otvos, J. W.; Calvin, M. *J. Phys. Chem.* **1990,** *94*, 7957-7960.
189. Ciampolini, M.; Fabbrizzi, L.; Licchelli, M.; Perotti, A.; Pezzini, F.; Poggi, A. *Inorg. Chem.* **1986,** *25*, 4131-4135.
190. Ferreira, K. Q.; Doro, F. G.; Tfouni, E. *Inorg. Chim. Acta* **2003,** *355*, 205-212.
191. Bianchini, C.; Mantovani, G.; Meli, A.; Migliacci, F.; Zanobini, F.; Laschi, F.; Sommazzi, A. *Eur. J. Inorg. Chem.* **2003,** *2003*, 1620-1631.
192. Haas, R. M.; Hern, Z.; Sproules, S.; Hess, C. R. *Inorganic Chemistry* **2017,** *accepted*.
193. Baidya, N.; Olmstead, M. M.; Mascharak, P. K. *J. Am. Chem. Soc.* **1992,** *114*, 9666-9668.
194. Coggin, D. K.; Gonzalez, J. A.; Kook, A. M.; Stanbury, D. M.; Wilson, L. J. *Inorg. Chem.* **1991,** *30*, 1115-1125.
195. Davis, R. N.; Tanski, J. M.; Adrian, J. C.; Tyler, L. A. *Inorg. Chim. Acta* **2007,** *360*, 3061-3068.
196. Crick, I. S.; Gable, R. W.; Hoskins, B. F.; Tregloan, P. A. *Inorg. Chim. Acta* **1986,** *111*, 35-38.
197. Hambley, T. W. *J. Chem. Soc. Dalton Trans.* **1986**, 565-569.
198. Kim, J. C.; Lough, A. J.; Park, H.; Kang, Y. C. *Inorg. Chem. Commun.* **2006,** *9*, 514-517.
199. Kannappan, R.; Rousselin, Y.; Jabri, R. Z.; Goze, C.; Brandès, S.; Guilard, R.; Zrineh, A.; Denat, F. *Inorg. Chim. Acta* **2011,** *373*, 150-158.
200. Marganian, C. A.; Vazir, H.; Baidya, N.; Olmstead, M. M.; Mascharak, P. K. *J. Am. Chem. Soc.* **1995,** *117*, 1584-1594.
201. Hartle, M. D.; Delgado, M.; Gilbertson, J. D.; Pluth, M. D. *Chem. Commun.* **2016,** *52*, 7680-7682.
202. Blake, A. J.; Gould, R. O.; Hyde, T. I.; Schröder, M. *J. Chem. Soc., Chem. Commun.* **1987**, 431-433.
203. El Ghachtouli, S.; Cadiou, C.; Déchamps-Olivier, I.; Chuburu, F.; Aplincourt, M.; Turcry, V.; Le Baccon, M.; Handel, H. *Eur. J. Inorg. Chem.* **2005,** *2005*, 2658-2668.
204. Barefield, E. K.; Freeman, G. M.; Van Derveer, D. G. *Inorg. Chem.* **1986,** *25*, 552-558.
205. Lewis, J.; Schröder, M. *Dalton Trans.* **1982**, 1085-1089.
206. Manuel, T. D.; Rohde, J.-U. *J. Am. Chem. Soc.* **2009,** *131*, 15582-15583.
207. Chu, T.; Belding, L.; Poddutoori, P. K.; van der Est, A.; Dudding, T.; Korobkov, I.; Nikonov, G. I. *Dalton Trans.* **2016,** *45*, 13440-13448.
208. Ciszewski, J. T.; Mikhaylov, D. Y.; Holin, K. V.; Kadirov, M. K.; Budnikova, Y. H.; Sinyashin, O.; Vicic, D. A. *Inorg. Chem.* **2011,** *50*, 8630-8635.
209. Hubin, T. J.; McCormick, J. M.; Collinson, S. R.; Alcock, N. W.; Clase, H. J.; Busch, D. H. *Inorg. Chim. Acta* **2003,** *346*, 76-86.
210. Fleischer, E.; Hawkinson, S. *J. Am. Chem. Soc.* **1967,** *89*, 720-721.
211. Hess, C. R.; Weyhermüller, T.; Bill, E.; Wieghardt, K. *Inorg. Chem.* **2010,** *49*, 5686-5700.
212. Shakya, R.; Powell, D. R.; Houser, R. P. *Eur. J. Inorg. Chem* **2009,** *2009*, 5319-5327.
213. **!!! INVALID CITATION !!! {}**.
214. Zhanaidarova, A.; Steger, H.; Reineke, M. H.; Kubiak, C. P. *Dalton Trans.* **2017,** *46*, 12413-12416.
215. Costamagna, J.; Ferraudi, G.; Matsuhiro, B.; Campos-Vallette, M.; Canales, J.; Villagrán, M.; Vargas, J.; Aguirre, M. J. *Coord. Chem. Rev.* **2000,** *196*, 125-164.

216. Dempsey, J. L.; Esswein, A. J.; Manke, D. R.; Rosenthal, J.; Soper, J. D.; Nocera, D. G. *Inorg. Chem.* **2005,** *44*, 6879-6892.
217. Bernhardt, P. V.; Jones, L. A. *Inorg. Chem.* **1999,** *38*, 5086-5090.
218. Rosenthal, J.; Bachman, J.; Dempsey, J. L.; Esswein, A. J.; Gray, T. G.; Hodgkiss, J. M.; Manke, D. R.; Luckett, T. D.; Pistorio, B. J.; Veige, A. S.; Nocera, D. G. *Coord. Chem. Rev.* **2005,** *249*, 1316-1326.
219. Hanson, G. R.; Gates, K. E.; Noble, C. J.; Griffin, M.; Mitchell, A.; Benson, S. *J. Inorg. Biochem.* **2004,** *98*, 903-916.
220. Stewart, C. A.; Dickie, D. A.; Kemp, R. A. *Inorganica Chimica Acta* **2012,** *392*, 268-276.
221. Ferreira, K. Q.; Doro, F. G.; Tfouni, E. *Inorg. Chim. Acta* **2003,** *355*, 205-212.

# 5 Appendix

**Table A 1.** Crystallographic data of **7**, **8**, **9** and **10**.

| | **7** | **8** | **9** | **10** |
|---|---|---|---|---|
| empirical formula | $C_{43}H_{52}F_{12}FeN_8OP_2$ | $C_{43}H_{48}F_{12}FeN_6OP_2$ | $C_{38}H_{42}Cl_2F_6N_4O_7S_2Zn$ | $C_{43}H_{45}F_6N_5O_7P_2Zn$ |
| fw | 1042.72 | 1010.66 | 981.14 | 987.33 |
| cryst. syst. | triclinic | monoclinic | monoclinic | monoclinic |
| space group | *P* -1 | *P* $2_1/n$ | *P* $2_1$/c | *P* $2_1$/c |
| *a* (Å) | 11.8732(14) | 17.6546(17) | 10.361(3) | 18.0907(15) |
| *b* (Å) | 12.7552(15) | 14.2997(14) | 15.945(4) | 14.3660(12) |
| *c* (Å) | 16.3941(18) | 18.8804(19) | 25.761(6) | 18.9329(15) |
| α (deg) | 76.579(5) | 90 | 90 | 90 |
| *β* (deg) | 83.331(5) | 92.641(5) | 93.772(14) | 91.824(4) |
| *γ* (deg) | 82.122(5) | 90 | 90 | 90 |
| volume (Å$^3$) | 2383.0(5) | 4761.4(8) | 4246.7(17) | 4918.0(7) |
| Z | 2 | 4 | 4 | 4 |
| $\rho_{calc}$ (mg mm$^{-1}$) | 1.453 | 1.410 | 1.535 | 1.333 |
| $\mu$ (mm$^{-1}$) | 0.474 | 0.471 | 0.881 | 0.657 |
| *F*(000) | 1076 | 2080 | 2016 | 2040 |
| reflns collected | 56160 | 203262 | 88748 | 138041 |
| indep. reflns /$R_{int}$ | 8733/0.0443 | 13923/0.0410 | 8356/0.0568 | 9693/0.0357 |
| data/restraints/para | 8733/85/684 | 13924/21/659 | 8356/84/549 | 9693/248/805 |
| GOF on $F^2$ | 1.042 | 1.024 | 1.019 | 1.056 |
| final R1 indexes [I≥2$\sigma$(I)] | 0.0340 | 0.0387 | 0.0339 | 0.0409 |
| final wR2 indexes (all data) | 0.0900 | 0.1105 | 0.0444 | 0.0508 |
| $\Delta\rho_{min/max}$ (e Å$^{-3}$) | 0.736/-0.302 | 0.807/-0.569 | 0.637/-0.729 | 0.622/-0.423 |

**Table A 2.** Parameters used to assign the $^1$H NMR signals of **8**.

| Label | Spin $\rho$ [a] x $10^{-3}$ [a.u.] | $\delta^{exp}_{298}$ rel. TMS [ppm] | Integral expl. | Half-width $\Delta$ [Hz] | Fe···H distance $r$ [Å] | Angle $\theta$ [deg] | $\delta^{dip}_{298}$ [ppm] | $\delta^{dia}$ from **10** [ppm] | $\delta^{para}_{298}$ [ppm] | $\delta^{theor}_{298}$ [ppm] |
|---|---|---|---|---|---|---|---|---|---|---|
| $H_6$ | 0.8713 | 224 | [b] | 260 | 3.874 | 105.8 | 1.3 | 9.83 | 214 | 227 |
| $H_1$ | 0.3283 | 140 | 1.0 | 600 | 3.265 | 90.6 | 2.9 | 8.69 | 131 | 86 |
| $H_{26}$ | 0.3135 | 123 | 2.1 | 950 | 3.564 | 56.1 | 0.1 | 5.06[e] | 118 | 114 |
| $H_{31}$ | 0.4385 | 81 | 2.2 | 720 | 3.093 | 40.1 | -2.5 | 7.86 | 73 | 82 |
| $H_{28}$ | 0.1410 | 54.8 | 2.8 | 75 | 5.029 | 24.2 | -1.2 | 7.53 | 47.3 | 36.7 |
| $H_{30}$ | 0.0675 | 51.9 | 2.9 | 60 | *5.091* | 23.1 | -1.2 | *7.33* | *44.6* | 17.6 |
| $H_4$ | 0.1960 | 50.3 | 1.5 | 55 | 5.034 | 104.1 | 0.6 | 8.42 | 41.9 | 51.1 |
| $H_2$ | 0.1598 | 49.2 | 1.4 | 55 | 5.234 | 95.6 | 0.7 | 7.83 | 41.4 | 41.6 |
| $H_{26'}$ | 0.0655 | 42 | 1.8 | *1000* | 3.174 | 53.3 | -0.2 | 5.09[e] | 37 | 17 |
| $H_{19}$ | 0.0333 | 17 | 1.6 | 20 | 6.364 | 89.5 | 0.4 | 7.48 | 9.5 | 8,7 |
| $H_{13}$ | 0.0038 | 15.7 | 1.4 | 30 | 6.346 | 99.6 | 0.4 | 7.66 | 8.0 | 1.0 |
| $H_{23}$ | 0.0038 | 15.1 | 1.5 | 25 | 4.896 | 82.5 | 0.8 | 7.98 | 7.1 | 1.0 |
| $H_8$ | -0.0083 | 4.5 | 1.8 | 55 | 4.845 | 105.4 | 0.7 | 8.06 | -3.6 | -2.1 |
| $H_{29}$ | -0.0118 | 2.3 | 2.9 | 35 | 5.829 | 1.1 | -1.0 | 8.01 | -5.7 | -3.1 |
| $H_{11}$ | 0.0020 | 1.1 | 13.2 | 15 | 7.853 | [c] | [d] | 1.42 | -0.3 | 0.1 |
| $H_{22}$ | 0.0005 | 0.4 | 13.2 | 15 | 7.800 | [c] | [d] | 1.39 | -1.0 | 0.5 |
| $H_{15}$ | 0.0000 | -0.4 | 8.6 | 20 | 6.451 | [c] | [d] | 1.53 | -1.9 | 0.0 |
| $H_3$ | -0.0653 | -0.9 | 1.3 | 55 | 5.915 | 100.9 | 0.4 | 8.42 | -9.3 | -17.0 |

[a] Spin per unpaired electron. [b] Not determined. [c] Not determined; see also next footnote. [d] Owing to the large distances $r$ the dipolar shifts should be very small. For this reason the averaging of the angle $\theta$ of the methyl and *t*-butyl groups has been abandoned. [e] Interchange of $H_{26}$ and $H_{26'}$ not excluded.

**Table A 3.** Parameters used to assign the $^1$H NMR signals of **7**.

| Label | Spin $\rho$ [a] x $10^{-3}$ [a.u.] | $\delta^{exp}_{298}$ rel. TMS [ppm] | Integral expl. | Half-width $\Delta$ [Hz] | Fe···H distance *r* [Å] | Angle $\theta$ [deg] | $\delta^{dip}_{298}$ [ppm] | $\delta^{dia}$ from **9** [ppm] | $\delta^{para}_{298}$ [ppm] | $\delta^{theor}_{298}$ [ppm] |
|---|---|---|---|---|---|---|---|---|---|---|
| $H_6$ | 0.6425 | 297 | [b] | 650 | 3.874 | 107.59 | 1,8 | 9.39 | 288 | 276.8 |
| $H_{31}$ | 0.3125 | 147 | 1 | 780 | 3.265 | 39.07 | -2.7 | 7.79 | 139 | 134.6 |
| $H_{26}$ | 0.2750 | 130 | 0.8 | 1200 | 3.564 | 59.11 | 0.5 | 5.08 | 125 | 118.5 |
| $H_a$ | 0.2550 | 96 | 0.9 | 920 | 3.093 | 79.66 | 2.5 | 8.66 | 87 | 109.8 |
| $H_4$ | 0.1500 | 85 | 1 | 490 | 5.029 | 104.7 | 0.6 | 8.27 | 77 | 64.6 |
| $H_2$ | 0.1250 | 63.6 | 1.2 | 380 | *5.091* | 86.7 | 0.7 | 7.66 | 55.9 | 53.8 |
| $H_{28}$ | 0.1175 | 62.9 | 1.2 | 350 | 5.034 | 25.0 | -1.1 | 7.36 | 55.5 | 50.6 |
| $H_{30}$ | 0.0850 | 52.7 | 1.3 | 130 | 5.234 | 22.1 | -1.2 | 7.30 | 45.4 | 36.6 |
| $H_{19}$ | 0.0225 | 22.3 | 0.9 | 440 | 3.174 | 83.0 | 0.3 | 7.33 | 15.0 | 9.7 |
| $H_{11}$ | 0.0010 | 1.2 | 11 | 15 | 7.929 | [c] | [d] | 1.34 | -0.1 | 0.4 |
| $H_{22}$ | -0.0005 | -2.5 | 11 | 10 | 7.734 | [c] | [d] | 1.29 | -3.8 | -0.2 |
| $H_{15}$ | 0 | -4.8 | 6.4 | 40 | 6.752 | [c] | [d] | 1.68[f] | -6.4 | 0 |
| $H_{15'}$ | -0,0005 | | | | 6.520 | [c] | [d] | 1.39[f] | | -0.2 |
| $H_3$ | -0,0275 | -12.3 | 0.4 | 260 | 5.972 | 97.1 | 0.4 | 8.20 | -20.5 | -11.8 |
| $H_{25}$ | -0.0975 | -58 | [b] | 2900 | 2.699 | 90.1 | 5.1 | 5.65 | -64 | -42.0 |

[a] Spin per unpaired electron. [b] Not determined. [c] Not determined; see also next footnote. [d] Owing to the large distances *r* the dipolar shifts should be very small. For this reason the averaging of the angle $\theta$ of the methyl and *t*-butyl groups has been abandoned.

**Figure A 1.** LIFDI-MS of **17**, **18** and **19** in DCM; expected isotope pattern above each spectrum.

**17**

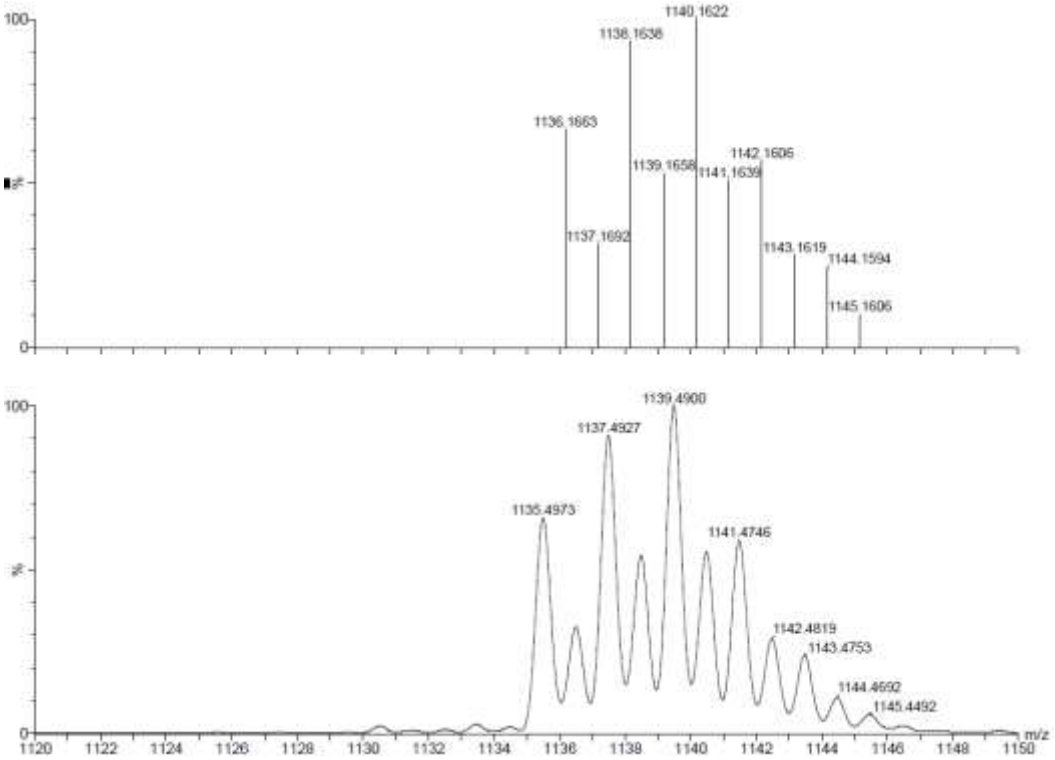


**18**

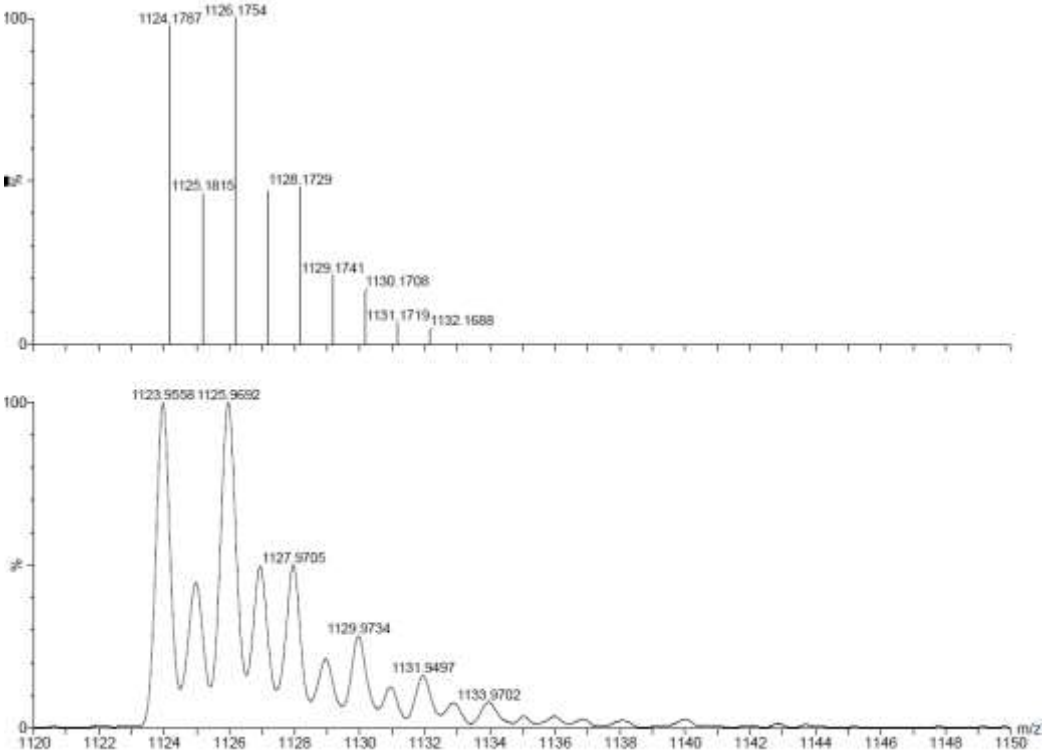

**19**

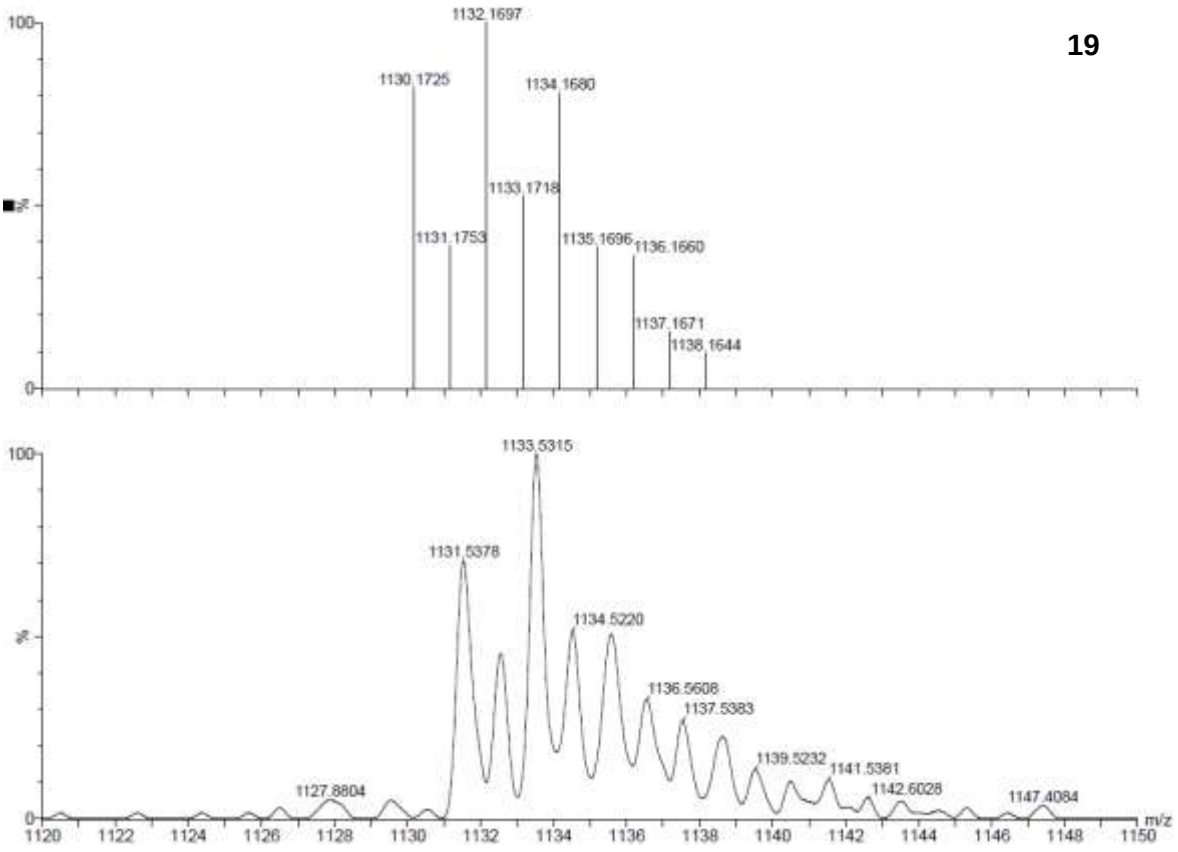
100
%
0
1132.1697
1130.1725
1134.1680
1133.1718
1131.1753
1135.1696
1136.1660
1137.1671
1138.1644
100
%
0
1133.5315
1131.5378
1134.5220
1136.5608
1137.5383
1139.5232
1141.5381
1142.6028
1127.8804
1147.4084
1120
1122
1124
1126
1128
1130
1132
1134
1136
1138
1140
1142
1144
1146
1148
1150
m/z

**Table A 4. .** Crystallographic data of **17**, **18**, **19**.

| | **17**·THF | **18**·THF | [**19**]$_2$·THF |
|---|---|---|---|
| Empirical formula | $C_{46}H_{71}F_{12}N_7O_{14}S_4Zn_2$ | $C_{46}H_{71}F_{12}N_7\ Ni_2O_{14}S_4$ | $C_{88}H_{134}F_{24}N_{14}\ Ni_2\ O_{27}S_8Zn_2$ |
| fw | 1433.07 | 1419.72 | 2780.74 |
| Cryst. syst. | monoclinic | monoclinic | monoclinic |
| Space group | P 1 21/c 1 | P 1 21/c 1 | P 1 21/n 1 |
| *a* (Å) | 15.3270(5) | 15.238(2) | 29.8465(13) |
| *b* (Å) | 16.5758(5) | 16.867(2) | 16.5015(8) |
| *c* (Å) | 29.9196(10) | 29.145(4) | 30.6747(15) |
| *α* (°) | 90 | 90 | 90 |
| *β* (°) | 103.8050(10) | 103.365 | 104.814(3) |
| *γ* (°) | 90 | 90 | 90 |
| Volume (Å$^3$) | 7381.7(4) | 7288.0(16) | 14605.5(12) |
| *Z* | 4 | 4 | 4 |
| $\rho_{calc}$ (mg mm$^{-3}$) | 1.289 | 1.294 | 1.265 |
| $\mu$ (mm$^{-1}$) | 2.606 | 2.471 | 2.532 |
| F (000) | 2960 | 2944 | 5744 |
| Reflns. collected | 95912 | 62002 | 135925 |
| Indep. reflns/$R_{int}$ | 13646 | 13771 | 26704 |
| Data/restraints/param. | 13646/385/854 | 13771/965/1072 | 26704/1066/1734 |
| GOF on $F^2$ | 1.072 | 1.083 | 1.044 |
| Final $R_1$ indexes [I ≥ 2σ(I)] | 0.0925 | 0.1002 | 0.1066 |
| Final w$R_2$ indexes | 0.2507 | 0.2677 | 0.2796 |
| (all data) | | | |
| $\Delta\rho_{min/max}$ (e Å$^3$) | 0.115 | 0.098 | 0.121 |

**Figure A 2.** Electronic spectra of **18** (blue) and **19** (red) in THF.